Technical Report

TR-09-34

Bentonite erosion

Final report

Martin Birgersson, Lennart Börgesson,
Magnus Hedström, Ola Karnland, Ulf Nilsson
Clay Technology AB

December 2009

Svensk Kärnbränslehantering AB
Swedish Nuclear Fuel
and Waste Management Co

Box 250, SE-101 24 Stockholm
Phone +46 8 459 84 00

Bentonite erosion

Final report

Martin Birgersson, Lennart Börgesson,
Magnus Hedström, Ola Karnland, Ulf Nilsson
Clay Technology AB

December 2009

Abstract

Low saline water may reach KBS-3 repository depth, e.g. during periods of glaciation. Under such aqueous conditions, the montmorillonite part of the bentonite buffer might transform into a sol and thereby be transported away with flowing water in fractures.

The primary aim with this report is to improve the understanding of the basic principles for this possible montmorillonite particle release. The report includes experimental and theoretical work performed at Clay Technology.

Natural bentonite and ion-exchanged purified montmorillonite from three different geographical origins, Wyoming (U.S.), Milos (Greece) and Kutch (India) have been studied. Experimental and/or theoretical investigations have been performed with respect to:

- Free swelling ability
- Rheological properties
- Rate of bentonite loss into fractures
- Filtering
- Ion exchange
- Sol formation ability
- Ion diffusion
- Mass loss due to erosion

The performed erosion experiments show that erosion does not occur in a mixed calcium/sodium montmorillonite with at least 20% calcium in exchange positions, when the external solution contains above 4 mM charge equivalents. This result is in agreement with the presented conceptual view of sol formation and measured equilibrium properties in mixed calcium/sodium montmorillonite.

The findings imply that the buffer will be stable for non-glacial conditions. However, erosion due to sol formation cannot be ruled out for glacial conditions.

Sammanfattning

Vatten med låg salthalt kan nå KBS-3 förvarsdjup, exempelvis under glaciala perioder. Under sådana förhållanden är det tänkbart att montmorilloniten i bentonitbufferten övergår i en solfas, vilken kan bli borttransporterad med flödande vatten i bergssprickor.

Rapportens huvudsakliga syfte är att öka förståelsen för de grundläggande principer som styr detta möjliga frigörande av separata montmorillonite partiklar. Rapporten omfattar experimentellt och teoretiskt arbete utfört vid Clay Technology.

Naturliga bentoniter och jonbytta renade montmorilloniter från tre olika geografiska ursprung, Wyoming (USA), Milos (Grekland) och Kutch (Indien), har undersökts. Experimentella och/eller teoretiska studier har genomförts med avseende på:

- Frisvällningskapacitet
- Rheologiska egenskaper
- Bentonitförlust via sprickor
- Filtrering
- Jonbyte
- Solbildningsförmåga
- Jondiffusion
- Erosionsorsakad massförlust

De genomförda erosionsförsöken visar att erosion inte uppträder i blandad kalcium/natrium-montmorillonit, i vilken minst 20% av motjonerna utgörs av kalcium, när den externa lösningen innehåller mer än 4 mM laddningsekvivalenter. Dessa resultat är i samklang med det framlagda konceptuella synsättet för solbildning och uppmätta jämviktsegenskaper hos blandad kalcium/natrium-montmorillonit.

Resultaten visar att bufferten är stabil under icke-glaciala förhållanden. Under glaciala förhållanden kan däremot erosion orsakad av solbildning ej uteslutas.

Executive summary

The exceptional uptake of water and resulting swelling of the bentonite buffer is normally counteracted by the walls of the deposition hole in a KBS-3 repository, and a swelling pressure develops in the bentonite. However, fractures intersecting a deposition hole mean that rigid swelling restrictions are not present everywhere, and that localized swelling continues into the fractures until an equilibrium is reached. This free swelling may lead to separation of individual montmorillonite layers (dispersion) and part of the buffer could thereby be transported away with the groundwater.

The primary aim with this report is therefore to describe the mainly experimental work, which has been performed in order to better describe and understand the basic principles for this possible montmorillonite particle release from a bentonite buffer.

Most of the performed work concerns bentonite from Wyoming, known under its commercial name MX-80. Both untreated MX-80 and purified montmorillonite in two homoionic forms (sodium and calcium) have been used as starting material in the presented experiments. In addition, Na- and Ca-exchanged montmorillonite from two other locations, Milos, Greece and Kutch, India, have been studied for comparison purposes. The three different montmorillonites are referred to as Wy-X, Mi-X, and Ku-X, respectively where X stands for the type of counterion.

In Chapter 1 an introduction to the possible erosion problem is presented and in Chapter 2 some qualitative and quantitative experiments are shown that illustrate how the swelling ability and colloidal properties depend on e.g. the valance of the charge compensating ions or the presence of excess ions in the external solution.

It is of interest to know how far bentonite can penetrate into fractures intersecting the deposition hole. A swelling model based on effective stress theory, previously developed at Clay Technology /Börgesson et al. 1995/, has been further adopted for the swelling into fractures and tested in Chapter 3. The model relies partly on an empirical relationship for hydraulic conductivity developed in our laboratory. From rheological measurements also presented and evaluated in Chapter 3, four rheological domains have been identified. The above mentioned swelling model is valid in the two regions with the lowest water to solid mass ratio, termed solid mass and gel (repulsive gel). Outside this region edge-face interactions that are not explicitly accounted for in the model start to influence the bentonite properties. In the modelling presented in Chapter 3, clay that has expanded beyond a water to solid mass ratio of 30 is assumed to be lost. Therefore the calculated mass loss may be too pessimistic if the water in the fracture has an ionic composition such that an attractive gel can be formed. We are however not aware of any model that correctly can describe the coagulation at the swelling front when the swelling clay meets a ground water with sufficient ionic composition for this to actually occur. However up to a water to solid mass ratio of about 35 the model presented here has been parameterized to experimental data /Börgesson et al. 1995/ and is in this report applied only within its domain of validity.

It is known from earlier experiments that colloid particles can penetrate filters. In Chapter 4 the question concerning what physical barriers can stop colloids is addressed. Homoionic calcium montmorillonite is found not to erode through stainless steel filters with pore size 100 µm. This observation is also consistent with the known fact that Ca-montmorillonite swells to a maximum interlayer distance and thus does not release colloids. For homoionic sodium montmorillonite the pore size needs to be 0.5 µm or less to prevent erosion. The idea that either accessory minerals present in MX-80 or added filler materials, e.g. kaolinite, could form a filter cake that may prevent erosion has also been tested. The outcome of those tests does not exclusively show that there is a mechanical filter effect of these materials.

Chapters 5–8 all discuss various physicochemical properties of bentonite and montmorillonite, especially at high water to solid mass ratios relevant for colloid formation. A large number of tests on the three different montmorillonites at solid-to-liquid mass ratios in the range 2 to 10 g clay per litre solution have been carried out in order to determine under what conditions montmorillonite forms a sol or coagulate, i.e. form an attractive gel. Although the sol/gel transition is in most cases obvious to the naked eye additional information, concerning, e.g. sedimentation kinetics and the gelling process, have been gained through turbidity measurements which are described in detail in Chapters 5 and 7.

Homoionic Ca-montmorillonite does not release colloids because of the well documented ion-ion correlation effect in systems with multivalent counterions. The problem of colloid release comes from monovalent counterions and low ionic strength of the external water. It is shown in Chapter 5 that as little as 20% sodium ions in the interlayer are sufficient, under unfavourable circumstances, to alter the behaviour of montmorillonite into a sol-forming state. Montmorillonite with ~90% calcium or more behaves similar to pure calcium montmorillonite and does not release colloids.

Commonly, the stability of montmorillonite sols is discussed in terms of a critical coagulation concentration, CCC. In NaCl solution the CCC is determined to be 25 mM for Wy-Na, 10 mM for Mi-Na and 5 mM for Ku-Na, respectively. The interlayer charge of Wy-Na and Mi-Na are similar, whereas it is higher for Ku-Na. In the so called primitive model (PM), or the DLVO approximation of the PM the repulsive osmotic force is balanced by the van der Waals interaction at the CCC /e.g. Evans and Wennerström 1999/. Mathematically this leads to increasing CCC with increasing layer charge. Thus, our results demonstrate that the CCC cannot be determined within the DVLO model for parallel clay layers. Also, the CCC from DLVO would be of the order of 1 M instead of around 10 mM. Clay particles contain two types of charges, negative on the faces and pH dependent charges on the edges. Standard DLVO theory for parallel layers neglects the latter type of charges and can therefore not be used for describing the coagulation of montmorillonite at low ionic strength. This point is further demonstrated by studying coagulation of Wy-Na in a mixture of tetrasodium pyrophosphate and NaCl. The presence of pyrophosphate that binds to the edges of the clay increases the CCC by an order of magnitude. Increasing pH also indicates a weaker gel at the CCC.

The presence of calcium in the clay and in the external electrolyte is of utmost importance to prevent colloid release. Na-montmorillonite produces colloids at low ionic strength conditions, pure Ca-montmorillonite does not, and relatively small amounts of sodium in exchange position in a calcium dominated montmorillonite makes the clay act similar to a sodium clay. The sodium–calcium charge ratio is consequently of major importance and a selectivity coefficient is needed in order to calculate the ratio for a specific ground-water composition. Several investigators have measured a selectivity coefficient in batch experiments, i.e. at high water to solid ratios. For the KBS-3 concept it is however important to know the Ca/Na selectivity coefficient at high compaction, in order to calculate the long-term cation distribution in the bentonite buffer. Using ion-selective electrodes as well as ICP/AES analysis the selectivity coefficient for Ca/Na exchange in Wy-montmorillonite has been determined at dry densities 1,000–1,500 kg/m^3. Our results reported in Chapter 6 gives a selectivity coefficient of 3.8–7.8 M in the Gaines-Thomas convention. This is similar to values around 4 M measured in batch experiment. Using a value of 4.5 M one can calculate that montmorillonite in contact with a glacial meltwater of Grimsel type would in thermodynamic equilibrium contain more than 95% divalent ions and thus not release colloids.

Chapter 7 presents a synthesis of the work in the previous two chapters. The investigation is further extended by having both NaCl and $CaCl_2$ in the external solution. Having two types of cations makes the problem of sol formation more complex and it cannot any longer be discussed in terms of CCC. The idea of a “beak-shaped” sol-formation zone (SFZ) is put forward. This is an area in a two-dimensional phase diagram with the Ca^{2+} concentration on the x-axis and the Na^+ concentration on the y-axis. The initial hypothesis was theoretically derived limits for a sol-formation zone in the [Ca^{2+}]-[Na^+]-diagram for montmorillonite limited at low ionic strength by a curve on which the Na/Ca-exchange reaction puts the Ca^{2+} population in the clay to approximately 90% (charge wise). At high ionic strengths the theory puts an upper limit by the line of constant ionic strength equal to the concentration at which the pure Na-system forms a gel. Numerous swelling and sedimentation tests have shown that the experimental SFZ is much smaller than given by the initial hypothesis. The measurements show that the SFZ is localized to very close to the [Na+]-axis in the [Ca^{2+}]-[Na^+]-diagram. This observation suggests that the ability to form a sol in a Ca/Na-solution is not just a matter of ionic strength but does explicitly depend on the calcium content of the system: relatively small amounts of calcium reduce the ability to form a sol significantly. This effect of calcium is additional to the well-documented correlation effects on lamellar swelling and we argue that it must be associated with the interactions with the edges of separate montmorillonite layers.

This additional effect of calcium has also been confirmed in performed erosion tests where highly Na-dominated clays (~80% sodium) have been shown to be prevented from eroding by solutions containing only small concentrations of calcium and NaCl concentrations in the range 1–5 mM.

Chapter 8 describes ion diffusion tests performed in pure montmorillonite systems contacted with crystalline gypsum in a controlled geometry or with gypsum saturated solution in order to gain understanding of the dissolution process of accessory minerals in water saturated bentonite. It is demonstrated that gypsum dissolving in Na-montmorillonite, contacted to deionized water will result in a Na_2SO_4 flux over the clay/external solution interface. Such behaviour is qualitatively easily explained by considering the basically infinite preference for Ca^{2+}- ions in clay for these types of boundary conditions.

The report ends with conclusions in Chapter 9.

Contents

1 Introduction

Bentonite consists mainly of montmorillonite, which is responsible for the swelling ability of bentonite in contact with an aqueous solution. The montmorillonite mineral belongs to the smectite group, in which all the minerals have an articulated layer structure. Each layer is composed of a central sheet of octahedrally coordinated cations, which on both sides is linked through shared oxygens to sheets of tetrahedrally coordinated cations, as pictured in Figure 1-1. The thickness of an individual mineral layer is around 1 nm (Figure 1-1) and the extension in the two other directions is often several hundred nanometres.

The octahedral sheet has aluminium as central ion, which is partly substituted principally by magnesium and iron. The tetrahedral sheet has silicon as central ion, which partly may be substituted principally by aluminium. The substitutions result in a net negative charge of the montmorillonite layer. The negative layer charge is balanced by cations located between the individual layers (interlayer space). The structure leads to a water affinity in the interlayer space and a variable number (n) of water molecules may be incorporated between the individual mineral layers to form an interlayer ionic solution /Newman and Brown 1987/. The chemical formula for an idealized Na-montmorillonite unit cell may be written as

$$\left[(Si_{8-x}Al_x)(Al_{4-y}Mg_y)O_{20}(OH)_4\right]^{(x+y)-}Na^+_{x+y}\cdot nH_2O\,,$$

where by definition the tetrahedral charge is lower than the octahedral charge (x<y) and 0.4 <x+y< 1.2. Smectite clay corresponding to the above chemical formula but with x>y is called beidellite. It is the mechanisms of hydrating the interlayer cations and osmotically transporting water into the interlayer solution that are the causes for bentonite swelling.

The swelling ability is strongly dependent on what type of charge compensating cation is dominating in the interlayer and on the chemical conditions of the external aqueous phase. For montmorillonite dominated by small monovalent cations (Li^+, Na^+, K^+) the swelling ability at low enough ionic strength can be so large that the clay transform into a sol state – a dispersion of in principle individual montmorillonite layers. However, in montmorillonite dominated by multivalent or larger monovalent ions (e.g. Cs^+, Mg^{2+}, Ca^{2+}), the swelling is restricted to a maximum mean interlayer distance of a few nm /Brindley and Brown 1980/.

The water uptake and resulting swelling of the bentonite buffer in a KBS-3 repository is normally counteracted by the walls of the deposition hole, and a swelling pressure develops in the bentonite. However, fractures intersecting the deposition hole mean that rigid swelling restrictions are not present everywhere, and that localized swelling continues into the fractures until an equilibrium or, in the case of erosion, a steady-state is reached. Certain chemical conditions during the repository lifetime, e.g. when glacial meltwater of low ion concentration interacts with the buffer during an ice age, may lead to sol formation in the fractures and part of the buffer could thereby be transported away with the groundwater. It is therefore of great importance to assess this possible cause for mass loss of the buffer.

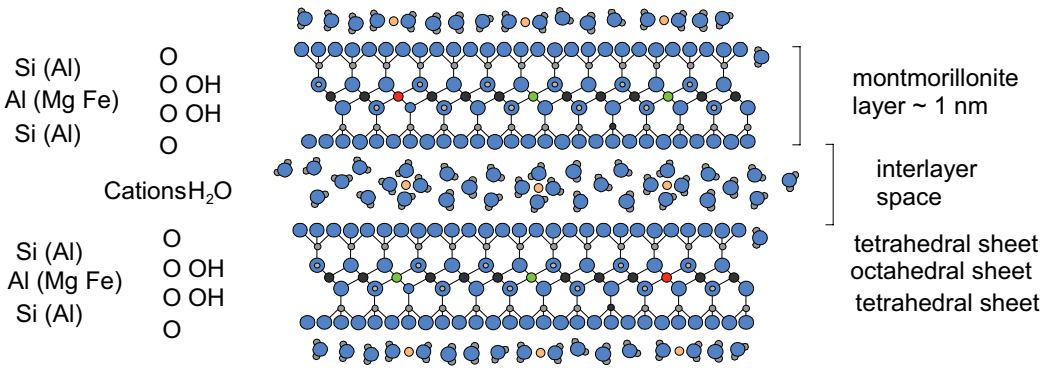

Figure 1-1. *Edge view cartoon of two montmorillonite layers with interlayer cations and water molecules.*

Montmorillonite shows different behaviour depending on water to solid (mass) ratio ($w_r = m_{water}/m_{clay}$) and the chemical composition of the aqueous phase. A schematic phase or state diagram of Na-montmorillonite is presented in Figure 1-2 where the water to solid ratio is plotted on the x-axis and the NaCl concentration of the water on the y-axis. At low w_r the repulsive forces (osmotic double layer forces and hydration) dominate the system and this phase is normally termed repulsive gel, /e.g. Abend and Lagaly 2000/. At very low water to solid mass ratios the repulsive gel behaves more like a solid (yield stress > 1 kPa) and in Chapter 3, on rheology, the term solid mass (Phase A) is used when $w_r < 10$ and the term gel (Phase B) when $10 < w_r < 35$. There are two more phases in the phase diagram and the commonly used terminology for those are attractive gel and sol /Abend and Lagaly 2000/. In case the NaCl concentration is below the critical coagulation concentration (CCC), which in the diagram is the concentration where repulsive gel, attractive gel and sol meet, a repulsive gel would continue to expand given free access to solvent. At a certain w_r the system behaves more like a fluid than a gel, the yield stress goes to zero. This is the sol phase, i.e. a suspension of montmorillonite particles (individual layers or aggregates) that are only weakly interacting. In Chapter 5 it is shown that aggregates are formed in the sol phase even when the clay is dispersed in deionized water. These aggregates have a limited size and do not form a network that span the available space, hence no yield strength. Above the CCC a gel phase, where attractive forces among the clay particles dominate, is formed. This attractive gel can be reached by either letting montmorillonite swell in a solution with NaCl concentration above the CCC or by adding NaCl to a montmorillonite sol such that the final NaCl concentration is above the CCC. In the former case the gel would swell to a maximum w_r (e.g. Figure 5-17 and Figure 7-28) where it meets the boundary separating the repulsive from the attractive gel. In the latter case we have found that a very low density gel can be formed where the average w_r may be more than an order larger than the water to solid ratio at which the clay particles can start to rotate freely. Our conceptual view of this attractive gel is a loose percolated network /Tanaka et al. 2004/ of clay particles interacting through edge to face attraction. We sometimes use the term percolation gel for the attractive gel that is formed when the sol-to-attractive-gel border is crossed. It should also be pointed out that the percolation gel is most probably a non-equilibrium structure where the clay particles are locked in their positions at local energy minima that are sufficiently low so that the thermal energy cannot bring the system to the global energy minimum. In the phase diagram in Figure 1-2 there is a dashed line at high w_r separating the attractive gel from the sol. This border has not been explored in this study but is deduced from the assumption that at sufficiently high w_r the system must be beyond the percolation threshold /Stauffer and Aharony 1994/ where the density of clay particles is too low to form a space filling network.

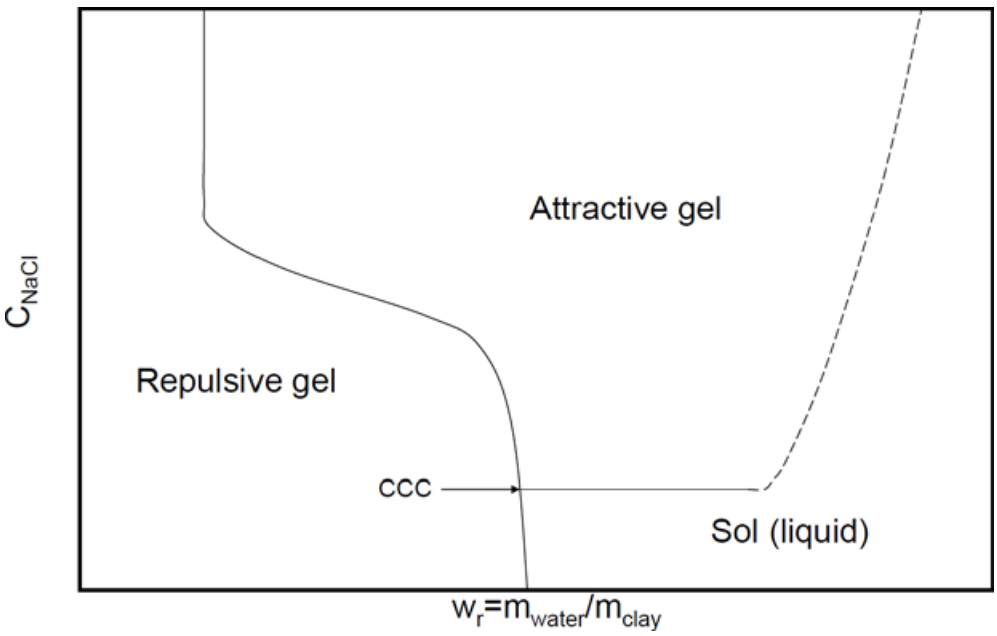

Figure 1-2. *Schematic phase/state diagram for Na-montmorillonite.*

In pure Ca-montmorillonite the sol phase is absent. Thus Ca-montmorillonite does not form colloidal sols even in contact with deionized water.

Mixed Ca/Na-montmorillonite may show the same phases as homoionic Na-montmorillonite. However, one needs to extend the phase diagram to include both Na^+ and Ca^{2+} concentrations. The complexity can be reduced by introducing a two-dimensional phase diagram (Chapter 7) with $CaCl_2$ concentration on the x-axis and NaCl concentration on the y-axis.

For a correct description of highly expanded systems where interlayer distances can be comparable with the lateral dimensions of the individual montmorillonite layers it becomes important to consider forces other than the pure osmotic repulsion, specifically forces associated with the edges of the montmorillonite layers /Lagaly and Ziesmer 2003, Tombácz and Szekeres 2004, Liu and Neretnieks 2006/. At the edges of the montmorillonite layers e.g. protonation/deprotonation reactions occur giving them a net positive or negative charge depending on pH. Also more complicated surface complexation reactions are associated with the montmorillonite edge sites which may greatly influence the interactions between individual layers in highly expanded systems.

Force interaction involving montmorillonite edges is a probable contribution to the very complicated rheological behaviour of bentonite gels (thixotophy, hysteresis, etc. see Chapter 3) and they are completely necessary in order to explain certain gel-sol transitions at very high water to solid mass ratios (Chapters 5 and 7).

The basic aim with this report is to describe the mainly experimental work, which has been performed in order to better describe and understand the basic principles for the possible montmorillonite particle release from a bentonite buffer material.

1.1 Investigated clays

Three different bentonites from different geographical origins have been investigated or used as raw material in this study; MX-80 from Wyoming, Deponit CA-N from Milos and ASHA 505 from Kutch, India. All the investigated bentonites have high percentage of montmorillonite (75–85%) but their composition regarding accessory minerals differ as well as the makeup of counterions, e.g. Deponit Ca-N is calcium dominated whereas MX-80 is dominated by sodium /Karnland et al. 2006/.

In this report the commercial names are used when the experiments are performed on the bentonite material whereas the geographical location of the bentonite deposit is used to label the extracted purified montmorillonite. Thus Wyoming (Wy) montmorillonite denotes the montmorillonite extracted from MX-80, Milos (Mi) montmorillonite is obtained from Deponit CA-N, and Kutch-39 (Ku39) montmorillonite from ASHA 505 /Karnland et al. 2006/. For simplicity the notation Ku will be used instead of Ku39.

Purified montmorillonites are ion exchanged to a homoionic form through dialysis and will be referred to as Wy-X, Mi-X and Ku-X, where X stands for the type of counterion. Some experiments are also performed on Ca/Na-montmorillonite obtained by mixing Ca-montmorillonite with Na-montmorillonite (see Chapters 2, 5 and 7 for details).

A comprehensive account of the chemical and physicochemical characteristics of the three clays used in this study can be found in the Technical Report by /Karnland et al. 2006/. In Table 1-1 we have extracted properties related to the layer charge. Note that Wy-Na1 and Wy-Na2 refer to the same mineral but the procedures of ion exchange to sodium montmorillonite differ in the two cases. The same comment pertains to the Milos montmorillonite. Ideally the layer properties should not be influenced by the ion exchange procedure. The differences seen in the two cases could possibly be ascribed to variation in the raw material, bentonite is after all a natural material and not engineered, as well as the sensitivity of the analysis. The layer charge distribution with respect to the octahedral and tetrahedral sheets can be deduced from the chemical analysis of the purified montmorillonite /Karnland et al. 2006/. The surface charge density σ is calculated from the total charge divided by the lateral dimensions of the unit cell and the cation exchange capacity (CEC) is the total charge divided by the mass of the unit cell, and is normally presented in units of mol equivalent charge/kg. Both Wy-Na and Mi-Na are dominated by octahedral charges whereas Ku-Na has an almost even division between tetrahedral and octahedral charges as shown in Table 1-1.

Table 1-1 Selected physical properties related to the permanent layer charges of the different montmorillonites investigated in this study (extracted from /Karnland et al. 2006/).

	Wy-Na1	Wy-Na2	Mi-Na1	Mi-Na2	Ku-Na
CEC [eq/kg]	0.87	0.88	0.97	1.09	1.04
σ [C/m^2]	–0.11(1)	–0.11(1)	–0.12(3)	–0.14(0)	–0.13(5)
Tetr. Charge [e]	–0.11	–0.05	–0.15	–0.27	–0.38
Octa. Charge [e]	–0.54	–0.60	–0.57	–0.55	–0.42
Total Charge [e]	–0.65	–0.65	–0.72	–0.82	–0.79

2 Swelling ability of montmorillonite

The maximum interlayer distance, for monovalent ions in the montmorillonite/water system, may be discussed in terms of the Debye screening length, which for a symmetric electrolyte is inversely proportional to the square root of solution concentration. The same dependence on the maximum interlayer distance has been experimentally found by /Norrish 1954/. The forces between parallel montmorillonite layers and only mono-valent ions present can ideally be calculated from DLVO theory, in which the entropic repulsive effects from ions and the attractive van der Waals forces are taken into account. In the case of only divalent ions in the system, additional attractive forces become significant /Kjellander et al. 1988/ which restrict the swelling to relatively short interlayer distances and no release of individual colloid particles takes place (Figure 2-1 and Figure 2-2).

The complexity of the swelling properties may further be illustrated by water vapour uptake tests, in which approximately 2 grams of montmorillonites with Li^+, Na^+, K^+, Mg^{2+} and Ca^{2+} as counterions were exposed to vapour from a free water surface (Figure 2-3). The materials and water were placed in an evacuated and sealed vessel, which in turn was placed in a climate chamber in order to keep the temperature constant (25°C). Not only had the clays with divalent ions a restricted swelling but also the K-montmorillonite.

A relatively small content of monovalent ions (Na^+) in a calcium dominated system may still lead to general colloid formation at low ion concentrations. The conditions may be illustrated by the performed series of simple swelling experiment shown in Figure 2-4 and Figure 2-5 with 0.5 grams of pure montmorillonite which was ion exchanged to pure Na^+ or Ca^{2+} states, and materials mixed in water and subsequently dried to give calcium-sodium ratios of 80/20 or 60/40. The pure Na-montmorillonite was further mixed with relatively large amounts of calcite or gypsum to show the effects of respective equilibrium concentrations of Ca^{2+} at saturation.

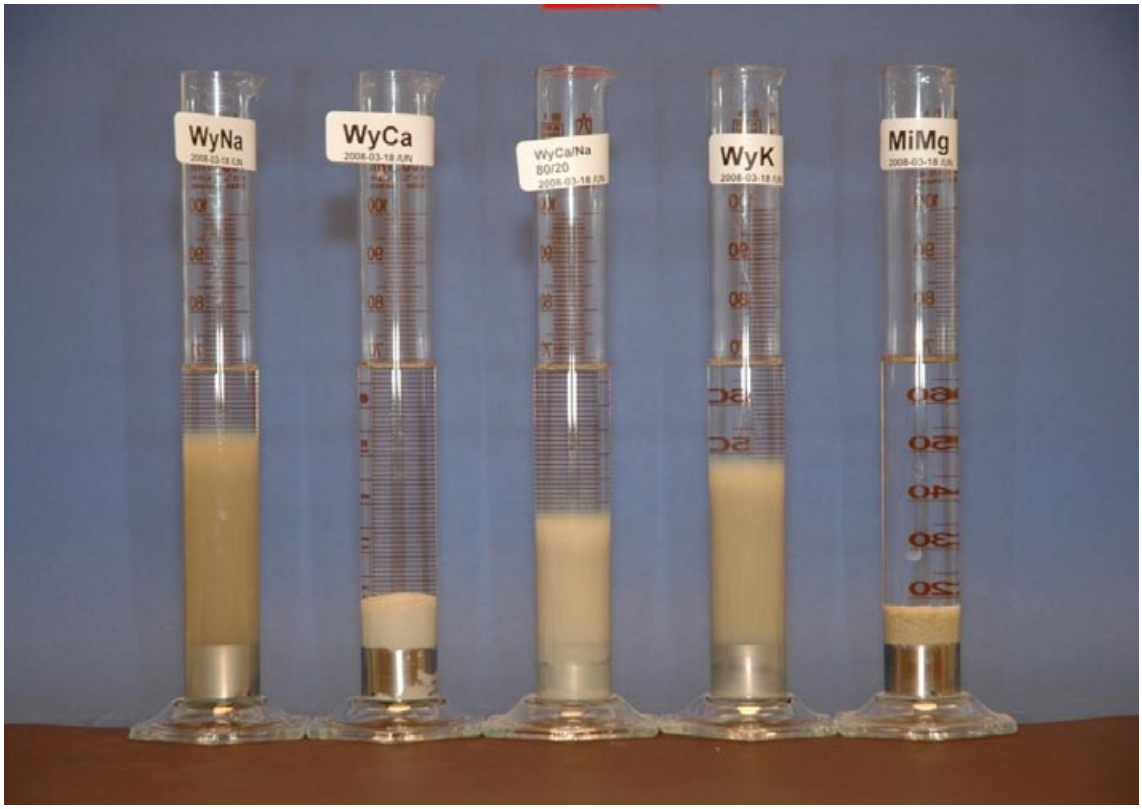

Figure 2-1. *Free swelling tests in ~65 ml deionized water with pure montmorillonites (~2 g) with only Na^+ as counterion (left), only Ca^{2+} as counterion (second from left), Ca^{2+}/Na^+ ratio of 80/20 (middle), only K^+ as counterion (second from right), and only Mg^{2+} as counterion (right).*

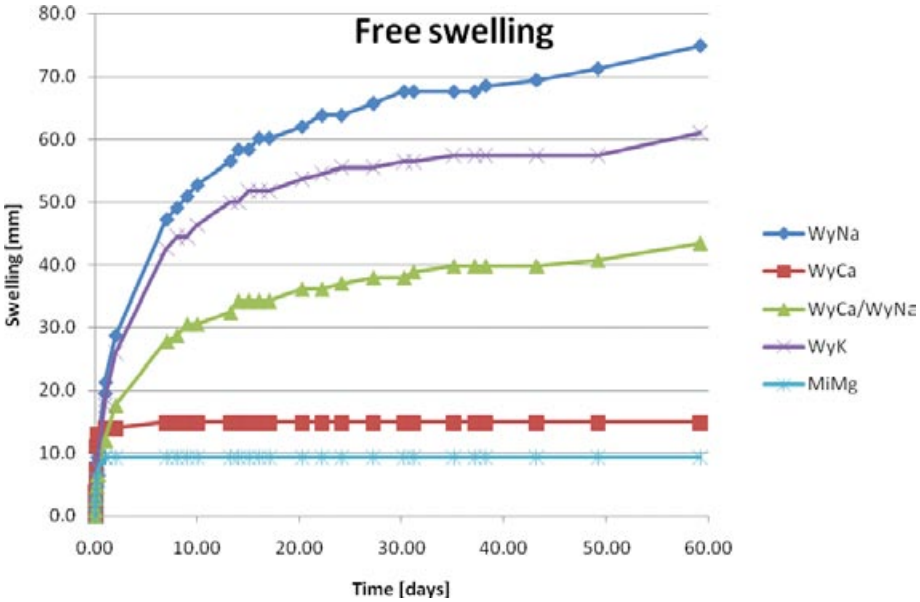

Figure 2-2. Height of test samples versus time measured for free swelling in deionized water. The initial height of the water-saturated samples was 2.5 mm. The samples final conditions are shown in Figure 2-1.

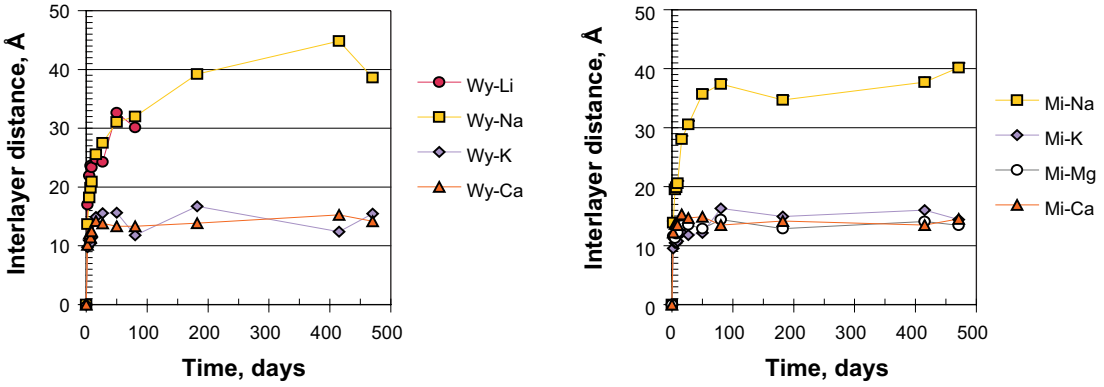

Figure 2-3. Mean interlayer distance (as deduced from gravimetric measurements) versus time in free swelling of approximately 2 grams of homo-ionic montmorillonites exposed to vapor from a free water surface in a closed system. Legends show the actual counterions.

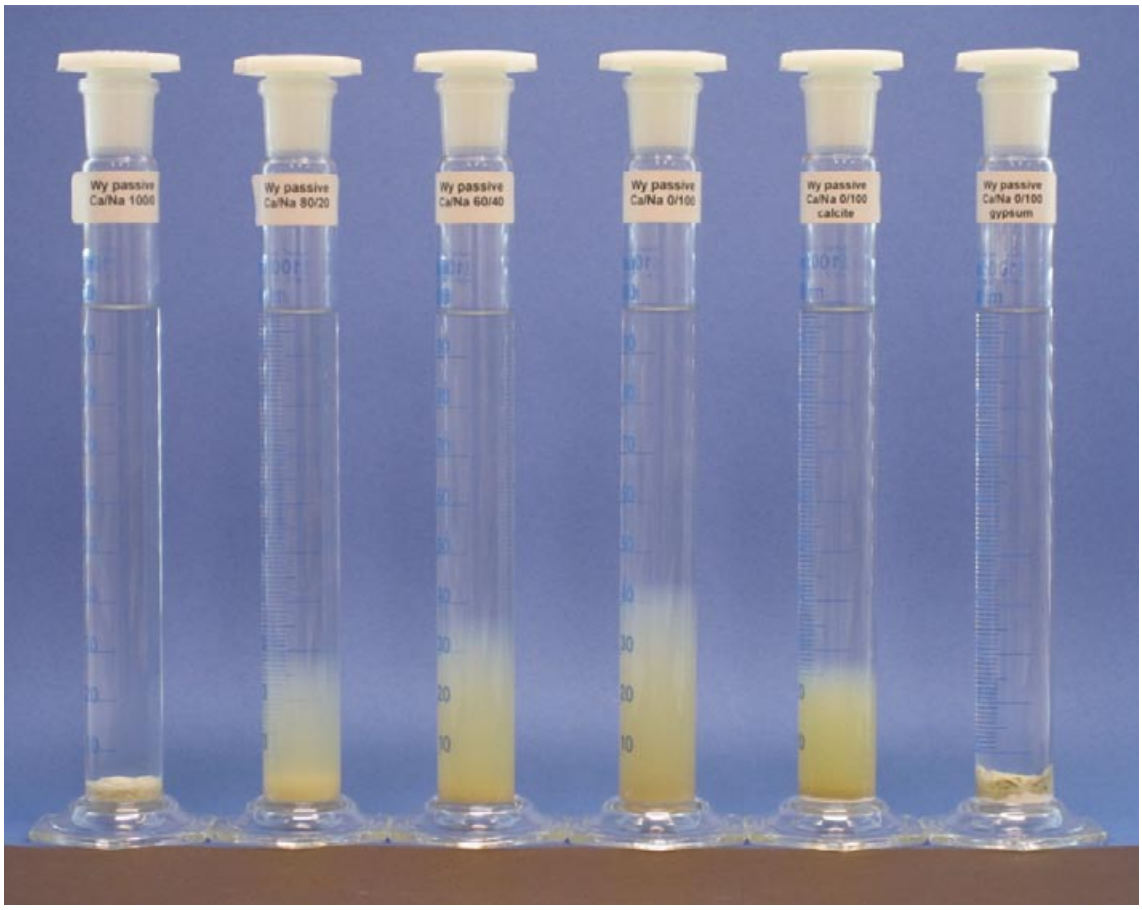

Figure 2-4. *Free swelling tests after 165 days with 0.5 grams of montmorillonite clay prepared to contain the following Ca^{2+}/Na^{+} ratios: 100/0 (left), 80/20 (second from left), 60/40 (third from left), 0/100 (third from right), 0/100 mixed with calcite (second from right), 0/100 mixed with gypsum (right). 100 ml deionized water is added to each cylinder.*

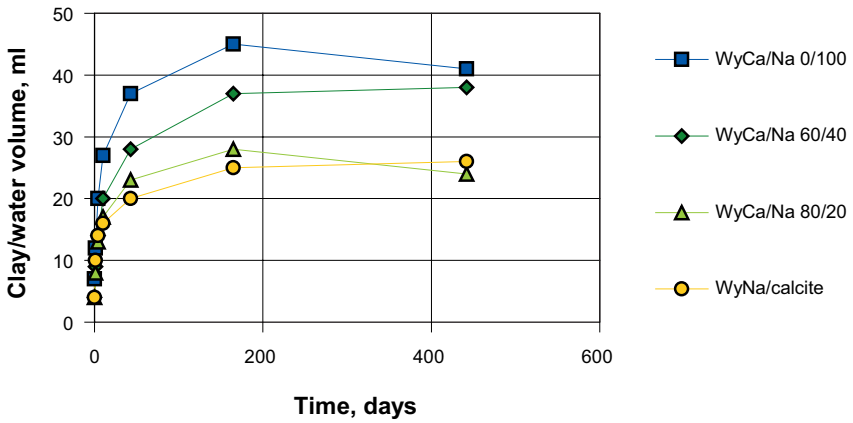

Figure 2-5. *Volume change of the clay/water system versus time in free swelling experiments with 0.5 grams of montmorillonite. Figures indicate the calcium/sodium ratios. The conditions at 165 days are shown in Figure 2-4.*

3 Rheology

3.1 Introduction

Bentonite that penetrates into fractures in a deposition hole will change its properties due to that it decreases its density with increasing distance from the highly compacted buffer material in the deposition hole. The rheological properties of the bentonite at the different phases have been investigated in order to understand and model how bentonite may be lost through a fracture.

3.2 Bentonite penetration into fractures

3.2.1 General

The buffer material in a deposition hole exposes the rock surface to a swelling pressure that is dependant mainly on the density of the bentonite inside the deposition hole, the stress history of the bentonite and the constant volume conditions of the deposition hole caused by the rock confinement. A fracture in the rock that intersects the deposition hole eliminates the constant volume conditions and allows the bentonite to penetrate into the fracture. If there is no resistance (counterforce) in the fracture the bentonite will not be at equilibrium and will continue to swell into the fracture until the fracture is filled or if the fracture is unlimited until the bentonite in the deposition hole is replaced by water that migrates inwards from the fracture to replace the bentonite that migrates out. The limiting factor in this case is the resistance to water flow of the bentonite-filled fracture.

Fortunately there is an inner resistance in the bentonite that limits free swelling into small open spaces. There is a resistance to shearing both internally inside the bentonite and externally at the interface with the fracture surface. This resistance, which can be described as friction or shear strength of the material, counteracts the swelling pressure from the bentonite and ultimately causes a state of equilibrium, when a portion of the fracture is filled with bentonite unless bentonite particles are lost by flowing water at the penetration front.

3.2.2 Conceptual model

The counteracting forces in the fracture that limit the swelling of the bentonite into the fracture create a state of equilibrium of bentonite with rapidly reduced density as function of the distance from the fracture opening at the buffer. The theoretical basis for this relation is described in Section 3.3.

The penetrating bentonite can be conceptualized as shown in Figure 3-1. A hypothetical fracture is visualized. The bentonite loses density as the distance from the buffer increases until there is virtually no bentonite but only natural ground water at the penetration front in the fracture. Due to the decreasing density with increasing penetration depth different states of the bentonite with different properties can be distinguished. As the bentonite loses its density it transforms from a solid state to a gel and further on to a liquid which finally has the same rheological properties as water.

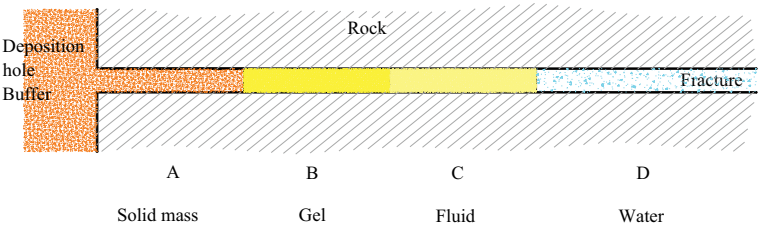

Figure 3-1. *Conceptual description of the rheological states of bentonite that swells from the deposition hole and penetrates into a fracture.*

In this chapter the following approximate definitions are used for the different states of the bentonite regarding rheological properties:

Solid mass: Shear strength higher than 1 kPa: τ_f>1 kPa

Gel: 1 Pa < τ_f< 1 kPa

Fluid: τ_f< 1 Pa

The existence, extent and properties of the different rheological states of the bentonite that penetrates into a fracture depend mainly on the bentonite composition and the chemistry of the ground water. For most natural conditions the bentonite forms a gel that is stable in contact with the free water. If the bentonite contains a high enough portion of Ca-ions in exchangeable positions both the fluid (sol) and the gel phase may be missing and if the ground water contains a high enough concentration of ions (NaCl) the fluid phase may be missing also for pure Na-bentonite (see further Chapters 5 and 7).

Figure 3-2 shows a visualisation of the mechanisms for transport of bentonite particles in a fracture. There are three different mechanisms. They can be separated in the following simplified way in relation to a fracture through a deposition hole (the transport directions are related to the deposition hole wall):

1. Radial transport by repulsion of the bentonite particles in still water (swelling).
2. Tangential transport by fluid flow driven by a water pressure gradient (viscous flow and erosion).
3. Axial (vertical) transport driven by gravity (sedimentation), which requires that the fracture is inclined.

These transport mechanisms are guided by different processes that must be modelled in different ways. Most tests in this report refer to the erosion and swelling properties (the tangential transport in a hydraulic gradient and the radial transport in still water). The properties have been investigated in the laboratory with different rheological equipment, which are described in Section 3.4.

An overview of the transport processes at the different zones in a fracture according to Figure 3-1 is shown in Table 3-1. The fluid phase has been divided into two phases (semi-fluid and fluid) so that it can be described with different models. The tests and models are described in this and other sections. The transport processes that have been investigated are marked yellow.

The solid mass is too stiff to yield any viscous flow or erosion. In the solid mass and gel phases the internal swelling forces are so strong that the sedimentation can be neglected.

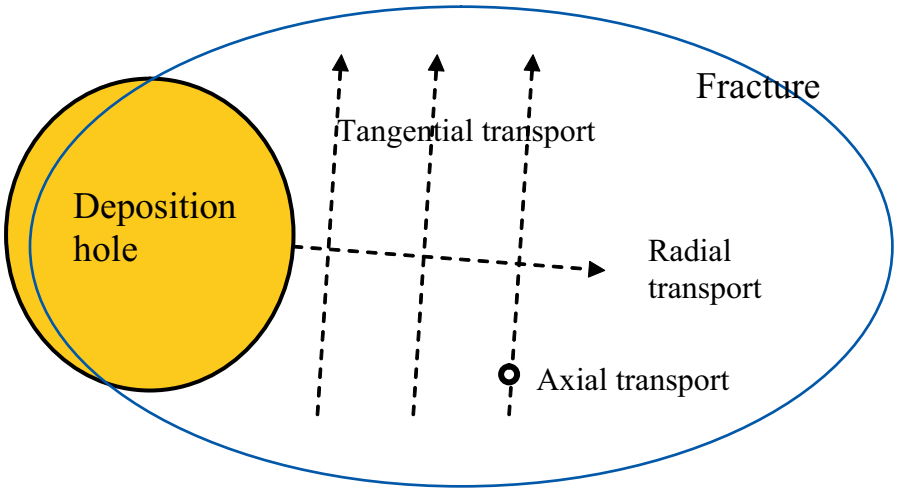

Figure 3-2. *Illustration of the mechanisms for transport of bentonite particles in a fracture.*

Table 3-1. Overview of the three bentonite transport processes in a fracture and the models or parameters used for analysing them. Processes investigated and reported are marked yellow.

Zone	Phase	Bentonite transport model		
		Radially (swelling)	Tangentially (viscous flow and erosion)	Axially (sedimentation)
A	Solid mass	A_R. Hydro-Mechanical friction	A_T. None	A_A. None
B	Gel	B_R. Hydro-Mechanical friction	B_T. Rheological stress/strain relation	B_A. None?
C1	Semi-fluid	$C1_R$ Hydro-Mechanical friction (?)	$C1_T$ Non-Newtonian viscosity, Power law	$C1_A$ Diffusion controlled aggregation?
C2	Fluid	$C2_R$ Diffusion?	$C2_T$ Viscosity, Newtonian	$C2_A$ Diffusion controlled aggregation
D	Water	D_R. Diffusion?	D_T. Viscosity of water	D_A. None?

3.3 Theoretical models

3.3.1 General

Different processes that can be modelled with different mathematical formulations are present during the transport of bentonite in a fracture system. The main subdivision used in this section is based on the transport mechanisms and states shown in Figure 3-1 and Figure 3-2. Since the theoretical knowledge of the basic laws (thermodynamics etc.) that drive these processes is judged to be insufficient, no geochemical or thermodynamic derivations have been done. All models are designed with test results as bases and are thus empirical. This is in agreement with most relationships derived for design purposes in soil mechanics and rheology sciences.

3.3.2 Swelling models

In this section the force equilibrium state that will prevail in a fracture after completed swelling into the fracture will be investigated and a formula for the swelling pressure distribution in the fracture derived without considering the path up to that state. Further ahead in Section 3.9 the time for the swelling will be investigated.

The bentonite swelling into an ideal plane fracture can be modelled as controlled by the swelling pressure of the bentonite and the friction against the fracture wall. The principle theory for the swelling behaviour is the effective stress theory that states that the effective stress in the bentonite (also named swelling pressure) is described by Equation 3-1.

When water is added to an unconfined specimen of bentonite the water to solid mass ratio[1] increases and the repulsion forces between the bentonite layers decrease. This causes the specimen to swell until a new equilibrium is established with a lower internal swelling pressure. If the volume is kept constant, a portion of the internal swelling pressure is instead transferred to an external swelling pressure, which can be measured. When a specimen with constant volume is completely water-saturated and the pore water pressure is kept positive, the entire swelling pressure becomes an external pressure. After full water saturation, the swelling pressure and the pore water pressure are mathematically independent quantities and give a total pressure that is the sum of the pressures (effective stress theory):

[1] See Equation 3-13.

$\sigma_t = \sigma + Au$ (3-1)

where

σ_t = total stress

σ = effective stress = swelling pressure

u = pore water pressure

$A \approx 1.0$

The water pressure will thus only affect the total stress and not the swelling pressure (except at very high water pressures), which means that the water pressure does not affect the behaviour of the bentonite.

Figure 3-3 shows the equilibrium situation of an infinitesimal part of a bentonite (dr) penetrating from a deposition hole into a horizontal fracture.

The shear stress between the penetrating bentonite gel and the fracture wall can be expressed as

$\tau = \sigma \tan\phi$

where

ϕ = friction angle between the bentonite and the fracture surface

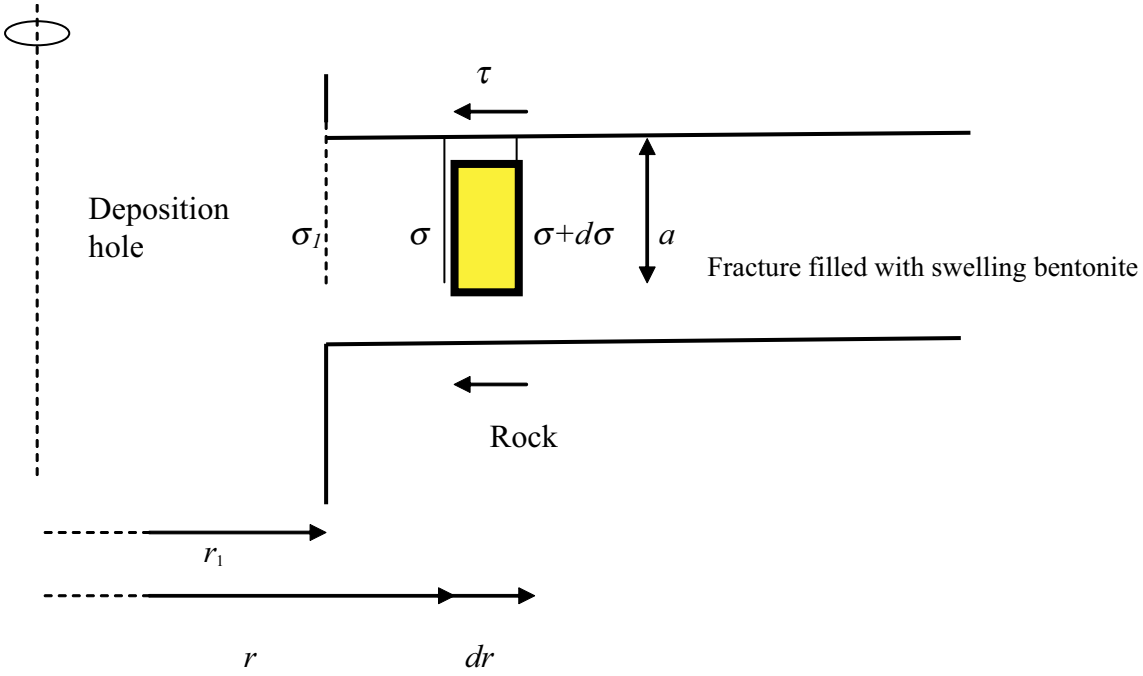

Figure 3-3. *State of equilibrium of an infinitesimal part of bentonite after swelling into a fracture where*
r1 = deposition hole radius
a = fracture aperture
σ_1 = swelling pressure at the deposition hole wall
σ = swelling pressure at the distance r-r_1 into the fracture
$d\sigma$ = change in swelling pressure at the increased distance dr
τ = shear stress at the fracture wall

Force equilibrium in radial direction yields according to Appendix 1:

$$\ln\sigma = \ln\sigma_1 + K\ln\frac{r}{r_1} - \frac{r-r_1}{a}\cdot 2\tan\phi \qquad (3\text{-}2)$$

where K is an anisotropy ratio (see Appendix 1) and r-$r_1 = z$.

The limit where $r/r_1 \approx 1$ (i.e. z small) yields

$$\ln\sigma = \ln\sigma_1 - \frac{z}{a}\cdot 2\tan\phi \qquad (3\text{-}3)$$

or

$$\sigma = \sigma_1 \cdot e^{-2\tan\phi(\frac{z}{a})} \qquad (3\text{-}4)$$

Equation 3-3 thus describes the relation between the swelling pressure σ in the fracture and the penetration depth z into the fracture at the fracture aperture a and the buffer swelling pressure σ_1 if the influence of axial symmetry is neglected (can be done since the radius of the deposition hole is large compared to the penetration depth). Equation 3-3 only describes the equilibrium state and does not consider the path or history.

Equation 3-3 can be used to determine the swelling pressure distribution in an ideal fracture i.e. a slot between two parallel plates. In order to be able to use this model for describing the tangential transport driven by a hydraulic gradient with the flow and erosion models the swelling pressure must be translated to density (or water to solid mass ratio). Such relations exist for high densities but not for swelling pressure below about 10 kPa.

An example of how Equation 3-3 can be used to calculate the penetration depth and penetration rate is shown in Section 3.9.

3.3.3 Rheological models (viscous flow and erosion)

3.3.3.1 General

Rheological models for bentonite gels or sols (clay/water systems) can be divided into three main types with different models and equipment to determine the properties. The common basic conditions for these models are that the bentonite/water system is considered as a unit so that the water and particles are transported together. Only the total stress is considered and the theories describe the relation between applied shear stress and resulting shear movement. There are a large number of different rheological models for gels and sols. The following ones that cover the phases and zones described in Figure 3-3 and Table 3-1 have been found to be useful for describing the flow properties of bentonite:

1. Newtonian viscosity
2. Power law
3. Stress-strain relations

Techniques to measure the parameters in these models are described in Section 3.4.

3.3.3.2 Newtonian viscosity

The viscosity of a fluid is defined according to Equation 3-5.

$$\tau = \mu\frac{du}{dy} \qquad (3\text{-}5)$$

where τ = shear stress at the actual shear rate (Pa)

μ = viscosity (Pas)

$du/dy = \dot{\gamma}$ = shear rate (1/s)

The shear rate is defined according to Figure 3-4.

Viscosity

$$\tau = \mu \frac{du}{dy}$$

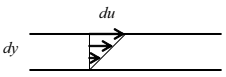

Figure 3-4. *The shear rate (rate of angular deformation) is defined as the difference in transport rate between two particles du (m/s) divided by the distance between the particles dy (m).*

If the shear stress increases linearly with the shear rate the viscosity will be a constant independent of the shear rate. This constant is called Newtonian viscosity. Water is a typical example of a material with Newtonian viscosity. For distilled water at room temperature the viscosity is

μ = 1.0 mPas

Bentonite sols with very high water to solid mass ratio (>100) usually show Newtonian behaviour and have a viscosity lower than 10 mPas.

3.3.3.3 Power law

At lower water to solid mass ratios the bentonite sols seem to decrease the viscosity with increasing shear rate, i.e. the shear stress – shear rate relation is not linear. If the relation is plotted in a double logarithmic diagram it becomes close to linear with an inclination less than 1. Such behaviour is well represented by a power law according to Equation 3-6.

$$\tau = m\left(\frac{\dot{\gamma}}{\dot{\gamma}_0}\right)^n \qquad (3\text{-}6)$$

where τ = shear stress at the shear rate $\dot{\gamma}$ (Pa)

$m = \tau_0$ = shear stress at the shear rate $\dot{\gamma}_0$ (Pa)

$\dot{\gamma}$ = shear rate = du/dy (1/s)

$\dot{\gamma}_0$ = normalized shear rate (=1.0 1/s)

n = inclination in a double logarithmic diagram (-)

n = 1.0 yields Newtonian behaviour

n = 1.0 yields viscosity $\mu = m/\dot{\gamma}_0$ (Pas)

$n \neq 1.0$ yields m = "fictive viscosity" evaluated at $\dot{\gamma}$ = 1.0 (1/s)

3.3.3.4 Stress-strain relation

At even lower water to solid mass ratios the sol turns into a gel which cannot be modelled according to Equation 3-6. Such a gel instead seems to behave more like normal sedimentary clay with a peak value of shear resistance that has to be overcome before further shearing followed by decreasing or constant shear stress at increasing shear displacement. They also show an increasing shear resistance at increasing shear rate but not as pronounced as for bentonites with higher water to solid mass ratios. Figure 3-5 shows an idealized example of such behaviour.

The shear stress increases until a maximum stress τ_f (failure stress) is reached. Then the shear resistance is reduced to τ_r (residual strength). The stresses τ_f and τ_r are also depending on the shear rate and increase slightly with increasing shear rate.

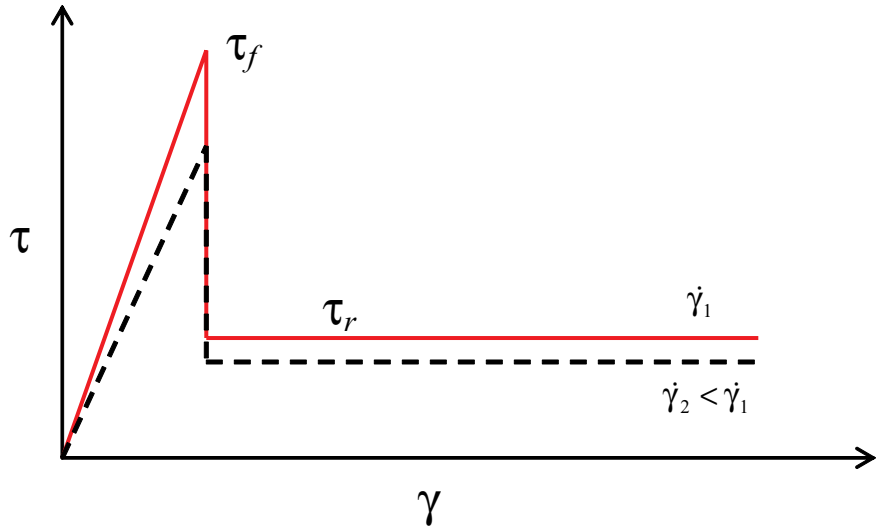

Figure 3-5. *Idealized stress-strain behaviour of bentonite gels with low water to solid mass ratio. The red curve represents a higher shear rate than the dashed curve at otherwise identical conditions.*

3.3.4 Sedimentation models

Sedimentation describes the motion of molecules in solutions or particles in suspensions in response to an external force such as gravity. The sedimentation of particles under gravity can be described by the Mason-Weaver equation. Assuming that the gravitational field is aligned in the z direction, the Mason-Weaver equation /Mason and Weaver 1924/ may be written according to Equation 3-7:

$$\frac{\partial c}{\partial t} = D\frac{\partial^2 c}{\partial z^2} + sg\frac{\partial c}{\partial z}, \qquad (3\text{-}7)$$

where t is the time, c is the solute concentration and the parameters D, s, and g represent the solute diffusion constant, the sedimentation coefficient and the acceleration of gravity, respectively.

Several laboratory tests on montmorillonite/water systems for evaluating the parameters in Equation 3-7 have been performed and are reported in Chapter 5.

3.3.5 Thixotropy

The viscous properties of bentonite/water systems change with time and stress history. They get stiffer with increasing time in rest, i.e. a sol with Newtonian viscosity increases its viscosity, a non-Newtonian sol increases its m-value and a gel may increase its shear strength. A sol may even transform from Newtonian to non-Newtonian and end up as a gel with shear strength according to Figure 3-5.

Bentonites are thus strongly thixotropic. Older tests (Figure 3-6) have shown that the shear strength of a bentonite gel can increase a factor of 10 if a gel with the water to solid mass ratio 7 has been allowed to rest for one week compared to if it is tested directly after mixing /Börgesson et al. 1991/.

The resting time is thus a very important parameter for evaluation of the rheological properties of bentonite/water systems. This fact complicates the description and modelling of the behaviour of the rheological properties. The actual resting times are much longer and the flow rates are much slower than in the laboratory measurements. On the other hand if laboratory results are used for modelling, the actual shear resistance should be higher than predicted by the model and the results are thus on the safe side (conservative) with respect to the long term performance of the bentonite in fractures and its vulnerability to erosion.

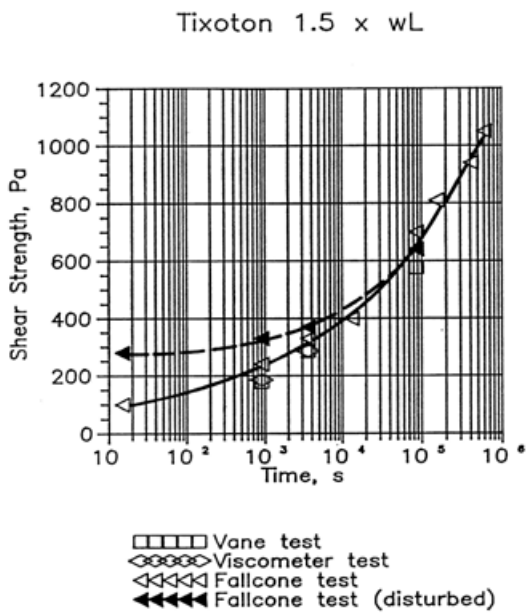

Figure 5-9 Shear strength of tixoton measured with different methods at different times after mixing. The filled triangles denote a tixoton that has been strongly disturbed after about 3 days ($2.4 \cdot 10^5$ s)

Figure 3-6. *Results from shear strength measurements with different methods on a sodium bentonite similar to MX-80 with water to solid mass ratio 7. The measured shear strength is plotted as function of the resting time before testing.*

3.4 Test methods

3.4.1 General

The rheological models described in Section 3.3.3 have been used to model the stress-strain properties of bentonite gels and sols after extensive testing in the laboratory. Different test instruments and different test techniques have been used depending on the properties of the tested material and on the model that can be used for evaluation.

3.4.2 Instruments

3.4.2.1.1 Viscometer

Most tests were made with a Brookfield LV viscometer, with attachments for different purposes. The test principle is described in Figure 3-7. This instrument was used to measure the parameters for Equations 3-4 and 3-5.

The shear rate $\dot{\gamma}$ and shear stress τ are calculated with Equations 3-8 and 3-9 (see /Brookfield Engineering Labs/).

$$\dot{\gamma} = \left(\frac{2R_c^2}{R_c^2 - R_b^2} \right) \varpi [s^{-1}] \tag{3-8}$$

$$\tau = \frac{M}{2\pi R_b^2 L} \left[N/m^2 \right] \tag{3-9}$$

where

R_c = radius of container (cup)

R_b = radius of spindle

M = torque

ω = angular velocity

L = effective length of spindle

The shear strain γ can be evaluated from the shear rate according to Equation 3-10.

$$\gamma = \dot{\gamma} \cdot t \tag{3-10}$$

where t = time (in s)

3.4.2.1.2 Laboratory vane

For gels the bob is not a good tool due to slip between the spindle and the gel. For such gels the spindle was replaced with a vane in order to measure the peak shear strength (stress strain relation according to Section 3.3.3.4).

The vane is made of four vertical blades fixed perpendicular to each other (see Figure 3-8).

The relationship between shear stress and torque in a vane test can be calculated according to Equation 3-11 /Hansbo 1975/.

$$M_{max} = \tau_{fu} \left(2\pi r^2 h + 2\int_0^r 2\pi Q^2 dQ \right) 2\pi r^2 h \tau_{fu} \left(1 + \frac{2r}{3h} \right) \tag{3-11}$$

where

M = torque (M_{max} = maximum torque)

τ = average shear stress (τ_{fu} = maximum shear stress (actually "undrained shear stress at failure")

If $h = 2d = 4r$ the relation can be simplified to Equation 3-12.

$$\tau_{fu} = \frac{6M_{max}}{7\pi d^3} \tag{3-12}$$

If the shear stress is plotted as function of the shear distance (the displacement of the periphery of the vane) the shear strength can be evaluated as the maximum shear stress.

For some tests the stiffness of the material was so high that the torque exceeded the measuring range. In those cases only half the vane was inserted into the gel and the shear stress accordingly recalculated.

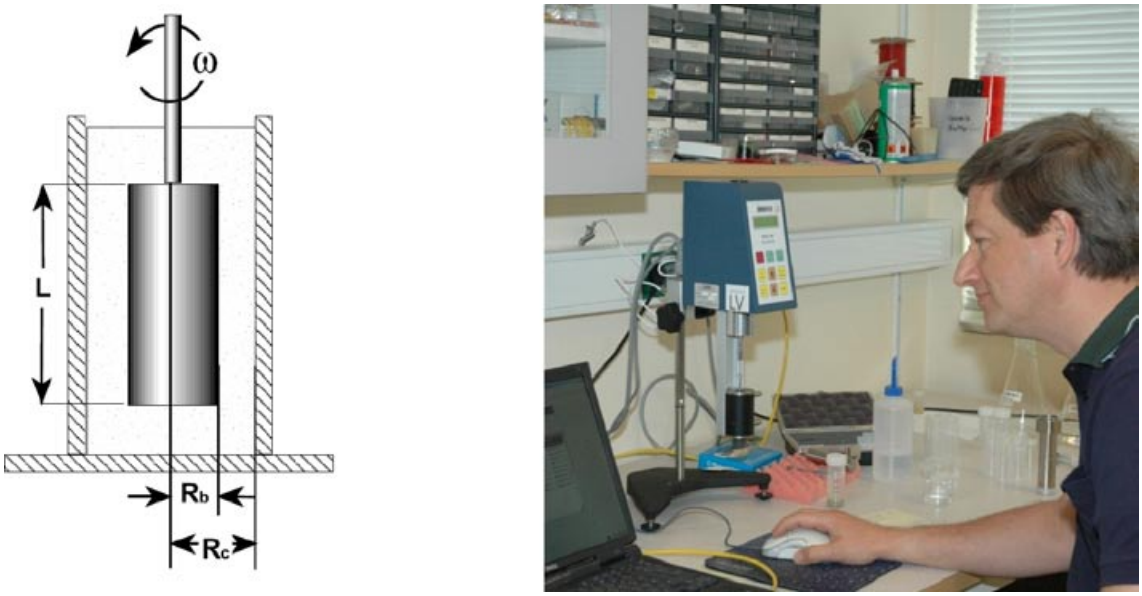

Figure 3-7. *Test principles for and a picture of the Brookfield viscometer. The spindle rotates inside the cup filled with the bentonite slurry and the torque and the torsional angle are measured.*

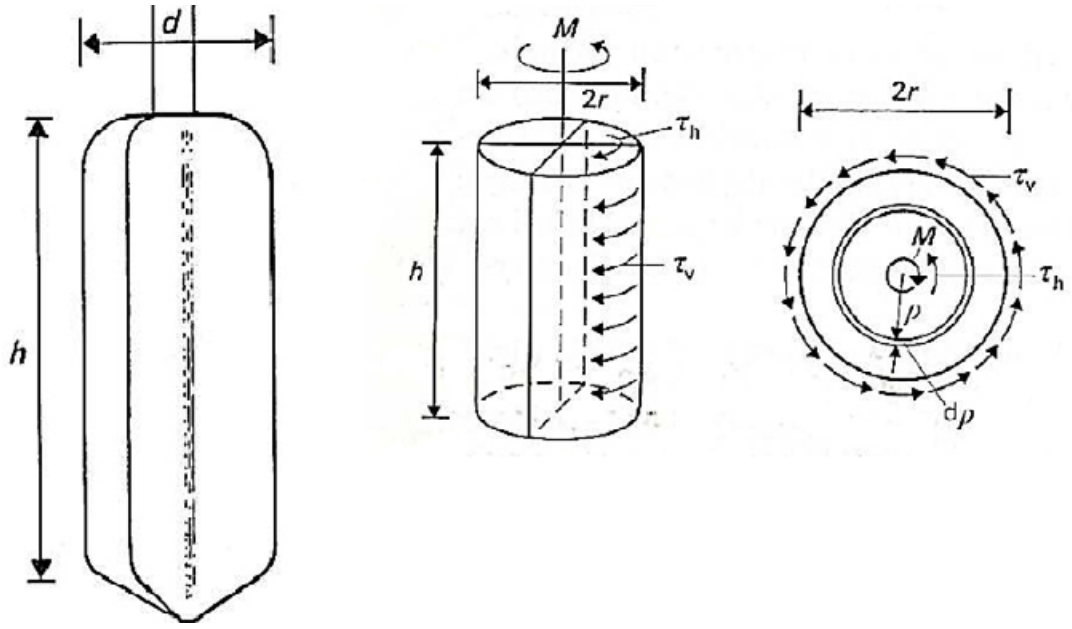

Figure 3-8. *Geometry of the vane and symbols for deriving the shear stress /Hansbo 1975/.*

3.4.3 Test techniques

3.4.3.1 Viscosity tests

The viscosity tests were done with stepwise increase in shear rate and measurement of the shear stress before changing speed. Normally 100 steps were used. The start was the lowest setting of shear rate for the viscometer. The shear rate usually started at 0.01 1/s and ended at 100 1/s, depending on the spindle/cup combination.

By plotting the relation between shear stress and shear rate the viscosity can be evaluated according to Equation 3-4 if the relation is a fairly straight line. If not the relation can be plotted in a double logarithmic diagram and the values of *m* and *n* can be evaluated according to Equation 3-5 if the relation is a straight line in such a diagram.

Mainly two geometries of the cup and spindle were used. The designations and geometries are

SC4-18

Spindle: diameter 17.48 mm, length 31.72 mm.

Cup: diameter 19.05 mm, depth 64.77 mm.

ULA

Spindle: diameter 25.15 mm, effective length 92.39 mm (actual length 90.74 mm).

Chamber: diameter 27.62 mm.

3.4.3.2 Rheology tests

The same equipment was also used to measure the stress-strain relation by applying a constant shear rate of 0.5 1/s and measuring the shear stress as a function of time. These tests are called rheology tests. By plotting the shear stress as a function of shear strain the rheological behaviour of the material could be studied.

For material with Newtonian behaviour the shear stress often increases to a stable constant value after some shear strain, while for stiffer materials there is often a peak shear stress in the beginning.

3.4.3.3 Vane tests

The dimensions of the vane used are

r = 6.335 mm

h = 25.35 mm,

which means that one revolution of the vane (360 degrees) corresponds to the shear distance 39.8 mm. The applied rotation rate was 0.1 rpm (revolutions per minute).

3.4.4 Reference method for preparation of the clay/water system

As indicated in Section 3.3 the results of the laboratory measurements of viscous and rheological properties of clay/water-mixtures are very much influenced by the preparation technique, the stress history and the resting time. Figure 3-9 shows a number of tests that were carried out on bentonite gels with identical water to solid mass ratio (w=20) and salinity (0.01 mM) but with different preparation techniques and resting times.

The figure thus shows that the results can vary depending on the preparation technique by more than a factor of 10. In order to be able to compare different slurries and to have results that can be used for modelling it is thus important to find a reference technique that resembles the actual conditions as much as possible.

After a number of initial tests which underscored the importance of preparation methodology, a standard method for MX-80 and WyNa was established.

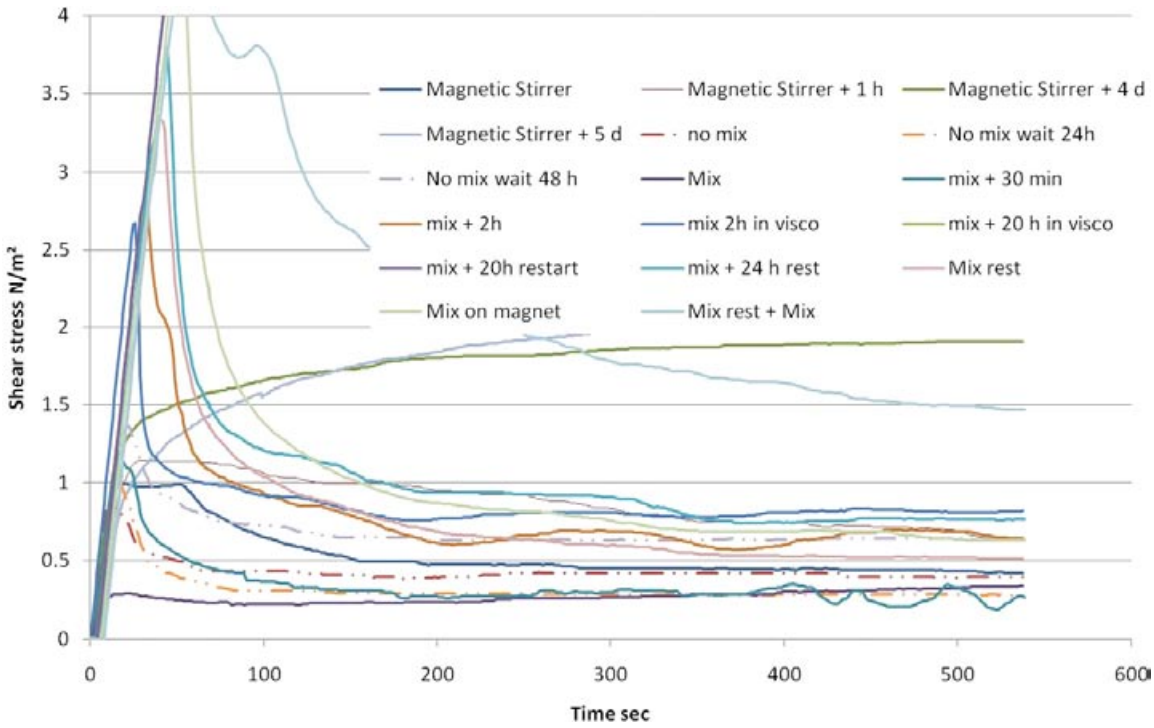

Figure 3-9. *Measured shear stress as function of time on bentonite gels with water to solid mass ratio 20 when shearing with constant rate with the viscometer. Tests with different preparation techniques. "Mix" and "magnetic stirrer" in the legend mean mechanical mixing with a propeller and a magnetic stirrer. "No mix" means undisturbed swelling of bentonite in water. Different waiting periods were also used.*

Based on above mentioned considerations and comparisons with other test methods the following method was established as the reference technique for preparation:

Dry clay powder is poured into water and left to rest for 24 hours.

Before testing the bentonite sample is shaken in order to obtain a fairly homogeneous mixture. This is especially important if the bentonite has settled.

The required amount of bentonite slurry is sucked up with a graded syringe and injected into the test cup.

The cup and spindle are mounted in the viscometer and the test starts.

The choice of method was mainly based on practicality reasons, but had also the purpose to avoid separation effects. A problem is of course that the process in a real fracture is much slower and includes a much longer resting time than can be applied in the laboratory. The effect of thixotropy is expected to yield stiffer gels/sols in a fracture than in the laboratory tests, which should lead to conservative modelling results.

3.5 Materials and water compositions used for the tests

Two clays and two derivates were used for these tests.

- MX-80, which is a Na dominated bentonite from Wyoming,
- WyNa, which is the clay fraction of MX-80 ion-exchanged to only Na,
- WyCa, which is the clay fraction of MX-80 ion-exchanged to only Ca,
- Deponit CA-N, which is a Ca dominated bentonite originating from Milos, Greece.

MX-80 clay was thus also tested in a homoionic form. The clay was separated so that only the clay fraction remained and then all exchangeable ions were changed to either Na or Ca ions yielding WyNa or WyCa. Detailed description of materials and treatment can be found in /Karnland et al. 2006/.

Deionized water was used for the mixtures (electric conductivity of less than 1 µS/cm) but the influence of the salinity of the pore water was also investigated. For those tests a 0.1 Molar solution was prepared and diluted to the required salinity. NaCl with the quality corresponding to *pro analysi* (best available) was used. When a saline solution was used, the standard technique was to pour the dry clay into the saline solution and allow it to rest for 24 hours before measurements were made. In some tests the salt was added afterwards.

The water to solid mass ratio (also named water content) w_r of the clay is defined according to Equation 3-13 (including the natural water in the clay).

$$w_r = \frac{m_w}{m_s} \tag{3-13}$$

where

m_w = mass of water

m_s = mass of solids (dry weight of clay)

3.6 Results from measurements on Na-bentonites

3.6.1 General

Only results from the tests made with the reference method for preparation of the clay/water systems are reported. Several test series with water to solid mass ratios varying from 25 to 300 (clay concentration 4%–0.33%) and water salinity varying from 0 to 100 mM NaCl have been made. The evaluation of the results from the viscosity and rheology tests is presented in Section 3.8.

3.6.2 Viscosity tests

3.6.2.1 MX-80

The technique used for the viscosity tests are described in Section 3.4. Table 3-2 summarizes the parameter variation used for the viscosity tests made on MX-80.

The results are displayed in Figure 3-10 to Figure 3-16 with the shear stress plotted as function of the shear rate. Figure 3-10 shows the influence of the water to solid mass ratio for the NaCl concentration 0 (corresponding to the left column in Table 3-2) while the rest of the figures show the influence of the NaCl concentration at certain water to solid mass ratios (corresponding to some of the rows in Table 3-2).

Table 3-2. Test plan for MX-80 with the tested combinations of water to solid mass ratio (w_r) and salinity of the mixing water. The squares marked green are performed tests.

MX-80	NaCl (mM)												
w_r	0	1	2	2,5	3	4	5	10	15	20	25	50	100
25	■	■		■				■					■
30	■												
35	■	■		■			■	■			■	■	■
40	■												
50	■	■		■				■					■
75	■												
100	■	■		■				■					■
150	■												
200	■	■		■									
250	■												
300	■												

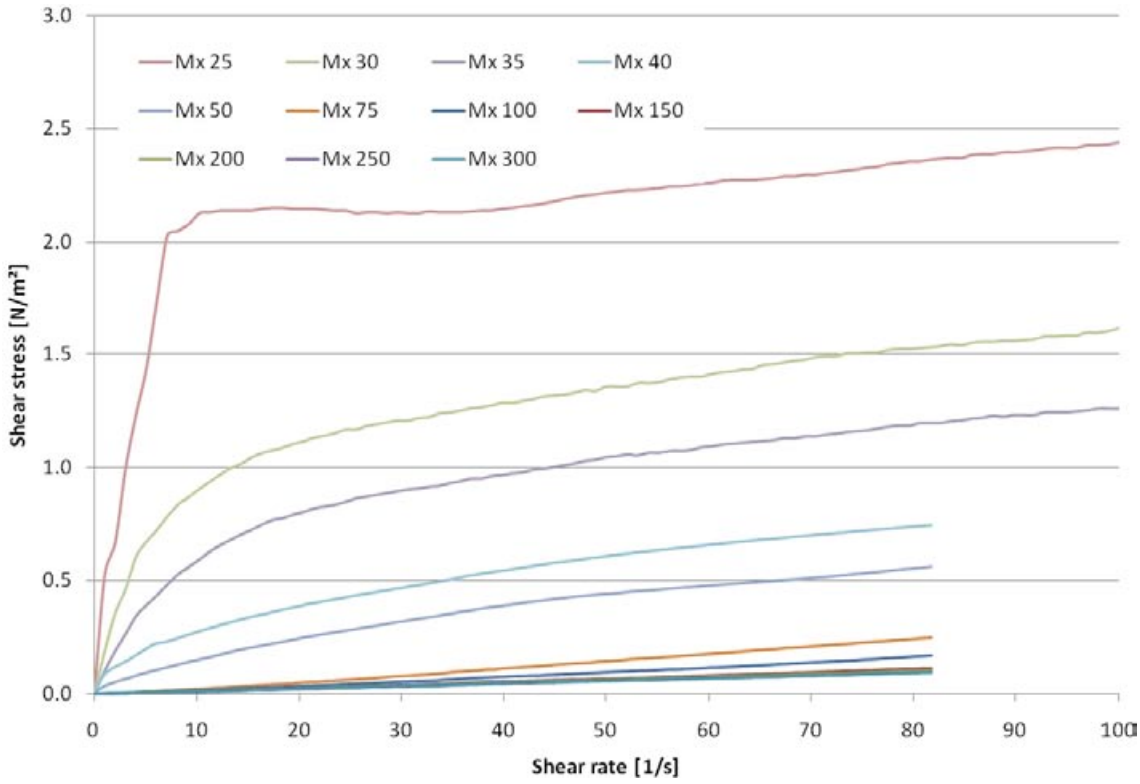

Figure 3-10. *Shear stress as a function of shear rate for MX-80 in distilled water at different water to solid mass ratios.*

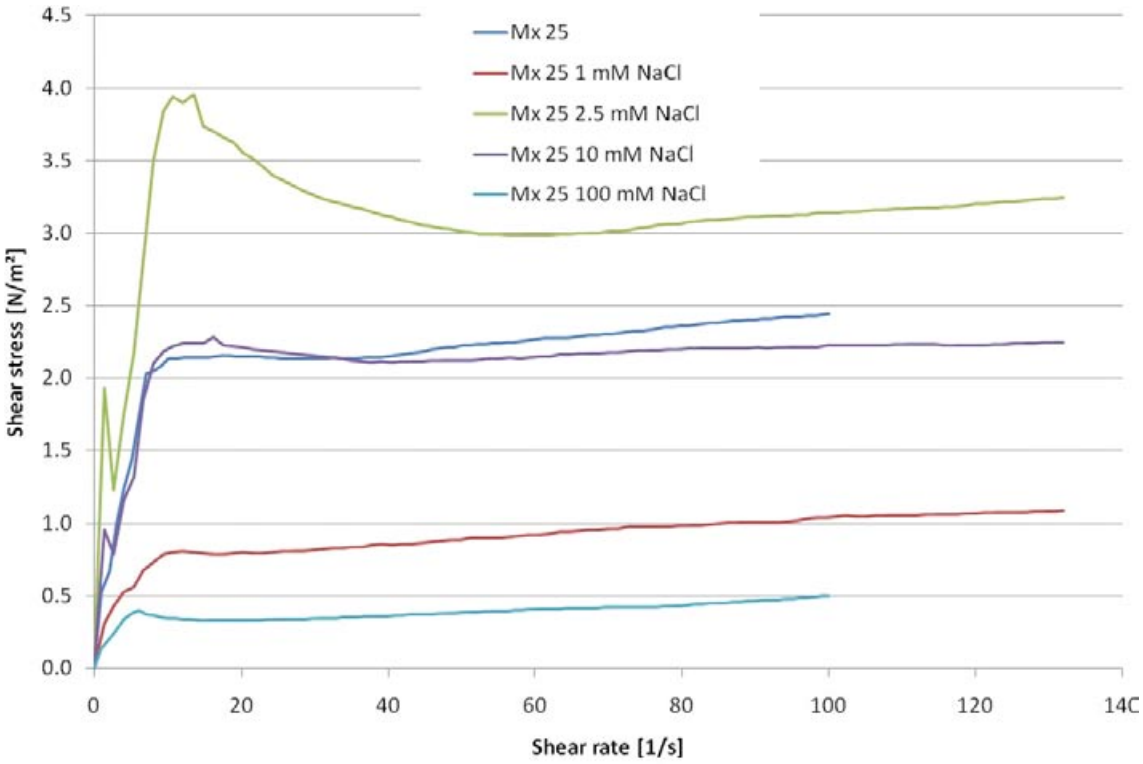

Figure 3-11. *Shear stress as a function of shear rate for MX-80 at the water to solid mass ratio 25 in water with different NaCl concentrations.*

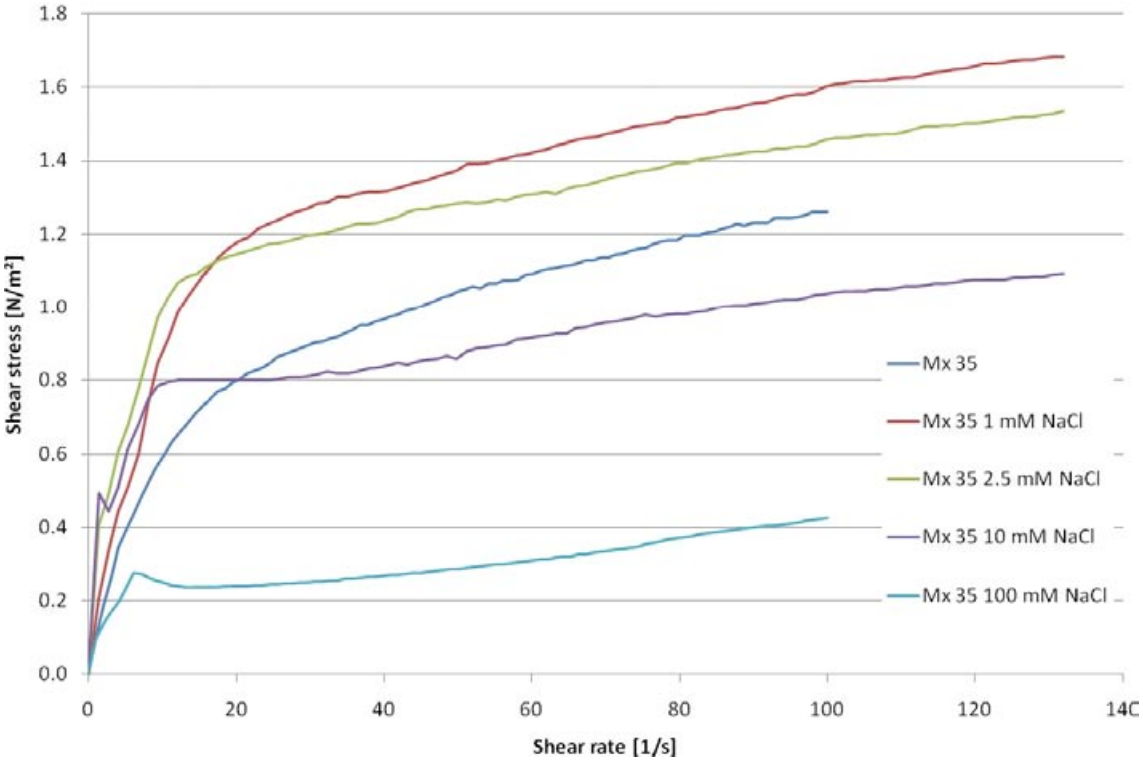

Figure 3-12. *Shear stress as a function of shear rate for MX-80 at the water to solid mass ratio 35 in water with different NaCl concentrations.*

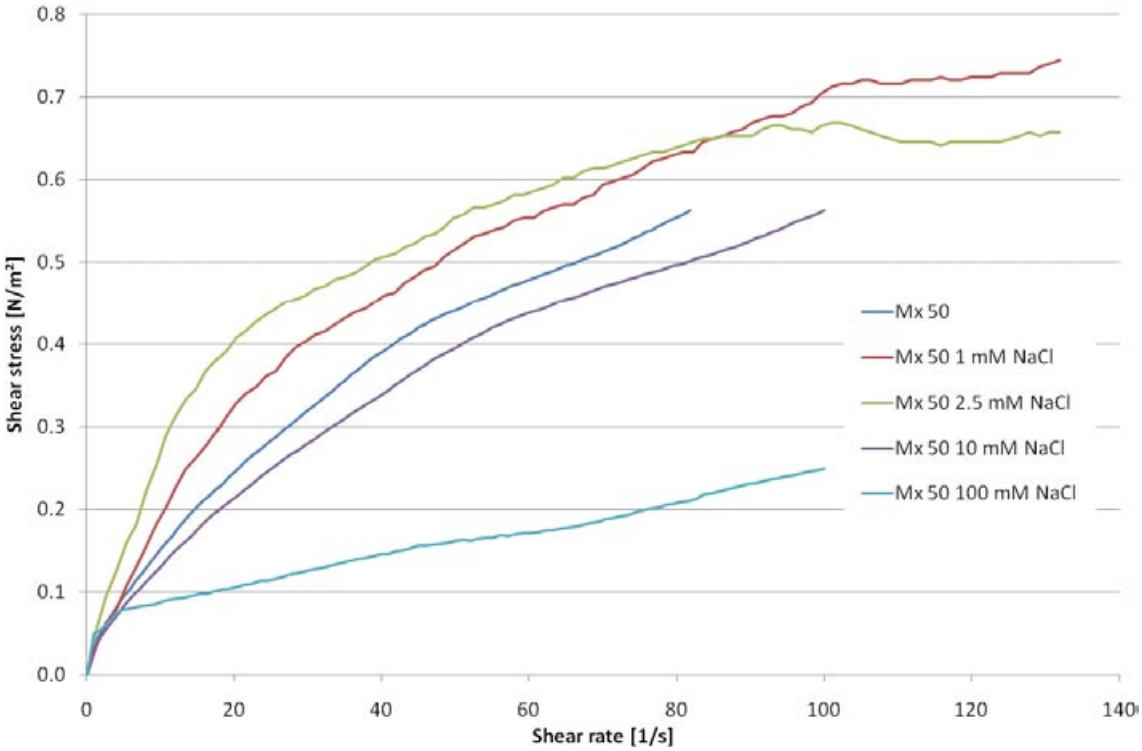

Figure 3-13. *Shear stress as a function of shear rate for MX-80 at the water to solid mass ratio 50 in water with different NaCl concentrations.*

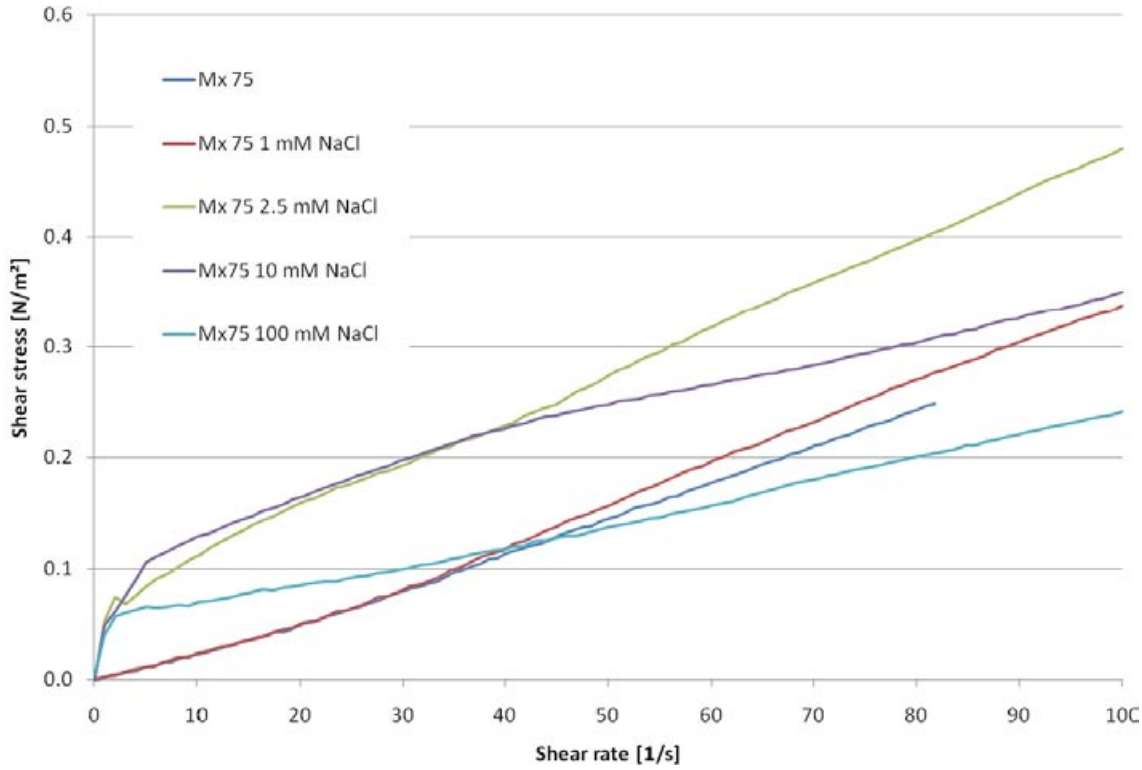

Figure 3-14. *Shear stress as a function of shear rate for MX-80 at the water to solid mass ratio 75 in water with different NaCl concentrations.*

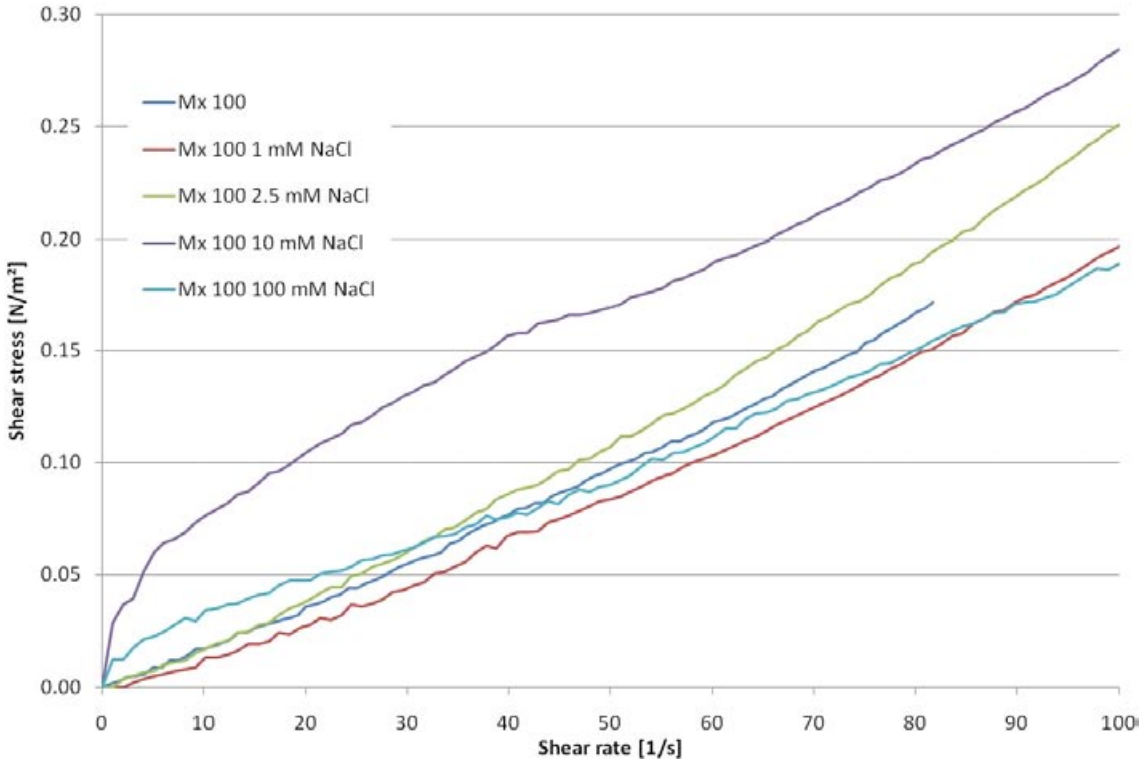

Figure 3-15. *Shear stress as a function of shear rate for MX-80 at the water to solid mass ratio 100 in water with different NaCl concentrations.*

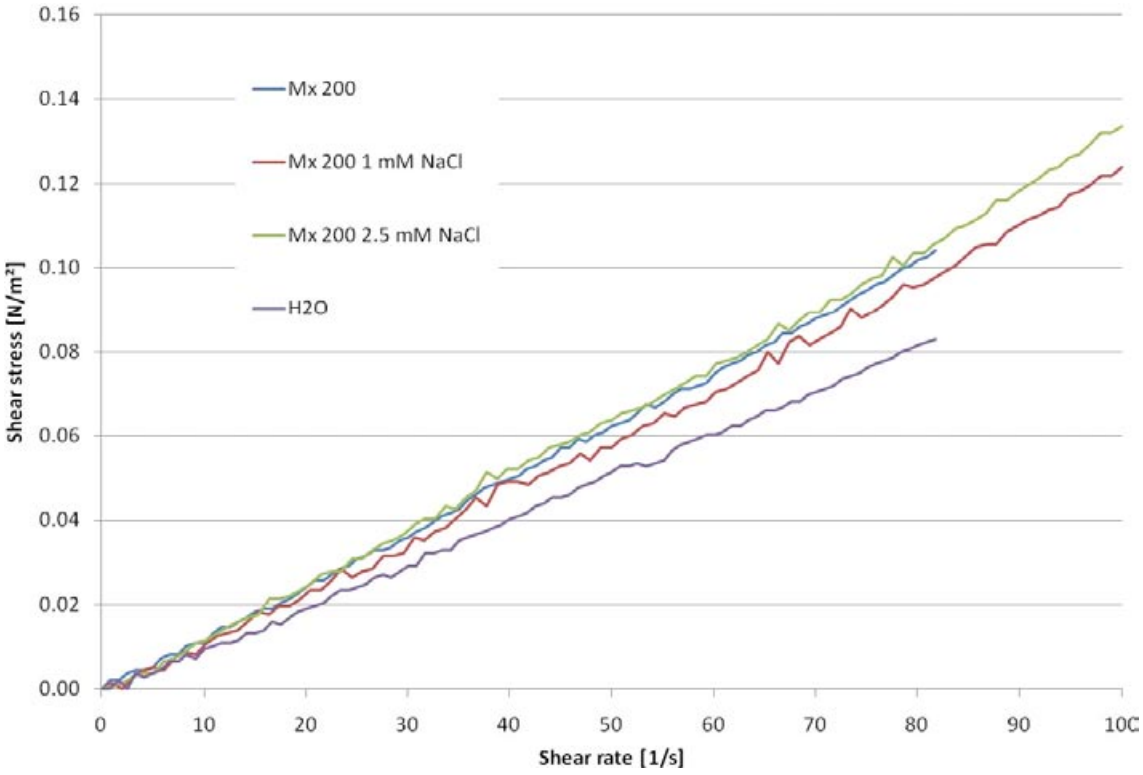

Figure 3-16. *Shear stress as a function of shear rate for MX-80 at the water to solid mass ratio 200 in water with different NaCl concentrations. Results from a test on free water is also displayed for comparison.*

3.6.2.2 WyNa

Similar test series as for MX-80 with variation of water content and NaCl concentration were also run on the purified homoionic WyNa material. Table 3-3 summarizes the tests. Gels with water to solid mass ratio below 35 were also tested but could not be run in this equipment (too stiff).

The results are displayed in Figure 3-17 to Figure 3-22 with the shear stress plotted as a function of the shear rate. Figure 3-17 shows the influence of water to solid mass ratio for the NaCl concentration 0 (corresponding to the left column in Table 3-3) while the rest of the figures show the influence of the NaCl concentration at certain water to solid mass ratios (corresponding to some of the rows in Table 3-3). The lack of conformity between some curves in Figure 3-17 and 3-19 is due to that they are made in different series and in some way reflex the scatter that in some cases may occur in these tests.

Table 3-3. Test plan for WyNa with the tested combinations of water to solid mass ratio (w_r) and salinity of the mixing water. The squares marked green are performed tests.

WyNa	NaCl (mM)													
w_r	0	0,5	1	2	2,5	3	4	5	10	15	20	25	50	100
35	■	■	■	■	■	■	■	■	■	■	■	■	■	■
40	■													
50	■		■		■			■	■					■
75	■													
100	■		■		■				■					■
150	■													
200	■		■		■				■					■
250	■													
300	■													

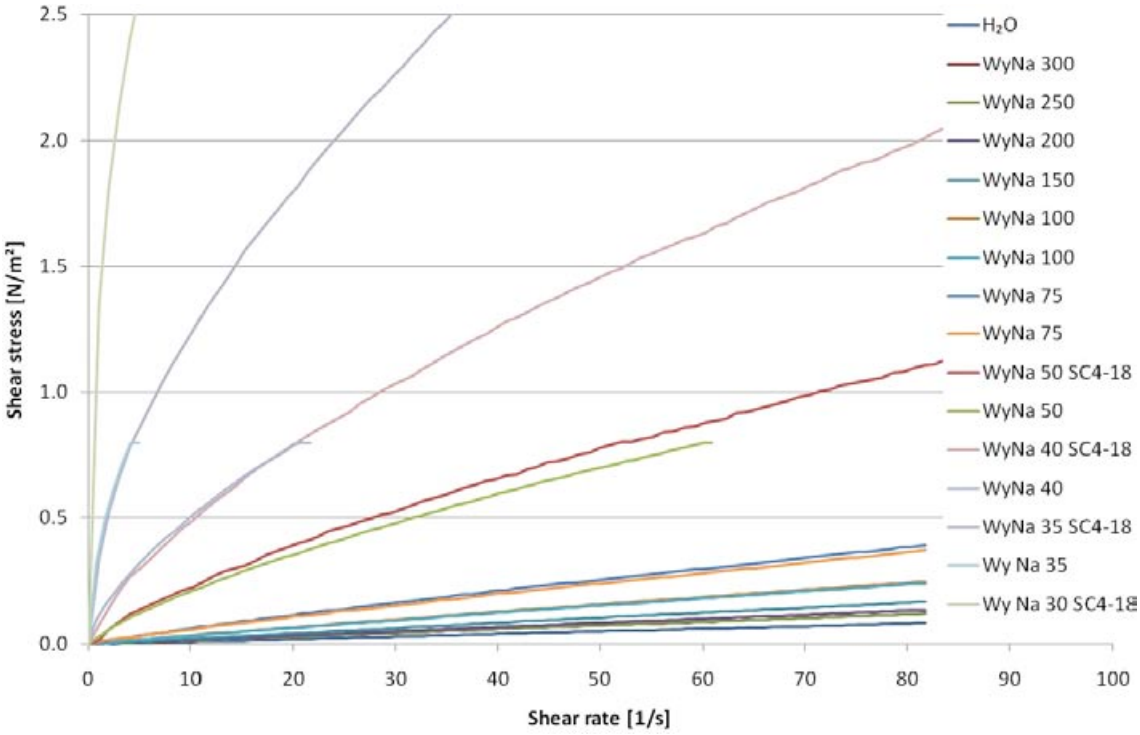

Figure 3-17. *Shear stress as a function of shear rate for WyNa in distilled water at different water to solid mass ratios. Curves with designation SC4-18 are made with another spindle/cup.*

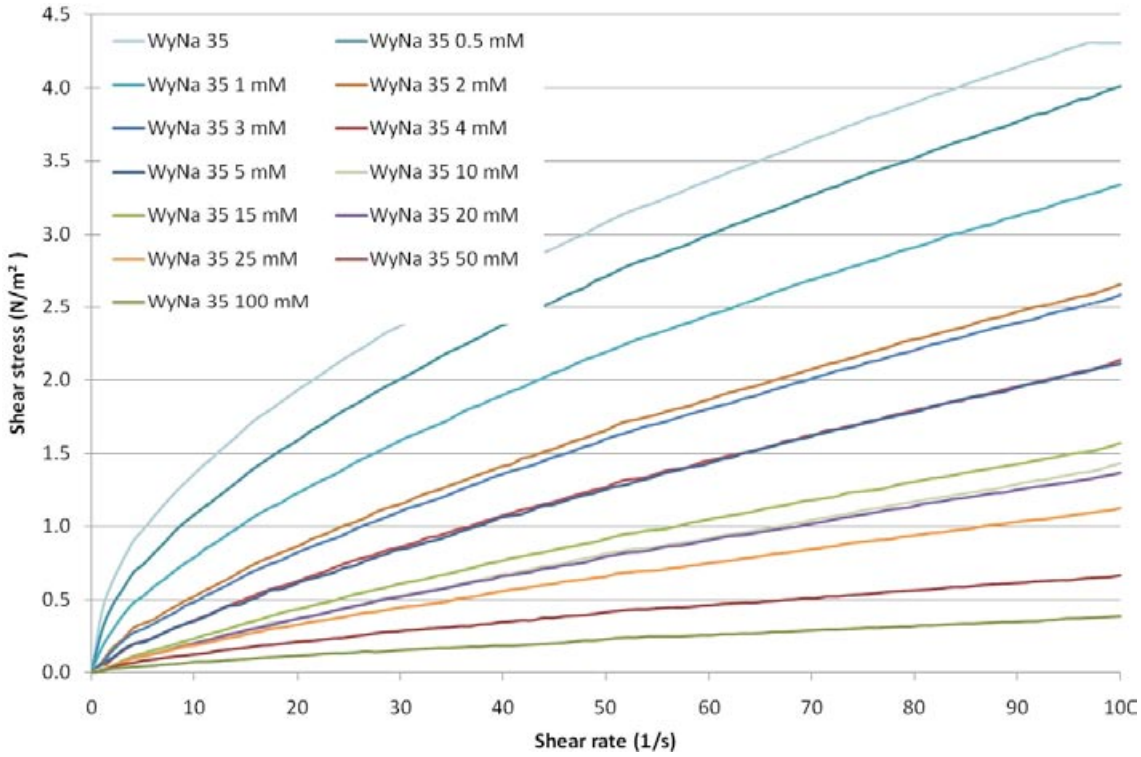

Figure 3-18. *Shear stress as a function of shear rate for WyNa at the water to solid mass ratio 35 in water with different NaCl concentrations.*

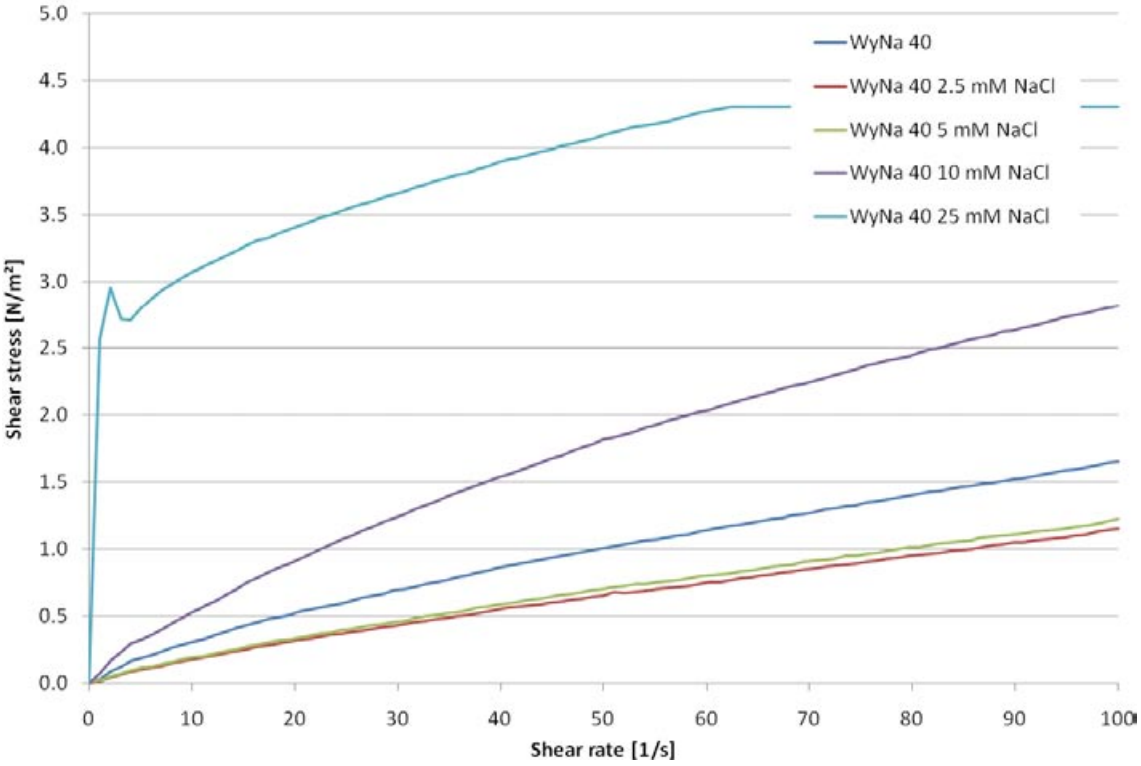

Figure 3-19. *Shear stress as a function of shear rate for WyNa at the water to solid mass ratio 40 in water with different NaCl concentrations.*

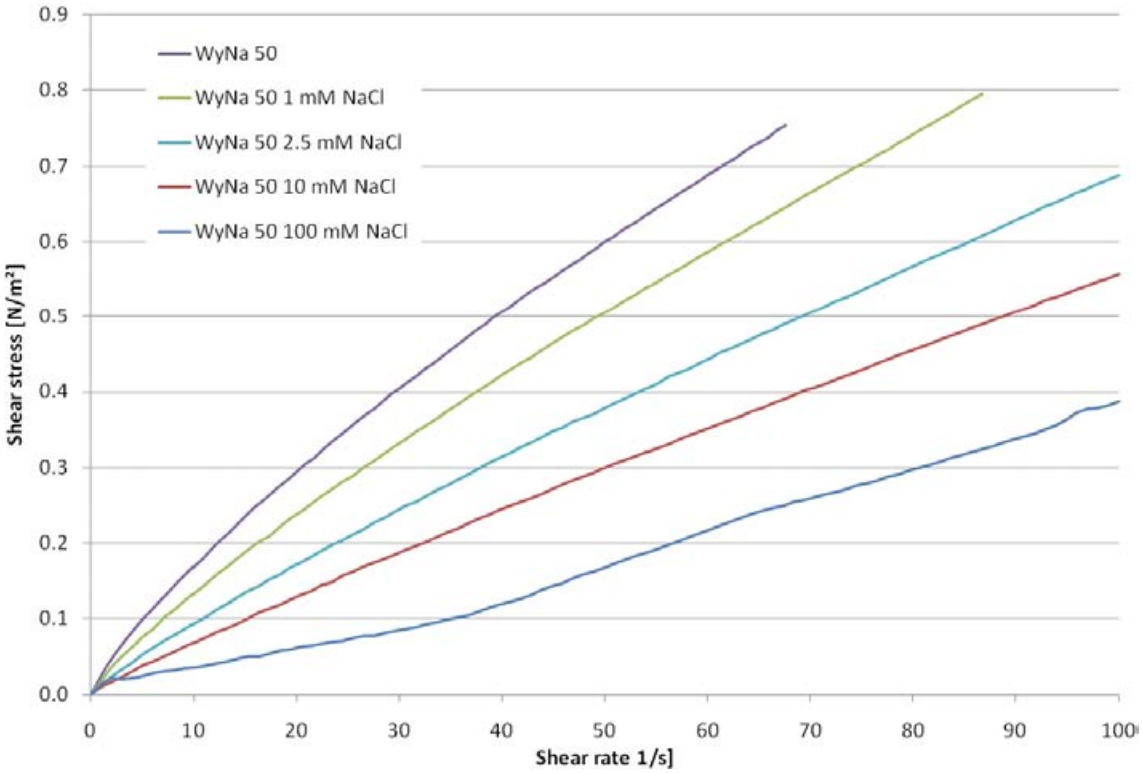

Figure 3-20. *Shear stress as a function of shear rate for WyNa at the water to solid mass ratio 50 in water with different NaCl concentrations.*

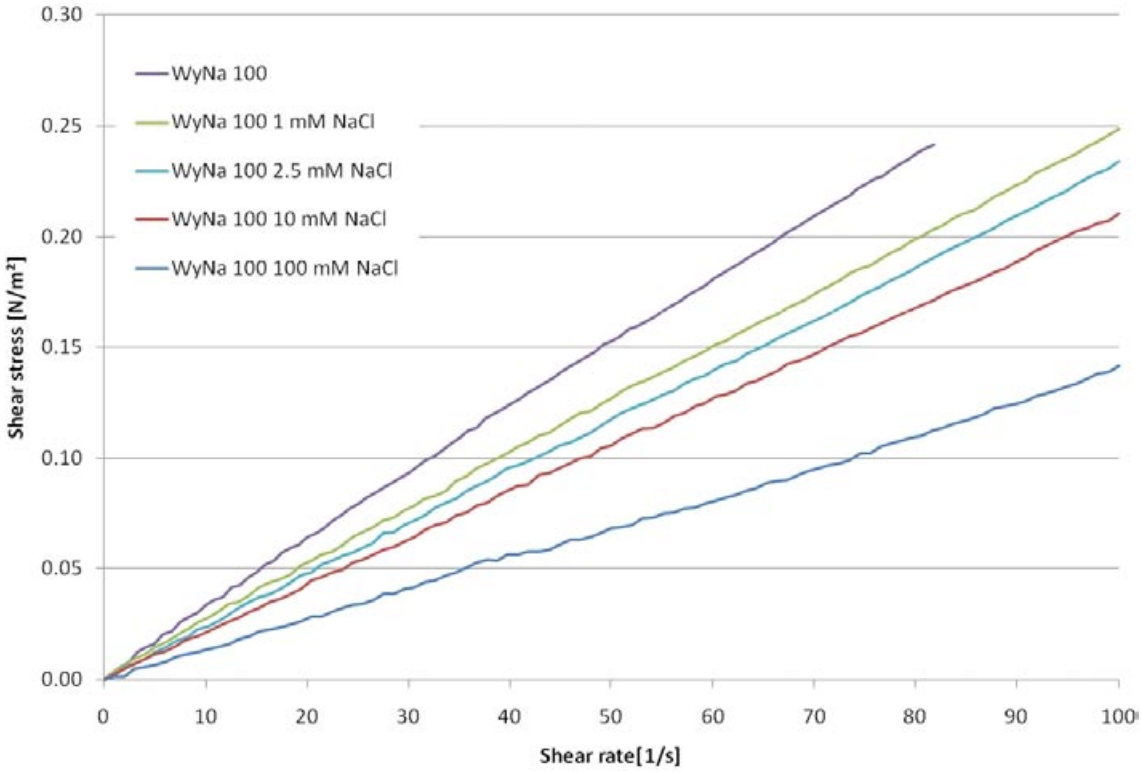

Figure 3-21. *Shear stress as a function of shear rate for WyNa at the water to solid mass ratio 100 in water with different NaCl concentrations.*

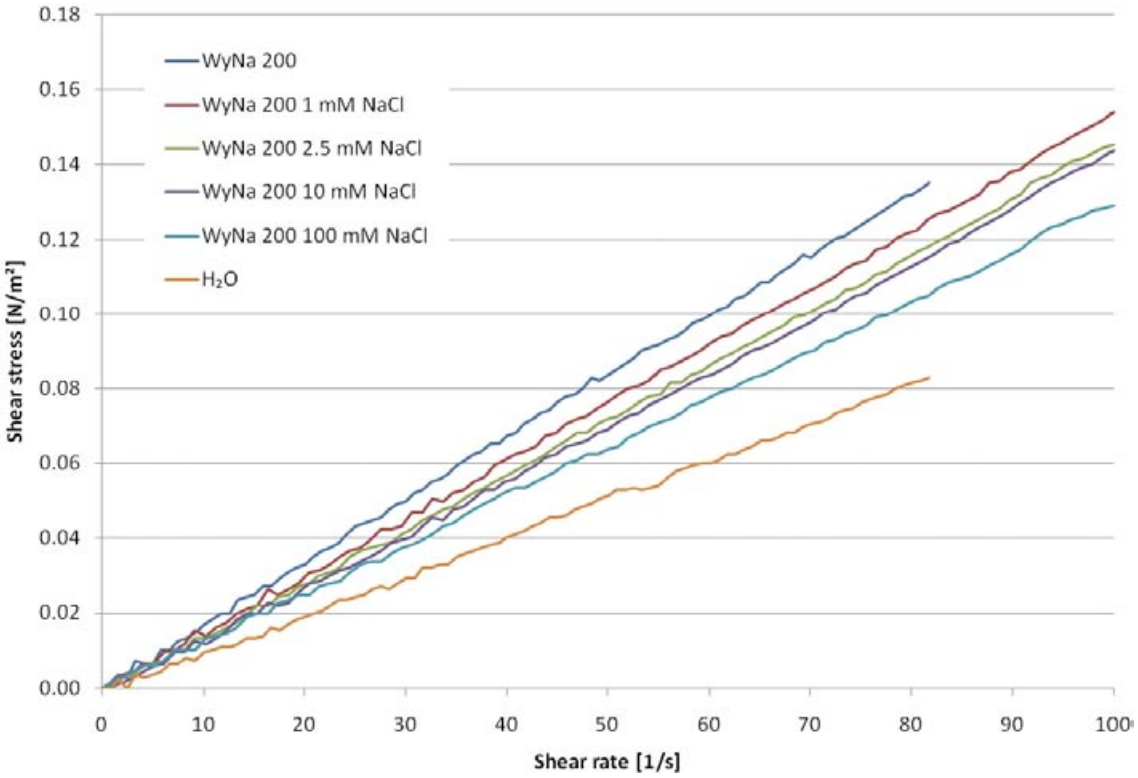

Figure 3-22. *Shear stress as a function of shear rate for WyNa at the water to solid mass ratio 200 in water with different NaCl concentrations. Results from a test on free water is also displayed for comparison.*

3.6.3 Rheology tests

3.6.3.1 MX-80

The technique used for the rheology tests are described in Section 3.4. The technique implies measurement of shear stress with increasing shear strain at constant shear rate. The test matrix of the viscosity tests (Table 3-2) was also used for the rheology tests. The results are displayed in Figure 3-24 to Figure 3-29 with the shear stress plotted as function of the shear strain. The rate of shear was 0.5 1/s in all tests. Figure 3-23 shows the influence of the water to solid mass ratio at the salt concentration 0 (corresponding to the left column in Table 3-2) while the rest of the figures show the influence of the NaCl concentration at certain water to solid mass ratios (corresponding to some of the rows in Table 3-2).

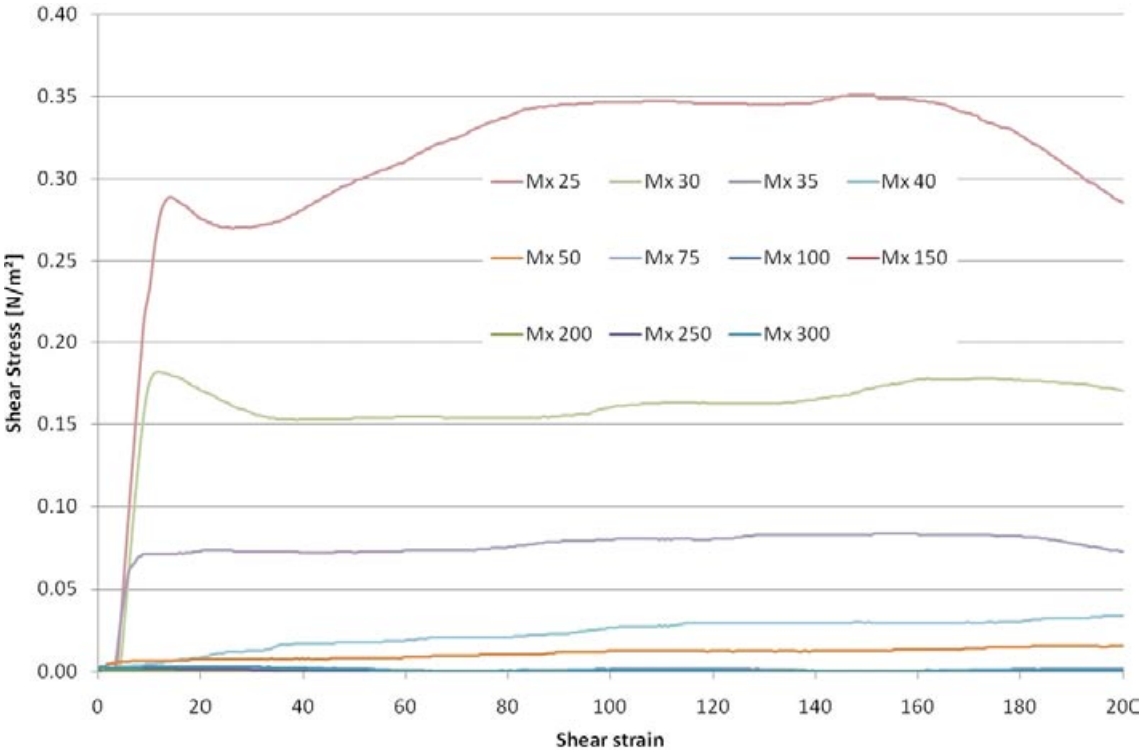

Figure 3-23. *Shear stress as a function of shear strain for MX-80 in distilled water at different water to solid mass ratios.*

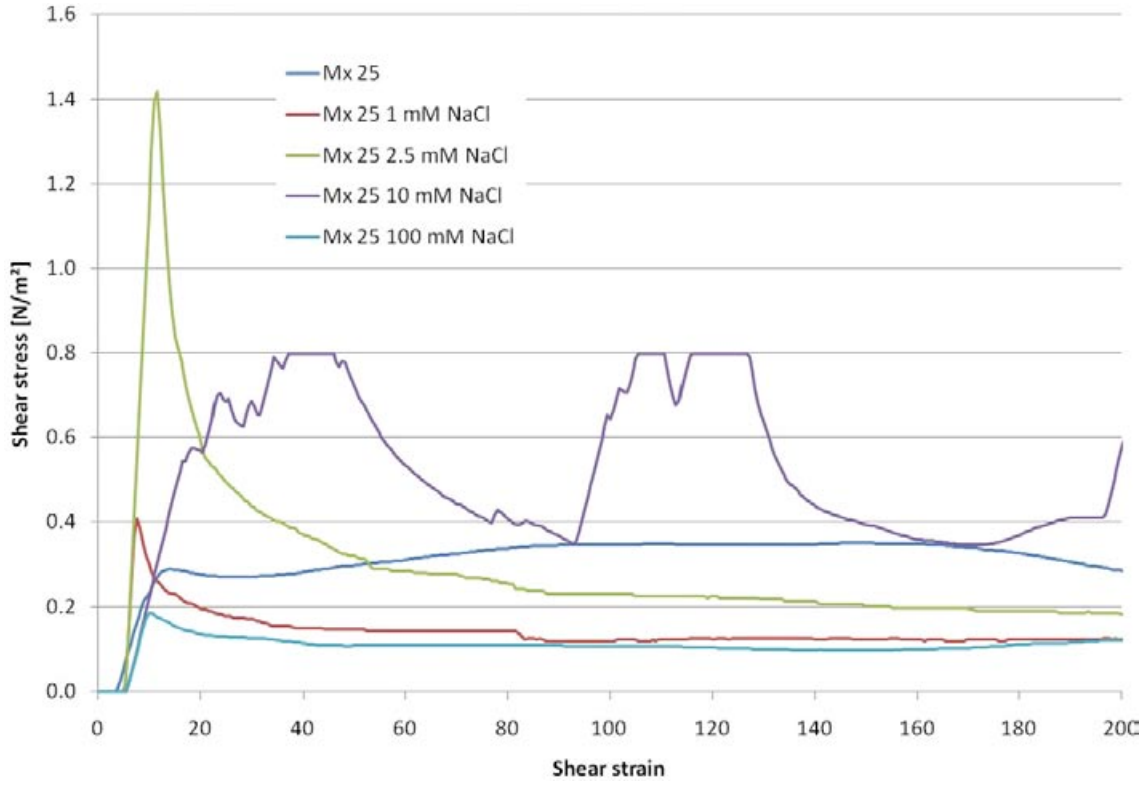

Figure 3-24. *Shear stress as a function of shear strain for MX-80 at the water to solid mass ratio 25 in water with different NaCl concentrations. In the case of 10 mM NaCl the instrument reached the maximum measurable value.*

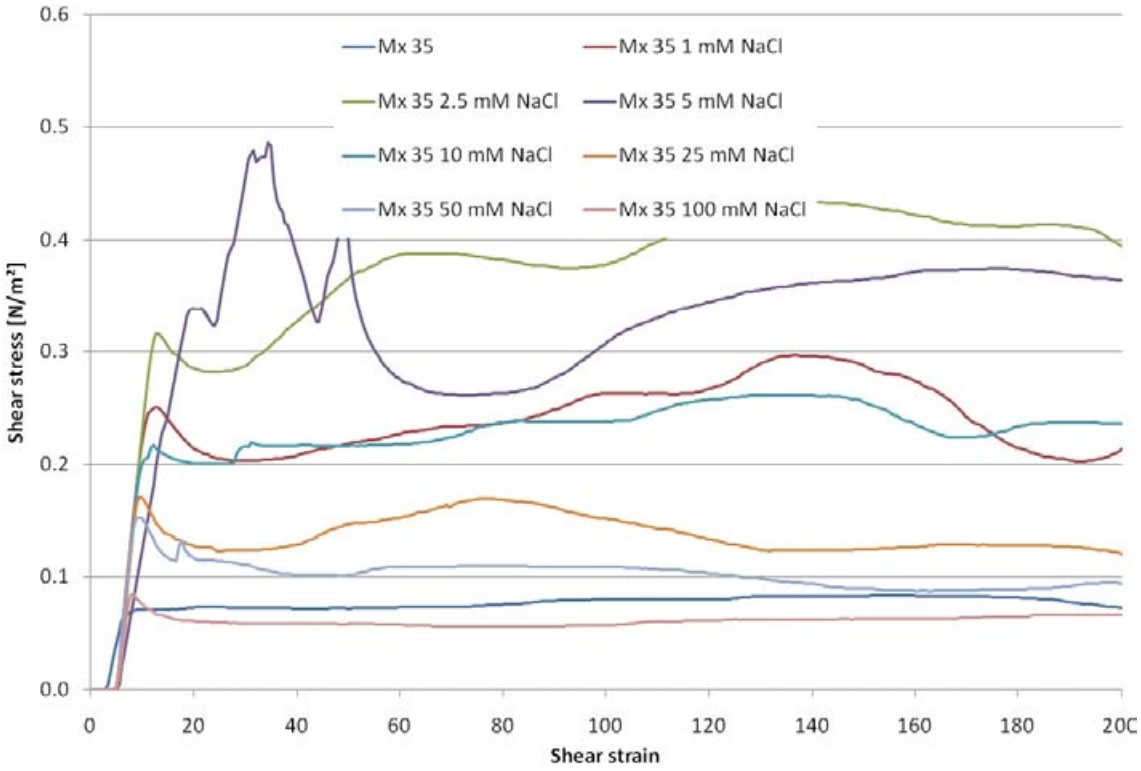

Figure 3-25. *Shear stress as a function of shear strain for MX-80 at the water to solid mass ratio 35 in water with different NaCl concentrations.*

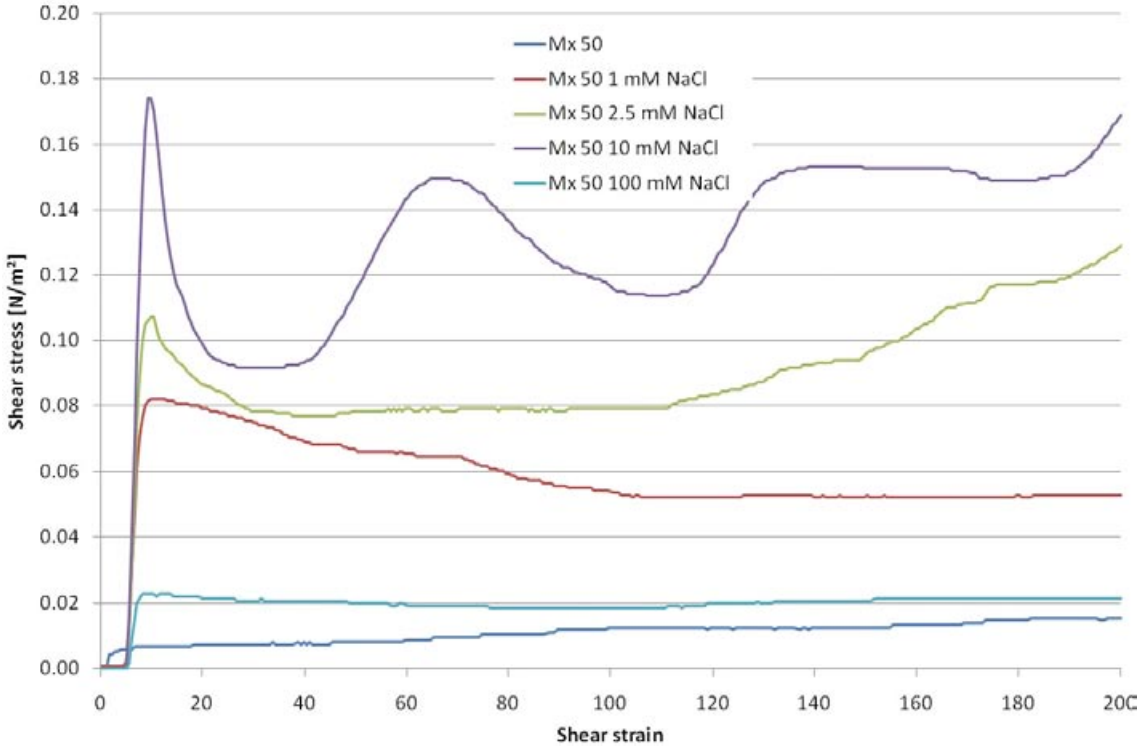

Figure 3-26. *Shear stress as a function of shear strain for MX-80 at the water to solid mass ratio 50 in water with different NaCl concentrations.*

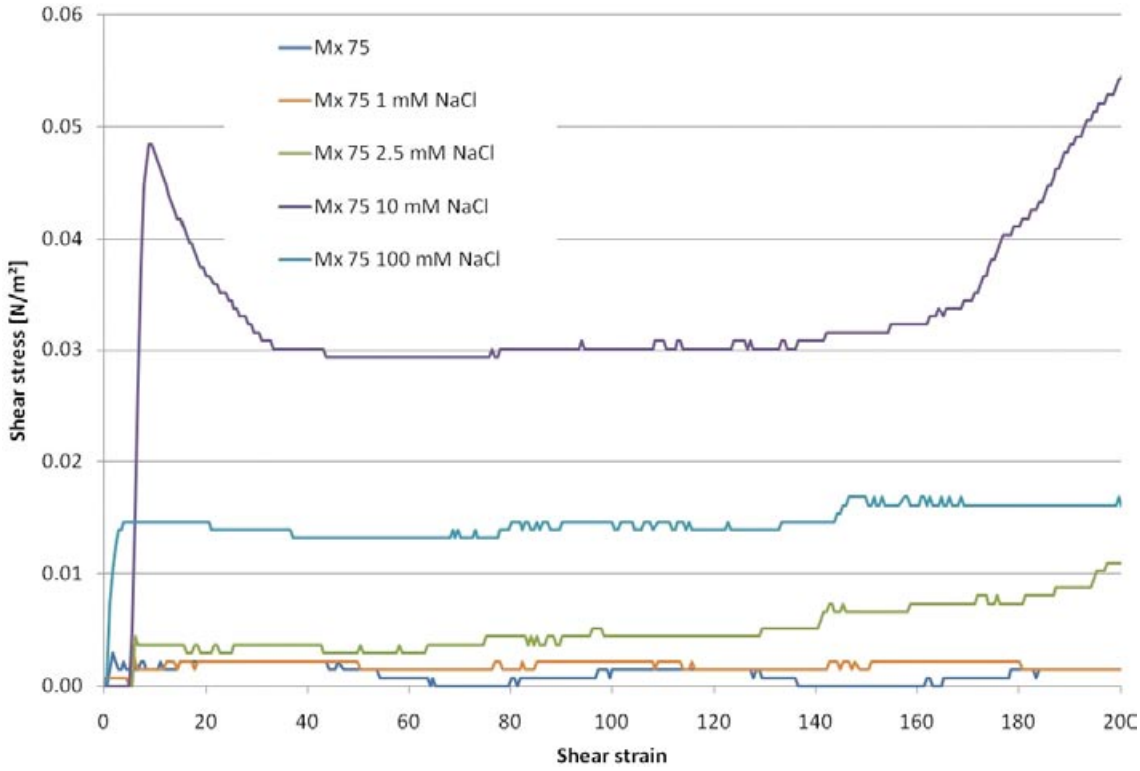

Figure 3-27. *Shear stress as a function of shear strain for MX-80 at the water to solid mass ratio 75 in water with different NaCl concentrations.*

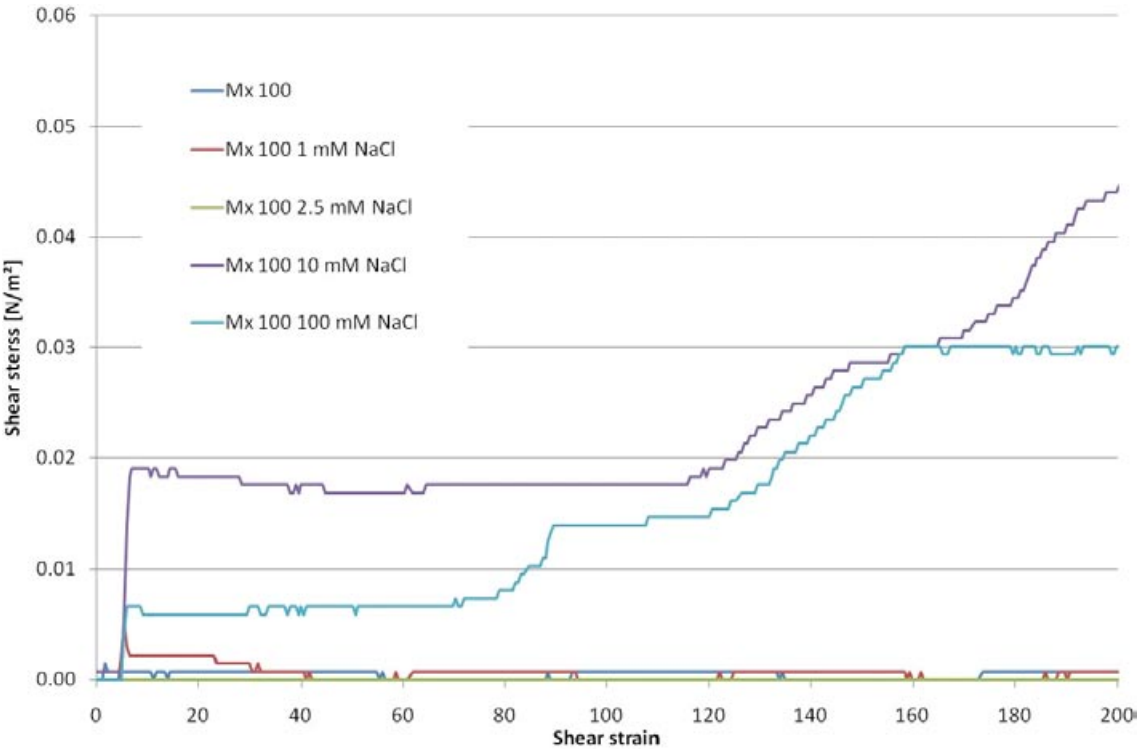

Figure 3-28. *Shear stress as a function of shear strain for MX-80 at the water to solid mass ratio 100 in water with different NaCl concentrations.*

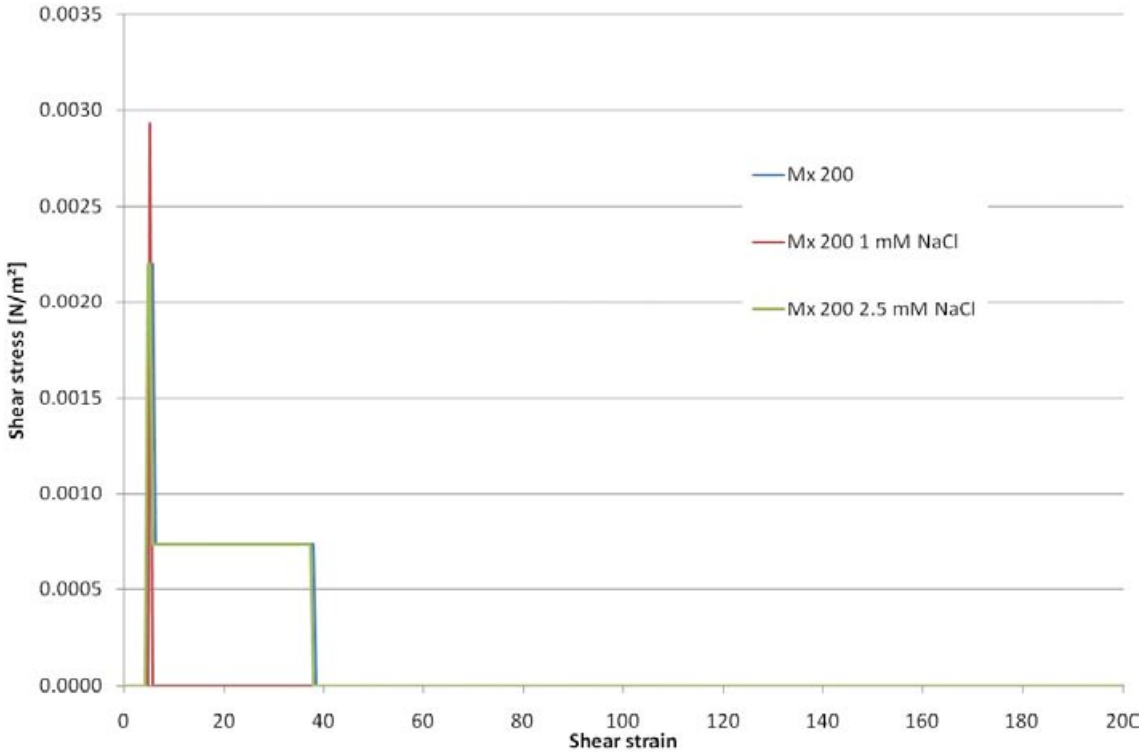

Figure 3-29. *Shear stress as a function of shear strain for MX-80 at the water to solid mass ratio 200 in water with different NaCl concentrations.*

3.6.3.2 Wy-Na

The same test matrix used for the viscosity tests on the purified bentonite Wy-Na (Table 3-3) was also used for the rheology tests. The results are displayed in Figure 3-30 to Figure 3-34 with the shear stress plotted as a function of the shear strain. The rate of shear was 0.5 1/s in all tests. Figure 3-30 shows the influence of the water to solid mass ratio at the salt concentration 0 (corresponding to the left column in Table 3-2) while the rest of the figures show the influence of the NaCl concentration at certain water to solid mass ratios (corresponding to some of the rows in Table 3-3). Figure 3-32 also includes some tests with different salt mixing procedures and mixing times.

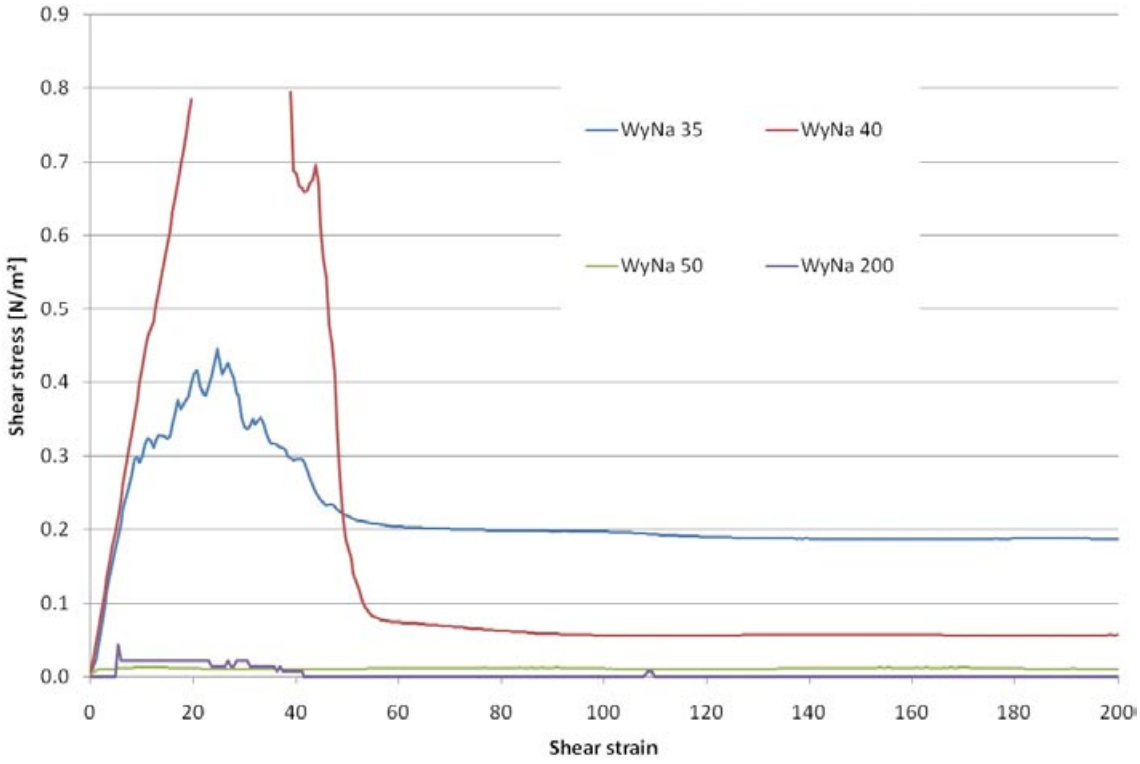

Figure 3-30. *Shear stress as a function of shear strain for WyNa in distilled water at different water to solid mass ratios.*

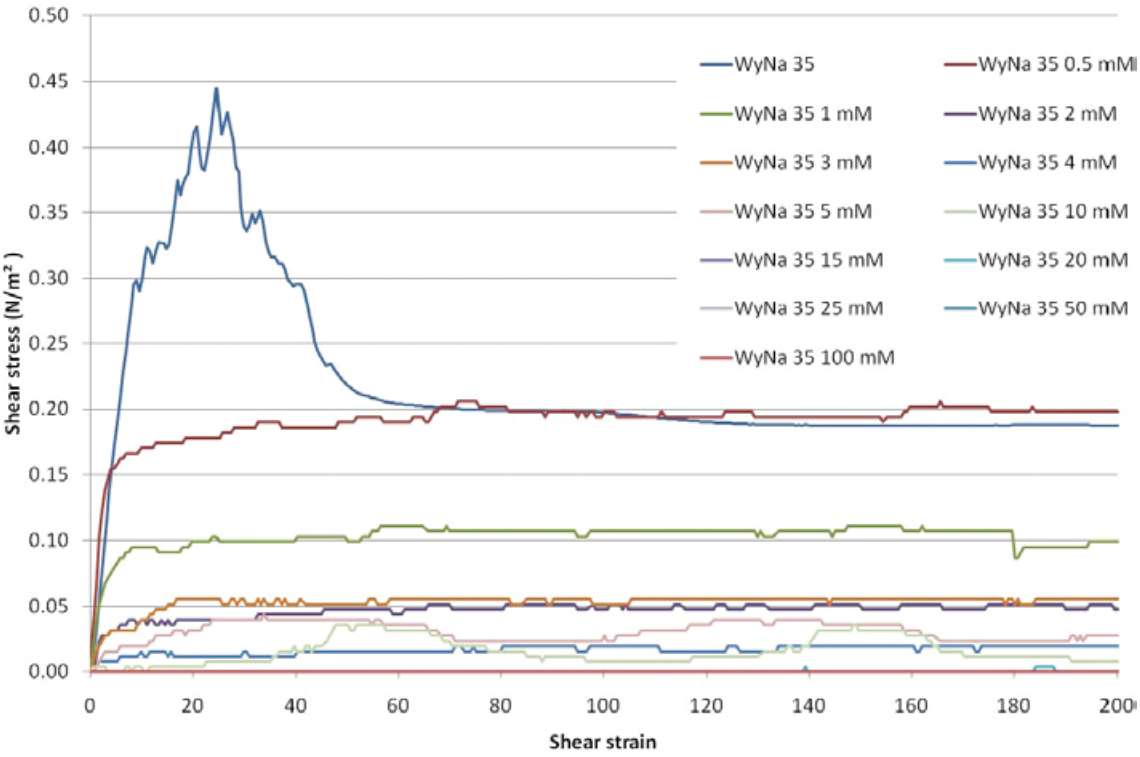

Figure 3-31. *Shear stress as a function of shear strain for WyNa at the water to solid mass ratio 35 in water with different NaCl concentrations.*

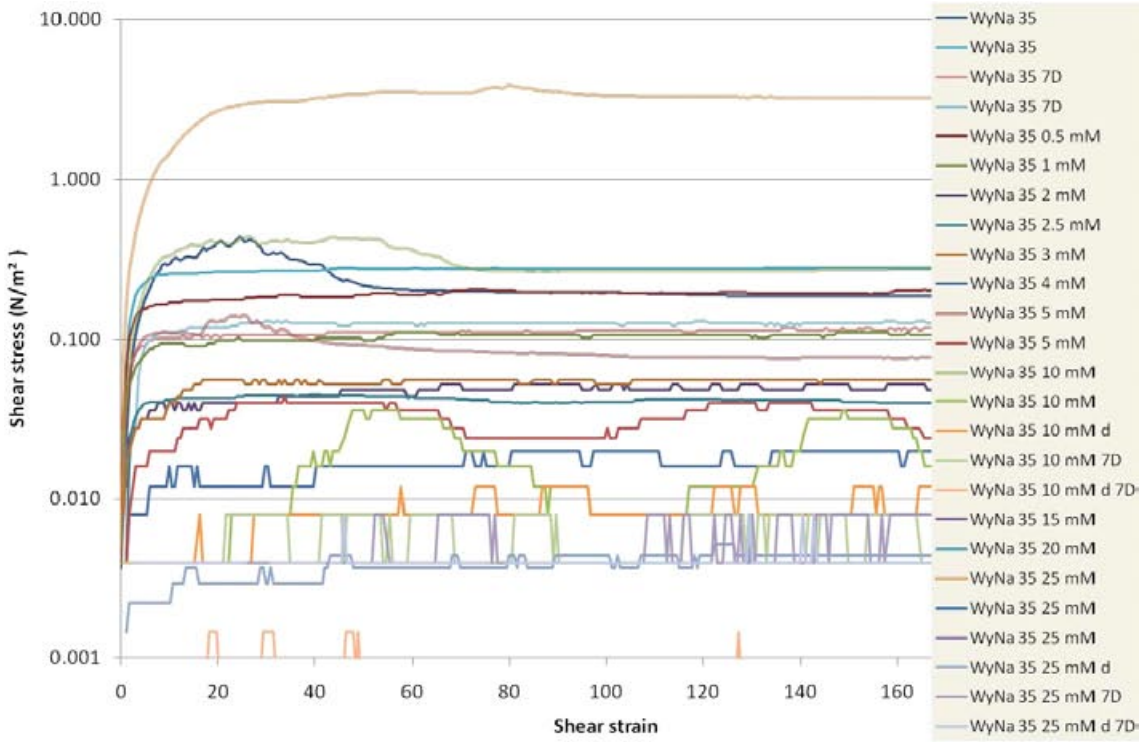
10.000
1.000
0.100
0.010
0.001
Shear stress (N/m²)
0
20
40
60
80
100
120
140
160
Shear strain
WyNa 35
WyNa 35
WyNa 35 7D
WyNa 35 7D
WyNa 35 0.5 mM
WyNa 35 1 mM
WyNa 35 2 mM
WyNa 35 2.5 mM
WyNa 35 3 mM
WyNa 35 4 mM
WyNa 35 5 mM
WyNa 35 5 mM
WyNa 35 10 mM
WyNa 35 10 mM
WyNa 35 10 mM d
WyNa 35 10 mM 7D
WyNa 35 10 mM d 7D
WyNa 35 15 mM
WyNa 35 20 mM
WyNa 35 25 mM
WyNa 35 25 mM
WyNa 35 25 mM
WyNa 35 25 mM d
WyNa 35 25 mM 7D
WyNa 35 25 mM d 7D

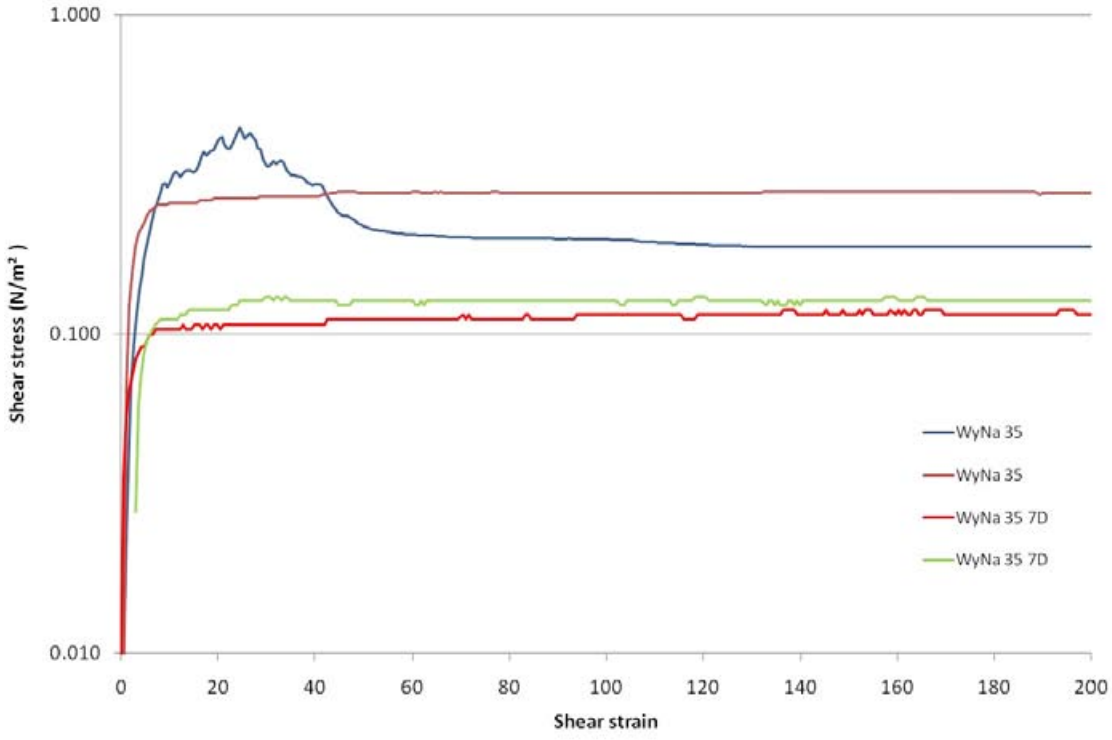
1.000
0.100
0.010
Shear stress (N/m²)
0
20
40
60
80
100
120
140
160
180
200
Shear strain
WyNa 35
WyNa 35
WyNa 35 7D
WyNa 35 7D

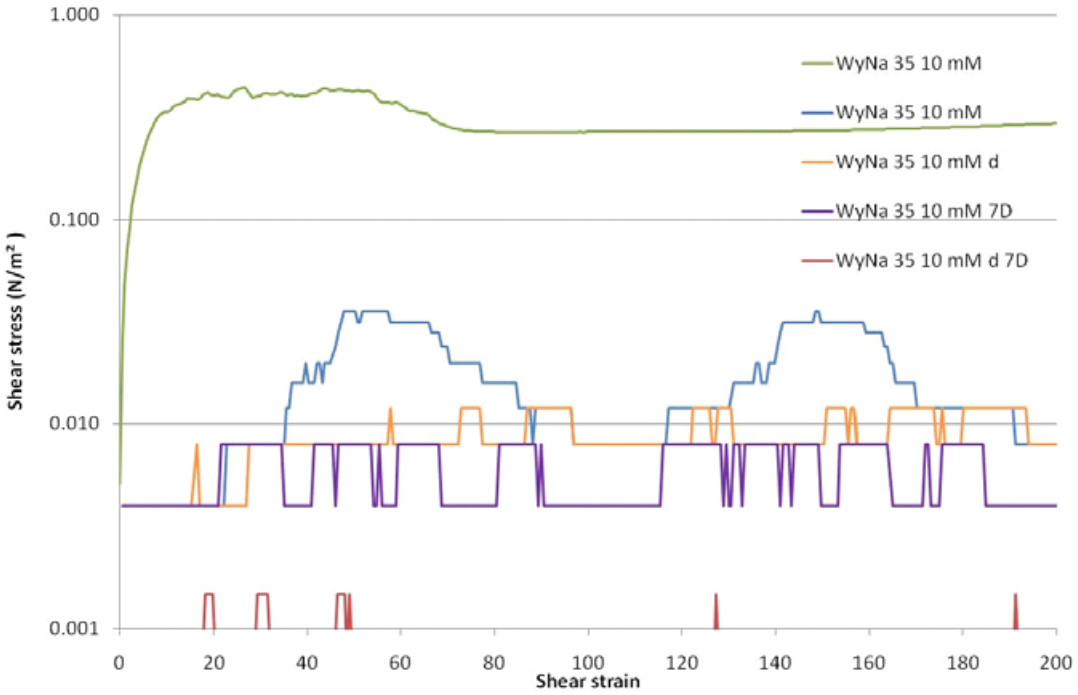

Figure 3-32. *Shear stress in logarithmic scale as a function of shear strain for WyNa at the water to solid mass ratio 35 in water with different NaCl concentrations. The same relations as shown in Figure 3-31 but with some extra tests with 7 days waiting time (marked 7D after the designation) and different mixing procedure (dissolving salt after the clay mixing: marked d after the salt concentration designation). The two following figures are pure WyNa and 10 mM NaCl mix.*

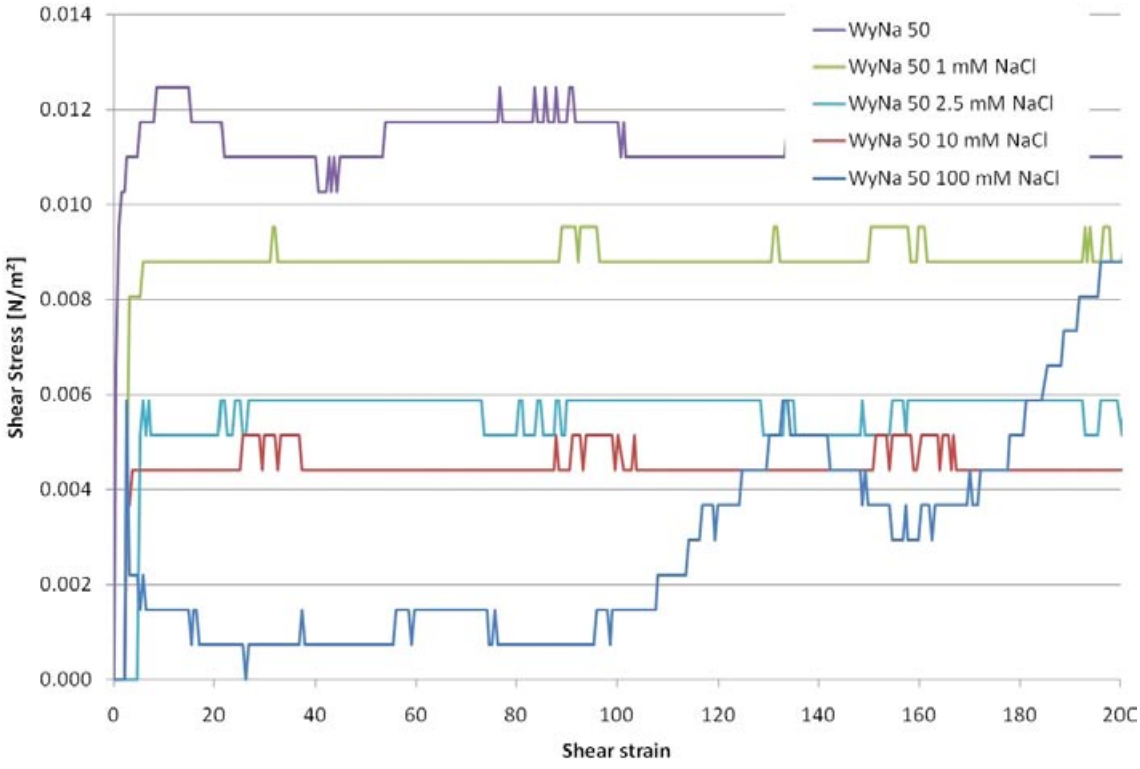

Figure 3-33. *Shear stress as a function of shear strain for WyNa at the water to solid mass ratio 50 in water with different NaCl concentrations.*

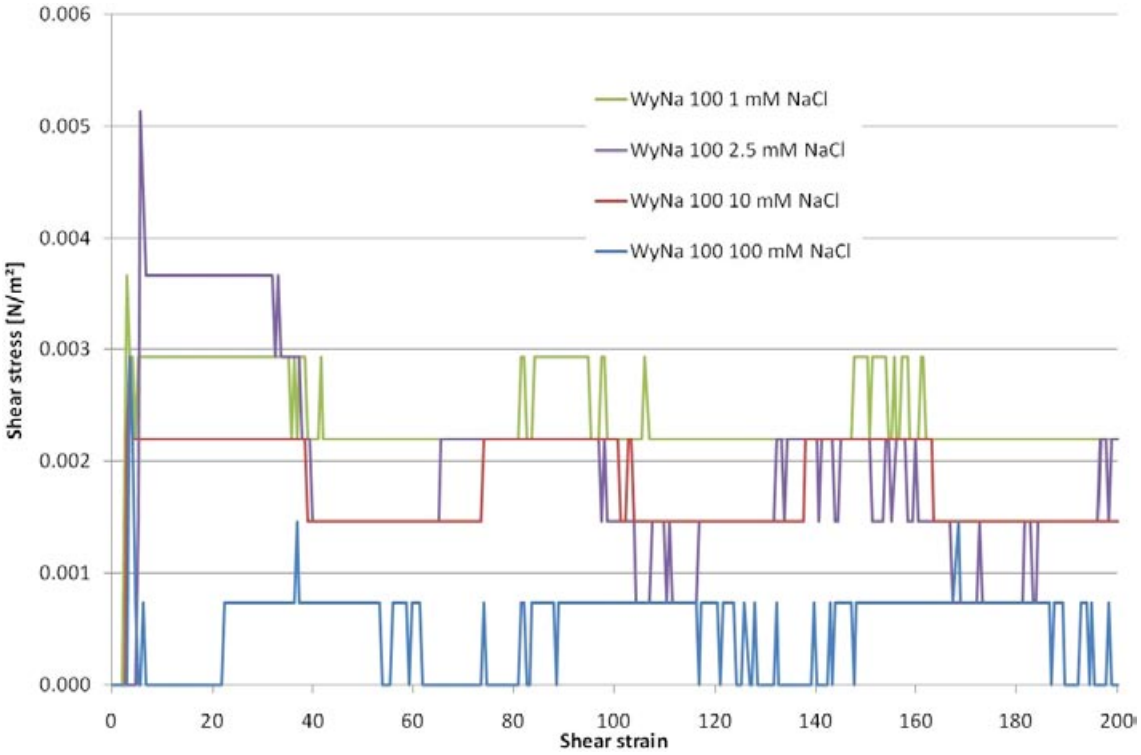

Figure 3-34. *Shear stress as a function of shear strain for WyNa at the water to solid mass ratio 100 in water with different NaCl concentrations.*

3.6.4 Vane tests

Since the rheology tests with a rotating spindle may be misleading for stiffer gels due to slip between the gel and the spindle some vane tests have also been done for measuring the shear strength of those materials.

MX-80 with water to solid mass ratios varying between 15 and 40 has been tested with three different resting times. Figure 3-35 to Figure 3-37 show the relation between shear stress and shear distance at no resting time, 24 hours resting time and three weeks resting time.

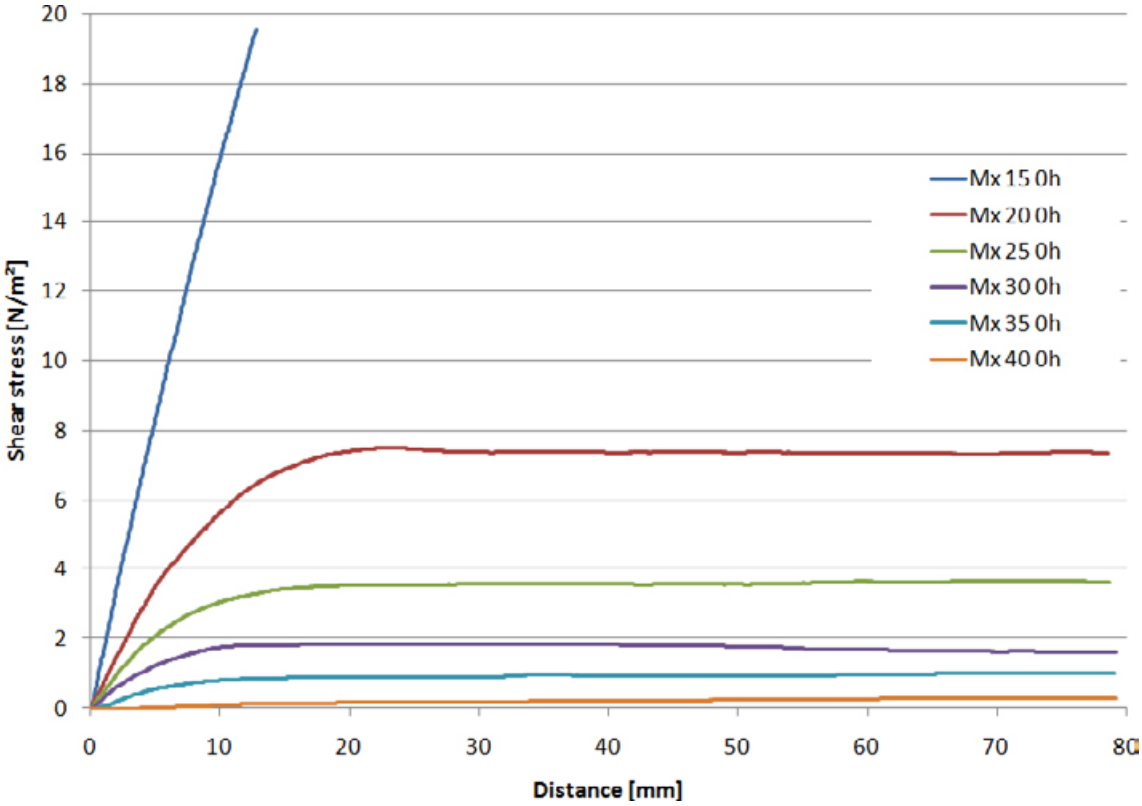

Figure 3-35. *Shear stress measured with the vane as a function of shear distance for MX-80 in distilled water at different water to solid mass ratios. Measured directly after agitation.*

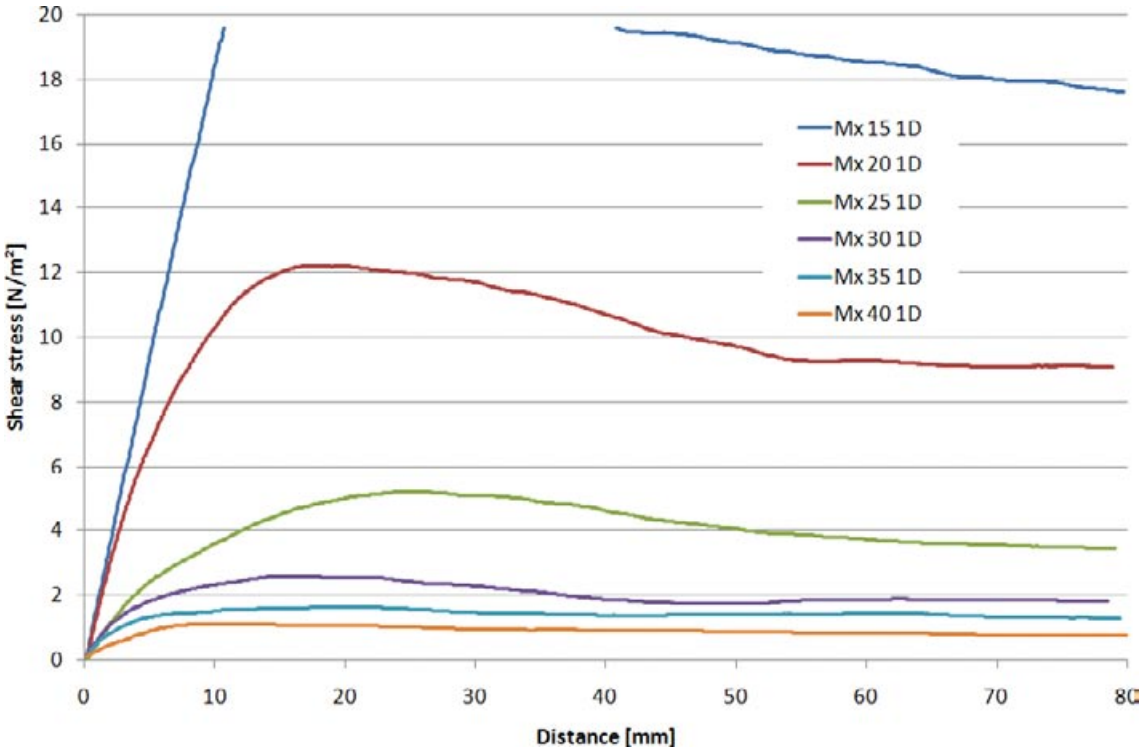

Figure 3-36. *Shear stress as a function of shear distance for MX-80 in distilled water at different water to solid mass ratios. Measured 24 hours after agitation.*

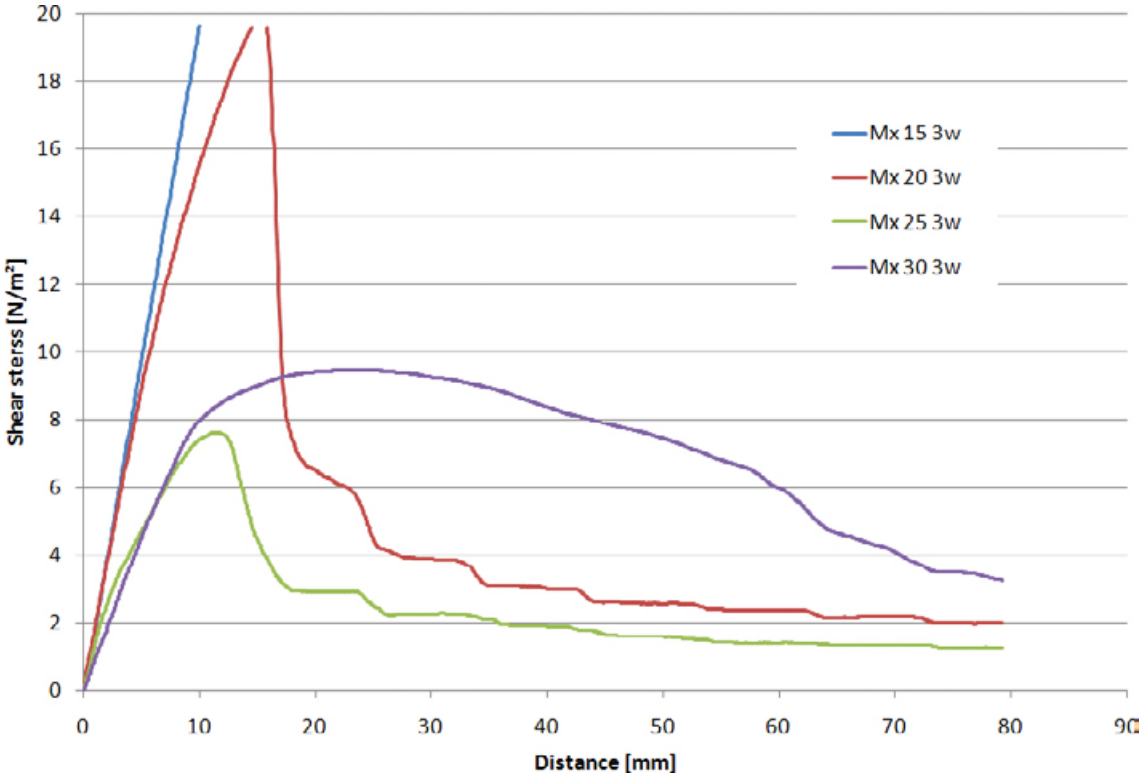

Figure 3-37. *Shear stress as a function of shear distance for MX-80 with distilled water at different water to solid mass ratios. Measured 3 weeks after agitation.*

3.6.5 Other tests

3.6.5.1 Viscosity of saline water

In order to verify that the NaCl concentration of the water itself does not affect the viscous properties of a bentonite/water system a comparison between deionized water and water with the different NaCl concentration has been made. Figure 3-38 shows the results of viscosity tests on water with different NaCl concentration. The conformance of the curves also verifies the accuracy of the measuring tool.

3.6.5.2 Influence of temperature

No tests at other temperature than room temperature have been done. The main reason is that the low temperatures will prevail during the critical time and the influence of decreased temperature is generally an increase in viscosity and the influence is rather low compared to all uncertainties of these tests.

3.7 Results from measurements on Ca-bentonites

Calcium bentonites (both natural and converted) are not easily rheologically characterized with the described methods. Figure 3-39 shows the difference in measured results when two different spindle/cup combinations were used. The difference is large as opposed to MX-80 and WyNa where no difference was noticed. One explanation for this is that one of the spindles (ULA adapter) is cylindrical and the other one (SC4-18) has conical ends. Another explanation is that the Ca-bentonite settles rapidly and the sediments cover different lengths of the bobs.

Figure 3-40 shows the results of viscosity measurements on Deponit CA-N at mean water to solid mass ratio 206. The properties agree with the properties of free water. The reason is that the bentonite has settled to a level below the bob and the measurements are done in the supernatant water above the sediments.

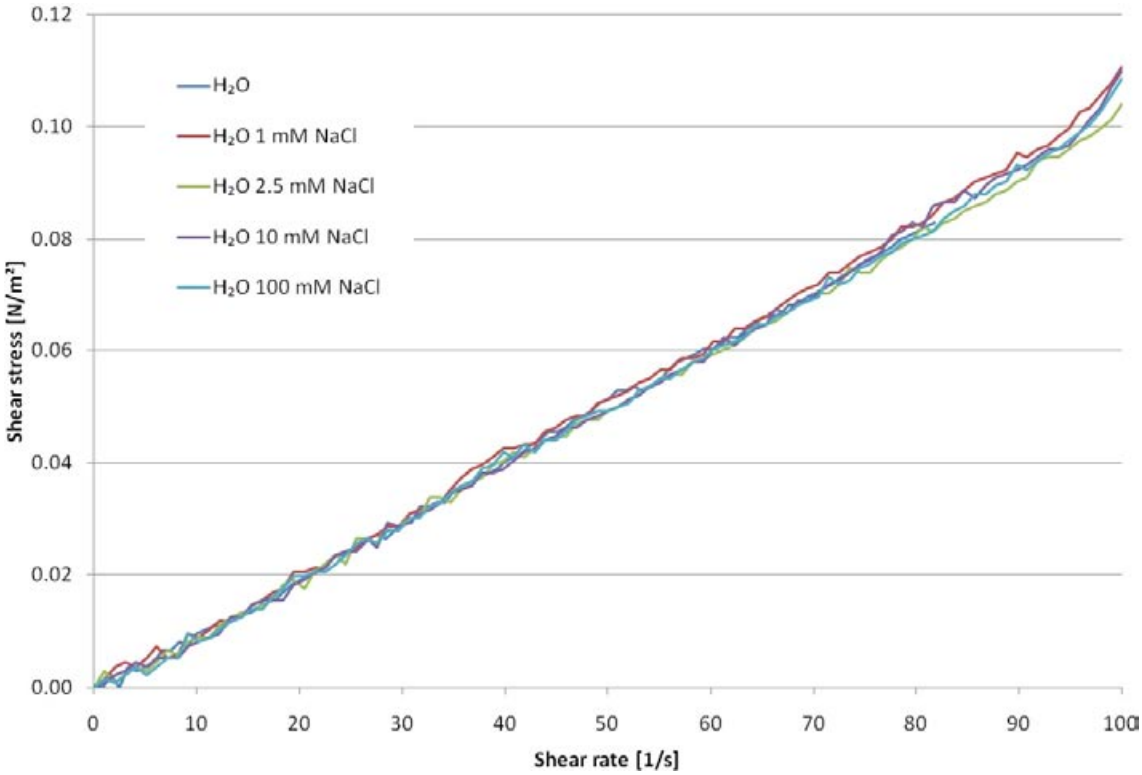

Figure 3-38. *Shear stress as a function of shear rate measured in water with different NaCl concentration.*

Figure 3-41 shows results from rheological measurements with constant shear rate (0.5 1/s) on WyCa with an average water to solid mass ratio of 7.7 with the same alternative spindle/cup combinations as in Figure 3-39. In one of the spindle/cup combinations the sediments gather below the bob so almost no shear resistance is registered. In the other combination the bentonite settles and the height of the sediments increase with time, which is seen as an increasing shear resistance with increasing shear deformation.

WyCa thus settles so rapidly that no rheological measurements can be made. The suspension will quickly become anisotropic with a sediment at the bottom and supernatant water above. The swelling and gelling ability of the Ca-bentonite is low. Figure 3-42 shows results of swelling tests. Samples with the dry mass 2.47 g have been placed in tubes that have been filled with water. After long time only a small swelling of the samples to a water to solid mass ratio of between 3 and 5 have taken place. Similar tests with well mixed powder of Wy-Ca show that the bentonite rapidly settles with similar results although to a little higher average water to solid mass ratio.

The Ca-bentonite thus seems to form a stable sediment with water to solid mass ratio well below 10, which has sand-like properties. Those properties cannot be measured with the equipment used for Na-bentonite. The strength of the sediment may possibly be measured with the vane although the strength mainly comes from the stress caused by the gravity of the overlying material as for friction materials like sand.

These results together with other results in this report show that Ca-bentonite is not a problem due to the low swelling capacity and the inability to form colloids.

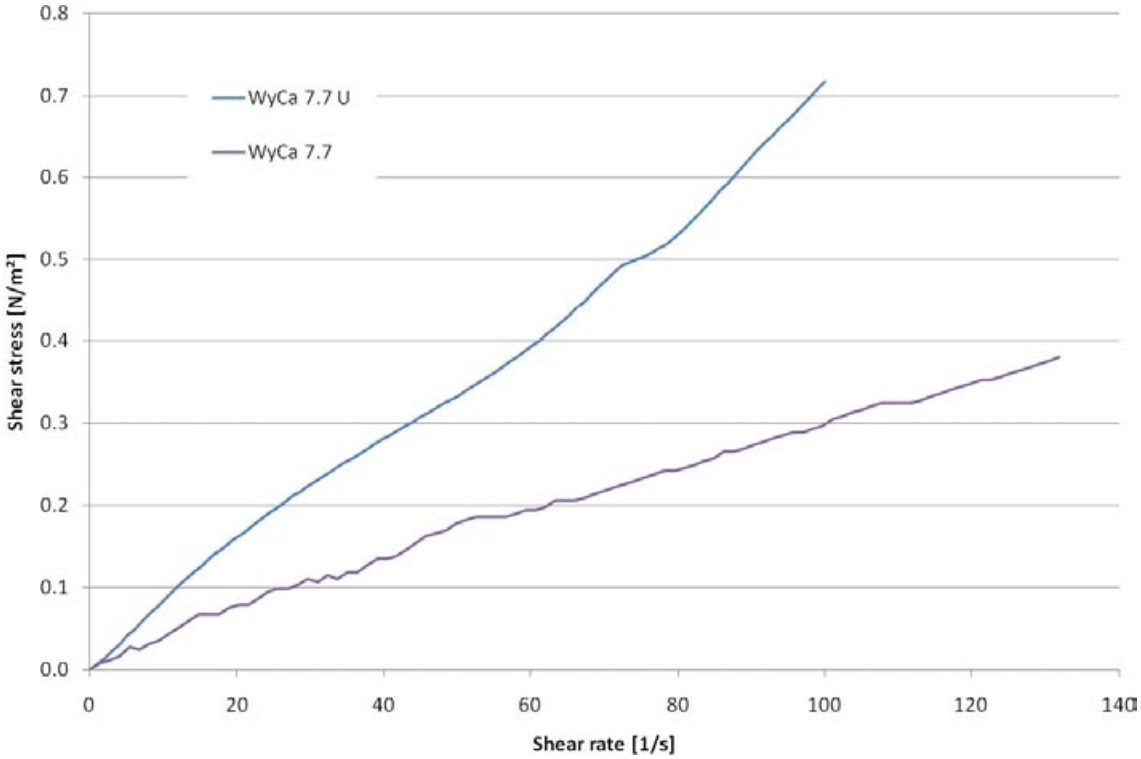

Figure 3-39. *Example of misleading results from viscosity measurements on Ca-bentonite. Shear stress measured as a function of shear rate for WyCa with water to solid mass ratio 7.7. Different equipment (spindle and cup) were used.*

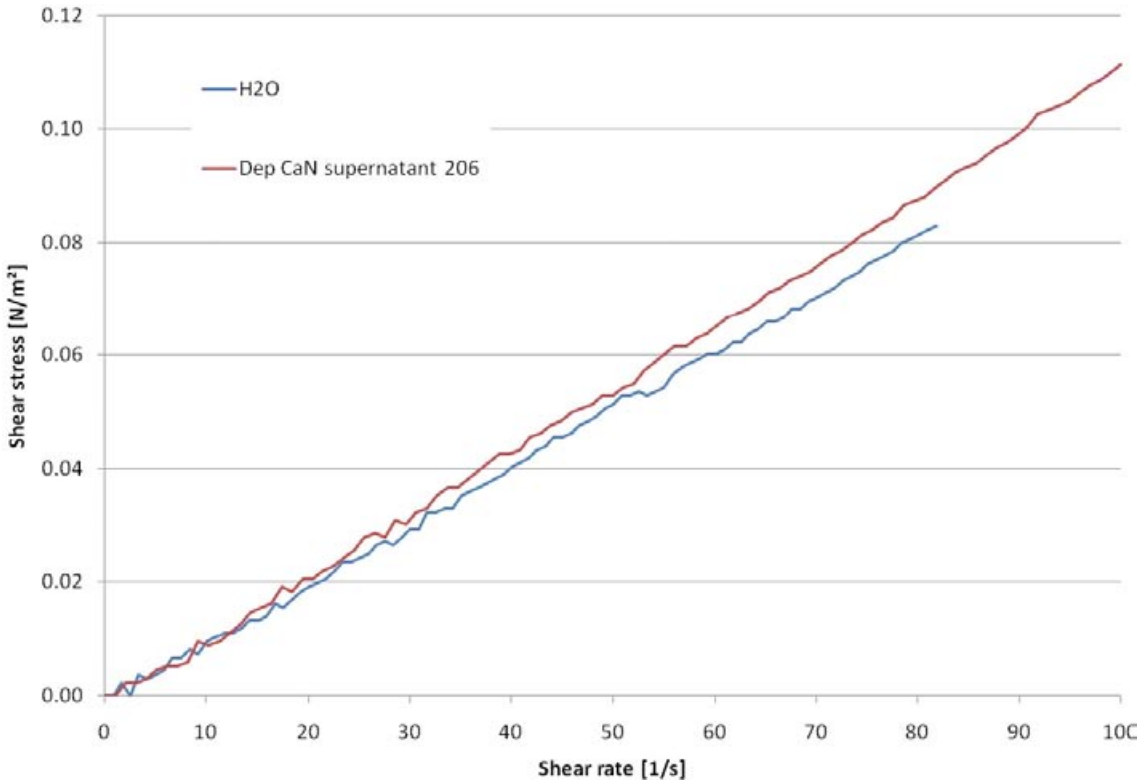

Figure 3-40. *Shear stress as a function of shear rate for Deponit CA-N with water to solid mass ratio 206. Water is included as comparison. The bentonite has settled below the bottom of the spindle.*

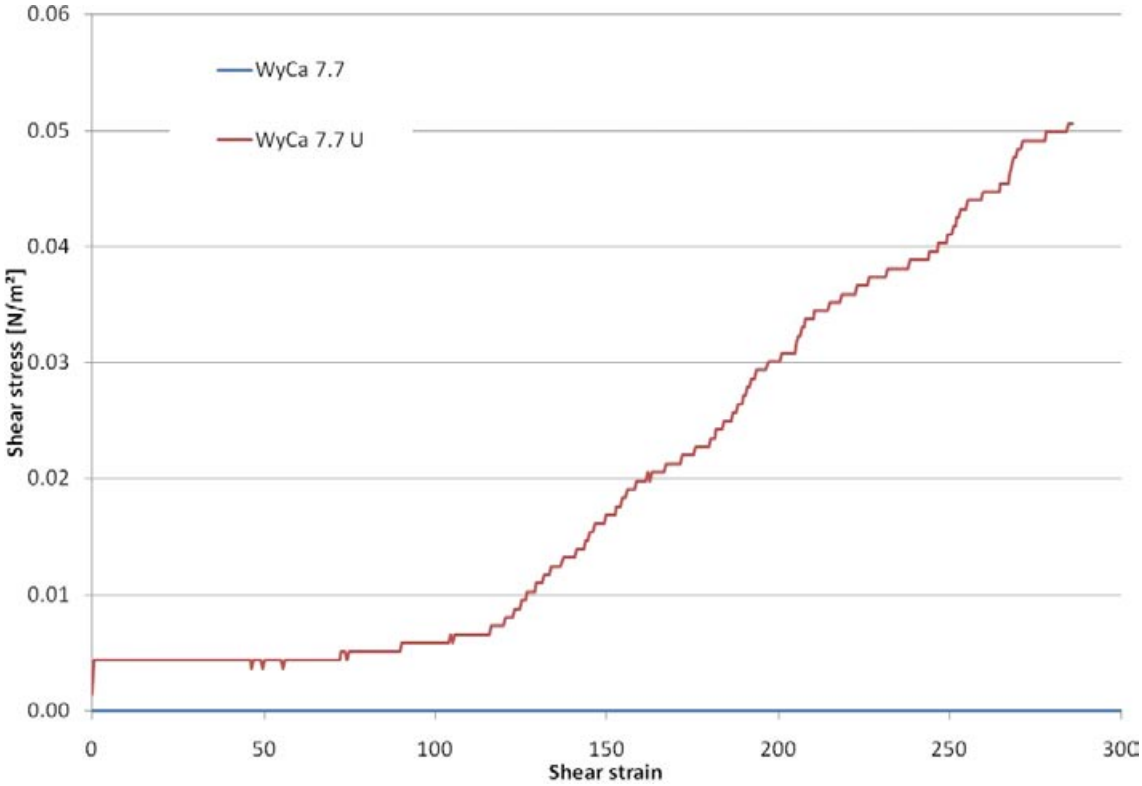

Figure 3-41. *Example of misleading results from rheology measurements on Ca-bentonite. Shear stress as a function of shear deformation for WyCa with the water to solid mass ratio 7.7. Different equipment (spindle and cup) were used.*

Figure 3-42. *Swelling of Wy-Ca with the dry mass 2.47 g from (left to right) powder, dry compacted sample and saturated sample.*

3.8 Evaluation

3.8.1 General

The measured results presented in Section 3.6 have been evaluated with the models presented in Sections 3.3 and 3.4.

3.8.2 Viscosity tests

Most results from the viscosity tests may be evaluated according to the power law (Equation 3-6) discussed in Section 3.3.3.3

$$\tau = m\left(\frac{\dot{\gamma}}{\dot{\gamma}_0}\right)^n \qquad (3\text{-}6)$$

where τ_0 is the shear stress at the shear rate $\dot{\gamma}$ and $m = \tau_0$ is the shear stress at the normalized shear rate $\dot{\gamma}_0 = 1.0(1/s)$.

An example of such evaluation for WyNa is shown in Figure 3-43 where the measured shear stress is plotted as a function of the shear rate in a double logarithmic diagram. The measured results are adapted to form a straight line. The parameter m in Equation 3-6 is evaluated as the shear stress at the shear rate 1.0 1/s and the parameter n is evaluated as the inclination of the line (tangent of the angle).

At water to solid mass ratio 35 this yields

$m = 0.33$ (Pa)

$n = 0.58$

while at water to solid mass ratio 200 we get

$m = 0.0017$ (Pa)

$n = 1.0$

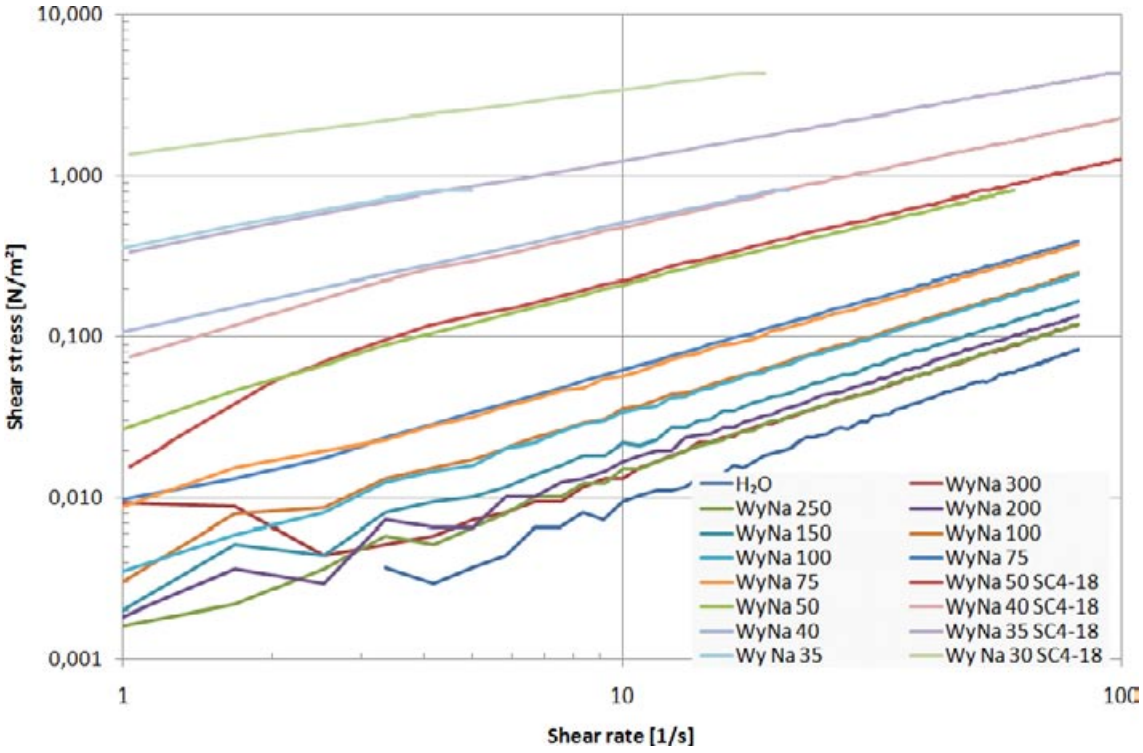

Figure 3-43. *Shear stress as a function of shear rate for WyNa in distilled water at different water to solid mass ratios plotted in a double logarithmic diagram (same curves as in Figure 3-17).*

WyNa at water to solid mass ratio 200 is thus Newtonian with the viscosity 1.7 mPas while at water to solid mass ratio 35 it is non-Newtonian but can be described according to Equation 3-6 with the derived *m* and *n* values.

In Figure 3-44 all the *m* and *n* values of the tests on MX-80 and WyNa with distilled water are evaluated. The mixtures turn Newtonian at water to solid mass ratios higher than 75–100.

The influence of salt concentration in the water on the parameters *m* and *n* for WyNa is shown in Figure 3-45. The influence of salt concentration is not quite consistent but a fairly general trend is that *m* decreases and *n* increases with increasing NaCl concentration. The results suggest that WyNa system becomes more liquid-like with increasing NaCl concentration due to the decreased electrostatic repulsion between the sheets, i.e. shorter Debye length.

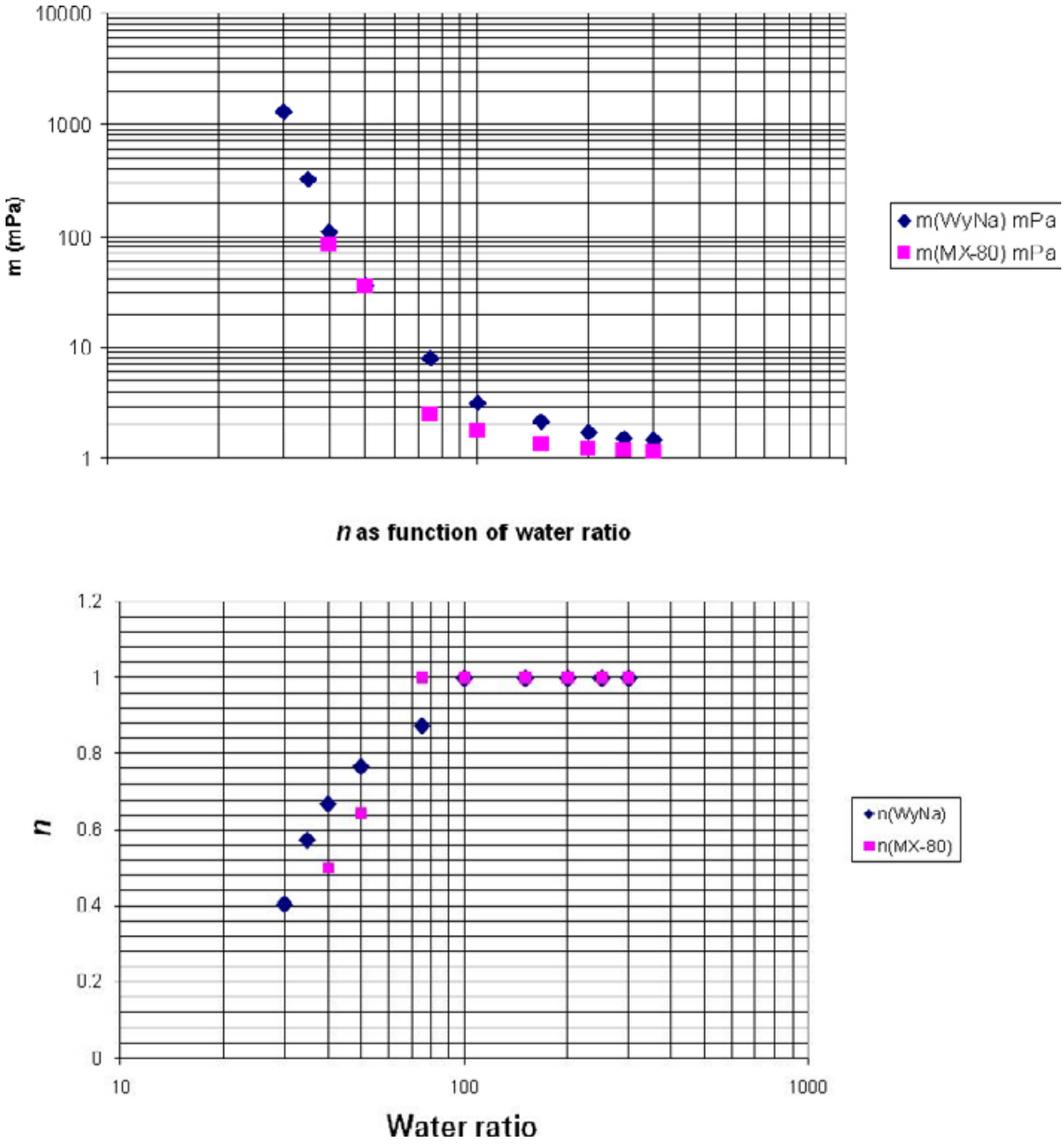

Figure 3-44. *Evaluation of the parameters m and n in Equation 3-6 as function of the water to solid mass ratio for MX-80 and WyNa in distilled water.*

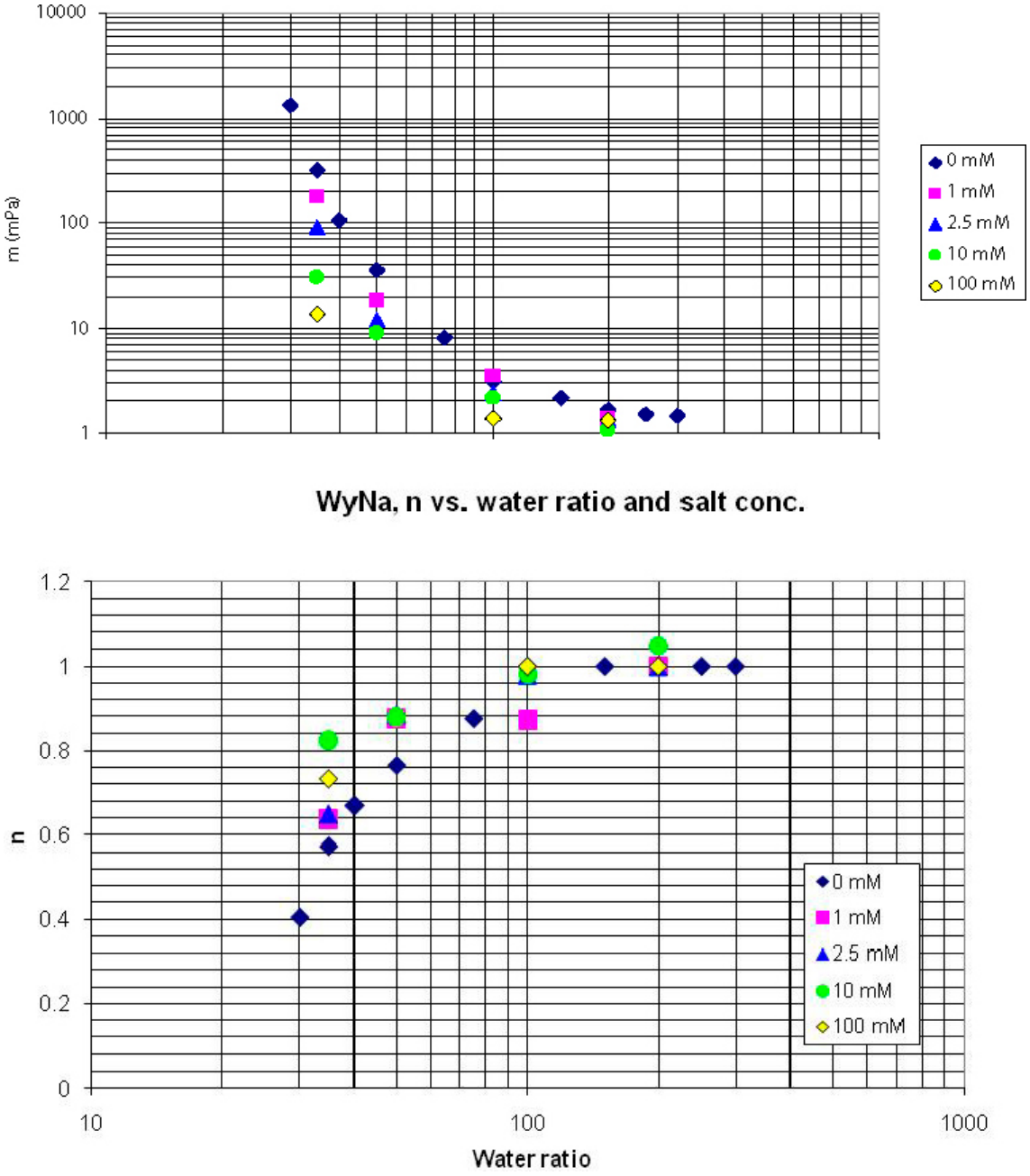

Figure 3-45. *Evaluation of the parameters m and n in Equation 3-6 as a function of the water to solid mass ratio for WyNa in water with different NaCl concentrations.*

The influence of NaCl concentration on WyNa is further illustrated in Figure 3-46. The *m* and *n* factors are plotted as a function of the NaCl concentration for clay/water systems with the water to solid mass ratio 35. The figure shows that at the water to solid mass ratio 35 WyNa never gets totally Newtonian. The *n*-value starts at n=0.55 at the NaCl concentration 0 and seems to stabilize at the $n \approx 0.8$ at NaCl concentrations higher than 5 mM. The *m* value though, strongly decreases with increasing NaCl concentration starting at m=0.4 Pa in water with zero NaCl concentration and ends at m=0.013 Pa in water with 100 mM NaCl concentration.

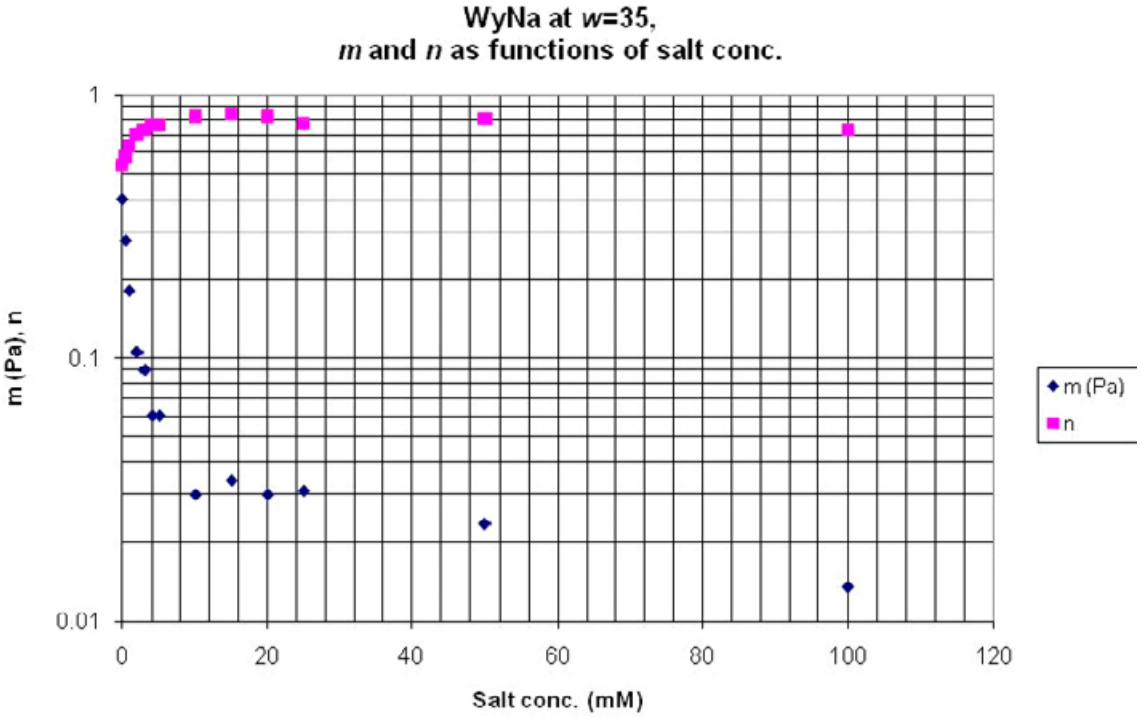

Figure 3-46. *Influence of salt concentration on the flow properties of WyNa at a water to solid mass ratio of 35. The values of m and n are plotted as a function of the NaCl concentration.*

3.8.3 Rheology tests

In the rheology tests the spindle rotates at the constant shear rate 0.5 1/s and the shear resistance is measured. Those tests can be used to evaluate the shear strength (failure stress) between the surface of the spindle and the sol. However, for gels this is not a good method to determine the shear strength of the material since the strength will be underestimated due to slipping between the spindle and the gel. Figure 3-47 shows the relation between the shear strength and the water to solid mass ratio of MX-80 and the influence of the salt concentration. Comparing these results at water to solid mass ratios below 40 to the shear strength measured with the vane (Section 3.8.4) reveals that the strength is significantly underestimated (factor of 10).

3.8.4 Vane tests

The results from the vane tests on MX-80 gels are summarized in Figure 3-48, which shows the measured shear strength as a function of water to solid mass ratio for the three different resting times. Although there is an obvious influence of resting time it is not as pronounced as measured earlier at lower water to solid mass ratios (see Figure 3-6).

Old measurements of shear strength at lower water to solid mass ratios are included in a double logarithmic diagram in Figure 3-49. The straight line seems to be a good model of the relation between shear strength and water to solid mass ratio.

3.8.5 Conclusions

Viscosity and rheology tests on MX-80 and WyNa clay/water systems have been made at different water to solid mass ratios varying from 25 to 300 in water with different NaCl solutions varying from 0 to 100 mM. The results have been evaluated and adapted to different models depending on the stiffness of the clay/water system.

Most sols could be tested in a viscometer and evaluated with the power law (Equation 3-6). A full set of parameters for this equation have been evaluated for those materials.

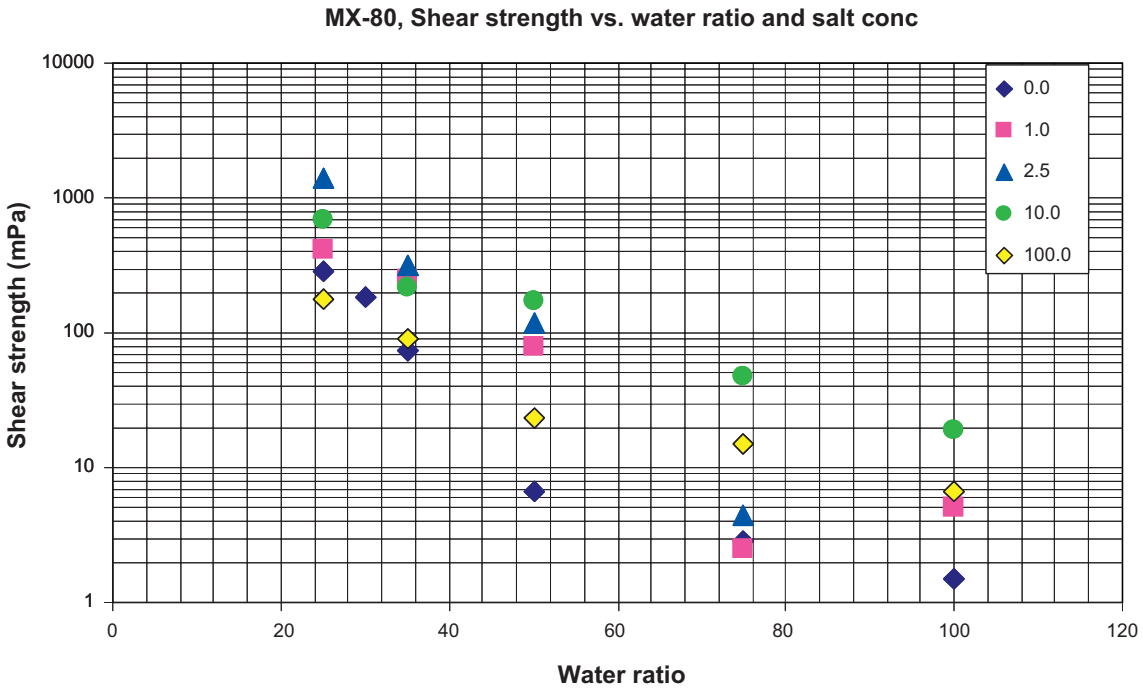

Figure 3-47. Shear strength of MX-80 measured with a rotating spindle as a function of the water to solid mass ratio in water with different NaCl concentrations in mM. Note that the strength is significantly underestimated and should not be used as data for modelling.

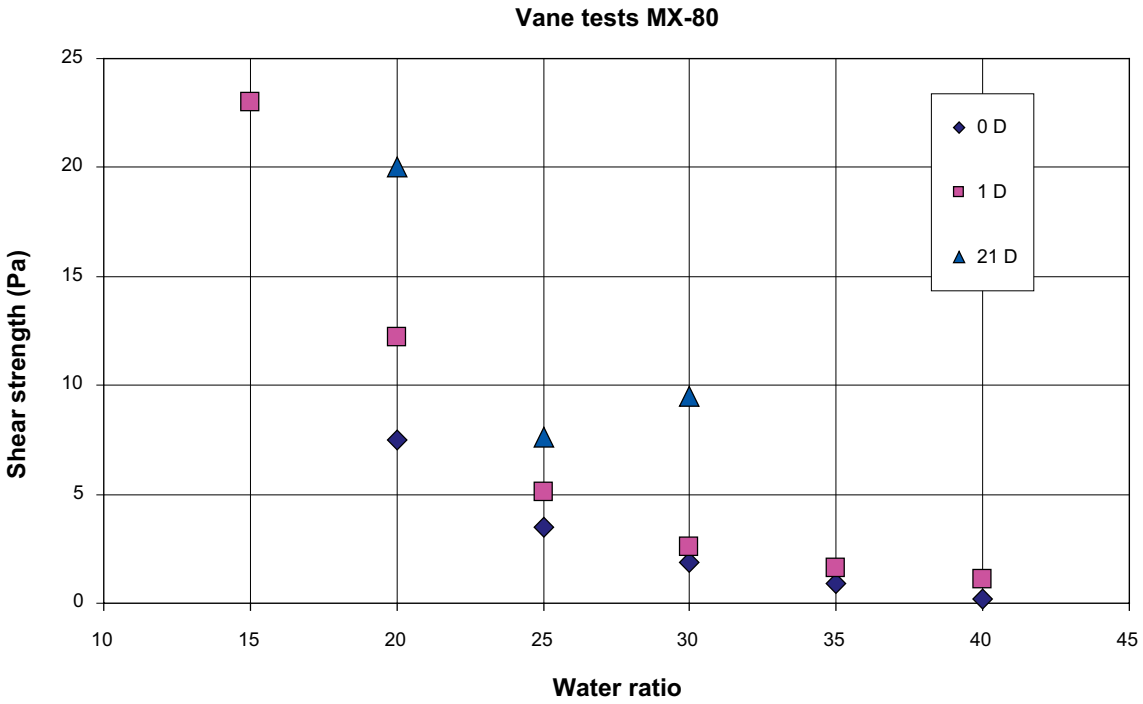

Figure 3-48. Measured shear strength of MX-80 in distilled water as a function of the water to solid mass ratio for three different resting times (Days).

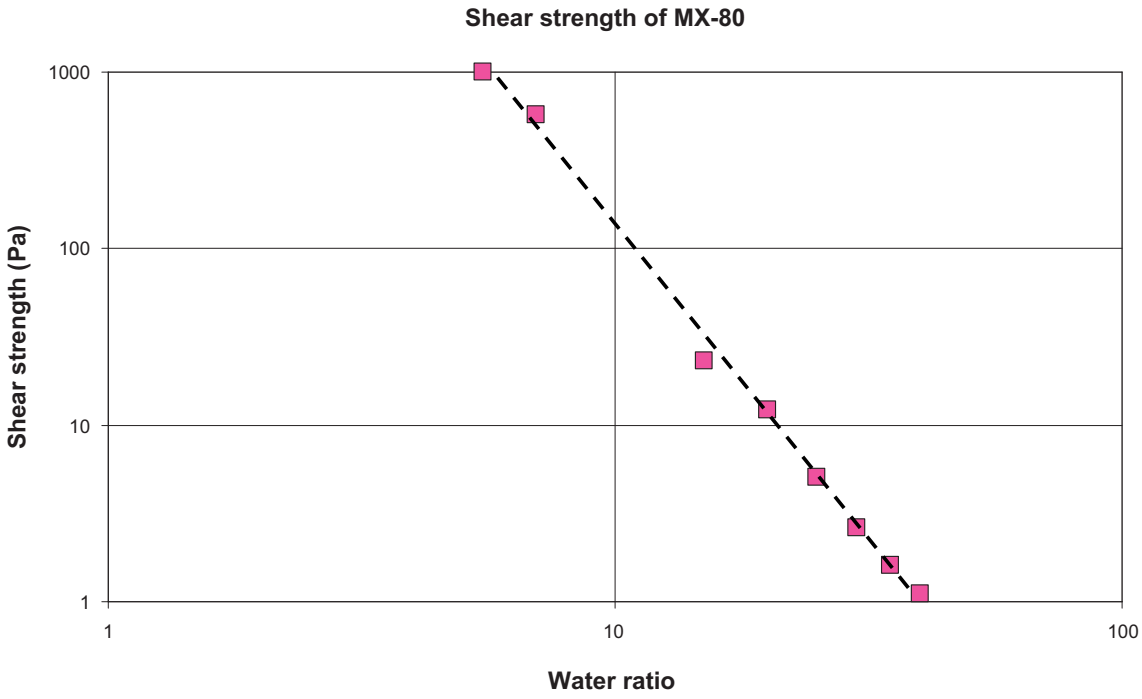

Figure 3-49. *Measured shear strength of MX-80 in distilled water as a function of water to solid mass ratio after 1 day of rest. Old measurements at low water to solid mass ratios are included.*

When the shear strength measured with the vane test exceeds about 1 Pa the power law is not suitable and instead the shear strength should be used for modelling the behaviour. For MX-80 in distilled water the limit is a water to solid mass ratio of about 35. A relation between shear strength and water to solid mass ratio has been evaluated for lower water to solid mass ratios.

Ca-bentonite seems to form a stable sediment with water to solid mass ratio well below 10, which has sand-like properties. These results together with other results in this report show that Ca-bentonite is not a problem due to the low swelling capacity and the inability to form colloids.

3.9 Modelling of the rate of bentonite loss

3.9.1 General

As noted in Section 3.2 there are three processes that drive the rate of bentonite loss in the fractures intersecting a deposition hole. These processes are swelling, erosion and sedimentation. All three must be included when modelling the loss of bentonite as a function of time. A way of estimating the time scale for swelling and erosion would be to model the rate of penetration into a fracture by swelling until the bentonite has been so diluted with water that the viscous properties allow the water flow past the deposition hole to transport the bentonite suspension.

Such a calculation would include two parts: at first the swelling of bentonite into the fracture opening and then the transport caused by the flow of the bentonite suspension in a hydraulic gradient. An attempt to estimate the first part of this calculation has been made in this section. It would probably also be possible to make an estimation of the second part if the boundary conditions are known because the viscous properties can be taken from the results derived in earlier sections, but this has not been done.

3.9.2 Swelling into a slot

Equation 3-4 derived in Section 3.3.2 can be used for modelling the swelling pressure distribution in a fracture.

$$\sigma = \sigma_1 \cdot e^{-2\tan\phi(\frac{z}{a})} \qquad (3\text{-}4)$$

where

σ = swelling pressure in the fracture at the distance z from the opening

σ_1 = swelling pressure in the deposition hole

a = fracture aperture

ϕ = friction angle between the bentonite and the fracture surface

z = distance from fracture opening

Figure 3-50 shows the swelling pressure distribution in a plane fracture with the aperture 0.1 mm at different friction angles calculated according to Equation 3-4.

Figure 3-50 shows that the swelling pressure drops rapidly. At the friction angle 10° it drops from 7 MPa at the deposition hole to below 10 Pa at 4 mm depth.

In order to be able to calculate the penetration rate not only the swelling pressure distribution but also the density or water to solid mass ratio distribution in the fracture must be known. Unfortunately no measurements of swelling pressure below about 40 kPa have been made so far due to measurement problems. However, according to such measurements at 40 kPa and higher (see /e.g. Börgesson et al. 1995/) the swelling pressure of MX-80 in distilled water is about 40 kPa at the void ratio e=10. In addition, estimations based partly on extrapolation of existing measured results and partly on the measured shear strength (the swelling pressure can be back-calculated from the strength shown in Figure 3-49 with the assumption of a friction angle of ~15º) indicate that the swelling pressure of MX-80 at the water to solid mass ratio 30 is about 10 Pa in distilled water. Water to solid mass ratio 30 corresponds to a void ratio of 73.

A probable void ratio vs. swelling pressure relation for MX-80 in distilled water would then look like in Figure 3-51.

Void ratio of a soil is defined as the ratio between the pore volume and the volume of the solids. In a water-saturated system the void ratio is related to the water to solid mass ratio through $e = w_r \times (\rho_s / \rho_w)$ where w_r is given by Equation 3-13 and ρ_s and ρ_w are the densities of the solid and water respectively.

3.9.3 Modelling of swelling time – example calculation

An example calculation of the rate of loss of bentonite can now be made with the following assumptions:

- The penetration into a fracture is only driven by the swelling pressure up to a water to solid mass ratio of 30 (no erosion or settling),
- At water to solid mass ratios higher than 30 the bentonite transport is driven by colloid dispersion, erosion and settling,
- The colloid dispersion etc. of bentonite is faster than the swelling into the fracture.

These assumptions mean that when the water to solid mass ratio exceeds 30 (void ratio exceeds 73) the bentonite can be assumed to be lost. The rate of bentonite loss can then be modelled in the following way: A fracture filled with bentonite with the swelling pressure and void ratio distribution according to Figure 3-50 and Figure 3-51 is modelled with ten finite elements according to Figure 3-52.

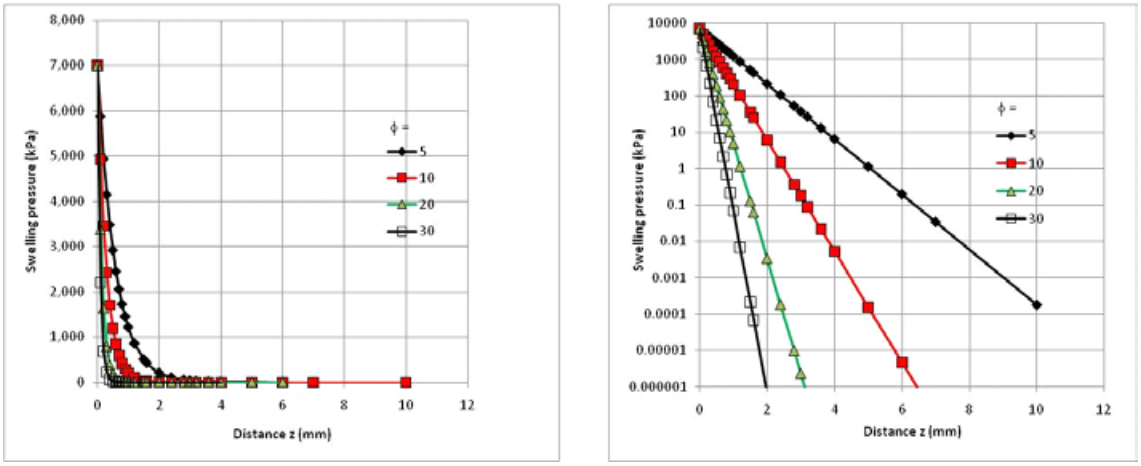

Figure 3-50. *Calculated swelling pressure as a function of depth after penetration of bentonite into a plane fracture with the aperture 0.1 mm at different friction angles.*

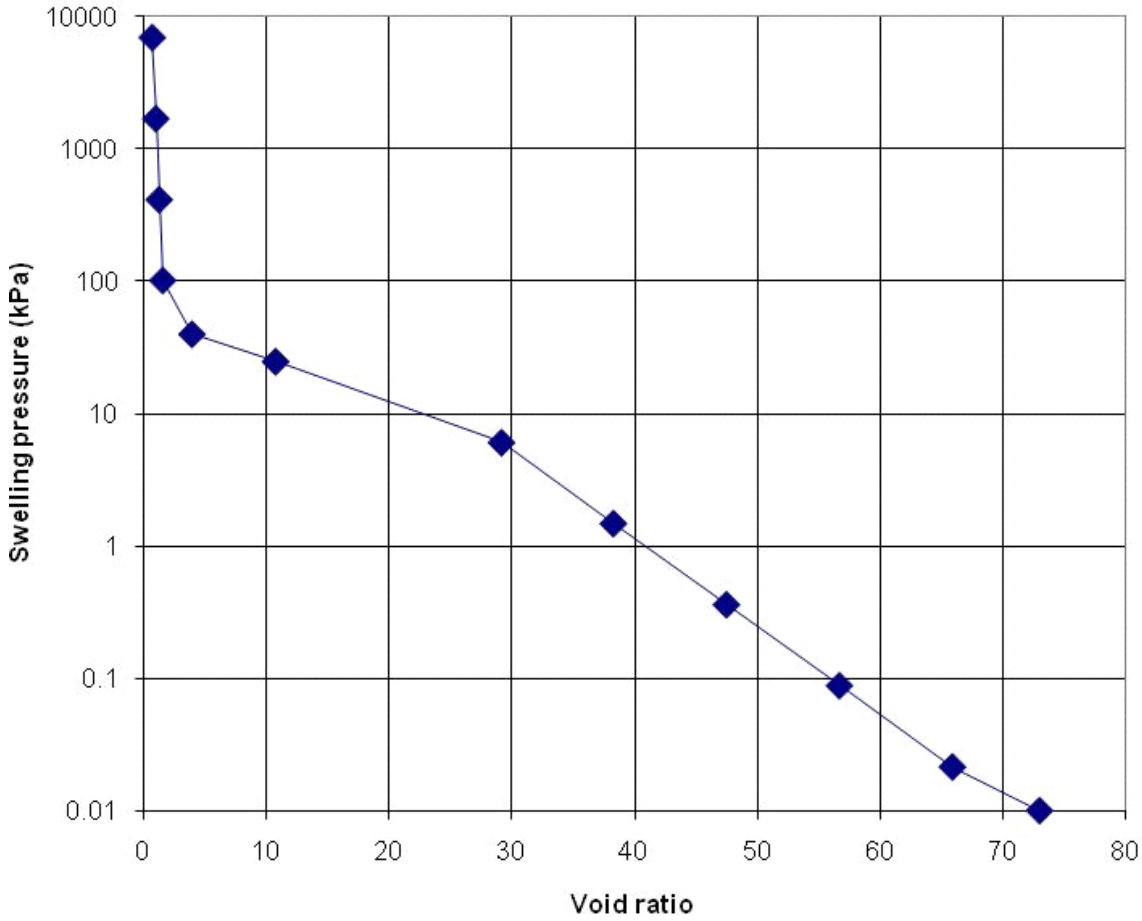

Figure 3-51. *Assumed relation between swelling pressure and void ratio for MX-80 in distilled water.*

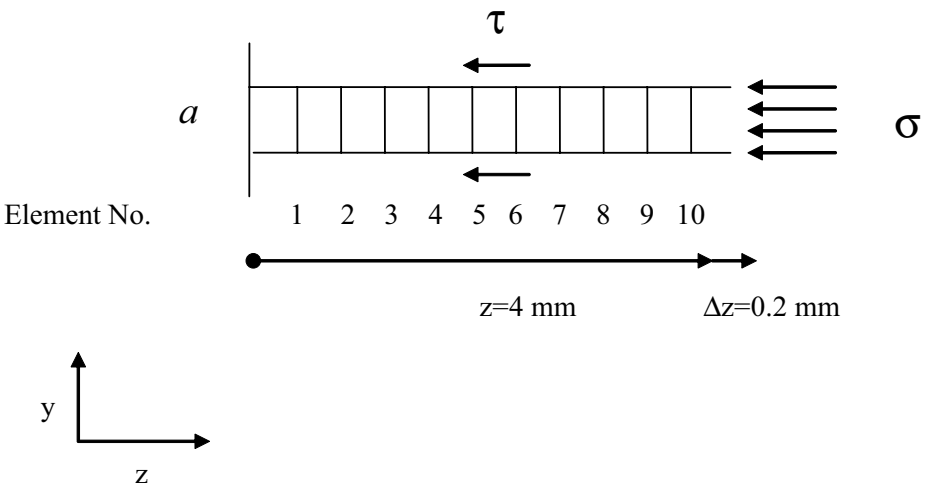

Figure 3-52. *Element mesh used for the penetration calculation. Aperture a=0.1 mm.*

With a friction angle of 10 degrees (conservatively chosen and based on triaxial tests on bentonite with high density – the results show that the friction angle increases with decreasing density) the penetration at the swelling pressure σ=10 Pa will according to Figure 3-50 be z=4 mm and the swelling pressure and void ratio at the right boundary are thus

σ = 10 Pa

e = 73

The purpose of the calculation is to study how long time it takes to replace a small amount of bentonite at the penetration front if the small amount of bentonite is assumed to be lost immediately.

In theory the modelling could start from time zero, but no such calculations have been possible to fulfil since there are large convergence problems due to the very large strains that occur. The end situation is likely to yield the same answer as Equation 3-4 since both are based on force equilibrium but Equation 3-4 does not take the time until equilibrium into account. So the initial conditions used for the modelling are taken from Equation 3-4 and only the time scale of the small swelling phase is modelled.

Outside the boundary in the model there is assumed to be a water filled slot with the depth Δz=0.2 mm that has lost its bentonite and thus contains only water. The bentonite wants to further penetrate the fracture since there is a swelling pressure and no limitation at the boundary. The slot is thus slowly filled as the swelling continues until equilibrium is reached.

The calculation of how the 0.2 mm swelling takes place has been done with finite elements and the same material models of porous materials that have been used for other swelling calculations (see /e.g. Börgesson and Hernelind 2006/). The finite element code ABAQUS was used. The boundaries of the fracture (i.e. the rock surfaces) are modelled with friction elements with the friction angle of 10 degrees. A constant swelling pressure of 7 MPa is applied at the left boundary (the deposition hole). A constant water pressure of 0 Pa is applied at the right boundary.

The porous elastic material model with the following properties was used.

ν = 0.4 (Poisson's ratio)

κ = see Table 3-4

The porous elastic modulus κ (see /Börgesson and Hernelind 2006/) and the initial conditions of the ten elements are shown in Table 3-4 where the void ratio and pressure correspond to the relation shown in Figure 3-51. The initial conditions of each element are thus different.

The hydraulic conductivity is made a function of the void ratio according to Table 3-5 (derived from /Börgesson et al. 1995/).

Table 3-4. Properties and initial conditions of the elements.

Element	κ	Void ratio (*e*)	Pressure σ (kPa)
1	0.2	0.77	7,000
2	0.2	1.05	1,708
3	0.2	1.33	416
4	0.2	1.62	102
5	6.5	10.8	24.8
6	6.5	29.2	6.05
7	6.5	38.3	1.48
8	6.5	47.5	0.36
9	6.5	56.7	0.088
10	6.5	65.9	0.0214

Table 3-5. Relation between hydraulic conductivity and void ratio.

Void ratio (e)	*K* (m/s)
0.4	$0.035 \cdot 10^{-13}$
0.6	$0.2 \cdot 10^{-13}$
0.8	$0.65 \cdot 10^{-13}$
1.0	$1.75 \cdot 10^{-13}$
1.5	$2.5 \cdot 10^{-12}$
2.0	10^{-11}
4	$5 \cdot 10^{-11}$
8	$2 \cdot 10^{-10}$
16	10^{-9}
30	$3.5 \cdot 10^{-9}$
45	10^{-8}
80	$3 \cdot 10^{-8}$

The calculation was done so that at first equilibrium was achieved in the model when the outer (10th) element is locked and not allowed to swell. Then the loss of bentonite was simulated by releasing this element and letting it and the other elements expand 0.2 mm.

3.9.4 Results

The interesting part is the time until the bentonite has filled the slot and the pore pressure thus dissipated to zero. Figure 3-53 shows the pore pressure evolution for each element when element 10 is released.

The swelling at the release of element 10 causes initially the pore water pressure in the bentonite in the slot to decrease since it is the pore water that resists the swelling, which needs to take place through water inflow. The swelling is completed when the pore pressure has returned to zero. Figure 3-53 shows that it takes about 2,000 seconds to fill the 0.2 mm deep space in the 0.1 mm wide fracture.

The void ratio of the filled space e=73 corresponds to a dry density of 37.6 kg/m^3, which with the void dimensions a=0.1 mm and Δz=0.2 mm results in a dry mass $\Delta m_s = 0.75 \cdot 10^{-6}$ kg bentonite being lost in Δt=2,000 seconds per meter fracture intersection.

Thus 1 kg bentonite (dry weight) will be lost in 85 years if the intersection of the fracture is 1.0 m. If the intersection is only 0.1 m it will take 850 years to lose 1 kg.

In order to see the influence of the fracture aperture, an identical calculation was made with a ten times smaller aperture (a=0.01 mm) and a ten times smaller swelling step (0.02 mm). According to Equation 3-3 the penetration depth is proportional to the aperture so the same swelling pressure and void ratio distribution will be achieved as in the 0.1 mm wide fracture but only to 0.4 mm. Figure 3-54 shows the results of the new calculation.

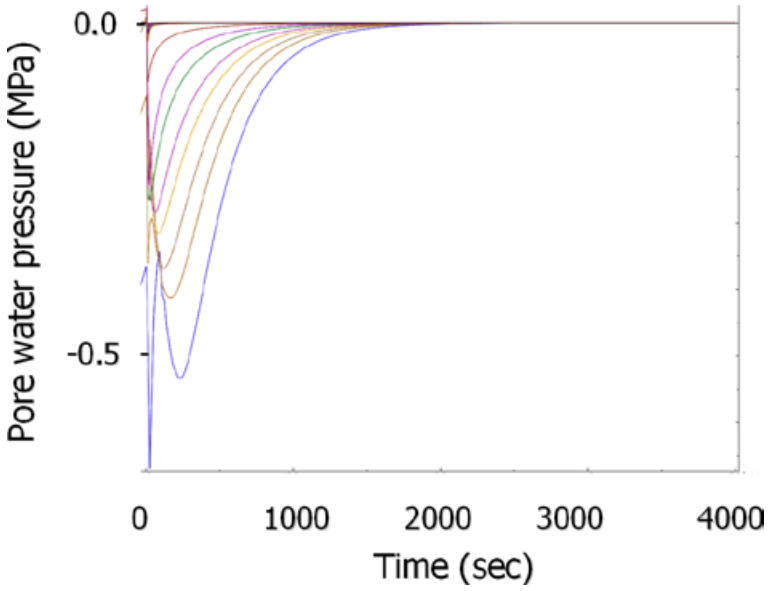

Figure 3-53. *Pore pressure evolution in the elements in the fracture during swelling to fill up the space where bentonite was lost. Fracture with the aperture 0.1 mm. The curves from left to right show the pore pressure evolution in the elements from the deposition hole to the water-filled slot.*

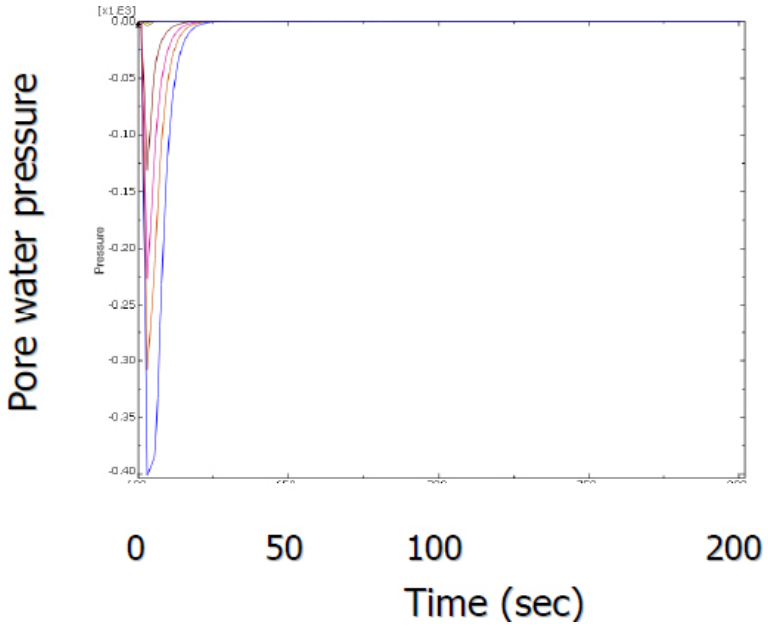

Figure 3-54. *Pore pressure evolution during swelling to fill up the space where bentonite was lost in a fracture with the aperture 0.01 mm.*

Figure 3-54 shows that it takes about 20 seconds to fill the 0.02 mm deep space in the 0.01 mm wide fracture.

The void dimensions a=0.01 mm and Δz=0.02 mm results in a dry mass $\Delta m_s = 0.75 \cdot 10^{-8}$ kg bentonite being lost in Δt=20 seconds per meter fracture.

Thus 1 kg bentonite (dry weight) will be lost in 85 years if the extension of the fracture is 1.0 m. If the extension is only 0.1 m it will take 850 years to lose 1 kg.

The same rate of bentonite loss will thus take place irrespective of the fracture aperture.

The reason for this performance is that although the mass is a factor 100 smaller the time will be a factor 100 faster since the penetration depth is a factor 10 smaller and the consolidation theory (or swelling theory) says that the time to equilibrium is the square of the distance to the water supply. The result is thus logical!

3.9.5 Sensitivity check

Many parameters used for the modelling are uncertain and in order to check the validity of the calculated rate of bentonite loss in the example calculation it is valuable to check the sensitivity to changes in those parameter values.

3.9.5.1 Friction angle

The friction angle ϕ=10º is used in the penetration model (Figure 3-50). This is probably too low a value that is valid for bentonites with high density (buffer density). Measurements at lower densities show that the friction angle increases with decreasing swelling pressure and density to $\phi \approx 17.5$º at the swelling pressure of 300 kPa and seems to continue to increase with further decreasing swelling pressure /Börgesson et al. 1995/. The friction angle has a rather strong influence on the penetration depth as shown in Figure 3-50. If ϕ=30º is used instead of ϕ=10º the penetration depth at the swelling pressure 10 Pa would only be 1.1 mm instead of 4 mm. Since the time to completed swelling is proportional to the square of the distance, the swelling will be about 13 times faster and 1 kg bentonite (dry weight) will be lost in 6.5 years instead of 85 years if the extension of the fracture is 1.0 m.

3.9.5.2 Swelling pressure – void ratio relation

The swelling pressure of gels is as mentioned previously not measured and the relation used in Figure 3-51 is rather uncertain. According to the theory of Poisson-Boltzmann /Evans and Wennerström 1999/ the relation between swelling pressure and void ratio will be according to Figure 3-55. These swelling pressure values are about a factor of 2 higher than the relation used in the calculation in the lower range of void ratio (e~10) and a factor of 100 higher in the upper range of void ratio (e~70). Observe that the Poisson-Boltzmann relation refers to purified Na-bentonite while the relation shown in Figure 3-51 refers to MX-80.

/Michot et al. 2004/ measured osmotic pressure of size-fractionated Wyoming Na-bentonite in low NaCl concentrations (10^{-2}–10^{-5} M). By equating the measured osmotic pressure and the swelling pressure a relation between void ratio and swelling pressure can be derived from those results. Such calculations yield swelling pressure – void ratio relation that is located between Poisson-Boltzmann and the values used in the example calculation.

The results from Poisson-Boltzmann can probably be considered an upper limit of the swelling pressure. If that relation is used the difference will depend on what boundary condition is used for when the bentonite is considered lost. The following two changes can be made:

1. The swelling pressure 10 Pa is used as boundary condition:

P=10 Pa will then correspond to the void ratio e=1,000 according to Poisson-Boltzmann's theory.

This case yields the same penetration depth 4 mm but a much higher average void ratio and thus much higher hydraulic conductivity. The hydraulic conductivity at such high void ratios is not known but would probably be several orders of magnitude higher than assumed in the calculation.

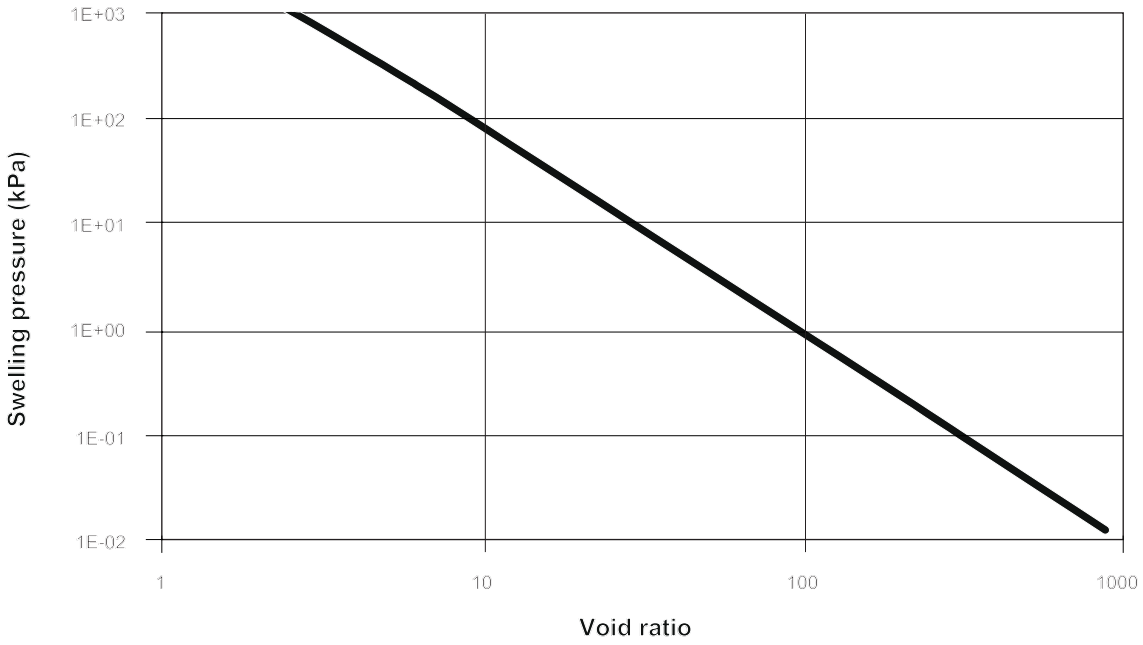

Figure 3-55. *Relation between swelling pressure and void ratio in a system of purified Na-smectite in distilled water according to the theory of Poisson-Boltzmann.*

The rate of bentonite loss would thus also be several orders of magnitude faster than for the calculation example.

2. The void ratio 73 is used as boundary condition:

e=73 will then correspond to the swelling pressure P=3 kPa according Poisson-Boltzmann's theory.

This case yields a penetration of only 2.2 mm instead of 4 mm. Since the average density is similar it means the same hydraulic conductivity of the gel and thus a much faster loss of bentonite (about a factor of 3 faster than the calculation example).

These examples show that the loss of bentonite will be faster if Poisson-Boltzmann's theory is used to describe the void ratio-swelling pressure relation instead of the relation used in the example calculation.

3.9.5.2.1 Hydraulic conductivity

The rate of bentonite loss is proportional to the hydraulic conductivity of the gel. Thus if the hydraulic conductivity is 10 times lower than assumed the loss will be 10 times slower. However, it is difficult to invoke such a change since the hydraulic conductivity that has been used in the example calculation is based on a relation that has been measured up to a void ratio of 20 and extrapolated above that value.

3.9.5.2.2 Boundary condition

The boundary where bentonite loss occurs is defined as having a swelling pressure of 10 Pa. This is a very uncertain figure. However, the influence on the results is not strong. If the boundary swelling pressure is decreased by a factor 1,000, i.e. to 0.01 Pa, the penetration depth for the calculation example will be about 6 mm instead of 4 mm. This yields an increased time until completed swelling with a factor 2.25, i.e.1 kg bentonite (dry weight) will be lost in 190 years instead of 85 years if the extension of the fracture is 1.0 m.

3.9.6 Conclusions

The modelling shows that the rate of bentonite loss, due to swelling from the buffer until the water to solid mass ratio of the swelling gel in the fracture is above 30, is the same irrespective of the fracture aperture. Only the length of fracture intersection has an effect on the time scale. Since the loss is rather fast (1 kg in 85 years for the fracture width 1 m) this process will probably not limit the bentonite transport.

The uncertainty of the data is rather large but the sensitivity to changes does not change the conclusion that the swelling rate cannot limit the bentonite loss. Most relevant changes yield an *increased rate*. Only a strongly reduced hydraulic conductivity can strongly reduce the rate of the loss since the swelling rate is proportional to the hydraulic conductivity.

3.10 Conclusions

Transport of bentonite particles from the buffer in a deposition hole into an intersecting fracture and further away can be divided into the following three main processes:

1. Transport of bentonite particles in still water by repulsion (swelling).
2. Transport by fluid flow driven by a water pressure gradient (viscous flow and erosion).
3. Transport driven by gravity (sedimentation).

Processes 1 and 3 are treated as “two-phase” problems with transport of clay particles in the water phase. For the second process the clay/water system is considered as a “one-phase” problem with water and particles transported together. The latter process has in the present project been investigated with rheological tests and modelled with rheological models.

Montmorillonite dominated clay/water systems exhibit very complicated rheological behaviour. The rheological properties are (in addition to water content and water chemistry) largely influenced by mixing procedure, chemical and mechanical history and resting time. Since it is impossible to test the rheological properties at realistic geometry and time scale the results from such measurements need to be treated with care and the sensitivity to changes of properties need to be carefully considered.

Rheology tests on MX-80 and WyNa clay/water systems have been made at different water to solid mass ratios varying from 25 to 300 in water with different NaCl solutions with NaCl concentration varying from 0 to 100 mM. The results have been evaluated and adapted to different models depending on the viscous properties of the clay/water system.

Most results could be evaluated with the power law relation (Equation 3-6). A full set of parameters for this equation has been evaluated for MX-80 and WyNa clay/water systems.

When the shear strength measured with the vane test exceeds about 1 Pa the power law is not suitable and instead the shear strength should be used for modelling the behaviour. For MX-80 in distilled water that limit is a water to solid mass ratio of about 40. A relation between shear strength and water to solid mass ratio has been evaluated for lower water to solid mass ratios.

Corresponding Ca-bentonites could not be tested with the rheological equipment or evaluated with those models since Ca-bentonite separates from the water, sediments to the bottom of the container and behaves as a friction soil with a water to solid mass ratio of about $w = 5$.

The penetration of MX-80 driven by the first process (transport of bentonite particles in still water by repulsion) into hypothetical fractures has been modelled for MX-80 in distilled water with the assumption that the bentonite is lost by diffusion and fluid flow when the clay concentration in the water has decreased to a certain level. The modelling shows that the rate of bentonite loss, due to swelling from the buffer until the water to solid mass ratio of the swelling gel in the fracture is above 30, is the same irrespective of the fracture aperture. Only the fracture width has an effect on the time scale. Since the loss is rather fast (1 kg in 85 years for the fracture width 1 m) this process is not expected to limit the bentonite transport if the bentonite is lost with at least the same rate by other processes at higher water to solid mass ratios.

The uncertainty of the data is rather large but the sensitivity analyses do not change the conclusion that the swelling rate cannot limit the bentonite loss. Most relevant changes yield an increased rate of bentonite loss. Only a strongly reduced hydraulic conductivity compared to the calculation example can strongly reduce the rate, which is caused by direct proportionality between hydraulic conductivity and swelling rate.

The bentonite transport mechanisms in distilled water are summarized in Table 3-6.

Table 3-6. Overview of the three bentonite transport processes in a fracture for the special case of distilled water and the models or parameters used for analysing them. Processes investigated and reported are marked yellow.

Phase		Properties		Bentonite transport model		
		WyNa in distilled water	MX-80 in distilled water	Radially (swelling)	Tangentially (viscous flow and erosion)	Axially (sedimentation)
A	Solid mass τ_f >1 kPa	w<10	w<5	A_R. Hydro-Mechanical friction	A_T. None	A_A. None
B	Gel 1 Pa <τ_f < 1 kPa	10<w<35	5<w<35	B_R. Hydro-Mechanical friction	B_T. Rheological stress/strain relation	B_A. None?
C1	Semi-fluid	35<w<100	35<w<70	$C1_R$ Hydro-Mechanical friction (?)	$C1_T$ Non-Newtonian viscosity,Power law	$C1_A$ Diffusion controlled aggregation?
C2	Fluid	100<w<1,000	70<w<500	$C2_R$ Diffusion?	$C2_T$ Viscosity, Newtonian	$C2_A$ Diffusion controlled aggregation
D	Water	w>1,000	w>500	D_R. Diffusion?	D_T. Viscosity of water	D_A. None?

4 Filtering

4.1 Introduction

It is known from earlier experiments that colloid particles can penetrate filters. A central issue is to determine under which circumstances this would happen. This work tries to answer the question of what physical barriers can stop colloids.

A number of tests have been made with both untreated MX-80 bentonite and homoionic sodium and calcium converted montmorillonite. Filters of different pore sizes have been tested. Combinations of these and filler materials such as kaolinite or diatomite as well as accessory minerals extracted from MX-80 were also tested.

Test time ranged from one to two months. Long term stability has not been tested. A number of combinations leaked colloids and suffered subsequent loss in swelling pressure. In some cases this leaking was so rapid that half of the swelling pressure was lost within 3 days.

4.2 Test methods

To test if colloids could penetrate a filter with a given pore size clay samples were placed in a test cell, saturated and water circulated over the filter. The swelling pressure and amount of particles in the water was measured. The test set-up is illustrated in Figure 4-1. Erosion of the tested material will lead to a lowering of the density of the (remaining) clay in the cell and a corresponding drop in swelling pressure. Thus, by monitoring swelling pressure as a function of time, information on the erosion process is gained.

4.2.1 Test cell

The test cell used is a 35 mm diameter cell with filters on both sides. Normal sample height is 5 mm. The swelling pressure was measured with load cells. Materials in the test cell are titanium in the ring and PEEK in the bottom and the piston, both highly inert materials that have been tested previously. On the backside of the filters there is a channel where water can be circulated by use of a peristaltic pump, see Figure 4-1.

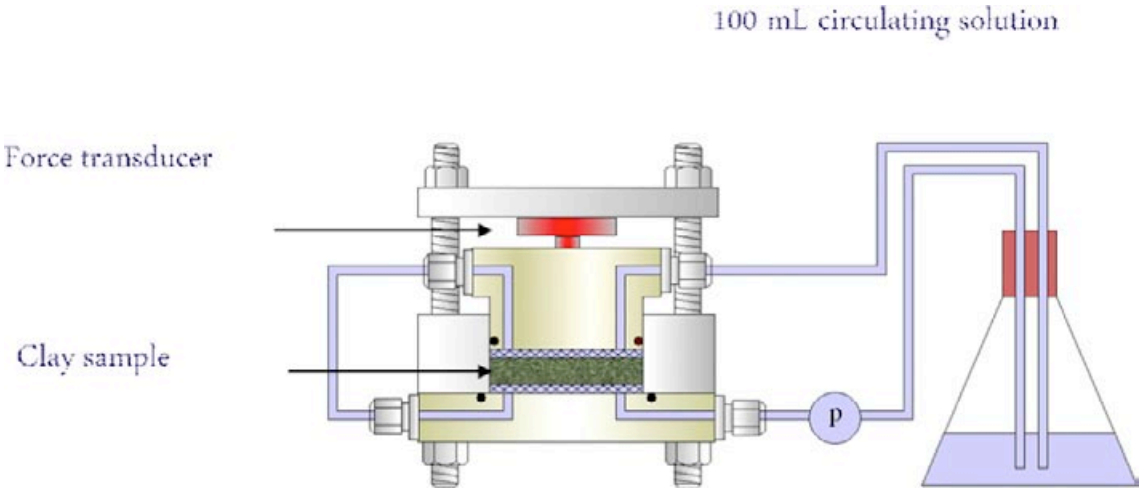

Figure 4-1. *Schematic illustration of the test set-up.*

4.2.2 Filters

The filters were sintered titanium or stainless steel. The thickness of the filter was 2 mm with a pore size ranging from 0.2 µm to 100 µm. Before each experiment they were cleaned in ultrasonic bath and repeatedly rinsed in deionized water to remove all loose materials.

The porosity of the filters varied from 11.6% to 54.9% calculated from the dimensions and mass of the filters, see Table 4-1

$$\phi = \frac{V_V}{V_T} \tag{4-1}$$

where ϕ is the porosity, V_V is the volume of void space and V_T is the total volume.

4.2.3 Measurements

The swelling pressure is measured with load cells. These are calibrated against a standard force ring before and checked after each test. The readings are recorded in a data acquisition system.

Turbidity was measured in the circulating water with a Eutech TN-100 turbidimeter. It is a clear indication whether colloids are present or not. The turbidity values can also be translated to a mass clay/volume number. A more detailed description of measuring turbidity is found in Section 5.2.

4.3 Materials used

The clays used were untreated MX-80 bentonite, as well as purified montmorillonite in two homoionic forms, sodium and calcium, Wy-Na and Wy-Ca respectively. Kaolinite and diatomite are tested as fillers both in a separate layer and mixed with Wy-Na (kaolinite).

Accessory minerals from MX-80 were collected from the coarse material that was rejected as larger than 2 µm in the previous process. The material was repeatedly washed and water soluble ions and colloid particles were rinsed from the accessory minerals. The material was dried at 60°C.

All samples were made to target buffer density, $\rho_{saturated}$ = 2,000 kg/m^3 (ρ_{dry} = 1,570 kg/m^3). Small variations in mass, volume of test cell and filter will end in deviating density leading to variation in swelling pressure.

Deionized water (electric conductivity < 1µS/cm) was used as circulating solution.

4.4 Results

4.4.1 10 µm filter

The first test was to see the difference, if any, between MX-80, Wy-Na and Wy-Ca. After an initial saturation phase without circulation, the circulation with 1 ml/min was started. As can be seen in Figure 4-2 below, the Wy-Ca sample maintained its initial swelling pressure while Wy-Na and MX-80 started to erode almost immediately. The solutions of water and clay from the MX-80 sample were measured with regard to turbidity and electric conductivity, and at the beginning the solution was replaced daily (workdays) with deionized water, see Figure 4-3.

Table 4-1. Filter porosity for used filters.

Filter	Porosity Φ
0.5 µm Ti	0.116
2 µm Ti	0.314
10 µm SS	0.380
40 µm SS	0.471
100 µm SS	0.549

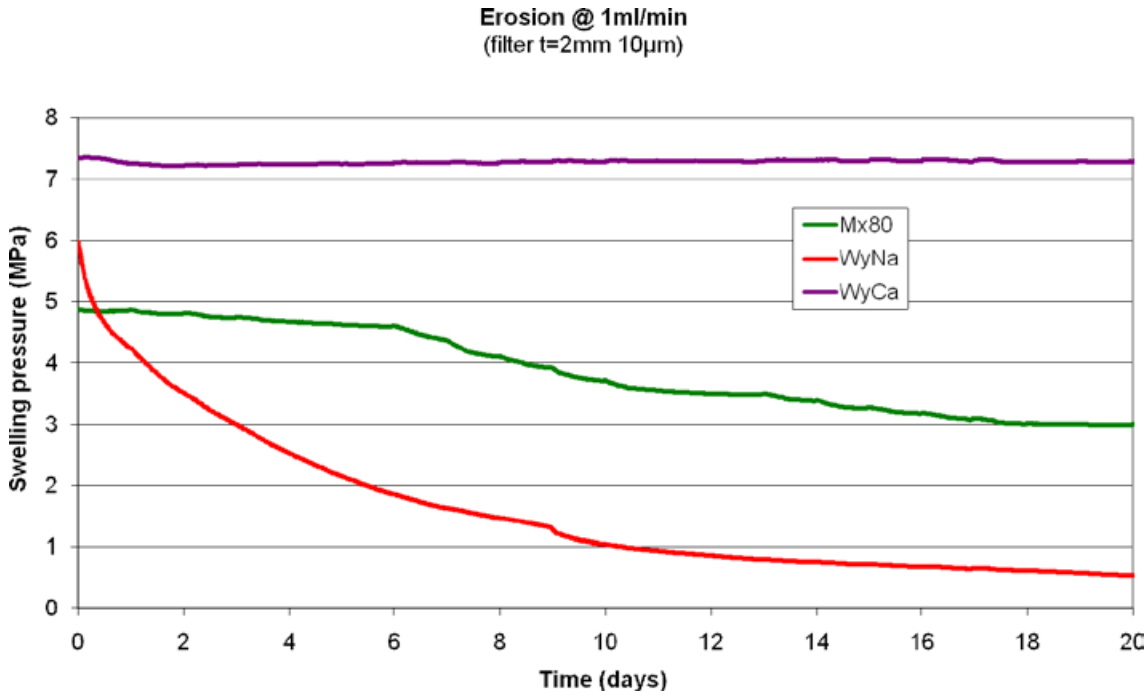

Figure 4-2. *Swelling pressure as a function of time for MX-80, Wy-Na and Wy-Ca samples flushed over 10 µm-filters.*

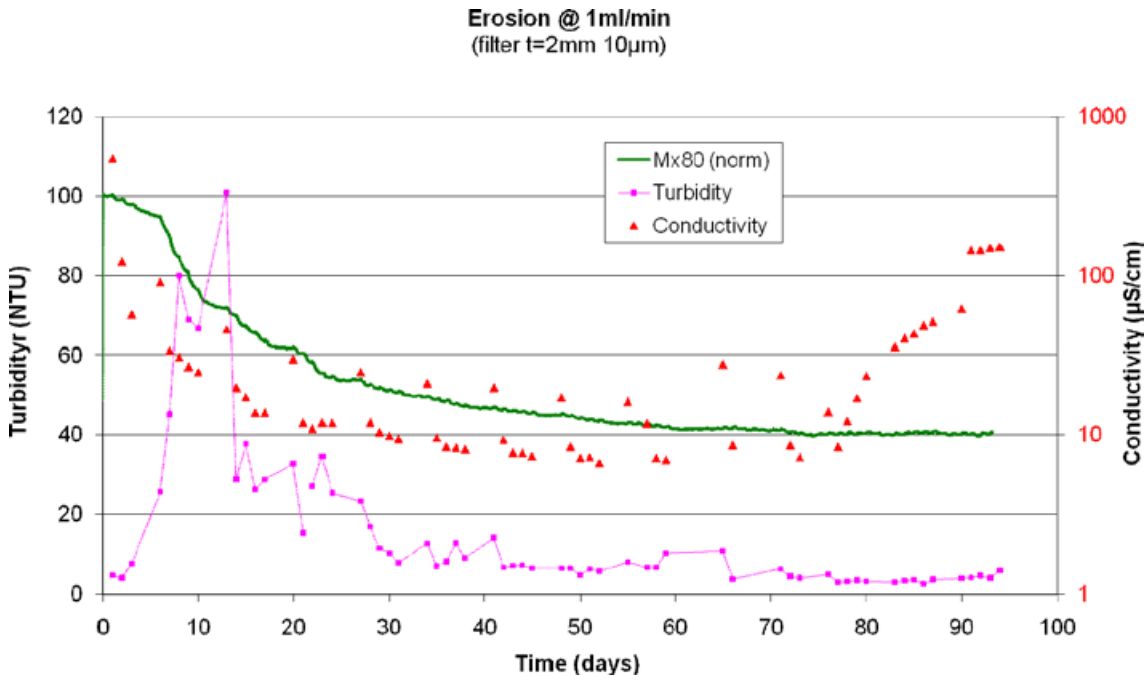

Figure 4-3. *The full evolution in time of swelling pressure (normalized), turbidity and electric conductivity of the MX-80 sample flushed over a 10 µm-filter. At 78 days replacement of water stopped and the same solution circulated continuously.*

A close examination of the drop in swelling pressure shows that it corresponds to lower electric conductivity. Already at day 60 (after holidays) the drop in swelling pressure had diminished and the electric conductivity was high. After 78 days the same solution was circulated continuously, which resulted in an increasing electric conductivity indicating the presence of ions in the solution, probably originating from dissolution of gypsum in the clay. Also the swelling pressure stabilized showing that erosion is halted due to the presence of excess ions in the circulating solution. These chemical or ion strength effects are further discussed in Section 7.5.

4.4.1.1 2 µm filter

To determine which pore size in the filter would stop Wy-Na and MX-80 from eroding new tests with 2 µm filters were made. Figure 4-4 shows the result, which is almost the same as in the case of 10 µm filters.

4.4.1.2 0.2–0.5 µm filter

Since the 2 µm filter did not stop the colloids, new tests with even finer filters were made. With these filters the swelling pressure remained constant for Wy-Na with both 0.2 and 0.5 µm filters and no colloids could be observed in the solution, Figure 4-5.

4.4.1.3 40–100 µm filter

Since no erosion could be observed for calcium montmorillonite (Wy-Ca) for the 10 µm filter, new tests were made with coarser filters. As can be seen in the Figure 4-6, the swelling pressure remained constant in both cases. A small initial drop can be observed in the test with the 100 µm filter and could be explained with some clay that propagates into the filter but no colloids could be observed in the solution.

This test shows that the sol phase is absent in the phase diagram of Ca-montmorillonite. Even the tiniest loss of montmorillonite would be manifested as a drop in swelling pressure as exemplified in the calculation. In Figure 4-7 the swelling pressure, P is plotted versus dry density, ρ_{dry} for Wy-Ca. The data taken from Table 4-7 of the report by /Karnland et al. 2006/ can be perfectly fitted to an empirical swelling pressure function of the form.

$$P = A\exp(B\rho_{dry}), \tag{4-2}$$

where A=0.5153 kPa and B=6.3739 cm^3g^{-1}. By differentiating Equation 4-2 we obtain an equation that relates a change in swelling pressure, ΔP to a clay mass loss, Δm

$$\Delta P = BP\Delta\rho_{dry} = BP\frac{\Delta m}{V}, \tag{4-3}$$

where V is the volume of the clay sample, in this case equal to $\pi \times 3.5^2 \times 0.5/4 = 4.8$ cm^3. A drop in swelling pressure of 100 kPa would be easily detected and at a swelling pressure of 5.5 MPa as in Figure 4-6 such a decrease would according to Equation 4-3 correspond to a mass loss of 14 mg. Furthermore, 14 mg clay in 100 ml (circulating) solution is well above the turbidity detection limit (<0.5 NTU). For Wy-Na a clay concentration of 0.14 g/l gives a turbidity of 16 NTU and Wy-Ca is found to be more turbid. Thus the absence of measurable turbidity at the initial drop in swelling pressure corroborates the explanation that clay penetrates into the filter but is not further eroded by the circulating deionized water.

4.4.1.4 Influence of gravity

In the previous tests the solution circulated on both top and bottom filter. To test if there was a difference due to gravity, two test cells with Wy-Na were prepared with 2 and 10 µm filters and the circulation on top and bottom was separated so colloids could be measured on both sides, see Figure 4-8. The same water circulated between the measurements and was exchanged simultaneously for all reservoirs when the turbidity values started to reach 800 NTU since the meter has an upper limit of 1,000 NTU. The initial values showed almost the same turbidity until after 11 days when the 10 µm filter started to rise, but after the next solution exchange it was the top 10 µm filter that had values above mean as can be seen in Figure 4-9. Gravity does not appear to influence the colloid release at these swelling pressures.

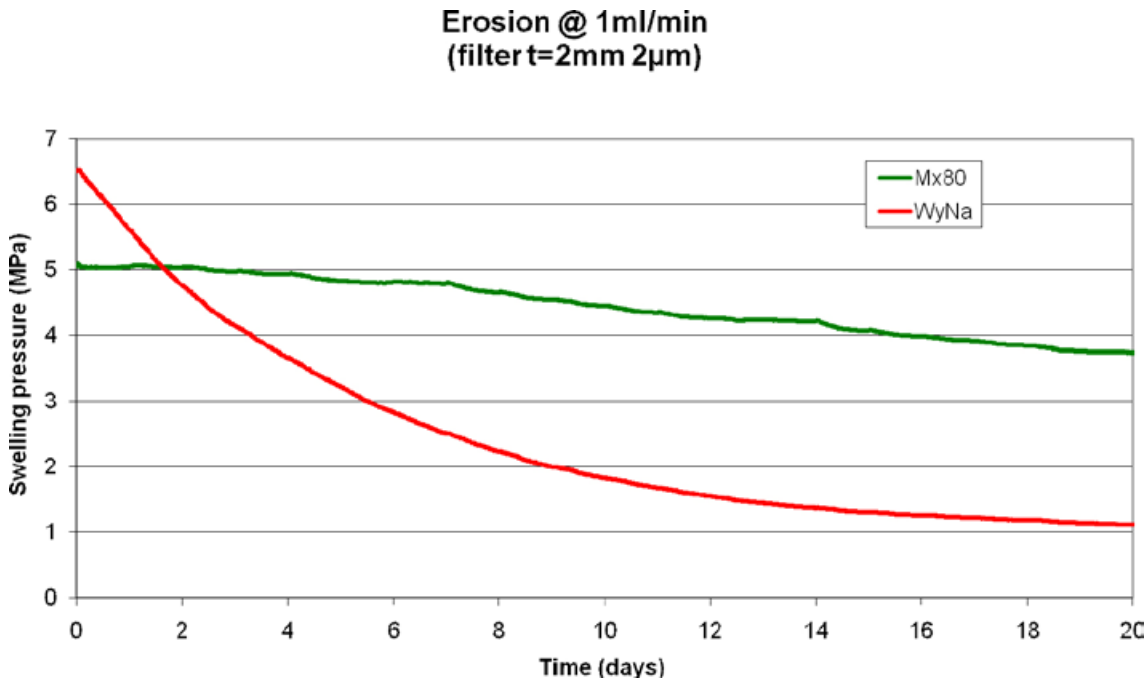

Figure 4-4. *Swelling pressure as a function of time for MX-80 and Wy-Na samples flushed over 2 µm-filters.*

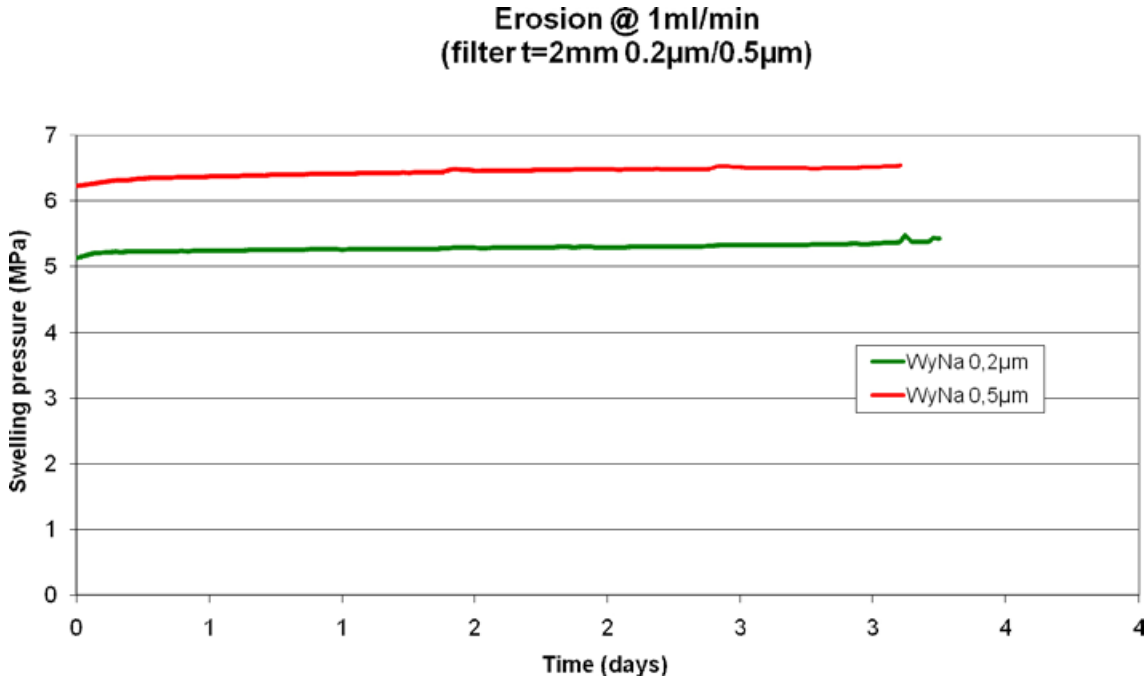

Figure 4-5. *Swelling pressure as a function of time for Wy-Na samples flushed over 0.2 and 0.5 µm-filters.*

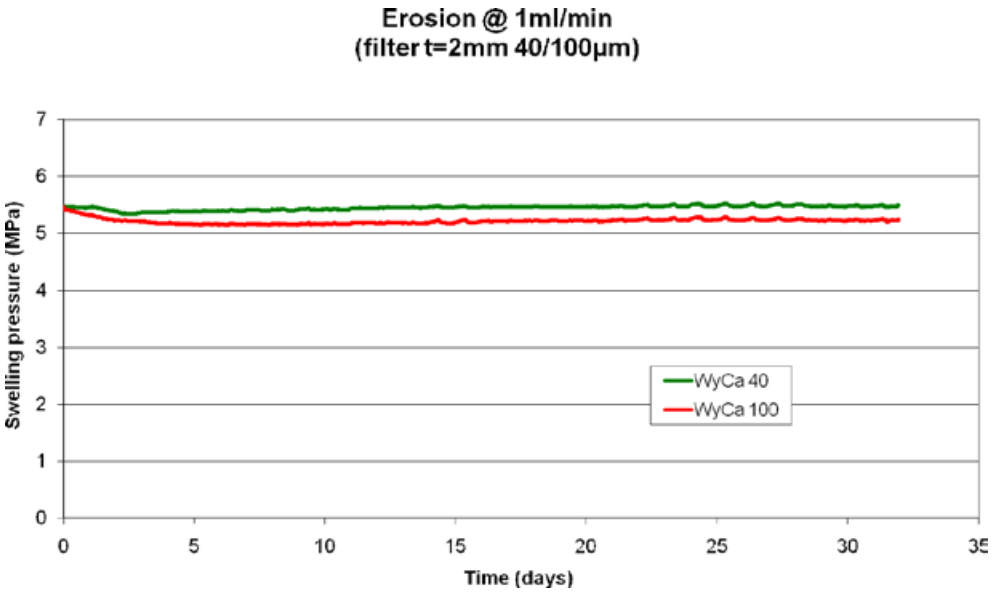

Figure 4-6. *Swelling pressure as a function of time for Wy-Ca samples flushed over 40 and 100 µm filters.*

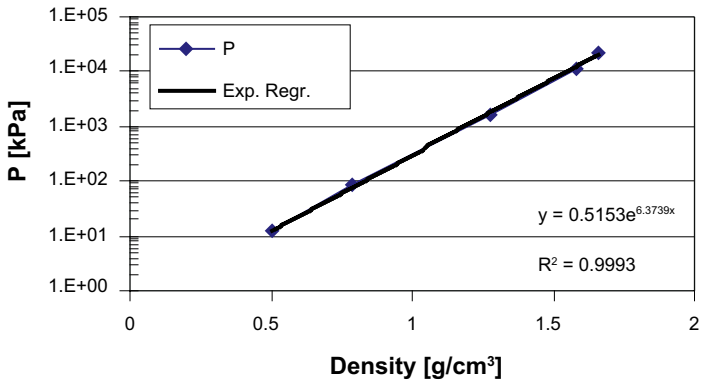

Figure 4-7. *Swelling pressure[kPa] vs. Wy-Ca dry density [g/cm³].*

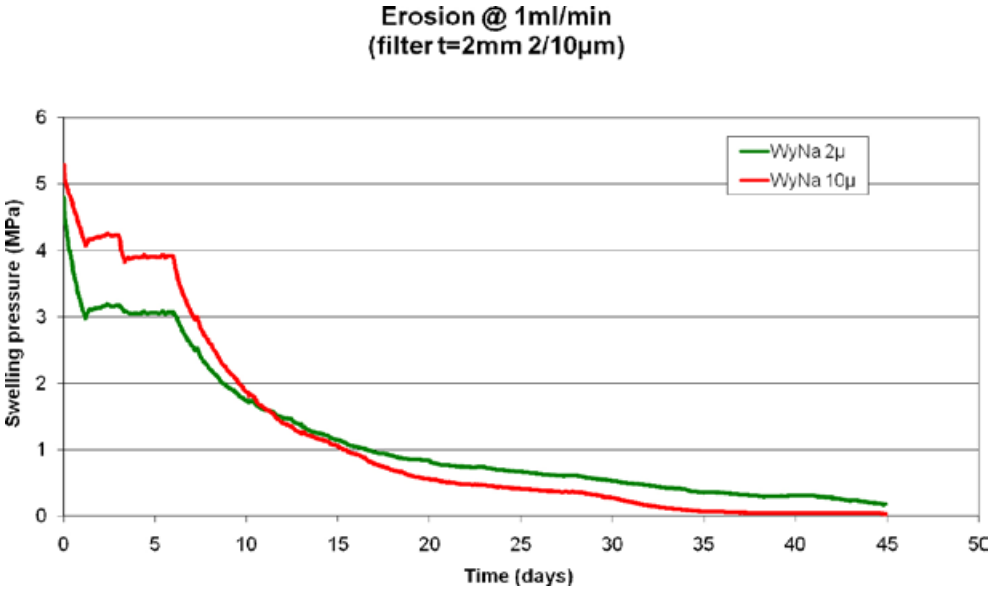

Figure 4-8. *Swelling pressure as a function of time.*

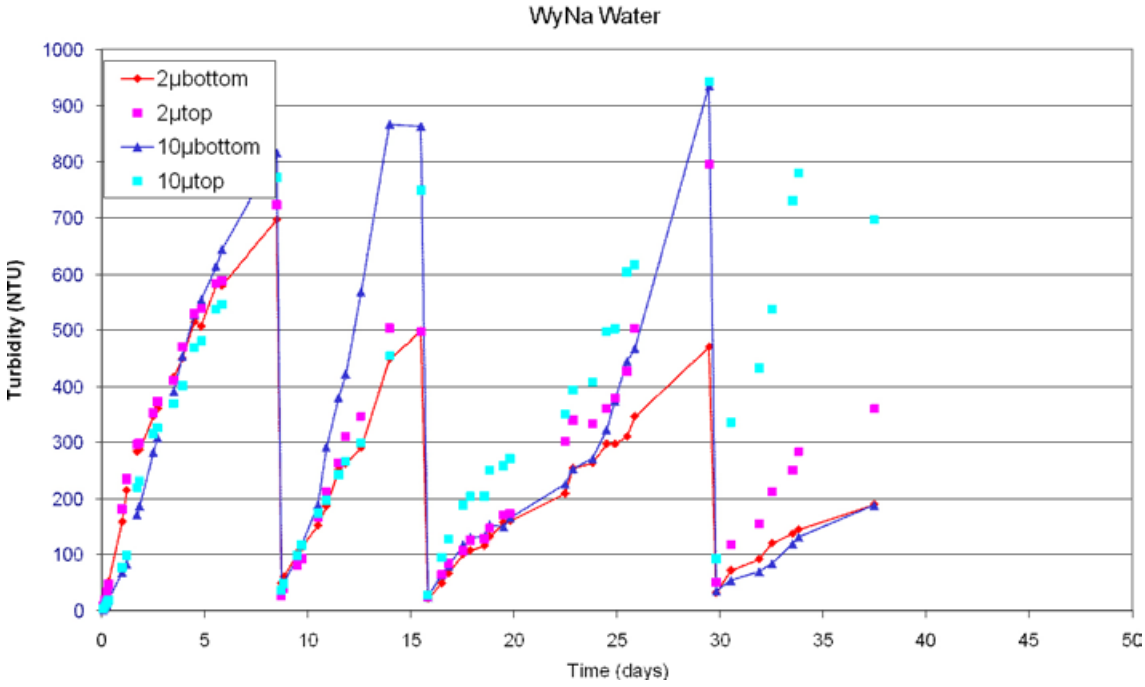

Figure 4-9. *Turbidity as a function of time.*

4.4.1.5 Influence of thicker filters

The question whether a thicker filter would stop or just delay the erosion was addressed with a new experiment. A test with three 2 µm filters on one side of the clay sample and a single filter on the other side, with separate circulation on top and bottom, was performed. When the water circulated on both sides, colloids were found on the single filter side. When the circulation was only on the triple filter side the swelling pressure drop was small but consistent as shown in Figure 4-10. The test cell was also inverted to see if orientation mattered, which it did not. The combination of three 2 µm filters only delayed the erosion.

4.4.1.6 Filler tests

Knowing that colloids could be stopped by a filter with a pore size less than 0.5 µm, tests were conducted with natural filler materials between the clay sample (Wy-Na) and the 10 µm steel filter in the test cell (see Figure 4-1): kaolinite, diatomite and MX-80 accessory minerals. In order to compare the effectiveness the same dimensions as the metal filters, 2 mm thick, was chosen for the filler dimensions.

The first test was a 2 mm thick layer of compacted kaolinite with Wy-Na bentonite. To make sure the kaolinite did not affect the bentonite, circulation on one side with two stacked standard filters was made. After an initial drop, the swelling pressure stabilized and no outflow of colloids could be detected (circulation only on the kaolinite side) see Figure 4-11.

Mixtures of Wy-Na and kaolinite in different proportions were then tested. The first test was a 50/50 by weight mix. The results are shown in Figure 4-12: initially there was a drop in swelling pressure and it dropped again slightly when the water was changed, but later it stabilized. In the long run a small leakage and subsequent drop in pressure can be seen. The hydraulic conductivity of the mix was $3.3 \cdot 10^{-12}$ m/s which is of the same order as MX-80 with a dry density of 600 kg/m^3 (saturated density 1,382 kg/m^3). Results from the 50/50 test were initially encouraging enough to test 80/20 and 90/10 mixes, shown in Figure 4-13. The 90/10 mix continued to lose swelling pressure but the 80/20 mix reached equilibrium at 1 MPa.

The second test was with diatomite, (diatomaceous earth or kieselguhr). Again a 2 mm thick compacted layer was used as a filter. Results are presented in Figure 4-14, where small variations in swelling pressure are seen but no apparent loss. Small amounts of particles were detected in the circulating water (2–4 NTU) which also had low electric conductivity measured (3–5 µS/cm).

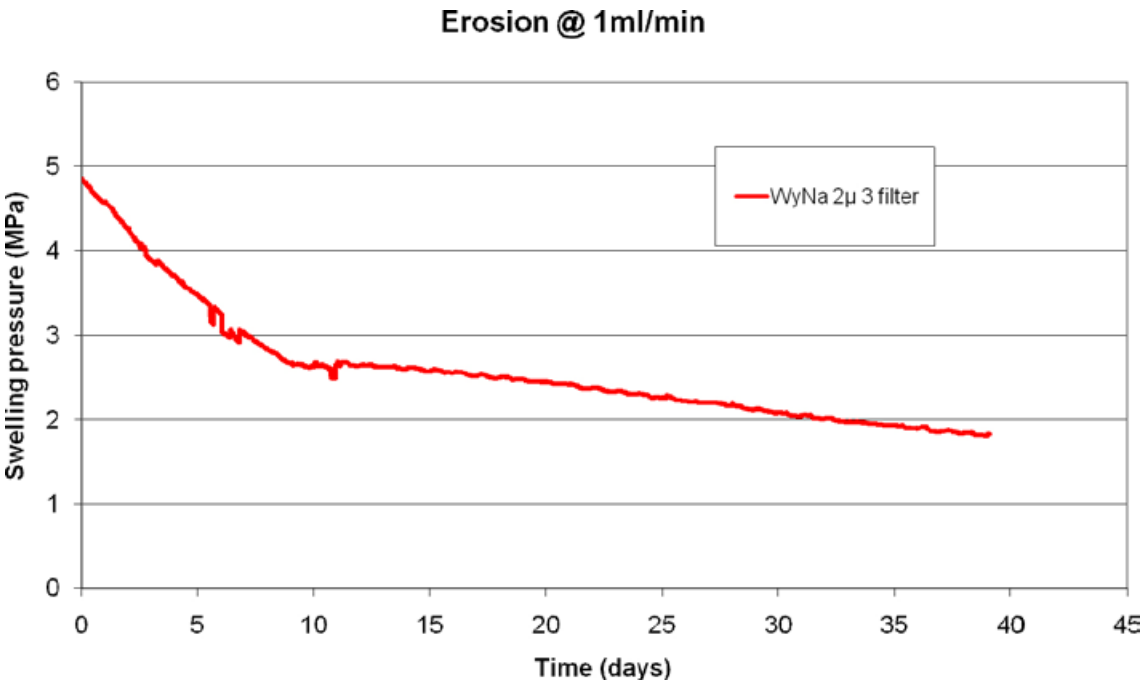

Figure 4-10. *Swelling pressure as a function of time for a Wy-Na sample in a test cell with a single filter on one side and three stacked filters on the other. After day 10, circulating water was applied only to the triple-filter side.*

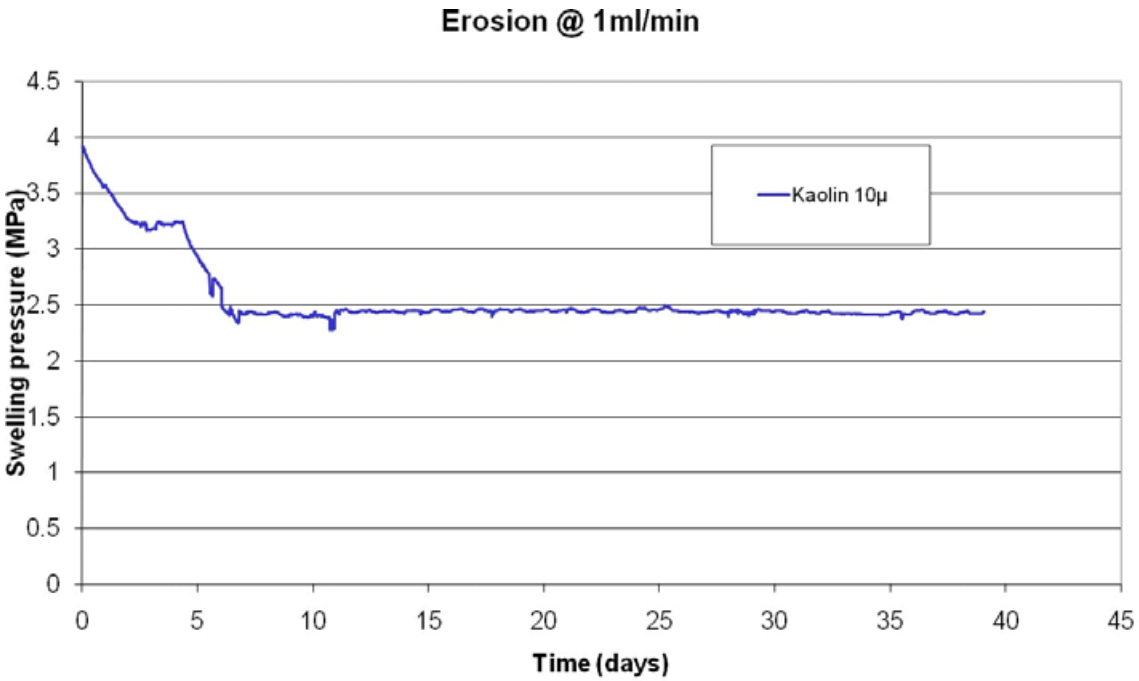

Figure 4-11. *Swelling pressure as a function of time for a Wy-Na sample with a 2 mm thick layer of kaolinite on one side and an extra steel filter on the other. After day 5, circulation of water was only made on the the kaolinite side.*

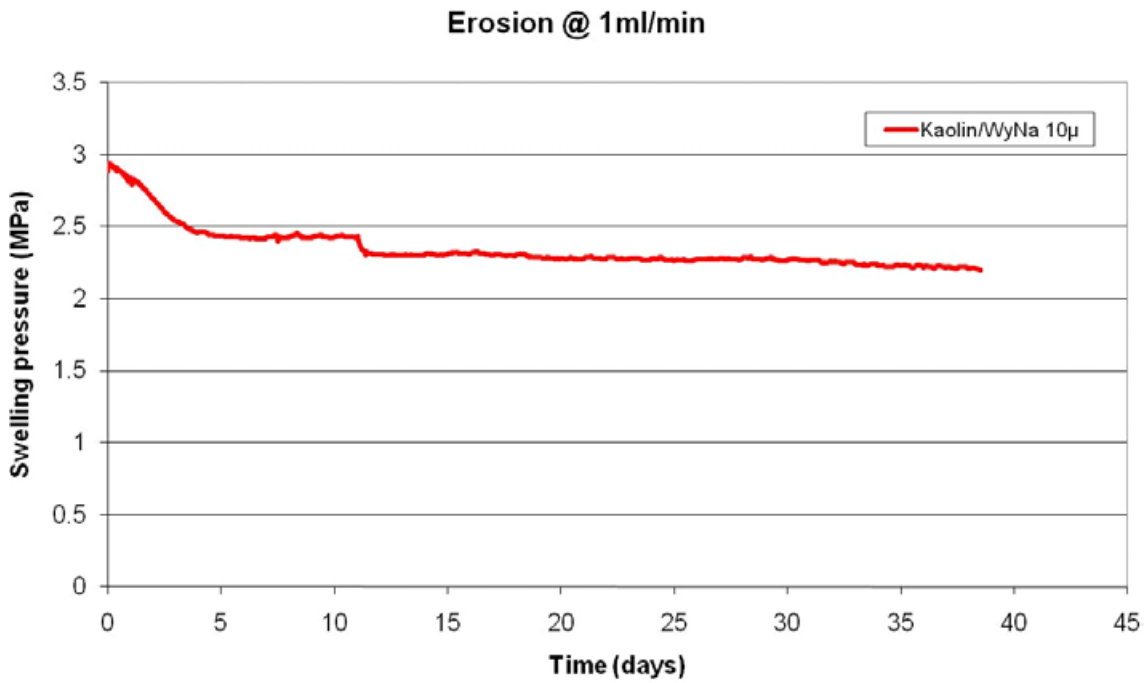

Figure 4-12. *Swelling pressure as a function of time for 50/50 mixture of Wy-Na and kaolinite. The circulating water was exchanged at 11 days.*

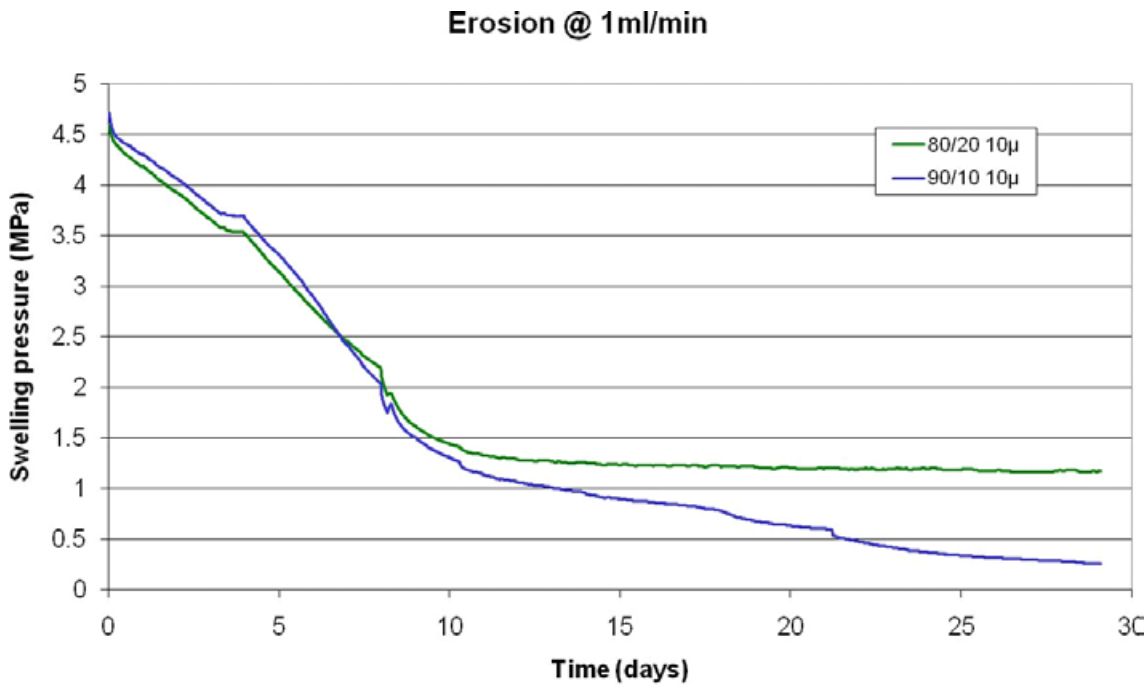

Figure 4-13. *Swelling pressure as a function of time for 80/20 and 90/10 mixtures of Wy-Na and kaolinite.*

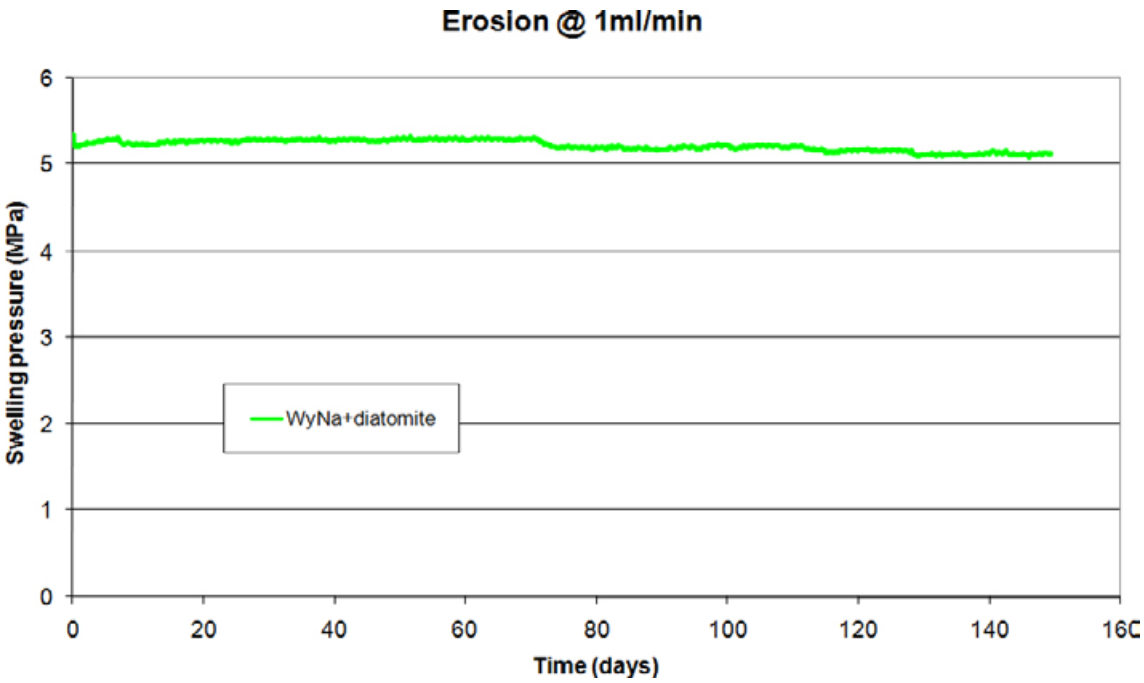

Figure 4-14. *Swelling pressure as a function of time for a Wy-Na sample with a 2 mm thick layer of diatomite.*

The accessory minerals in MX-80 were also tested in two experiments, see Figure 4-16. The first sample is a standard 5 mm thick Wy-Na at density 2,000 kg/m3 with an extra 2 mm thick cake of accessory minerals in the bottom. The second test is with a 10 mm MX-80 sample and only circulation on one side to see if the normal accessory minerals could form a filter cake. The slow pressure drop is not in agreement with the behaviour in Figure 4-2 where the swelling pressure drops significantly within 20 days. The difference between the two experiments is the difference in proportions of the sample and the ratio between the water reservoir and clay mass. Later measurements of electric conductivity (see Figure 4-17) show values that are consistent with the values that stopped erosion in the earlier experiments. The apparent stop for colloid release is mainly due to the ionic content in the circulating solution.

These experiments show that a material with particles smaller than 10 µm can be compacted into a filter that stops colloids. There has been no attempt to optimize the composition or investigate long term effects. The diatomite is mainly silica and is soluble in water and is therefore not well suited in this application. In Figure 4-15 the grain size distribution from the different materials are shown. It can be noted that the diatomite has no particles smaller than 2 µm while the other materials has about 40–50% of the amount below that limit (of finer than 63 µm).

4.4.1.7 Ongoing experiments

4.4.1.7.1 Long test cell

A test with a test cell with diameter 50 mm and length 350 mm and MX-80 is running. This length corresponds with the actual buffer thickness. Filter pore size is 10 µm. The test is saturated from one side only (rockside).

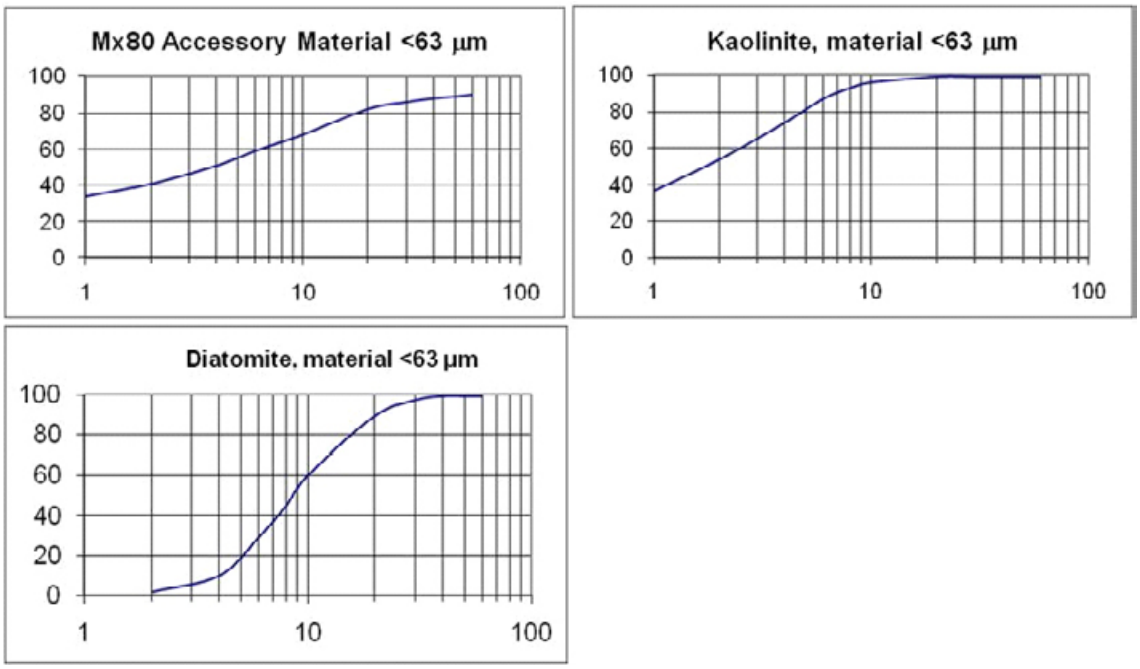

Figure 4-15. *Sedigraph results for MX-80 accessory minerals, kaolinite and diatomite. Particle size in µm is shown on the x-axis and accumulated percentage on the y-axis.*

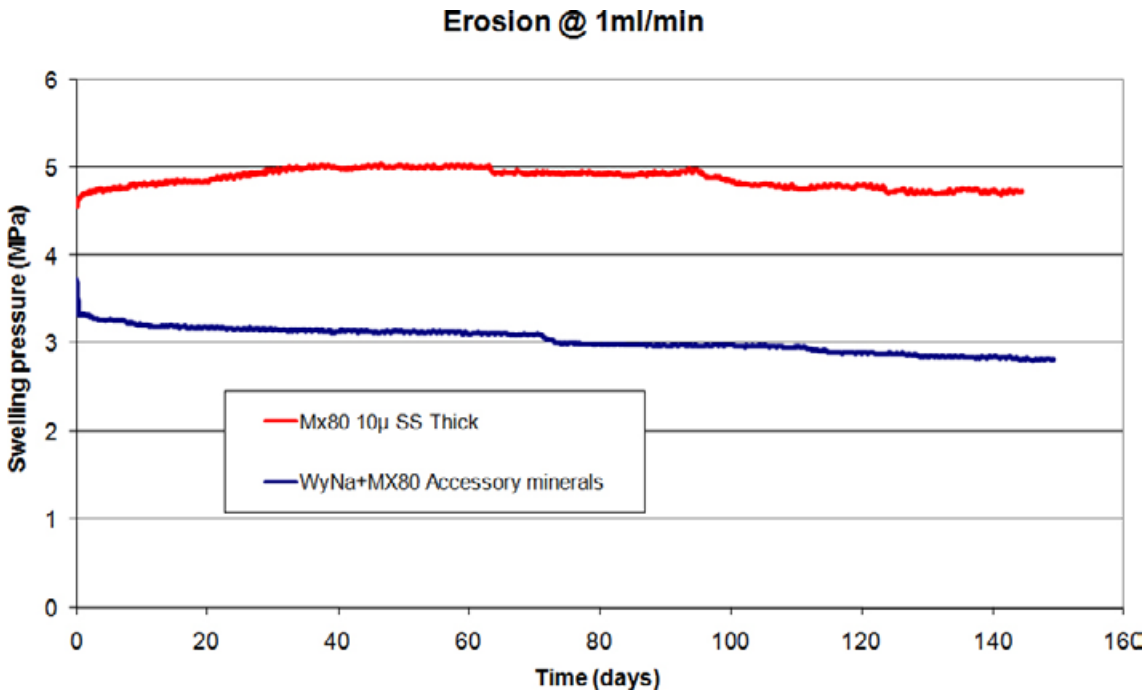

Figure 4-16. *Swelling pressure as function of time for a 10 mm thick untreated MX-80 sample and a Wy-Na sample with a 2 mm thick layer of accessory minerals.*

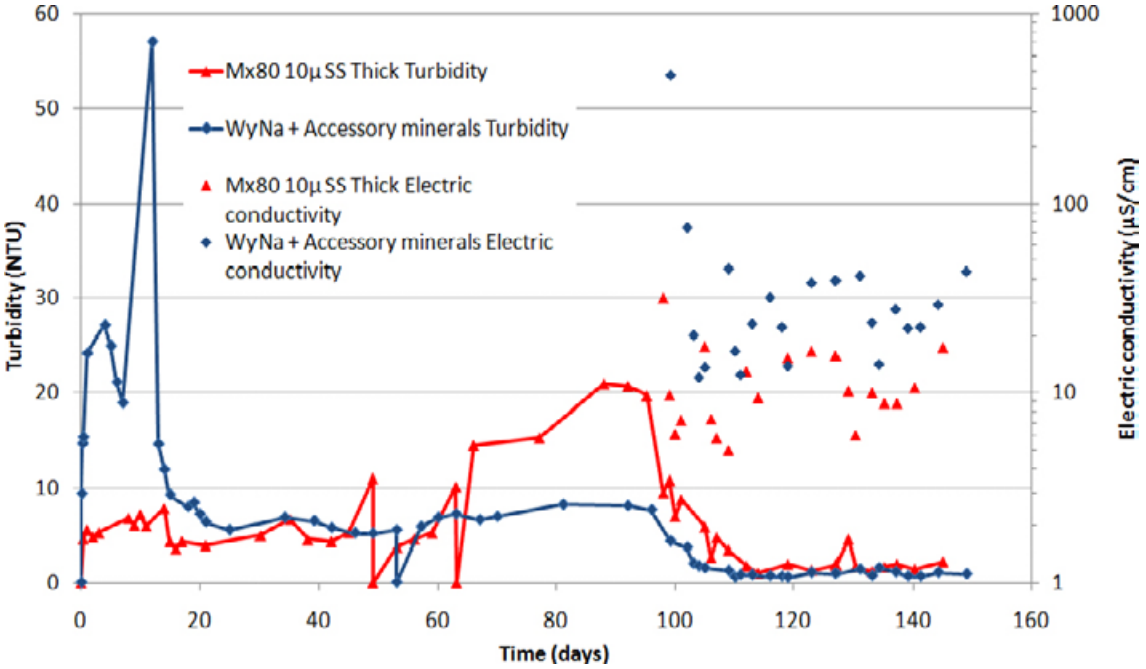

Figure 4-17. *Turbidity and electric conductivity as a function of time for the same samples as in Figure 4-16.*

4.5 Conclusions

A number of tests have been made with both untreated MX-80 bentonite from Wyoming and homoionic sodium and calcium converted clays (montmorillonite). Combinations of these and filler materials such as kaolinite, diatomite and accessory minerals were tested. Also a number of filters with different pore sizes have been tested.

In short the following combinations have been found to stop colloid release in deionized water at a flow of 1 ml/min:

- Homoionic calcium clay and pore size <100 µm (largest pore size tested),
- Homoionic sodium clay and pore size <0.5 µm,
- Homoionic sodium clay and a compacted 2 mm layer of either kaolinite or diatomite.

Other filler materials can be expected to have similar sealing properties as kaolinite provided they have similar grain size distribution.

5 Sol formation without influence of ion exchange

5.1 Introduction

This study focuses on the low solid to liquid ratio region (m_{clay}/m_{water} <1%), or equivalently the high water to solid mass ratio, i.e. to the right of the repulsive gel-sol transition in the schematic phase or state diagram in Figure 5-1. At low ionic strengths the montmorillonite-water system under study is a liquid sol. By increasing the ionic strength the colloidal particles in the sol form an attractive gel that may phase separate to an almost colloid free supernatant and an aggregated system. Depending on the ionic strength and the water to solid mass ratio the attractive gel may fill the vial or slowly consolidate under gravity until an equilibrium height is reached. In other words gravity induces a phase separation in the system under certain conditions. It should be pointed out that the swelling experiments are performed at high *average* water to solid mass ratio, but the actual water to solid mass ratio in the clay is at first at least as low as it is intended to be in a repository for spent nuclear fuel. Thus in the swelling experiment the clay is initially in the repulsive gel phase and evolves towards either the sol or the attractive gel depending on the NaCl concentration in the solution.

5.2 Experimental methods

The swelling and sedimentation behaviour of Wy, Mi, and Ku montmorillonite are investigated with respect to counterion (Na or Ca), excess NaCl and pH. The experiments are performed using cylindrical glass vials, with outer dimensions: height 35 mm and diameter 23 mm. In swelling experiments a given amount of montmorillonite is dried-in at the bottom of the vials and 10 ml of either deionized water or NaCl solution is added. The swelling and colloidal release vertically, i.e. against gravity is monitored by measuring the change in turbidity with time at approximately 12–13 mm above the bottom. At low particle concentrations the turbidity is directly proportional to the concentration. Similarly for sedimentation the same equipment is used. However in order to ensure complete delamination, the montmorillonite is first dispersed in 5 ml deionized water and later 5 ml NaCl solution (of double the desired final concentration) is added.

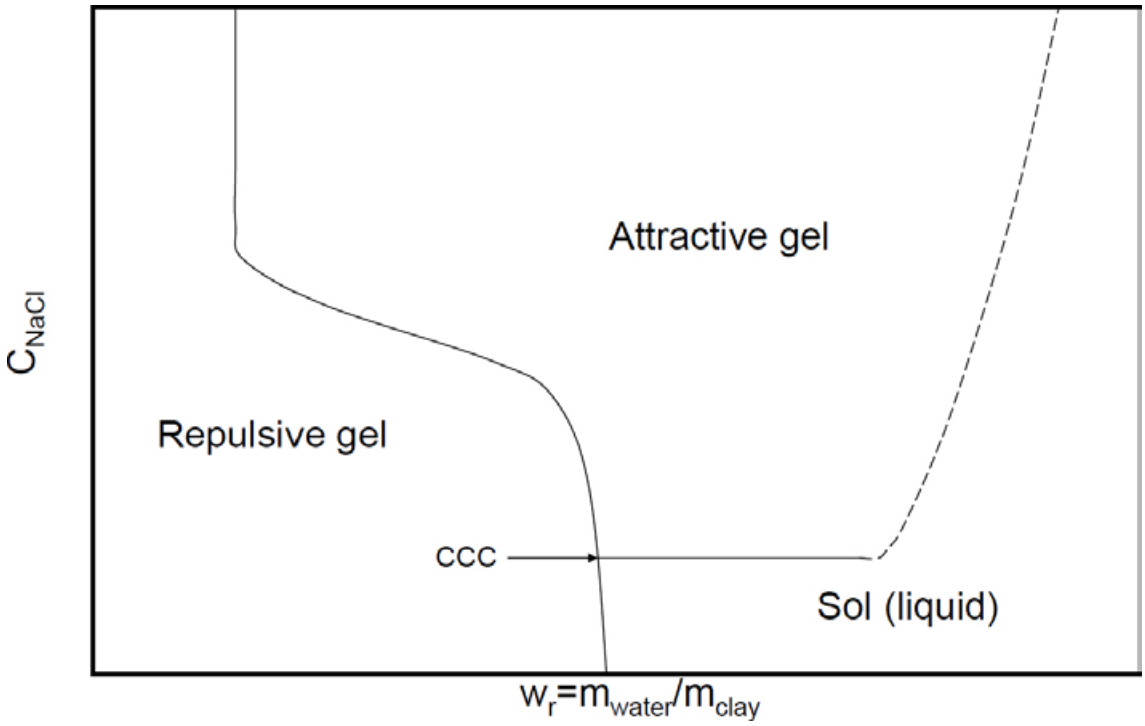

Figure 5-1. *Schematic phase (state) diagram for Na-montmorillonite.*

Turbidity is measured with a portable turbidimeter TN-100 from Eutech Instruments. The light source in TN-100 is an infrared-emitting (850 nm) diode. Light scattered from the (clay) particles in the suspension is detected at an angle of 90 degrees with respect to the light source, thus formally the TN-100 is a Nephelometer. The intensity of the scattered light is directly converted to nephelometric turbidity units (NTU) and the TN-100 operates in the turbidity range 0–1,000 NTU. As mentioned above the standard turbidimeter measures the turbidity at 12–13 mm height. A second TN-100 was purchased and rebuilt to allow the registration of turbidity at different heights in the vials, thereby offering the possibility of obtaining time-resolved swelling or sedimentation profiles. Turbidity at low colloidal concentrations is proportional to the concentration or equivalently the particle number density ρ, i.e. the number of particles per unit volume, according to

$$I(90°) \propto \frac{I_0}{r^2}\frac{V_p^2}{\lambda^4}\left(\frac{n_{21}^2-1}{n_{21}^2+2}\right)^2\left(1-\frac{(4\pi)^2}{\lambda^2}\frac{R_g^2}{6}\right)\cdot\rho, \qquad (5\text{-}1)$$

where $I(90°)$ is the intensity of the scattered light at 90 degrees detection angle, r is the distance from the scattering centre to the detector, V_p is the volume of the clay particle, λ is the wavelength of the light source, n_{21} the relative refractive index of the clay particle to the suspending medium, and R_g the radius of gyration of the clay particle. One notices from Equation 5-1 that the turbidity is proportional to the square of the clay particle size. As a consequence, large particles contribute more to the measured turbidity in a heterogeneous mixture of various sizes. It is found that different clays give different turbidity responses. In addition, increasing, e.g. NaCl content in the solution also increases the turbidity, which suggests that it is not only individual clay particles (1 nm thick layers) that contribute to the scattering but also aggregates of particles. Up to a certain density the turbidity response is linear and beyond the linear regime the turbidity increases less than the increase in density. For Wy-Na the turbidity response is linear up to 5 g clay/litre deionized water and the measured values together with a linear fit through the origin are displayed in Figure 5-2. The measured turbidities at 7.5 and 10 g/l are 684 and 780 NTU respectively which are clearly below the extrapolation of the linear fit. Mi-Na shows linear response to approximately 4 g/l (194 NTU/g/l) and Ku-Na to 2.5 g/l (315 NTU/g/l).

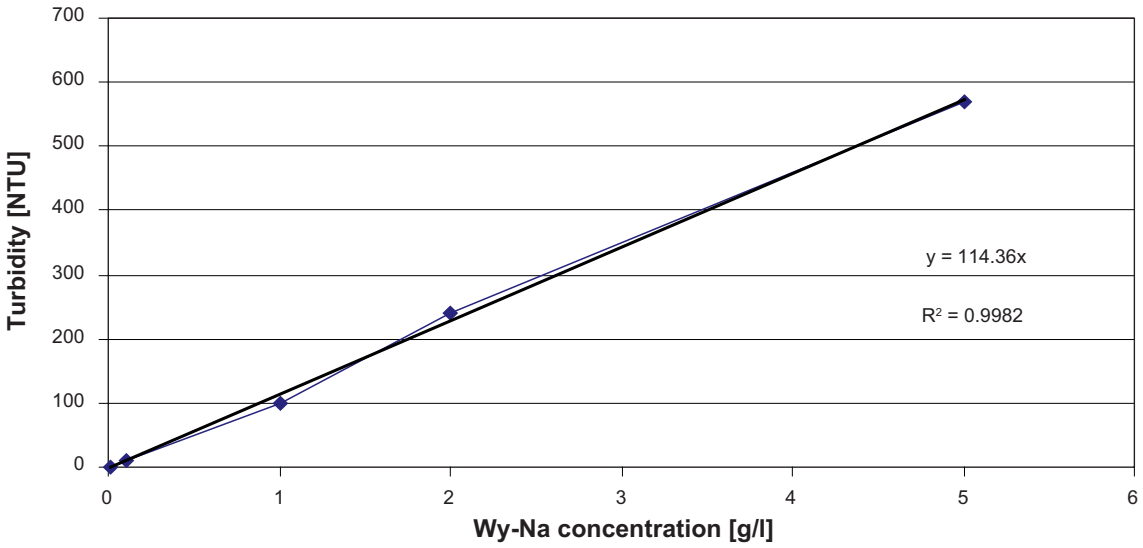

Figure 5-2. *Turbidity vs. Wy-Na concentration in the linear regime.*

5.3 Results

Before discussing the results from the experiments we would like to reflect upon the quantities of montmorillonite used and the dimensions of the vials. To cover the bottom area of the vials by one clay layer, h = 1 nm, requires $m = \rho_c \pi r^2 h$ kg of montmorillonite. With ρ_c = 2,750 kg/m^3 being the grain density of montmorillonite and the vial inner radius r~11 mm, the mass m becomes approximately 1 µg. Typically in the experiments 0.02 to 0.1 g of clay is used, which translates to 20,000 to 100,000 layers of clay. If these amounts of clay were evenly dried-in at the bottom, the height would be 0.02–0.1 mm, and after water uptake to a basal distance of 200 nm, roughly the distance where one could expect free rotation of a typical Wy-Na particle /Michot et al. 2004/, the height would be 4 mm in the case of 0.02 g and 20 mm for 0.1 g montmorillonite. The height of 10 ml liquid in the vials is ~25 mm so swelling to the point of free rotation means that 0.1 g of clay fills the whole sample, 0.05 g barely reaches the detection height and 0.02 g reaches one third of the detection height. However, gravity and, as we will see later, aggregation will strongly influence the distribution of montmorillonite along the height of the vials.

5.3.1 Influence of divalent counterions

Numerous experiments have shown that montmorillonite with calcium or magnesium as counterion does not form colloidal sols, even if placed in deionized water. In other words the critical coagulation concentration of Ca^{2+} for Ca-montmorillonite is zero. The problem with extensive swelling and colloid release only occurs when monovalent counterions are present. Is it possible to prevent colloidal sol formation by replacing some of the monovalent counterions by divalent counterions? To answer this question compound Ca/Na montmorillonites were prepared by mixing given amounts of pure Ca-montmorillonite with given amounts of pure Na-montmorillonite. In total 2 g of clay was dispersed in 250 ml deionized water for each Ca/Na combination. To facilitate the mixing, the suspension was agitated with ultrasound for 15 minutes and then mixed with a magnetic stirrer for at least 12 h, after which the water was removed in 60°C oven. Initially Ca/Na clays were made at mass ratios 100/0, 80/20, 60/40, 40/60, 20/80 and 0/100, where 100/0 and 0/100 means pure Ca-montmorillonite and pure Na-montmorillonite respectively. The mass ratios also reflect the ratio of the cation exchange capacity (CEC) compensated by either Ca^{2+} or Na^+, i.e. in the 80/20 montmorillonite 80% of CEC is compensated by Ca^{2+} and 20% by Na^+.

The swelling of mixed Ca/Na Wyoming montmorillonite is monitored by measuring the turbidity at vial mid-height as the clay expands and disperses against gravity. Initially the clay is dried-in at the bottom and 10 ml deionized water is added. The results for clay contents of 0.100 g and 0.020 g are displayed in Figure 5-3 and Figure 5-4, respectively. Pure Wy-Ca (100/0) behaves totally different from the other clays with 20% Na^+ or more in exchange position. In practice there is no release of colloids from Wy-Ca and the measured low turbidity reflects the fact that Wy-Ca swells to a maximum distance. Furthermore, the original grains of Ca-montmorillonite on the bottom of the vials are intact, albeit considerably swollen compared to the dry state. Inclusion of as little as 20% Na^+ makes the Wy-Ca/Na clay display predominantly sodium montmorillonite behaviour and no sign of the original grains is visible in the vials. It is instructive to compare the curve for Wy-80/20 (B4) in Figure 5-3 with the curve for Wy-0/100 (D11) in Figure 5-4. Sample B4 consists of 0.08 g Wy-Ca and 0.02 g Wy-Na, whereas sample D11 contains 0.02 g Wy-Na. Thus both samples have the same amount of Na^+ but their swelling behaviours are entirely different.

In the literature one sometimes encounters speculations that mixed Ca/Na smectite systems segregate into Ca-layers and Na-layers, a process termed de-mixing /Shainberg and Otoh 1968, Iwasaki and Watanabe 1988, Verburg and Baveye 1994, Laird 2006/.

For de-mixing to occur there must exist an interaction energy that dominates over the entropy of mixing as described in /e.g. Evans and Wennerström 1999/. It is very hard to envisage any such force that would make e.g. Ca^{2+} ions to prefer to be surrounded by other Ca^{2+} ions over Na^+ ions. Our results, on the other hand strongly suggest that the mixing of Ca-montmorillonite with Na-montmorillonite results in a clay where the ions are mixed in the interlayer and not to a situation where there are Ca-layers and Na-layers. The latter situation would correspond to 80% Wy-Ca that do not release colloids and 20% Wy-Na that would give a maximum turbidity of approximately 25 NTU in accordance with Figure 5-4. Instead the Wy-80/20 clay gives a turbidity maximum above 160 NTU as seen in Figure 5-3. Furthermore, the

turbidity maximum of series B4 in Figure 5-3 occurs after 27 days, whereas the turbidity maximum in swelling series D11 in Figure 5-4 takes place after 57 days. If the de-mixing hypothesis were the dominating mechanism here, one would expect a much slower increase in turbidity for sample B4 because clay particles would not fully exfoliate, which would have two effects that both reduce the transport of clay against gravity. First, clay particles would be heavier (stacks of Ca-montmorillonite with Na-ions on the outer surfaces) and more affected by gravity. Second, osmotic pressure will be lower. This follows from the fact that the osmotic pressure at large particle separations is inversely proportional to square of the separation /Eq. 5.1.18 in Evans and Wennerström 1999/ and distances between stacks are necessarily larger than they would be between fully exfoliated clay layers at a given water to solid mass ratio.

Undoubtedly Wy-80/20 clay enters the osmotic swelling regime where the basal distance surpasses by far 20 Å and water is absorbed in a continuous manner (up to a basal distance of ~20 Å, the crystalline swelling regime, water uptake is discretized and X-ray crystallography can discern up to four hydration levels). With that in mind it is also clear that an increase of the percentage of sodium should give higher swelling pressures at long distance due to a larger number of ions in the interlayer. This is reflected at the initial stage of the turbidity response, where we notice higher maximum turbidities the higher the sodium fraction. Below we will discuss the correlation between swelling pressure and maximum turbidities in more detail. With higher total clay content the initial swelling-dominated increase in turbidity is more rapid and with 0.1 g clay/10 ml the turbidity for Wy-0/100 reaches a maximum after 8 days (Figure 5-3) whereas with 0.02 g/10 ml the maximum occurs after 57 days (Figure 5-4).

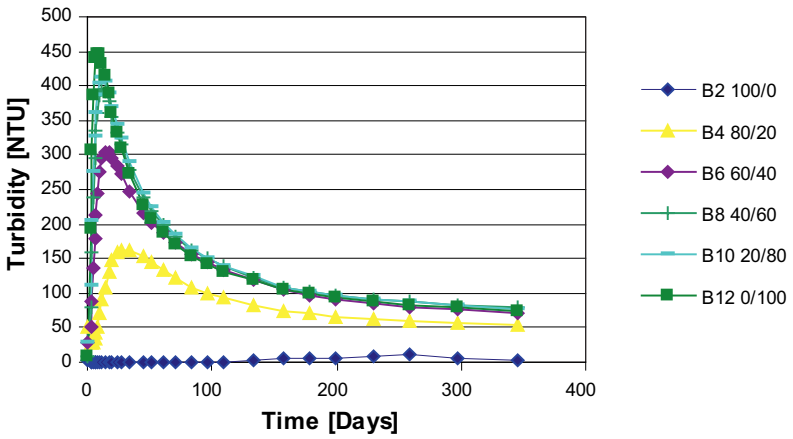

Figure 5-3. *Swelling series B: Turbidity at vial mid-height vs. swelling time of Wy-Ca/Na montmorillonite for various Ca/Na combinations. Clay content is 10 g/l.*

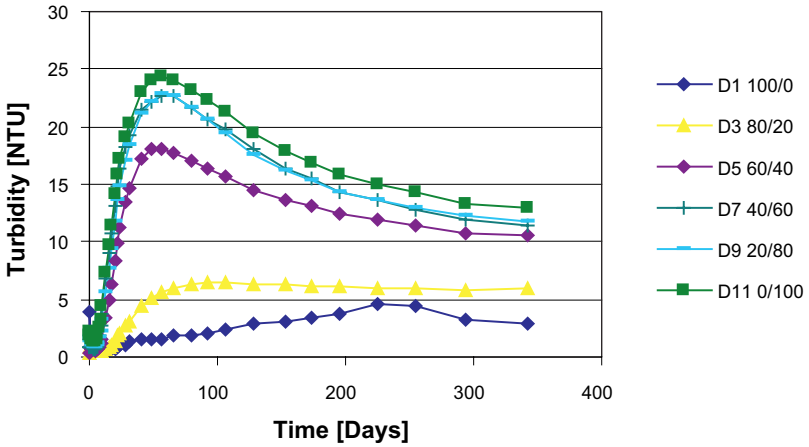

Figure 5-4. *Swelling series D: Turbidity at vial mid-height vs. swelling time for Wy-Ca/Na montmorillonite. Clay content is 2 g/l.*

It comes as no surprise that an intermediate clay content of 0.05 g/10 ml, presented in Figure 5-5 and Figure 5-6, gives maximum turbidities and turbidity-increase rates in between the values obtained at 0.02 and 0.1 g /10 ml respectively. It is also clear that the maximum turbidities at vial mid-height do not vary linearly with clay content. For a diffusion-driven process one expects a linear variation of turbidity with the amount of dried-in clay at all times. However, at the termination of the experiments (after ~1 year) the mid-height turbidities appear proportional to the amount of clay in the vials. The initial non-linearity can be explained on the basis of the osmotic pressures in lamellar systems at low densities where according to the Poisson-Boltzmann (PB) equation the swelling pressure ρ_s is inversely proportional to the square of the mean interlayer distance /Eq. 5.1.18 in Evans and Wennerström 1999/ or, equivalently, proportional to the square of the solid to water mass fraction which follows from the relation

$$\frac{m_{\text{clay}}}{m_{\text{water}}} = \frac{\rho_{\text{clay}} d}{\rho_{\text{water}} h} \propto \frac{1}{h},$$

where d = 1 nm, i.e the thickness of a single clay layer and h is the interlayer separation. Therefore the swelling pressures in the systems discussed here with 0.1, 0.05 and 0.02 g total amounts of montmorillonite obey the relation $P_s(0.1\text{ g}) = 4P_s(0.05\text{ g}) = 25P_s(0.02\text{ g})$. Let $N_{\text{m}}^{\text{Ca/Na}}$ denote the maximum turbidity for a given Ca/Na clay in the swelling experiments. From Figure 5-3, Figure 5-4 and Figure 5-6 one finds that the turbidities for the 0/100 clays at maximum obey the relation $N_{\text{m}}^{0/100}(0.1\,\text{g}) = 4.4N_{\text{m}}^{0/100}(0.05\,\text{g}) = 18.3N_{\text{m}}^{0/100}(0.02\,\text{g})$and for the 80/20 clays the relation is similar; $N_{\text{m}}^{80/20}(0.1\,\text{g}) = 3.9N_{\text{m}}^{80/20}(0.05\,\text{g}) = 25.1N_{\text{m}}^{80/20}(0.02\,\text{g})$ The fact that the maximum turbidities behave as the swelling pressures can be rationalized as follows: Turbidity is proportional to clay concentration, therefore N_{m} is proportional to the mass of clay in a cross-section of thickness δ at detection height, where δ is the width of the scattering region. The weight of this mass is balanced by the swelling pressure exerted by the clay below, i.e. $P_s \approx \rho\delta g$, where g is the acceleration of gravity. Thus the ratio of maximum mid-height turbidities or densities for tests with initially dried-in amounts m_1 and m_2 of clay is envisaged to approximately obey the relation

$$\frac{\rho(m_1)}{\rho(m_2)} \approx \frac{P_s(m_1)}{P_s(m_2)} \approx \left(\frac{m_1}{m_2}\right)^2.$$

This relation is of course only approximate and one source of imprecision is the neglect of the weight of the clay above the detection height. On the other hand, the maximum turbidities show that the concentrations at mid-height are much lower than the average concentration, which is a sign that most of the clay remains below detection height. This is also confirmed by measuring the turbidity profiles along the height of the vials which is further discussed in Section 5.3.2.3. Furthermore, the decrease in midheight turbidity after the maximum value is primarily due to aggregation and sedimentation of the formed heavier aggregates (Sections 5.3.2.1 and 5.3.2.3) and not to further swelling and diffusion of montmorillonite upwards.

In view of the relationship between N_{m} and P_s it is also clear from the turbidity measurements that the swelling pressure at high water to solid mass ratios for the 80/20 Wy-Ca/Na is in the order of at most 30–40% of the swelling pressure for the pure Wy-Na, if one assumes the same relation between turbidity and concentration to be valid for both clays. In fact we have noticed that the Wy-80/20 is more turbid than Wy-0/100 (i.e. Wy-Na) which we ascribe to a higher rate of aggregation for Wy-80/20. Even if one disregards this fact, the lower swelling pressure for Wy-80/20 at high water to solid mass ratios is still less than what a simple Poisson-Boltzmann reasoning would suggest. In that case the swelling pressure for Wy-80/20 at high water to solid mass ratios would be in the order of 60% of that for Wy-0/100, because the number of ions in the interlayer for 80/20 clays is 60% compared to pure sodium clays. Lower swelling pressures at high dilution also means a less active release of colloids. This may have importance for the actual repository conditions, especially if the water composition is such that a gel can be formed. Lower swelling pressures imply weaker repulsive forces that need to be overcome to form an attractive gel. However, in the experiments performed by us on erosion of highly compacted montmorillonite through 2 mm thick steel filters and pore size of 2 µm, the Wy-80/20 sample lost material at the same rate as Wy-Na, when deionized water was circulated over the filter (see Section 5.5.1).

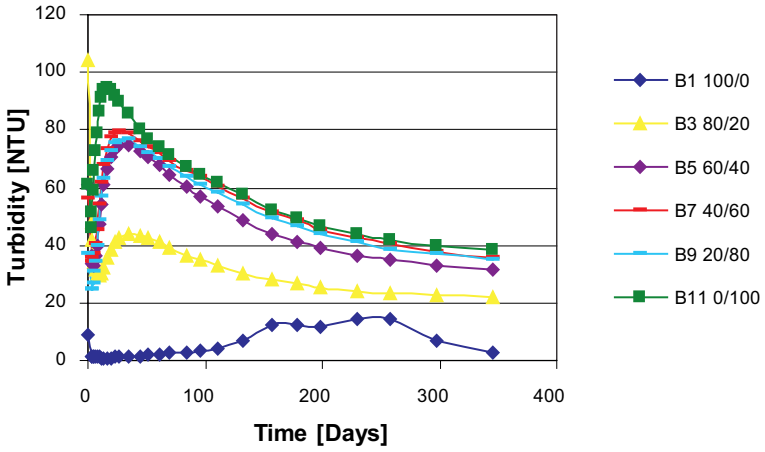

Figure 5-5. *Swelling series B: Turbidity at vial mid-height vs. swelling time of Wy-Ca/Na montmorillonite for various Ca/Na combinations. Clay content is 5 g/l.*

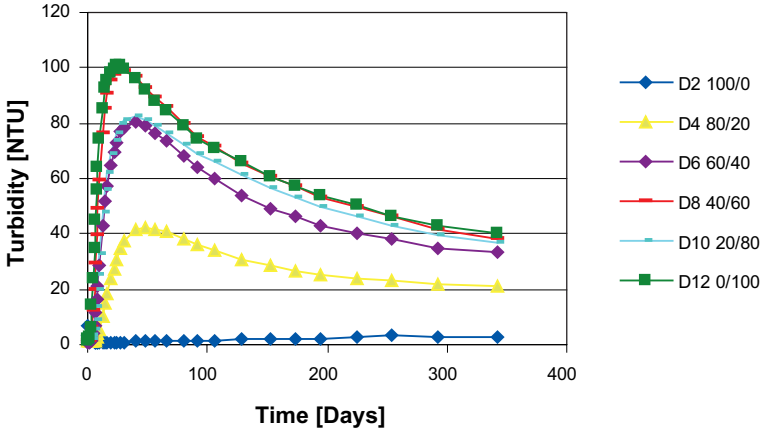

Figure 5-6. *Swelling series D: Turbidity at vial mid-height vs. swelling time of Wy-Ca/Na montmorillonite for various Ca/Na combinations. Clay content is 5 g/l. Swelling series D is a duplicate of swelling series B in Figure 5-5, with the difference that more care have been taken not to stir up clay when water was added, thus avoiding large initial turbidities, c.f. curve D4 with curve B3.*

Kutch-Ca/Na behaves similarly to Wy-Ca/Na as can be seen in swelling series E in Figure 5-7. Kutch is more turbid than Wyoming montmorillonite, which is reflected in the high turbidities despite the fact the clay content in series E is 0.05 g/10 ml, i.e. half of the clay content in Series B (Figure 5-3). We also notice a larger correlation between Na content and turbidity at maximum for Ku-Ca/Na than for Wy-Na/Ca. As time progress the initial differentiation among the clays containing sodium is faded out both for Ku and Wy. Swelling experiments on Ku-Ca/Na were also performed for 0.02 g/10 ml and the non-linear dependence on N_m with clay content seen for Wy-Na/Ca was confirmed and for the pure Ku-Na clay the relation was found to be $N_m^{0/100}(0.05\ \mathrm{g}) = 9.1 N_m^{0/100}(0.02\ \mathrm{g})$ and similar for the other Na^+ containing clays.

Increasing the calcium content beyond 90% of CEC makes the limited swelling behaviour typical for calcium montmorillonite to dominate as can be seen in Figure 5-8. Note that when water is added some grains of clay are stirred up which gives relatively high initial turbidities. These grains are quite large and sediment rapidly leading to a minimum in the turbidity after a few days. As can be seen in Figure 5-8, Wy-90/10 still shows some active colloidal release but the turbidity increase at vial mid position is very minor and reaches a maximum of 5.6 NTU after 130 days. In comparison Wy-80/20 at 5 g/l gives a turbidity maximum above 40 NTU in 40 days. Furthermore Wy-80/20 appears similar to pure Wy-Na with no sign of limited swelling, whereas in free swelling of Wy-90/10 original grains of clay are present at the bottom of the vial.

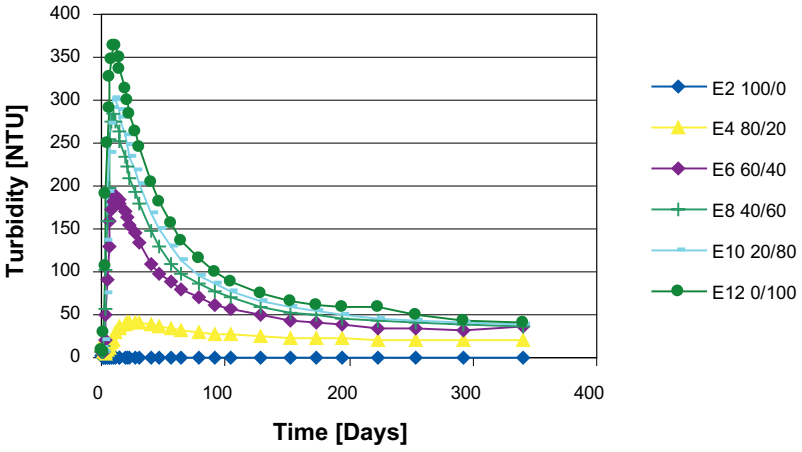

Figure 5-7. *Swelling series E: Turbidity at vial mid-height for Ku-Ca/Na montmorillonite. Clay content is 5 g/l.*

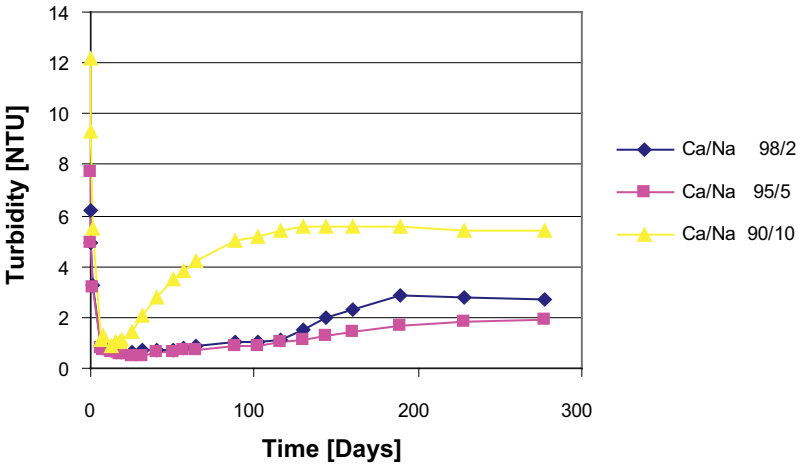

Figure 5-8. *Turbidity at vial mid-height as a function of swelling time for Wy-Ca/Na at a clay content of 5 g/l.*

Sedimentation of Wy-Ca/Na confirms the above picture that 90% Ca or more is needed for behaviour similar to pure Wy-Ca to occur, as shown in Figure 5-9. With 60% Ca or less the sedimentation follows the same pattern as for pure Wy-Na. Wy-80/20 sediments slightly faster and Wy-90/10 falls in between the fast sedimentation of Wy-Ca and the slower sedimentation of Wy-80/20. The gradual increase in turbidity for Wy-100/0, 98/2 and 95/5 after 90 days has only been observed in Wyoming montmorillonite and not in Kutch. We have at present no explanation for this pattern but the turbidity at maximum after 250 days (Wy-100/0) is only 10 NTU and obviously these particles aggregate in suspension and re-sediment. The same effect is seen in the swelling experiments of Wy-Ca/Na, but appears more pronounced in Figure 5-9 due to the logarithmic scale.

In order to gain more insight into this, in view of the results in Section 4.4.1.3, unexpected turbidity increase in Wy-Ca (Wy-100/0) the concentration profiles were measured after 214 days, using the modified turbidimeter, and the results for sedimentation series C are displayed in Figure 5-10. Zero means the topmost measurement position and 18 mm is the deepest measurement position. However one realizes that most of the montmorillonite is located below the 18 mm depth if one bears in mind that initially (time 0) after shaking the vials the concentration is even and gives a turbidity of ~570 NTU for Wy-0/100 (sample C11). The turbidity N is displayed on a log scale so straight lines mean exponential decay in accordance with

$$N(z) \propto N_0 \exp\left(-\frac{mgz}{k_B T}\right), \qquad (5\text{-}2)$$

where m is the buoyant mass and z, the height above a reference level, k_B Boltzmann's constant and T is the absolute temperature. The samples containing some 20% or more sodium all show the expected exponential concentration profile and from the data in Figure 5-10 one can evaluate m. If one also makes the assumption that the clay particles are 1 nm thick circular discs the extracted buoyant mass would translate to clay particles with radii of approximately 100 nm.

The profile for the 100/0, i.e. Wy-Ca, shows the presence of colloids that are evenly distributed throughout the vial and therefore not affected by gravity on the length scale of the vials (h=25 mm). These particles must therefore have a very small buoyant mass that can be roughly estimated from $m \leq 0.1 k_B T / gh$, which becomes in the order of 10^{-21} kg, or converted to montmorillonite, clay particles with radii of less than 10 nm for Ca-montmorillonite. Maybe these particles instead are silica residues (or other minerals) that have not been completely removed in the purification. There is nothing in the experiment suggesting that Ca-montmorillonite presents a problem with respect to colloid sol release. In fact the slow increase in mid-height turbidity seen in the experiments on Wy-100/0, shows that this process is diffusion governed and not related to swelling. Furthermore, no loss of Wy-Ca has been observed in swelling pressure test cells, even at filter pore size of 100 µm (Section 4.4.1.3).

In summary, we find at very low concentrations of excess salt (ionic strength governed by dissolution of the mineral itself) close to 90% of the CEC needs to be compensated by Ca^{2+} to prevent colloidal sol formation in mixed Ca/Na-montmorillonite.

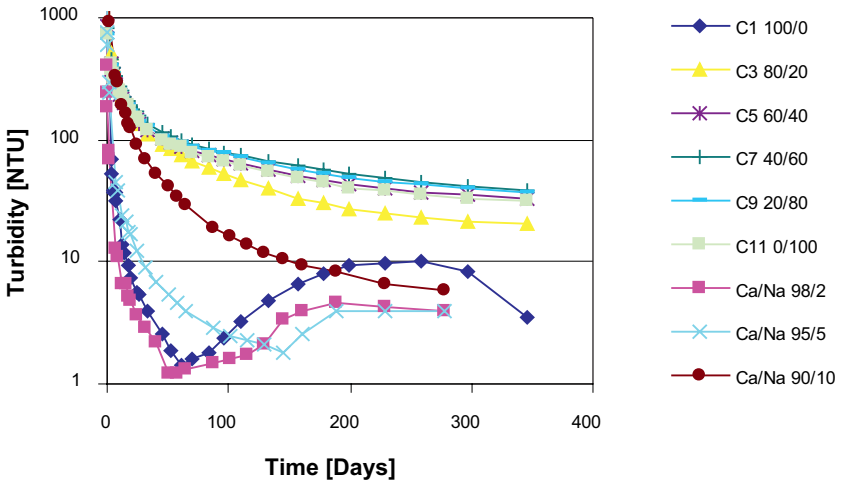

Figure 5-9. *Turbidity at vial mid-height as a function of sedimentation time for Wy-Ca/Na at 5 g/l.*

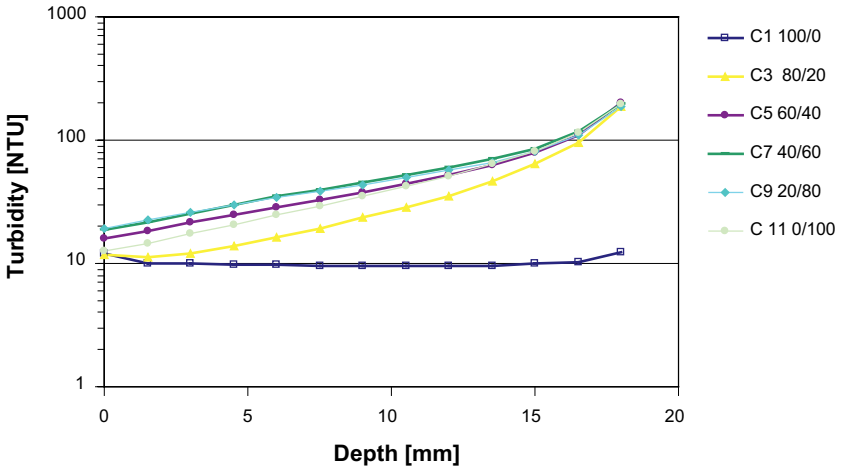

Figure 5-10. *Concentration profiles after 214 days of sedimentation for Wy-Ca/Na at initial concentration of 5 g/l.*

5.3.2 Influence of excess NaCl on the reduction of colloidal sol formation

We have seen that pure Ca-montmorillonite does not pose a problem with respect to sol formation in deionized water, i.e. the CCC for this system is 0 M Ca^{2+}. Adding NaCl(aq) to a Ca-montmorillonite or $CaCl_2$(aq) to Na-montmorillonite will lead to a mixed Ca/Na-montmorillonite in a mixed NaCl/$CaCl_2$ solution. Such systems may or may not release colloids and their stability must be discussed in terms of a sol formation zone that will be described in detail later (Chapter 7). Here the focus will be on the effect of NaCl on Na-montmorillonite, where the sol formation zone is reduced to a CCC in terms of external NaCl concentration.

5.3.2.1 Sedimentation experiments

Sedimentation experiments show two major patterns of the clay –electrolyte mixture. Below a critical concentration of NaCl, which we here call CCC, the sol sediments as aggregates and above the CCC there is a rapid formation of a percolation gel that slowly consolidates under gravity. As most of the experiments are done at concentration of 5 g clay/litre or less, i.e. very dilute suspensions, we first tested the assumption that sedimentation could be explained by non-interacting 1 nm thick clay discs by numerically solving the diffusion equation for thin discs in a gravitational field (Equation 3-7 of Section 3.3.4) for various particle radii /Mason and Weaver 1924/. The results for particles with radii 100 nm are shown in Figure 5-11. It is evident from the calculation that such assumption leads to a too slow sedimentation as is clearly demonstrated by comparing to measured sedimentation profiles for Mi-Na in deionized water shown in Figure 5-12. In other words individual clay particles are too light to be substantially influenced by gravity and it would take several weeks to get a lowering of the mid-height turbidity, whereas in reality the drop in turbidity is registered within a few hours even in deionized water. Increasing the radius to 700 nm gives a somewhat faster sedimentation but no change in density (turbidity) at mid-height is obtained within 16 days.

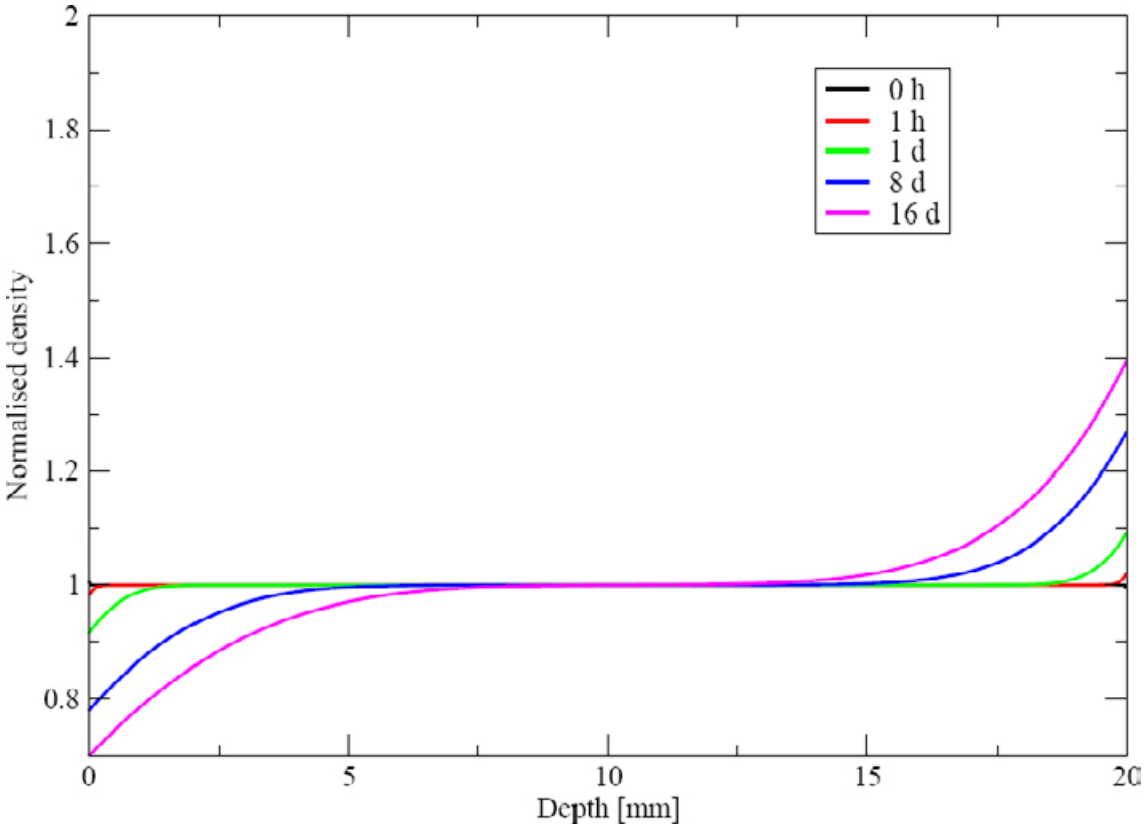

Figure 5-11. *Sedimentation profiles at various times for thin non-interacting clay particles of radii 100 nm. The particle density at mid-height (10 mm) is unchanged even after 16 days.*

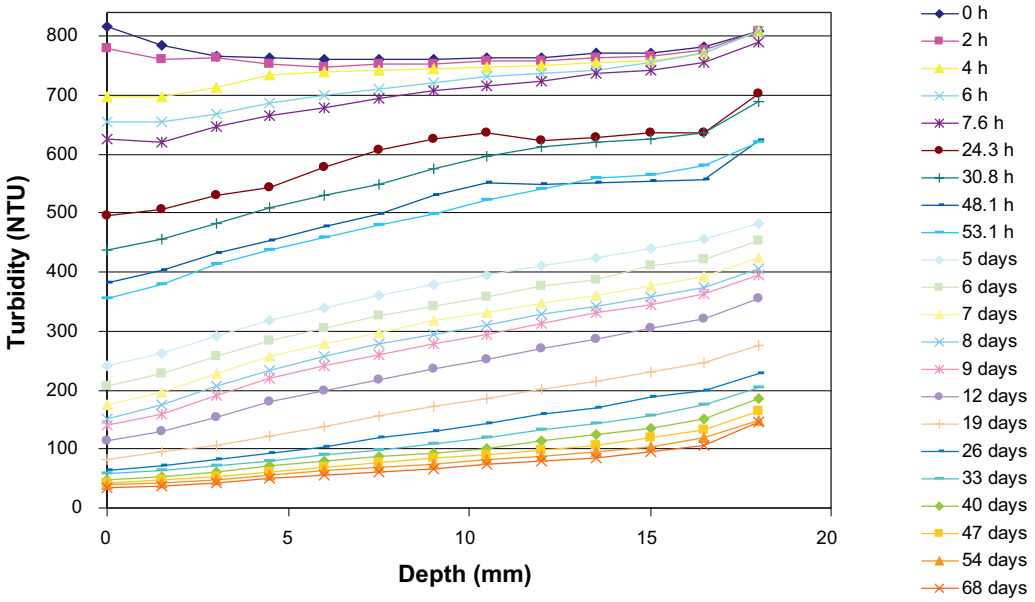

Figure 5-12. *Sedimentation profiles (0–68 days) for Mi-Na 4 g/l deionized water. The meniscus at the top and the curvature of the vial at the bottom gives a distortion in the turbidity measurement seen in the initial curve which bends upwards at both ends.*

If one disregards Brownian motion then the settling velocity v_s of a spherical particle of radius r is given by

$$v_s = \frac{\Delta\rho V g}{6\pi\eta r} \tag{5-3}$$

where Δρ is the difference in density between the particle and the fluid medium, V the particle volume, η the viscosity of the fluid, and g the acceleration of gravity. If one further makes the approximation that a clay particle or an aggregate of clay particles is spherical then

$$v_s = \frac{\Delta\rho g V^{2/3}}{6\pi\eta(3/4\pi)^{1/3}}. \tag{5-4}$$

Note that, the assumption that clay particles are spherical makes Equation 5-4 conservative in the sense that it gives an upper limit for v_s. Still the settling times for clay particles (ρ = 2,750 kg/m^3) to fall 10 mm in water (η = 1.0 mPa·s) using v_s from Equation 5-4 are ~80 days for a 100 nm disc and almost 4 days for a single particle with radius of 1,000 nm, respectively. An aggregate of 1,000 clay particles with a 100 nm radius each would, according to the velocity in Equation 5-4, sediment 10 mm in 8 hours.

In Figure 5-13 one notices how sedimentation patterns for Wy-Na in 0, 5 and 10 mM NaCl are similar showing a steady decrease in mid-point turbidity. Above the CCC there is no drop in the mid-point turbidity at the initial stages. From Figure 5-13 one sees that there is a gradual increase in turbidity especially with 50 and 100 mM NaCl but also with 25 mM. The suspension has become a gel that slowly consolidates giving a two-phase system, a gel at the bottom with a clear almost clay-free electrolyte above. When the upper border of the gel phase has arrived at the detection height in the vial there is a rapid lowering of the turbidity as can be seen for the 25 mM curve, but not for 50 and 100 mM. It turns out that the equilibrium height, which also reflects the strength of the gel, is above the height of detection when the NaCl concentration is 50 mM or higher. With the modified turbidimeter we have been able to follow the sedimentation profile at a 1.5 mm resolution in the vial and the result for Wy-Na in 25 mM NaCl is shown in Figure 5-14. During the first week there is almost no change in the turbidity at any height and only after two weeks is there a tendency to consolidation seen as an increase in turbidity at the lower section of the vial. Thus, at and above the CCC the sedimentation behaviour is entirely different from that observed in NaCl solutions below the CCC where the sedimentation profiles always resemble those depicted in Figure 5-12.

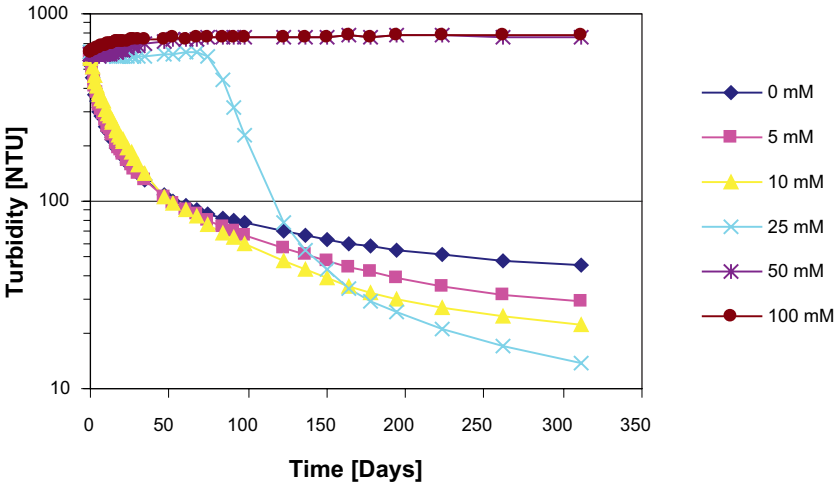

Figure 5-13. *Turbidity vs. sedimentation time for Wy-Na 5 g/l at different NaCl concentrations.*

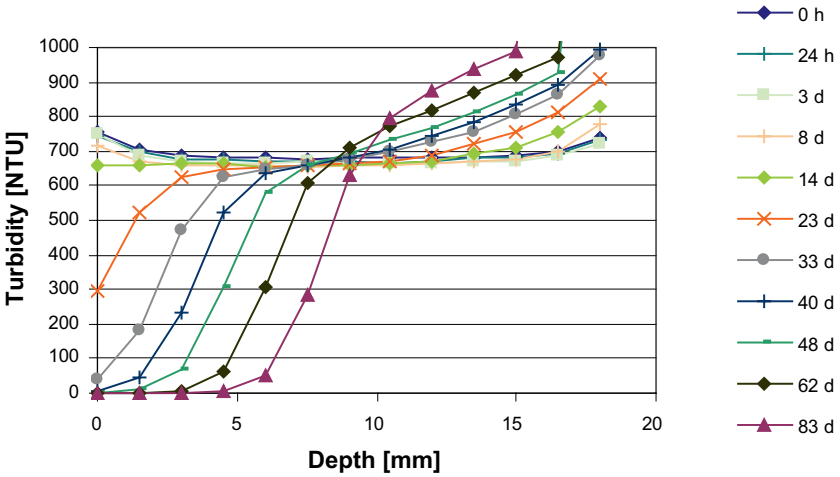

Figure 5-14. *Sedimentation profiles of 5 g/l Wy-Na in 25 mM NaCl.*

Above the gel phase the turbidity is essentially zero as is very clear from the profile at 83 days. The limit of the turbidimeter is 1,000 NTU so one cannot expect to monitor the conservation of particles by integrating the curves. Furthermore the turbidity is not measured at the top and the very bottom where the meniscus and the glass curvature, respectively, would give a distortion, which already affects the turbidity at relative depth 0 and 18 mm (curves bend initially upwards at both ends).

It is interesting to note that even in deionized water the colloidal sol is not stable but aggregates are formed that settle. Aggregation in colloidal systems is normally described assuming bimolecular association of colloidal particles, $A + A \rightarrow A_2$ and the formation rate of dimers follows a second order rate equation /Evans and Wennerström 1999/. It should be noted here that dimers do not refer to two clay particles but an aggregate of much larger size, in the order of 1,000 clay particles, to give high enough settling velocity (Equation 5-4) compatible to the observed rapid decrease in turbidity. We find that the sedimentation of Na-montmorillonite at 10 and 15 mM NaCl follow a second order rate law but at lower salt concentrations the sedimentation rate is too slow to fit a second order law and show rather a third order behaviour, especially in deionized water. Third order aggregation is unusual but has been discussed in the literature, e.g. /Jiang et al. 1990, ben-Avraham 1993, Connaughton et al. 2008/. Plotting $\ln(-dN(t) / dt)$ vs. $\ln(N(t))$ where $N(t)$ denotes the turbidity at time t should ideally give a straight line with a slope that corresponds to the order of the reaction. The graphs for 2 g/l Wy-Na in Figure 5-15 demonstrate that initially, i.e. when N and dN / dt are larger, sedimentation follows a third order law but when excess NaCl is present there is a shift to a second

order law. In deionized water the third order process seems to dominate during the whole experiment (~260 days) although there seems to be a mixture of both second and third order processes after the kink in the curve (at $\ln(-dN/dt) \approx -1$).

The turbidity change rate for an nth order process is described by

$$\frac{dN(t)}{dt} = -k_n N^n(t), \qquad (5\text{-}5)$$

where k_n is the rate constant. Equation 5-5 captures the lowering of turbidity with time due to the formation of clusters that rapidly fall below the detection height in the vial (gravity dominates over Brownian motion). The solution for $n \geq 2$ is given by

$$\left(\frac{N_0}{N(t)}\right)^{n-1} - 1 = (n-1)N_0^{n-1}k_n t, \qquad (5\text{-}6)$$

where N_0 is the initial turbidity. By plotting the left hand side of Equation 5-6 against sedimentation time one can fit a straight line through the origin from which the rate constant is evaluated.

The third and second order rate constants from the sedimentation experiments using Wy-Na 2 g/l are shown in Table 5-1 and Table 5-2 respectively. As stated above without excess NaCl there is no clear transition from a third to a second order rate law so k_2 is not evaluated for 0 mM NaCl. If one neglects that sedimentation in 10 mM follows a third order law during the first six days and instead fit a second order process to the whole time period $k_2 = (7.1 \pm 0.3) \times 10^{-4}$ l/(mol s), i.e. slightly larger than the value in Table 5-2. Sedimentation of 2 g/l Wy-Na in 15 and 20 mM NaCl shows initially a decrease in turbidity, due to aggregation leading to sedimentation and there is a build-up of sediment at the bottom of the vial. However there is also a process of forming a gel in these systems and after about three weeks there is a low-density gel visible in the 20 mM solution and after 4 months there is a phase separation discernible also in the 15 mM solution. Clearly Equation 5-6 is not meant to capture this type of behaviour and consequently no rate constants have been evaluated for gelling situations. With 5 g Wy-Na/l no gel formation is observed below 25 mM NaCl.

Now returning to sedimentation of Wy-Na at 5 g/l: A linear fit of $\ln(-dN(t)/dt)$ vs. $\ln(N(t))$ gives n=3 for 0 mM, n=2.4 for 5 mM, and n=2 for 10 and 15 mM. These reaction orders were determined over the whole sedimentation time interval and there is no indication of a change from third to second order in the 5 mM NaCl solution. There is instead a mixture of second and third order processes at all times giving an average n of 2.4. The rate constant ($k_{2.4}$) for 5 mM is not evaluated but we see from Figure 5-13 that in 5 mM NaCl the sedimentation rate falls in between that of 0 mM and 10 mM. The rate constants for 0, 10 and 15 mM are found to be $k_3 = (6.1 \pm 0.1) \times 10^{-2}$ l^2/(mol^2 s) for 0 mM, $k_2 = (1.58 \pm 0.03) \times 10^{-4}$ l/(mol s) for 10 mM and $k_2 = (1.57 \pm 0.05) \times 10^{-4}$ l/(mol s) for 15 mM NaCl in the solution.

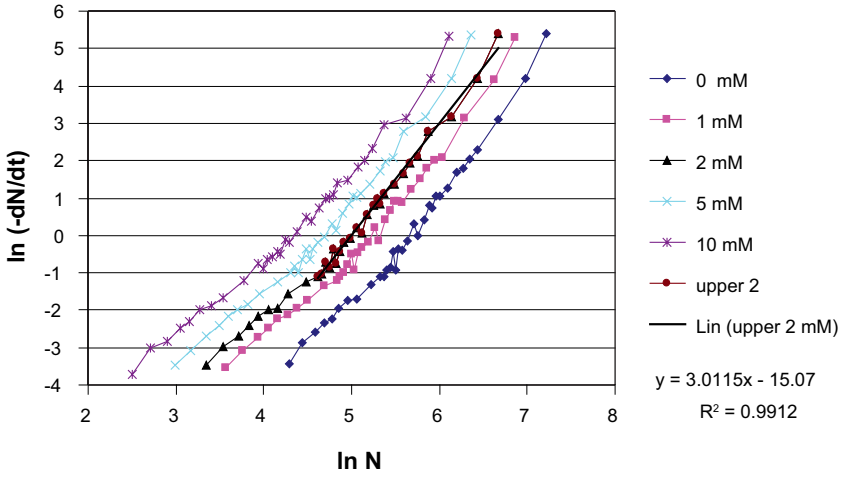

Figure 5-15. ln(–dN(t) / dt) vs. ln(N(t)) *for 2 g/l Wy-Na at different NaCl concentrations. The linear fit refers to the upper sections of the 2 mM data. The curves are translated on the* ln(N) *axis for visualization purposes.*

Table 5-1. Evaluated third order rate constants for Wy-Na 2 g/l at different NaCl concentrations (C). The time span where the rate law is valid is denoted by t and the R^2 values indicate the quality of the linear fit. The error in k_3 is estimated to be ±4%.

t [days]	C [mM]	k_3 [$l^2/(mol^2\,s)$]	R^2
0–73	0	1.05	0.9972
0–45	1	1.15	0.9997
0–45	2	1.16	0.9995
0–42	5	1.17	0.9979
0–6	10	1.02	0.9966

Table 5-2. Evaluated second order rate constants for Wy-Na 2 g/l at different NaCl concentrations (C). The time span where the rate law is valid is denoted by t and the R^2 values indicate the quality of the linear fit.

t [days]	C [mM]	k_2 [l/mol s] $\times 10^{-4}$	R^2
45–262	1	4.8 ± 0.2	0.9985
45–262	2	4.9 ± 0.2	0.999
42–262	5	5.3 ± 0.2	0.9987
6–262	10	6.8 ± 0.3	0.9986

It is found that Mi-Na forms a gel when dispersed in 10 mM NaCl and for Ku-Na the critical value is 5 mM NaCl. Figure 5-16 shows a snapshot of sedimentation in Ku-Na and it illustrates the difference in sedimentation behaviour between consolidating gels and an aggregating sol. The sedimentation experiments on Ku-Na were done at the clay concentration of 2 g/l and at the NaCl concentrations 0, 5, 10, 20, 25 and 50 mM. As stated above the aggregation model does not describe gel formation (the gel is a percolation cluster that spans the whole vial) so Equation 5-6 is only applied to the 0 mM case. In contrast to Wy-Na, Ku-Na in deionized water sediments according to a second order rate law and the rate constant k_2 is found to be $(7.6 \pm 0.3) \times 10^{-4}$ l/(mol s), which is similar to the value obtained for 2 g Wy-Na per litre at 10 mM and almost 5 times larger than k_2 (10 or 15 mM) with Wy-Na content of 5 g/l. A dilute dispersion (sol) of Ku-Na is less stable than a dispersion of Wy-Na. This is consistent with the fact that the (percolation) gel is formed at a lower NaCl concentration for Ku-Na.

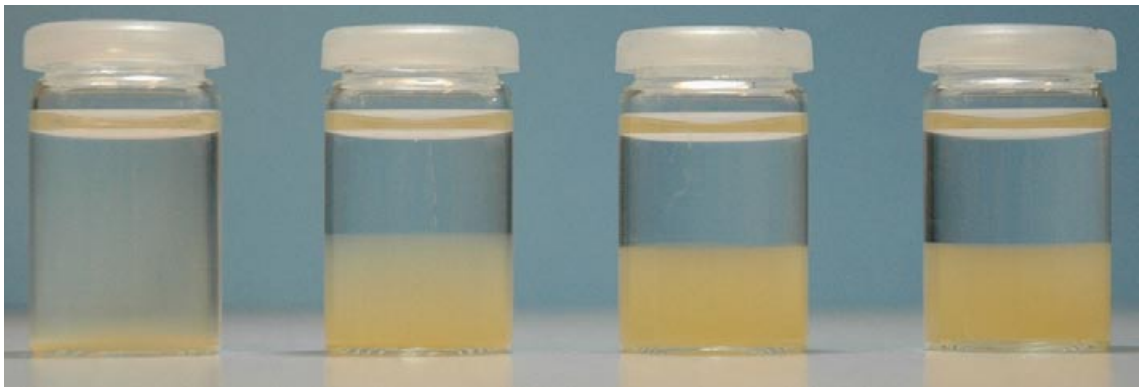

Figure 5-16. *Sedimentation of Ku-Na 2 g/l. NaCl concentrations are from left to right 0, 5, 10, and 50 mM respectively. Note the sharp interface between attractive gel and supernatant at the CCC and higher concentrations.*

5.3.2.2 Swelling experiments

Excess NaCl has a significant influence on the swelling of Na-montmorillonite. For Wy-Na and Ku-Na 0.05 g clay /10 ml solution is used, and the experiments on Mi-Na are made at 0.04 g/10 ml. When the NaCl concentration is above the CCC, the clay shows limited swelling and many of the grains stay intact, although swollen several times their original size, giving rise to the appearance of a "lunar landscape" as can be seen in Figure 5-17. The gel at the bottom of the vials in, e.g. Figure 5-17 consists of regions that are optically isotropic and parts that are birefringent. The latter appear as bright sections, embedded in isotropic, therefore dark, gel, when observed between crossed polarizers. We interpret these sections as the expanded original grains with the mineral layers highly oriented. In the isotropic parts one would expect no favoured direction of the layers on a macroscopic scale. A striking feature in Figure 5-17 is the extent to which the montmorillonite swells. As we reasoned earlier, 0.05 g montmorillonite evenly dried-in at the bottom would have a height of 0.05 mm and the gels in the picture seem to have expanded 50–100 times.

The CCC for Wy-Na is found to be around 25 mM NaCl and the swelling behaviour at CCC is similar to the systems with 50 and 100 mM in Figure 5-17. It is worth noting that the critical NaCl concentration for limited swelling is the same as for gel formation seen in the sedimentation experiments. This suggests that the same physical interactions are involved when the attractive gels are formed irrespective of whether that phase is approached from the sol or the repulsive gel phases. In Figure 5-18 the turbidity at vial mid-height versus swelling time is shown for Wy-Na at six different electrolyte concentrations. Above the CCC, i.e. 25 mM the measured turbidity is indeed very low as expected. For 5 and 10 mM NaCl one notices a very slow increase in turbidity which also agrees with the appearance of a dispersion of particles in the vials and not a gel at the bottom. However, the maximum turbidities are much lower in comparison to the reference in deionized water. Small amounts of excess electrolyte have large effects on the swelling pressure at high water to mineral ratios, which can be understood from the PB equation and Donnan equilibrium /Karnland et al. 1995/. Thus the slow turbidity increase for the samples with 5 and 10 mM NaCl is governed by diffusion and not an effect of active transport due to swelling. Theoretically, the diffusion coefficient for a thin disc undergoing Brownian motion in water with viscosity η is given by $D = k_B T / 12\eta r$ /Cadene et al. 2005/. With $r = 100$ nm, one obtains $D = 3.4\times10^{-12}$ m^2/s at $T = 298$ K so the time for diffusion over a distance of 1 cm ($\sqrt{2Dt}$) is 170 days which agrees fairly well with Figure 5-18.

For Ku-Na it was found in the sedimentation experiments that the CCC is 5 mM NaCl and from the swelling tests it is clear from the turbidities reported in Figure 5-19 that 5 mM NaCl or higher gives no colloidal sols. Swelling of Ku-Na in 1 mM NaCl causes the formation of a sol. However, the swelling is substantially reduced and the maximum turbidity is only about 1/10 of the turbidity at maximum for swelling and colloid release in deionized water (sample E12 in Figure 5-7).

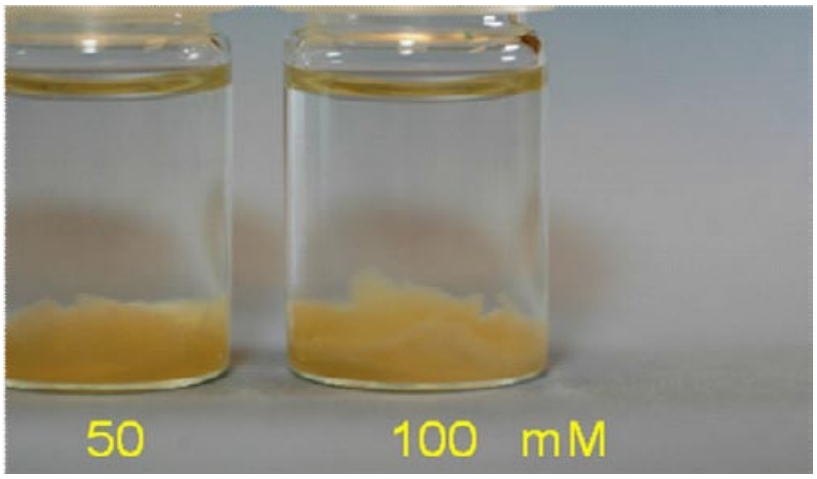

Figure 5-17. *Limited swelling of Wy-Na in NaCl solution above the CCC for NaCl. Notice the rough texture "lunar landscape" of the gel reflecting the original grains of clay.*

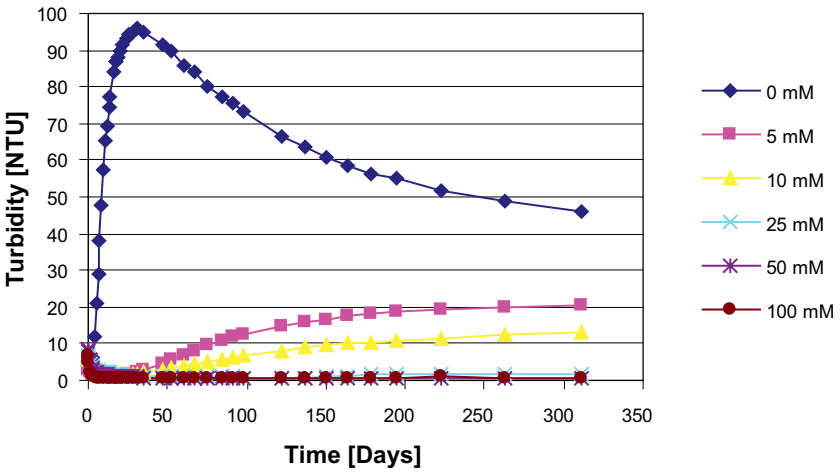

Figure 5-18. *Turbidity at vial mid-height vs. swelling time for Wy-Na at various concentrations of NaCl. Clay amount is 5 g/l electrolyte.*

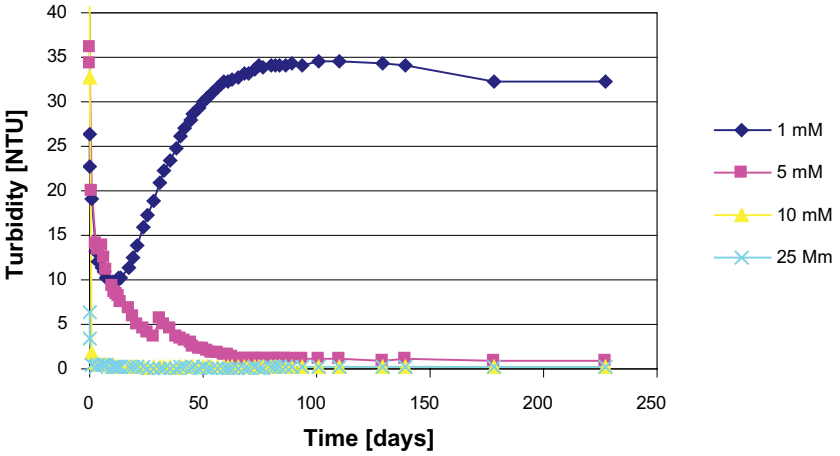

Figure 5-19. *Turbidity at vial mid-height vs. swelling time for Ku-Na at various concentrations of NaCl. Clay amount is 5 g/l electrolyte.*

Similarly, swelling tests on Mi-Na also show the same consistency with the sedimentation experiments and 10 mM NaCl gives a limited swelling. The CCC for Mi-Na is thus higher than for Ku-Na but lower than for Wy-Na. An important consequence of this is that the theoretical and most conservative sol-formation zone (Chapter 7) for Milos montmorillonite is considerably smaller than for Wyoming montmorillonite.

5.3.2.3 Density profiles for swelling of sodium montmorillonite

Having realized that aggregation is the main mechanism for sedimentation we will use this insight in the analysis of the swelling profiles below the critical NaCl concentration. When swelling was monitored by measuring turbidity at vial mid-height it was noted especially at low ionic strength, that the turbidity reached a maximum value after 10–20 days, as for Wy-Na in deionized water shown in Figure 5-18. Earlier it was argued that the rapid increase in turbidity at mid-height was caused by swelling. We will here demonstrate that the subsequent decrease in turbidity is mainly due to sedimentation, which is, as has been shown, caused by aggregation.

The swelling profiles for 0.04 g of Mi-Na in 10 ml deionized water are shown in Figure 5-20. Vial mid-height corresponds approximately to the depth 12 mm. The profile is recorded every 1.5 mm between 0 and the depth of 18 mm. The bottom of the vial corresponds to a depth of approximately 24 mm. Initial turbidities are about 20 NTU all over, due to the stir-up of clay particles when the

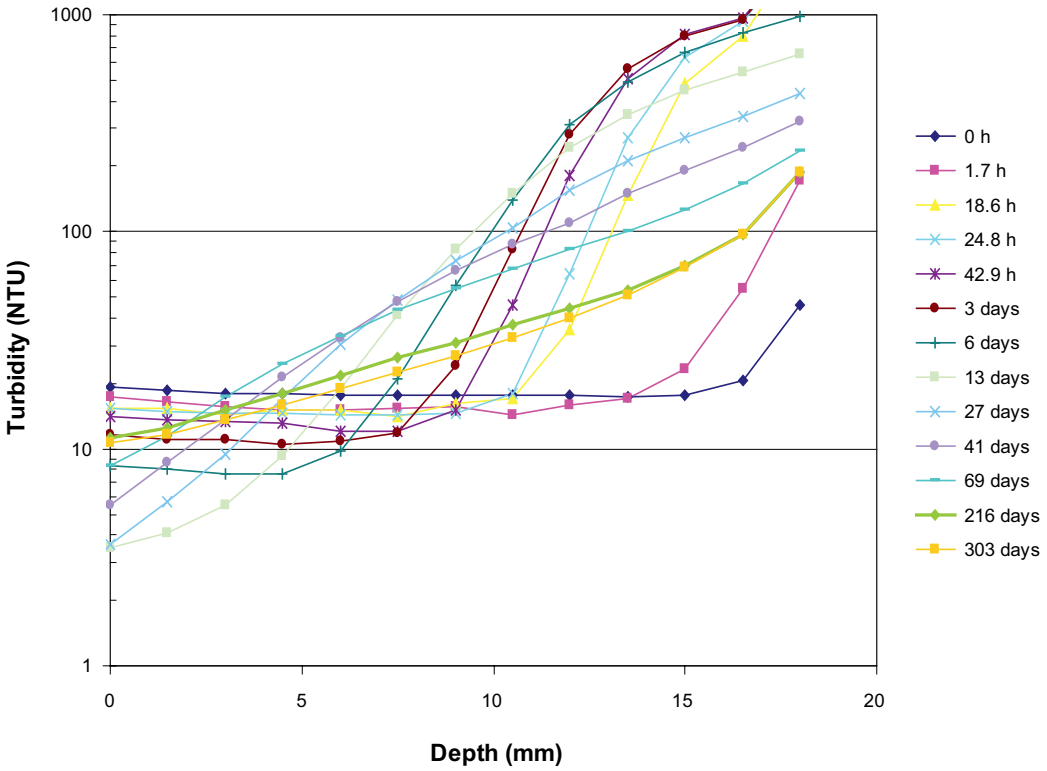

Figure 5-20. *Swelling profile (0–303 days) for 0.04 g Mi-Na in 10 ml deionized water.*

liquid is added. This undesired effect has been minimized by drying-in clay at the bottom, but it cannot be totally avoided. At the lowest three points 15–18 mm we see a rapid increase in turbidity due to swelling already after 1.7 h. After 6 days the turbidity has reached its maximum at 12 mm and at all later times the turbidity at that depth is decreasing. An inspection of the graph suggests that the integrated turbidity (= particle content) from 0–18 mm also is maximal after 6 or possibly 13 days. This means that clay particles are forming a deposit below the lowest detection height. Thus we conclude that the main cause of lowering the turbidity at vial mid-height is aggregation and not particles diffusing upwards, which might have been the other possibility.

The swelling of Mi-Na in 1 mM NaCl is very different from swelling in deionized water as can be seen in Figure 5-21. First of all, the turbidities are much lower, and second, the rate at which the swelling front moves upwards is also slower. The amount of clay brought out into the suspension by swelling is very limited compared to the results for deionized water. Therefore aggregation and sedimentation seem to be important only at the lowest two or three measured depths. Instead diffusion is the mechanism for redistributing particles.

Swelling tests in 5 mM NaCl solution shows that diffusion is the main upward transport mechanism of clay and the integrated turbidity across the monitored heights is slowly increasing (but at a decreasing rate) during the time span of 303 days.

From the data in Figure 5-20 and Figure 5-21 one can see that a steady-state is almost reached as the profiles at 303 days do not significantly differ from those at 216 days. The upper 13.5 or 15 mm of the profiles are straight lines in the log-scale which means that the expected exponential distribution of colloids has been reached. By fitting the equilibrium profiles to Equation 5-2 we find the clay particles in the suspension to have a radius of around 100 nm. As we have shown earlier, the settling of the sol is due to the formation of aggregates of size in the order of 1,000 clay particles. Now, we conclude from Equation 5-2 that the particles in the dilute sol at equilibrium are essentially single clay particles with radius of 100 nm. These two views are compatible if one assumes that the aggregates are not stable but have a probability to break-up. Sedimentation occurs when the formation rate of aggregates is higher than the disintegration rate. As the particle concentration in the suspension decreases, the aggregation rate decreases and at steady state disintegration and aggregation rates are balanced and essentially only individual clay particles or very small clusters remain. When the NaCl

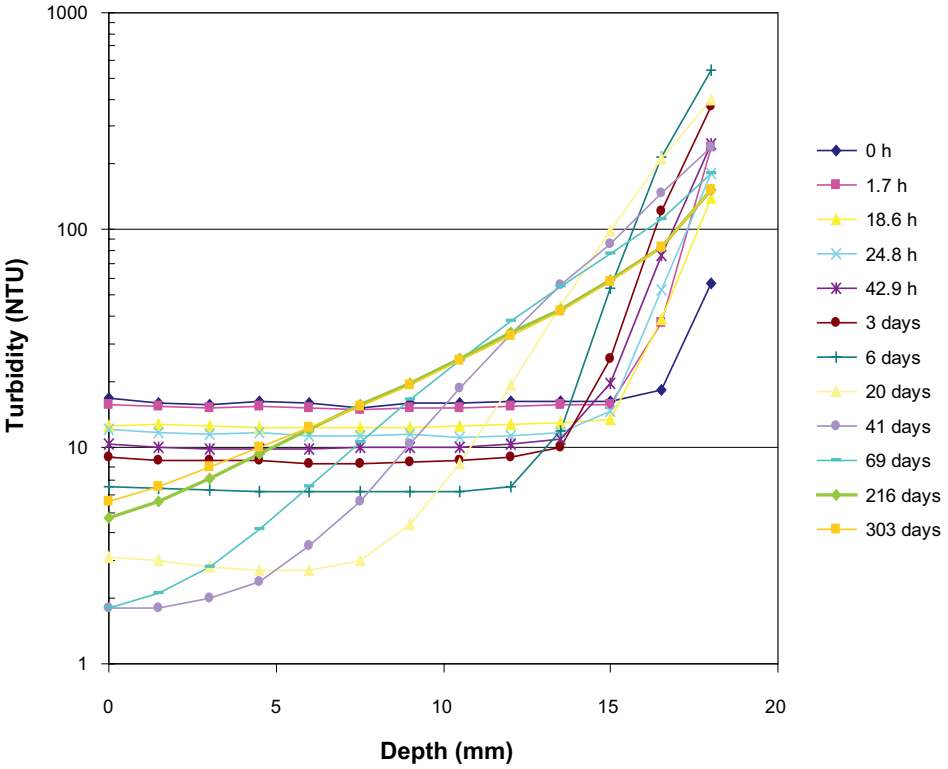

Figure 5-21. *Swelling profile (0–303 days) for 0.04 g Mi-Na in 10 ml 1 mM NaCl solution.*

concentration is above the critical value the aggregates do no longer disintegrate by thermal motion and instead a percolation gel is formed.

If one would shake the vials and then measure the turbidity it would be more or less constant at all heights as can be seen in the first profile in Figure 5-12. For Mi-Na the concentration 1 g/l corresponds to a turbidity of 194 NTU, thus 4 g/l gives the turbidity 776. The total height of liquid in the vials is 24 mm so the total amount of Mi-Na in Figure 5-20 and Figure 5-21 can be expressed as 776×24=18,624 NTU·mm. Integration of the profiles at 303 days and division by 18,624 gives the fraction of clay in the upper 18 mm of the vials. This turns out to be 4% in the case of deionized water and 3% in the 1 mM NaCl solution.

The swelling of 0.05 g Wy-Na in 10 ml solution follows the same pattern, as shown here for Mi-Na. The evaluated particle size is approximately the same, 100 nm. However the steady state amounts of Wy-Na in suspension are 7% in deionized water and 6% in 1 mM NaCl which is approximately twice of the amounts for Mi-Na. The stability (strength) of aggregates in Wy-Na is less as shown by the higher CCC. Whether this is the cause for the higher amounts of Wy-Na in suspension or if it is due to the 25% larger total amount of clay one cannot tell on the basis of the data at hand.

5.3.3 Effect of OH^- on gel formation of homoionic sodium montmorillonite

The approach taken in this work to judge whether a certain concentration of NaCl can cause coagulation of montmorillonite is based on the observation of the presence or absence of a macroscopic gel. To completely rule out sol formation in a swelling type of experiment may take up to a week. Similarly in sedimentation experiments, the compaction of the percolation gel to the point where a clear supernatant can be discerned also takes several weeks as indicated in the sedimentation profile of Wy-Na in 25 mM NaCl shown in Figure 5-14. This poses a slight problem for the investigation of gel-sol transition in the presence of added NaOH, because on the timescale of days or weeks the pH response will be governed by the dissolution of the mineral and not the titration of the edge Al- or Si-OH groups, /e.g. Duc et al. 2005, Tertre et al. 2006/. Thus to investigate the influence of pH on the protonation state of the edges the commonly used practice is to measure the pH response after only a short equilibrium time, /e.g. Wanner et al. 1994/ use 10 minutes in their titration experiments on Wy-Na from MX-80.

In order to make the timescale for the assumed pH response of the edge sites compatible with the observation of macroscopic gel formation we use a centrifuge to speed-up the emergence of a supernatant above the percolation gel. Due to the dimensions of the centrifuge and the vials, the force-field inside the vials shows a large difference between top and the bottom. For example, at an angular frequency of 1,020 rpm, the acceleration at the top (radial distance r=85 mm) is 100 g and at the bottom (r=120 mm) 140 g (g being the acceleration of gravity). Increasing the angular frequency to 1,600 rpm gives centrifugal accelerations of 240 and 340 g at the top and bottom respectively. For Wy-Na at a solid to liquid ratio of 5 g/l we find that the percolation gel formed in 25 mM NaCl cannot withstand these force gradients. Similarly for Ku-Na the force gradient pulls the percolation gel formed at the CCC =5 mM NaCl apart when the clay content is 2 g/l. Increasing the NaCl concentration to 10 mM gives a gel at 2 g/l that can be compacted in the centrifuge at an angular frequency of 1,020 rpm during 20 minutes. Without added NaOH the pH was measured to be 6.64 (Metrohm 691 pH meter with a pH glass electrode). The pH was changed in steps by adding 0.05 ml 20 mM NaOH followed by centrifugation and measurements of turbidity and pH. The gel appeared to become weaker at higher pH, noticeably above pH 9.

In another test series on Ku-Na the centrifugation was done 600 rpm for 60 minutes or longer in total, with inspection of the vials after 5, 10, 20 and 40 minutes of centrifugation. Even at this lower frequency the gel formed at 5 mM NaCl was pulled apart in the inhomogeneous force field so also in this case 10 mM NaCl is needed in order to use the centrifugation method. pH was changed by adding 0.2 ml 5 mM NaOH at a time. Initial pH in the vial with 10 mM NaCl was 7.04 and changed to 7.6 and 8.8 after the first and second addition of NaOH. A percolation gel was formed at all pH values up to 8.8 (the highest investigated pH in this test). The initial pH in the vial containing 5 mM NaCl was 7.4. Thus gel formation of Ku-Na at 5 mM does not require acidic conditions.

For Wy-Na we followed a different strategy and decided to make the percolation gel stronger by increasing the clay content to 10 g/l. Clay was dispersed overnight in two vials containing deionized water and 25 mM NaCl solution respectively. The vials were shaken vigorously and left to rest for 5 minutes, then centrifuged at 1,600 rpm for 10 minutes. The result after centrifugation is shown in Figure 5-22. A clear phase separation can be noticed in the system with 25 mM NaCl as expected. The pH in the suspension without added NaCl is 9.9 and 7.8 in the supernatant of the system with 25 mM NaCl. After addition of 1 µmol NaOH (0.05 ml 20 mM NaOH) again followed by shaking and 5 minutes rest and centrifugation, we find that the gel becomes weaker (the supernatant is somewhat cloudy after 10 minutes of centrifugation). After an additional 20 minutes of centrifugation at a lower frequency (1,020 rpm) a clear supernatant is obtained as shown in the photograph to the left in Figure 5-23. The pH in the supernatant is 9.1, whereas for the system with no NaCl the pH barely changes (9.95) after the addition of NaOH. In order to verify that the montmorillonite containing sediment is a gel and not a viscous liquid the vial was tilted and the gel shows no tendency to flow as can be seen in the photograph to the right in Figure 5-23.

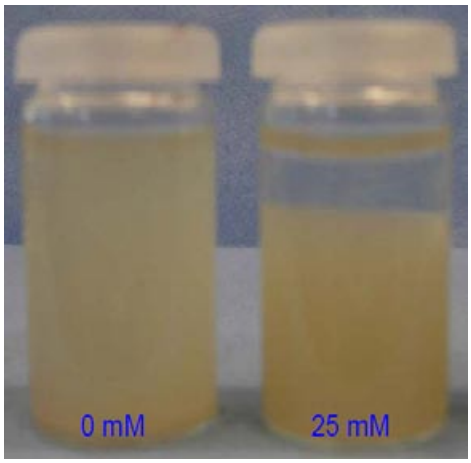

Figure 5-22. *Wy-Na (10 g/l average) after 10 minutes centrifugation at 240–340 g. An attractive gel is formed in the 25 mM NaCl solution (CCC) with a clear supernatant. No NaOH is added and the pH in the supernatant (right sample) is 7.8.*

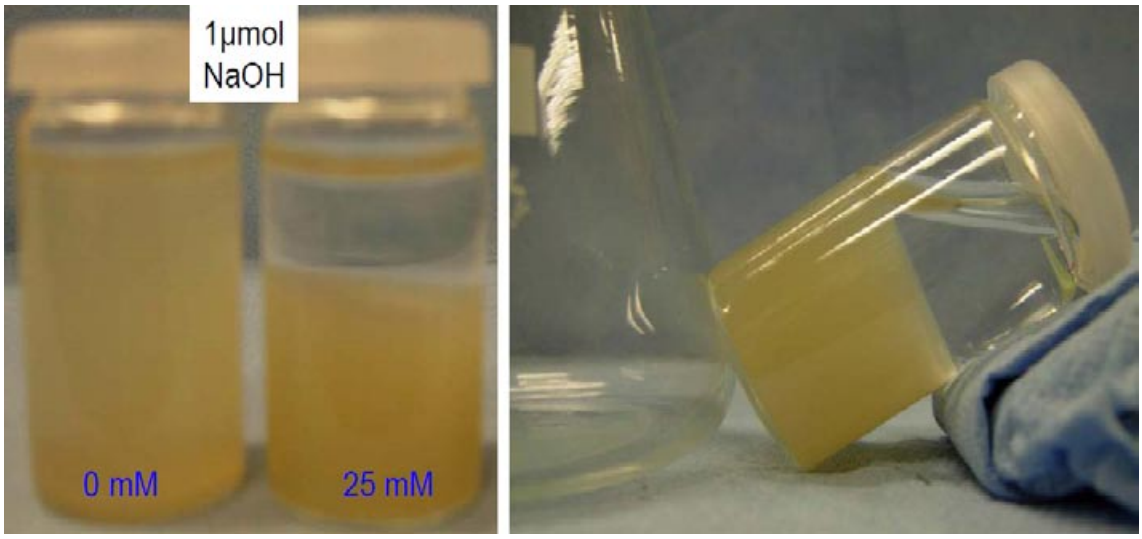

Figure 5-23. *Wy-Na (10 g/l average) after 20 minutes centrifugation at 100–140 g. The pH in the supernatant is 9.1. The photo to the right is taken 1.5 h after tilting the 25 mM sample. The gel is clearly attractive.*

Thus both for Ku-Na and Wy-Na the addition of NaOH leads to weakening of the formed percolation gel but not to sol formation as long as pH is within 7-9. This is in agreement with the findings for SWy-1 (Wyoming type montmorillonite) and Otay-montmorillonite by /Hetzel and Doner 1993/ who find only a weak dependence of CCC (NaCl) with pH in the above mentioned range.

The deionized water used in all our experiments is initially in equilibrium with the atmosphere giving a pH of about 5.9 due to CO_2. Obviously, montmorillonite buffers this initial acidic solution to a slightly basic solution. At NaCl concentration of 25 mM the equilibrium pH is found to be ~7.5 with 2 as well as 5 g Wy-Na per litre. We have also observed a trend of decreasing pH with increasing NaCl concentration. This is consistent with the shift of the point of zero net proton consumption (the intersection between raw titration curves for the blank and for the suspension) towards lower pH with increasing ionic strength, /e.g. Wanner et al. 1994, Avena et al. 2003, Tombácz and Szekeres 2004, Tertre et al. 2006/. This feature is not present in oxides without permanent layer charge, e.g. for kaolinite the point of zero net proton consumption is near pH=7 irrespective of the ionic strength /e.g. Kraepiel et al. 1998/. Naturally part of this observation in the case of montmorillonite is explained by sodium/hydrogen exchange to compensate the permanent layer charge. With increasing concentration of sodium more H^+ is replaced which results in lower pH. In addition to the surface exchange reaction, the proton affinity at the edge sites could be influenced by the permanent negative charge which is considered in the modelling by /Wanner et al. 1994/ and /Kraepiel et al. 1998/ using the same experimental data. An increase in ionic strength leads in the model used to more screening which results in a decreased proton affinity at the edge site. Thus there are two mechanisms that both suggest a lowering of pH in the clay suspension with increasing ionic strength.

The percolation gel is found to be formed at very high water to solid mass ratios. Most sedimentation tests have been performed at 2–5 g montmorillonite per litre, i.e. w_r in the range 200–500 which is beyond the water to solid mass ratio where montmorillonite particles can start to rotate freely (about 100 for a circular disc of radius 200 nm). For Ku-Na we have continued to dilute the dispersions and found gels at water to solid mass ratios as high as 1,300 (0.75 g/l). The so called house-of-card structure could not be space filling beyond $w_r = 100$ and a laminar structure of parallel clay layers is hardly a realistic model for an attractive gel at these high water to solid mass ratios ($w_r = 100$ corresponds to an average interlayer distance of 270 nm) since the van der Waals force, which is the only attractive force in the DLVO theory, is negligible. As said in the introduction, we arrive at a conceptual view of this attractive gel as a loose percolated network /Tanaka et al. 2004/ of clay particles interacting through edge to face attraction. The force of attraction is electrostatic between the negative faces and positively charged edges. The addition of NaOH led to a weaker gel, which we interpret as being caused by an increase of negative edge charge as pH increases. Still in order to have an attractive gel, the net edge charge must be positive even at pH 9, i.e. there are more,

presumably $Al-OH_2^{+1/2}$ groups than Si–O^- groups. The notion that the net edge charge may be positive in this pH range is by no means in conflict with titration data. In their review over acid-base properties of clays, /Duc et al. 2005/ find that published pK values are spread over 10 pH units. The most frequently found values were mainly located in three domains, pH 4–5, pH 6–8 and pH 10–11. Acidic pKs were normally attributed to the tetrahedral sites (Si–OH) and the basic pKs to the octahedral sites ($Al-OH^{-1/2}$). /Avena et al. 2003/ suggest a pK value of 10 for the latter sites, which thus are predominantly positively charged ($Al-OH_2^{+1/2}$) below pH 10.

As stated earlier the CCC for Ku-Na was found to be 5 mM NaCl (pH =7.4 in the supernatant solution). However, in 5 mM NaOH Ku-Na does not form a gel (pH=11.5) and remains a sol even after adding NaCl to a final sodium concentration of 15 mM. This observation fits the suggestion that above pH 10 the aluminol sites become largely negatively charged, thus the net edge charge is negative at pH=11.5.

In order to further test the notion of positive edge charges playing the major role in the formation of attractive gels, additional sedimentation and swelling experiments were performed on Wy-Na (5 g/l) in a mixture of 0.25% tetrasodium pyrophosphate ($Na_4P_2O_7{\cdot}10H_2O$) solution and NaCl of various concentrations (25, 50, 100, 250, 500 mM). Colloids were formed in the swelling experiments up to 100 mM NaCl. Equally, in the sedimentation experiments a dispersion of particles was developed in samples with 100 mM NaCl or less, and a weak gel was formed in 250 mM NaCl. Bear in mind that the 0.25% tetrasodium pyrophosphate also contributes 22.4 mM Na^+. Addition of $Na_4P_2O_7$ increases the critical concentration of NaCl by almost one order of magnitude. /Lagaly and Ziesmer 2003/ make the same observation for montmorillonite and the effect has also been quantified for synthetic hectorite (Laponite) by, e.g. /Mongondry et al. 2004/ who states that pyrophosphate screens the positive rim charges very effectively.

5.4 Discussion

5.4.1 Aggregation and gelation caused by edge-face interactions

The sedimentation experiments reported here show that even at low ionic strength (deionized water) there exist attractive forces among the clay particles that come into play at high water to solid mass ratios. The clay particles form aggregates that grow in size and eventually reach a point where gravity dominates over Brownian motion. The most likely force of attraction is electrostatic, between positive edge charges and negative faces, probably leading to overlapping coin configurations rather than house of cards /Jönsson et al. 2008/. This means that there are positive edge-charges present also at basic pH, somewhat in conflict with the commonly expressed view that the edge is positively charged below pH 6.5 /Tombácz and Szekeres 2004, Lagaly and Ziesmer 2003/. On the other hand there are numerous experiments performed on the synthetic hectorite named Laponite at pH 9–10 also suggesting the presence of positive edge charges. /Martin et al. 2002/ state that the edges are positive below pH 11 and at higher pH some of the surface sites may become ionized as SiO^- groups. We do see an effect of pH on CCC: Ku-Na does not form a gel in 5 mM NaOH but it does in 5 mM NaCl. This is a rather extreme case and the pH of the suspension is found to be above 11.5. In the pH range 7–9, there are no significant changes in CCC, which is also the finding by /Hetzel and Doner 1993/, so one may suspect that very high pHs are needed to make negative edge charges dominate over positive ones.

The influence of the edge charges on the aggregation process was further confirmed in sedimentation and swelling experiments on Wy-Na (5 g/l) in a mixture of 0.25% tetrasodium pyrophosphate ($Na_4P_2O_7{\cdot}10H_2O$) solution and NaCl of various concentrations. Pyrophosphate ions adsorb to the positively charged edge and thereby make the total net edge charge negative /Lagaly and Ziesmer 2003, Mongondry et al. 2004/. The addition of $Na_4P_2O_7$ increased the critical concentration of NaCl by almost one order of magnitude.

In Table 5-2 it is shown that an increase in the NaCl concentration leads to an increase in the second order rate constant for sedimentation. This is intuitively easy to comprehend as an increase in ionic strength increases the screening which has an effect on the face to face repulsion. There may also be the effect of screening the spillover of the negative electric field that somewhat bury the positive

edge at long distance as described by /Secor and Radke 1985/. We also notice that by increasing the ionic strength there is a change from a third to a second order rate law describing sedimentation in Wy-Na. A rate law in itself cannot be used to deduce a mechanism, but a proposed mechanism may lead to a rate law that can be tested experimentally. Therefore, for Wy-Na at low ionic strength there must be another mechanism operating in addition to bimolecular association of colloidal particles.

Ku-Na sediments according to a second order rate law already at 0 mM and the rate constant is as high as the rate constant for Wy-Na at 10 mM NaCl. A possible explanation for this lies in the difference in charge distribution between Wy and Ku, the latter having a considerable amount of tetrahedral charges /Karnland et al. 2006/, which should give a larger edge-face attraction /Hetzel and Doner 1993/.

At the CCC for Na-montmorillonite in NaCl (aq) there is yet another change in behaviour, where the edge-face association becomes irreversible. Aggregates formed in the sedimentation experiments actually span the whole vial initially even at 1 g montmorillonite per litre or less. This is a particle concentration that is almost ten times lower than the concentration where free rotation of clay particles can take place. This supports a picture that the attractive gel consists of branched chains of overlapping coins rather than a house-of-cards structure, which hardly could be space filling at these low particle concentrations.

Some scoping sedimentation experiments have also been performed on Wy-Na using sodium sulphate (Na_2SO_4) at concentrations 1, 5 and 15 mM which corresponds to ionic strengths of 3, 15 and 45 mM, respectively. 1 mM Na_2SO_4 is too low concentration to form a gel. A clear phase separation is seen both at 5 and 15 mM. Clearly sulphate ions do not have the same effect on edge charges as pyrophosphate ions. Furthermore the strength of the edge-face attraction seems to be related to the ionic strength, although one might conclude that CCC for Wy-Na seems to be in the vicinity of an ionic strength of 15 mM in the case of Na_2SO_4 and 25 mM in NaCl.

5.4.2 The critical coagulation concentration CCC

The CCC for either finite swelling or attractive gel formation in sedimentation studies is found to be the same. The percolation gel that is reached in sedimentation experiments has a much larger water to solid mass ratio than the attractive gel that is formed at the bottom of the vial in the swelling studies. This indicates that the percolation gel is not an equilibrium structure but rather a configuration where the clay particles are being locked-in. However, it is clear that the CCC found can only be explained in terms of edge-face interactions and not in terms of screening and van der Waals attraction, normally discussed in DLVO theory. A simple such calculation of CCC for Wy-Na would give something in the order of 1 M /Evans and Wennerström 1999/ and the measured CCC is around 25 mM. Furthermore in the DLVO treatment, the CCC is proportional to $\sigma^{4/3}$, σ being the surface charge, which means that the CCC for both Mi-Na and Ku-Na should be above that of Wy-Na. Instead, exactly the opposite is found in the experiments reported here. CCC for Mi-Na is 10 mM NaCl and as low as 5 mM for Ku-Na. In the primitive model (DLVO) for parallel clay layers, edge charges are never involved so there is no pH dependence on CCC, but Ku-Na does not coagulate in 5 mM NaOH not even after increasing the Na^+ concentration to 15 mM by adding NaCl to the suspension. Even more striking is the fact that CCC for Wy-Na is an order of magnitude larger than the value in NaCl, when edge charges are screened by pyrophosphate. These facts have substantial significance for theoretical modelling of colloidal release in montmorillonite. Any such modelling must consider the effect of edge-face interaction. Models based on, e.g, the DLVO theory for parallel clay layers without considering edge charges, do not contain the physical interactions needed for predicting the observed relatively low critical NaCl concentrations where coagulation occurs.

5.4.3 Mixed Ca/Na montmorillonite in deionized water

The swelling and sedimentation behaviours were studied for mixed Ca/Na-montmorillonites in order to determine at what percentage of sodium the limited swelling seen in pure Ca-montmorillonite is lost. This property of Ca-montmorillonite has been described in the literature and stems from ion-ion correlations in the interlayer that strongly influence the swelling pressure so it actually becomes negative beyond interlayer distance of approximately 10 Å /Guldbrand et al. 1984 Kjellander et al.

1988/. In order to separate the correlation effect of divalent ions from ionic strength effects or edge-face coagulation, these experiments were performed in deionized water.

An important finding is the fact that approximately 90% of CEC needs to be compensated by Ca^{2+} in order to have a calcium-dominated system, i.e. where correlation effects give a stable minimum. At first it appeared contradictory that as little as 10–20% sodium in the interlayer would make the clay qualitatively similar to a pure Na-montmorillonite. We made Prof. Bo Jönsson aware of these findings and he was able to demonstrate in numerically exact solutions of the primitive model that the delicate balance between osmotic repulsion and correlation effects indeed gives clays that show "unlimited" swelling when the sodium content is 20% and clays with limited swelling when the sodium content is 10% of CEC /Jönsson et al. 2009/.

We have argued that our experiments can only be explained if one assumes that the mixing of Ca^{2+} and Na^{+} occurs in the interlayer and not as de-mixed Ca- and Na-layers. Mixing at the interlayer level is also inherent in the calculations by /Jönsson et al. 2009/.

Both Kutch and Wyoming montmorillonite showed unlimited swelling at 20% sodium content. For Kutch montmorillonite no experiments with 10% sodium were carried out, but nothing suggests that Kutch montmorillonite would behave differently from the Wyoming material. If any difference, theory predicts higher correlation attraction the higher the layer charge, which means that Ku-Ca/Na would possibly need to contain more sodium than Wy-Ca/Na before forming a sol.

Montmorillonite with ~90% calcium or more behaves as pure calcium montmorillonite and does not release colloids. Furthermore it has been shown in the erosion tests that no Ca-montmorillonite is lost even when the filter pore size is as large as 100 μm. These results show that there would be no problem of buffer erosion in the repository provided that the sodium content of the clay at the swelling front in contact with the seeping ground water never exceeds 10%.

5.5 Erosion

5.5.1 Erosion test with Wy-80/20

To test how an 80/20 Wy-Ca/Wy-Na mixed clay behaves compared to the homoionic materials an experiment was run with this compound clay and 2 μm filters. Swelling pressure as a function of time is shown in Figure 5-24. The rate of decrease in swelling pressure is equal to that of Wy-Na (cf. Figure 4-4) despite the high content (80%) of Ca^{2+} in the clay. This confirms the earlier experimental and theoretical findings that an 80/20 montmorillonite behaves similar to pure Na-montmorillonite in deionized water. The Wy-80/20 clay appears to completely delaminate as it is flushed out through a 2 μm filter. Had there been any grains (stacks) of Wy-Ca present one would have expected some reduction in the erosion rate, bearing in mind that pure Wy-Ca does not erode even through a 100 μm filter.

5.5.2 Ionic strength effects

In this experiment Wy-Na clay was used since it is a clean homoionic clay with no water soluble contaminations. Sodium chloride, of various concentrations was circulated over the filters. As a first test deionized water was circulated in the cell until a drop in swelling pressure was seen, usually within hours, to verify that the cell was working. The measurements with different ionic strength were done with a stepwise increase in ionic strength. Between the different steps the swelling pressure was observed. When the swelling pressure was stable over days, the erosion was considered to have stopped. The swelling pressure response is presented in Figure 5-25. For comparison a test with deionized water is also shown. After 23 days the swelling pressure in the test with circulating NaCl is stabilized. At this point the NaCl concentration is 20 mM and no further solution exchange is done. Previously the CCC for Wy-Na has been determined to be 20–25 mM and this erosion experiment confirms that value. More importantly, the strength of the gel formed when Wy-Na is swelling in NaCl solution above the CCC is sufficient to prevent erosion.

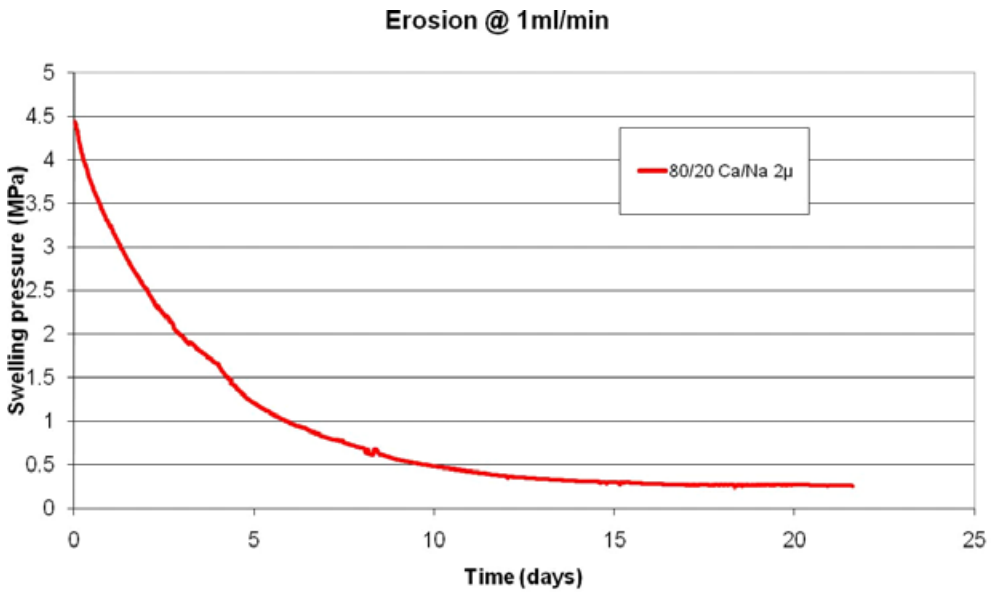

Figure 5-24. *Swelling pressure as a function of time for Wy-80/20 erosion test (pump stops excluded).*

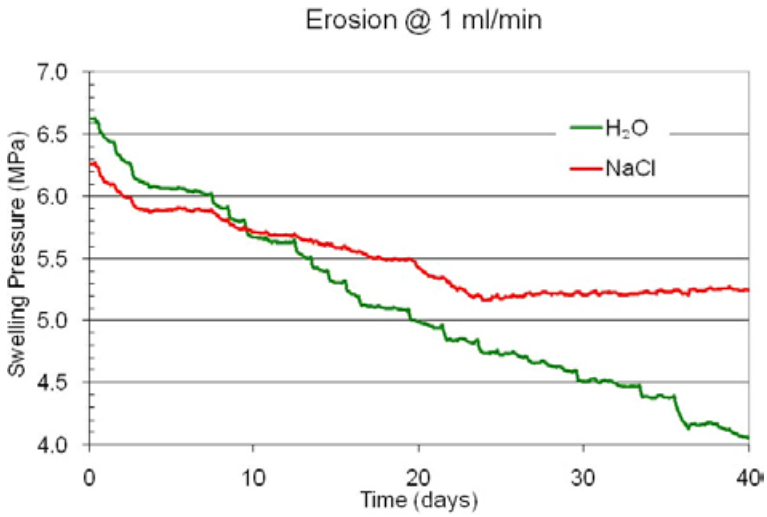

Figure 5-25. *Swelling pressure as a function of time. The NaCl concentration at the stabilization of swelling pressure is 20 mM.*

6 Ca/Na ion exchange equilibrium

6.1 Background

Na-montmorillonite produces colloids at low ionic strength conditions, pure Ca-montmorillonite does not, and relatively small amounts of sodium (20%) in the exchange position in an otherwise calcium dominated montmorillonite makes the clay act as a sodium clay (see Chapter 5). The sodium–calcium ratio is consequently of major importance and a selectivity coefficient is needed in order to calculate the ratio for a specific ground-water composition. Several investigators have measured a selectivity coefficient in batch experiments, i.e. in high water to solid mass ratios /e.g, Bradbury and Baeyens 2003/ and /Missana and García-Gutiérrez 2007/. The conditions in highly compacted bentonite are, however, radically different in many respects, e.g. the interlayer space is in the nanometer scale and the concentration of counter-ions is in molar range. The basic aim with the present part of the project was therefore to quantify selectivity coefficients for sodium/calcium exchange at short basal distances, and thereby give a relevant basis for calculating the long-term cation distribution in a KBS-3 bentonite buffer.

The law of mass action for the Ca^{2+}/Na^{+} exchange reaction is:

Ca^{2+} (solution) + 2 Na^{+} (clay) ↔ Ca^{2+} (clay) + 2 Na^{+} (solution)

According to the Gaines-Thomas convention /Gaines and Thomas 1953/, the selectivity coefficient K_{GT} may be expressed as:

$$K_{GT} = \frac{X_{Ca} \cdot \left[Na^{+} \right]^2}{(X_{Na})^2 \left[Ca^{2+} \right]} \qquad (6\text{-}1)$$

where X_{Ca} and X_{Na} are the equivalent charge fractions of Ca^{2+} and Na^{+} in the clay, $[Na^{+}]$ and $[Ca^{2+}]$ are the concentrations of sodium and calcium in the external solution, respectively. The experimental mission was consequently to determine the Na^{+} and Ca^{2+} distribution in systems with an external solution in equilibrium with a highly compacted clay sample. In addition, the swelling pressure evolution was measured as a response to the ion exchange, which is of general interest and gave additional information of when equilibrium was reached.

6.2 Experimental

6.2.1 Test principle

Homoionic Na and Ca-montmorillonite were prepared from commercial Wyoming bentonite (brand name MX-80 from American Coll. Co.) by removal of the fraction larger than 2 µm, repeated dispersion in 1 M chloride solutions of the relevant salt, removal of excess salt by centrifugations and successive dialyses. The resulting material was finally dried at 60°C /Karnland et al. 2006/.

Defined amounts of Wy-montmorillonite materials were compacted in 6 separate test cells (Table 6-1, Figure 6-1) All samples were confined by the titanium filters, which were completed with semi-permeable membranes (Spectrapore 3, 3,500 MWCO) in the Na-montmorillonite samples in order to prevent release of colloidal particles. Water saturation was started by circulating 0.1 l deionized water behind the filters by use of a peristaltic pump. The swelling force was measured, and ion exchange was started when constant force was measured. The test material was equilibrated with 0.1 l $CaCl_2$ solutions in the case of Na-montmorillonite, and NaCl solutions in the case of Ca-montmorillonite. In a first step, the content of cations in the solution corresponded to 25% of the total cation exchange capacity (CEC) in the test samples. The Na^{+} and Ca^{2+} concentrations in the test solutions were determined frequently by use of ion selective electrodes (Metrohm). At equilibrium, the content of replacing cations was increased to correspond to 50% of the CEC of each sample, and at new equilibrium to 100%. An exception was sample WyNa(Ca) 03 where the 50% step was overleaped due to the slow exchange in the first step. Consequently, the final conditions in all clay/solution systems contained equal charge from sodium and calcium ions, and the sum was twice the layer charge of the clay.

Table 6-1. Test program with intended saturated sample density (Dm), dry sample density (Dd), and the successive test solution concentrations (C1 to C3). Solution indicated by italics was not used.

Sample no.	Dm kg/m³	Dd kg/m³	C1 moles/L	C2 moles/L	C3 moles/L
WyNa 01	1,650	1,021	0.0057	0.0113	0.0226
WyNa 02	1,900	1,414	0.0078	0.0156	0.0313
WyNa 03	2,100	1,729	0.0096	*0.0191*	0.0383
WyCa 04	1,650	1,021	0.0113	0.0226	0.0452
WyCa 05	1,900	1,414	0.0156	0.0313	0.0626
WyCa 06	2,100	1,729	0.0191	0.0383	0.0765

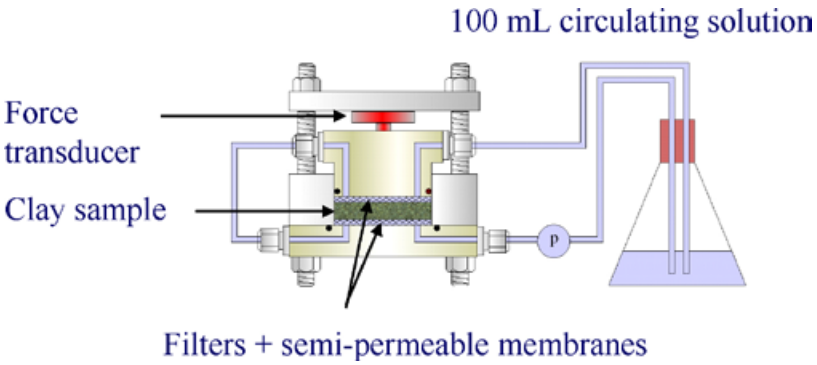

Figure 6-1. *Schematic drawing of the sample holder and external test solution.*

Swelling pressure was continuously measured in order to monitor the effects of the successive ion exchange and to verify equilibrium conditions.

6.2.2 Sample examination after test

At test termination, each test sample was removed as quickly as possible and split in two sections, one was placed in a ventilated oven at 105°C for 24 h in order to determine the water content (w). The second part was used for CEC determinations (Table 6-2) by use of the Cu-trien method /Meier and Kahr 1999/. The dried part was sent for chemical analyses by ICP/AES and Leco carbon analyzer.

The water content (w) was calculated according to

$$w = \frac{m - m_d}{m_d} \qquad (6\text{-}2)$$

where m is the specimen mass and m_d is the mass of the dry sample. The saturated sample density (D_m) was calculated from:

$$D_m = \frac{w + 1}{\frac{w}{D_w} + \frac{1}{D_s}} \qquad (6\text{-}3)$$

where D_w is the water density and D_s is the mean grain density. A water density of 1,000 kg/m³ and a mean grain density of 2,780 kg/m³ were used. The presented dry densities (D_d) were calculated according to:

$$D_d = \frac{D_m - D_w}{1 - \frac{D_w}{D_s}} \qquad (6\text{-}4)$$

6.3 Results

6.3.1 Swelling pressure

The swelling force (F) was measured and recorded hourly during the testing time, and the swelling pressure (P_s) was calculated from the measured force according to:

$$P_s = \frac{F}{A} \tag{6-5}$$

where A is the sample cross area perpendicular to the measure force. The swelling pressures (P_s) are shown in Figure 6-2 to Figure 6-7 (right hand scale), and the evaluated equilibrium swelling pressures are shown in Table 6-2.

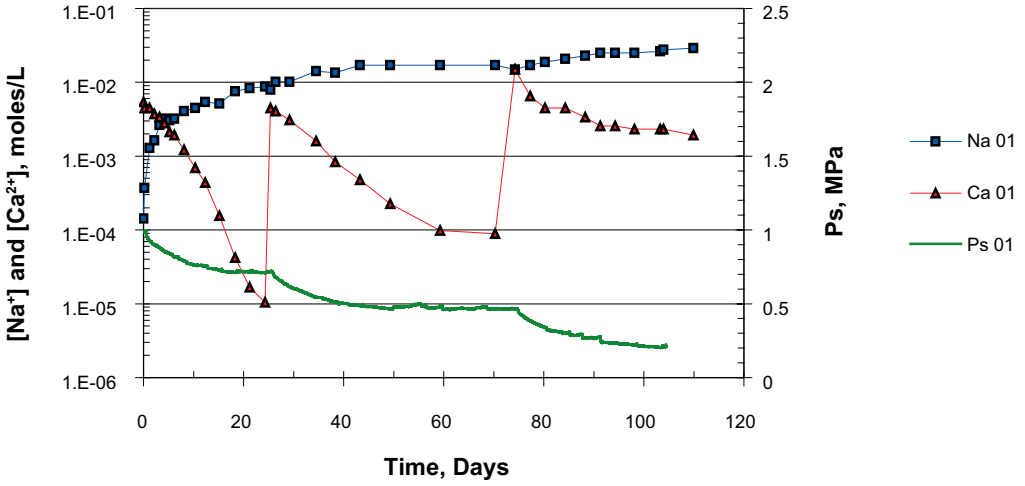

Figure 6-2. Sodium and calcium concentrations and swelling pressure (right-hand scale) in sample WyNa(Ca)01 as a function of time. Time represents elapsed time after the replacement of pure water by the first test solution.

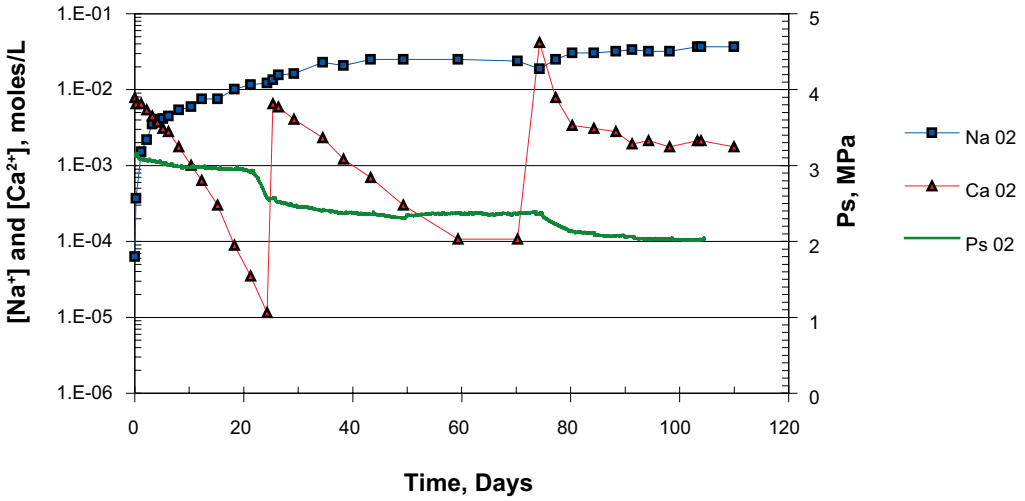

Figure 6-3. Sodium and calcium concentrations and swelling pressure (right-hand scale) in sample WyNa(Ca)02 as a function of time. Time represents elapsed time after the replacement of pure water by the first test solution.

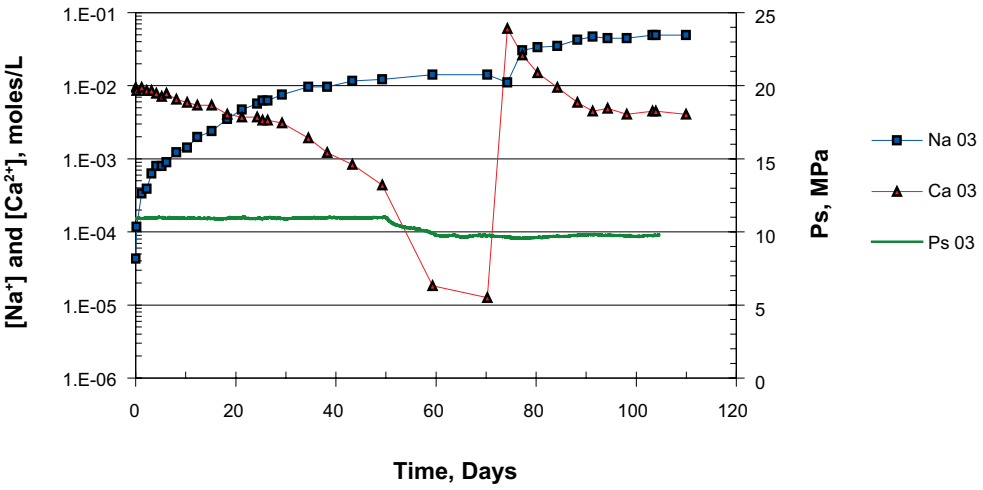

Figure 6-4. *Sodium and calcium concentrations and swelling pressure (right-hand scale) in sample WyNa(Ca)03 as a function of time. Time represents elapsed time after the replacement of pure water by the first test solution.*

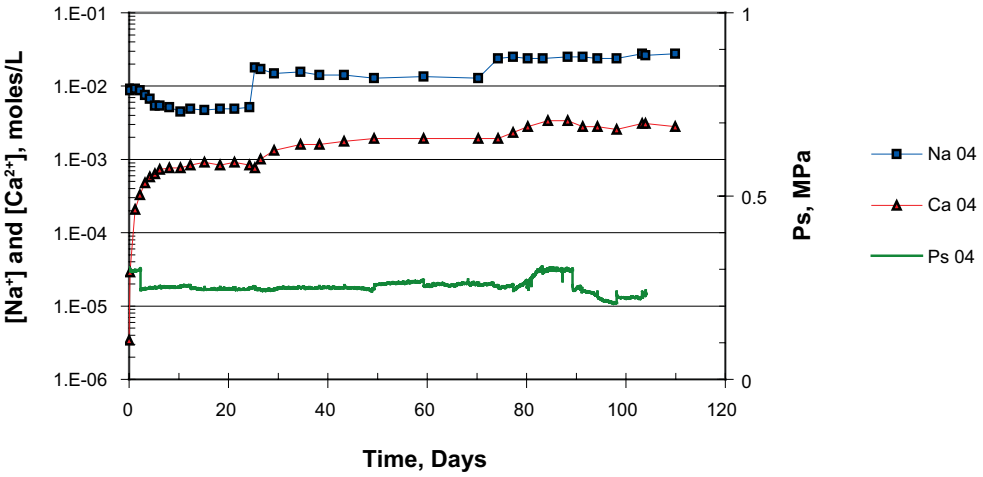

Figure 6-5. *Sodium and calcium concentrations and swelling pressure (right-hand scale) in sample WyCa(Na)04 as a function of time. Time represents elapsed time after the replacement of pure water by the first test solution.*

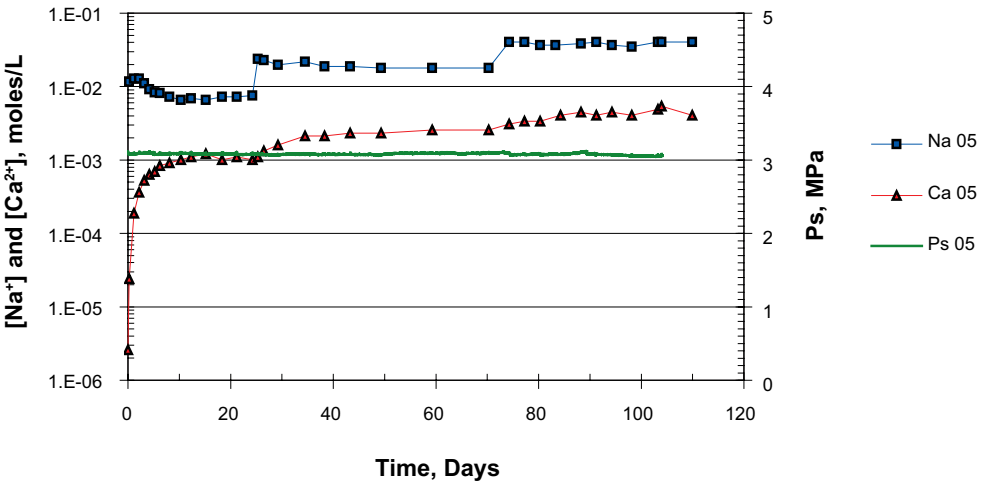

Figure 6-6. *Sodium and calcium concentrations and swelling pressure (right-hand scale) in sample WyCa(Na)05 as a function of time. Time represents elapsed time after the replacement of pure water by the first test solution.*

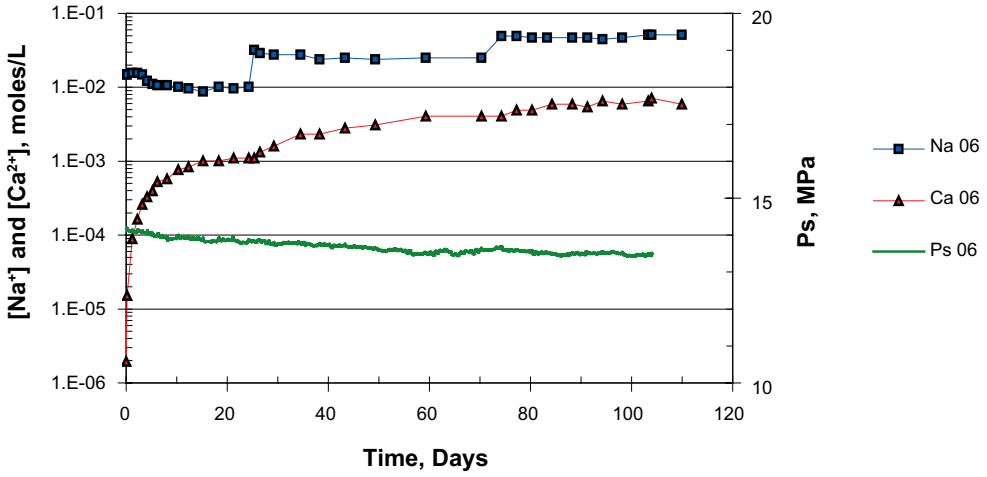

Figure 6-7. Sodium and calcium concentrations and swelling pressure (right-hand scale) in sample WyCa(Na)06 as a function of time. Time represents elapsed time after the replacement of pure water by the first test solution.

Table 6-2. Calculated final saturated density (Dm), dry density (Dd) and swelling pressure at equilibrium in all samples for the various boundary conditions (pure H_2O and C1 to C3).

Sample	Dm kg/m³	Dd kg/m³	H_2O MPa	C1 MPa	C2 MPa	C3 MPa
WyNa 01	1,615	967	1.0	0.70	0.47	0.21
WyNa 02	1,799	1,255	3.1	2.9	2.4	2.0
WyNa 03	1,979	1,538	10.9	11.0	-	9.7
WyCa 04	1,670	1,053	0.3	0.3	0.3	0.3
WyCa 05	1,825	1,296	3.1	3.1	3.1	3.1
WyCa 06	1,969	1,523	14.1	13.8	13.5	13.5

6.3.2 Ion analyses

pH increased from initial values around 5.3 to around 7 within one month in the three solutions which were contacted to sample WyNa 1 to 3. In the solutions contacted to samples WyCa 4 to 6, the initial pH was around 6.5 which rose to around 7 within a month. pH was thereafter relatively constant around 7 in all test solutions. The pH evolution was in principle the same for the test solutions as for the reference solutions. The Na^+ and Ca^{2+} ion selective electrodes were carefully calibrated against standard solutions, but still, the accuracy is generally not very impressive. The results should consequently only be used as supplementary information to the ICP/AES results of the final solution, and as an "online" measurement of the redistribution of the ions. The fast reduction of Ca^{2+} from the test solution and replacement by Na^+ correlates well with the response in swelling pressure in the originally sodium saturated clay samples (Figure 6-2 to Figure 6-4). The equilibrium concentration values were used to calculate the ion content within the clay by simple subtraction, and selectivity coefficients for each test solution and sample were calculated according to Equation 6-1. The ICP/AES results from the solid test materials (Table 6-4) were used to calculate the full structural formula for the six samples (Table 6-6) according to the technique presented in /Karnland et al. 2006/. The carbon analyses were made in order to examine whether $CaCO_3$ was formed by uptake of atmospheric CO_2 (Table 6-3). The small amount of inorganic carbon was compensated for by subtraction of the corresponding amount of Ca from the ICP/AES analyses. The structural formulas were used to calculate equivalent charge fractions, which were used together with the ICP/AES results from the test solutions to calculate selectivity coefficients for the 6 samples. All calculated selectivity coefficients from measured results are shown in Table 6-7.

Table 6-3. Water to solid mass ratio (w), Cation exchange capacity (CEC) and carbon content in the final test samples.

Sample	w	CEC Eq/kg	TOT/C %	CO2 %
WyNa 01	0.671	0.93	0.18	<0.02
WyNa 02	0.433	0.93	0.15	0.03
WyNa 03	0.286	0.92	0.15	0.05
WyCa 04	0.586	0.94	0.18	0.04
WyCa 05	0.408	0.94	0.17	0.07
WyCa 06	0.293	0.95	0.19	0.09

Table 6-4. ICP/AES main element results from the solid test materials.

Sample	SiO2 %	Al2O3 %	CaO %	Fe2O3 %	K2O %	MgO %	Na2O %	TiO2 %
WyNa 01	56.7	19.5	1.65	3.60	0.12	2.37	0.70	0.13
WyNa 02	57.0	19.6	1.66	3.61	0.12	2.37	0.71	0.13
WyNa 03	59.1	20.4	1.69	3.73	0.09	2.46	0.79	0.14
WyCa 04	57.6	19.8	2.03	3.67	0.11	2.32	0.47	0.14
WyCa 05	56.2	19.3	1.98	3.58	0.09	2.26	0.47	0.13
WyCa 06	58.0	19.9	2.04	3.70	0.10	2.33	0.52	0.14

Table 6-5. ICP/AES results from the final test solutions.

Sample	Na moles/L	Ca moles/L	K moles/L	Cl moles/L
WyNa 01	0.0293	0.0020	0.0008	0.0319
WyNa 02	0.0358	0.0021	0.0006	0.0277
WyNa 03	0.0479	0.0045	0.0004	0.0481
WyCa 04	0.0284	0.0031	0.0005	0.0283
WyCa 05	0.0416	0.0053	0.0004	0.0399
WyCa 06	0.0482	0.0069	0.0004	0.0565
WyCa (Na) ref.	0.0400	0.0000	0.0002	0.0366
WyNa (Ca) ref.	0.0012	0.0197	0.0003	0.0354

Table 6-6. Calculated structural formulas for the six test samples based on the ICP/AES analyses after the performed tests. Structural values shows atoms per $O_{20}(OH)_4$. X_{Ca} and X_{Na} are the calculated molar charge fractions used for the selectivity coefficient calculations. CEC are given in charge eq/kg.

Sample:	WyNa 01	WyNa 02	WyNa 03	WyCa 04	WyCa 05	WyCa 06
Si	7.95	7.95	7.93	7.95	7.95	7.95
Al	0.05	0.05	0.07	0.05	0.05	0.05
Sum tetrahedral	8.00	8.00	8.00	8.00	8.00	8.00
Al	3.11	3.12	3.12	3.12	3.13	3.13
Ti	0.01	0.01	0.01	0.01	0.01	0.01
Fe(III)	0.22	0.21	0.23	0.19	0.19	0.18
Fe(II)	0.16	0.17	0.14	0.19	0.19	0.20
Mg	0.49	0.49	0.49	0.48	0.48	0.47
Sum octahedral	4.00	4.00	4.00	3.99	4.00	4.00
O	24.00	24.00	24.00	24.00	24.00	24.00
H	4.00	4.00	4.00	4.00	4.00	4.00
Ca	0.25	0.25	0.24	0.30	0.29	0.29
Mg	0.00	0.00	0.00	0.00	0.00	0.00
K	0.00	0.00	0.00	0.00	0.00	0.00
Na	0.19	0.19	0.21	0.13	0.13	0.14
Unit cell weight	745	745	745	745	745	745
Layer charge	–0.69	–0.69	–0.69	–0.70	–0.70	–0.71
Interlayer charge	0.69	0.68	0.68	0.72	0.71	0.71
X_{Ca}	0.72	0.72	0.70	0.82	0.82	0.80
X_{Na}	0.28	0.28	0.30	0.18	0.18	0.20
Evaluated CEC	0.93	0.93	0.92	0.94	0.94	0.95
Measured CEC	0.93	0.93	0.92	0.94	0.94	0.95

Table 6-7. Evaluated selectivity coefficient (given in M) according to the Gains-Thomas convention. ISE indicate that ion selective electrodes were used to determine the ion concentrations in the test solutions, and that the ions content in the clay were calculated. ICP/AES indicate that ion content/concentration in both solids and solutions were determined by this method.

Method		ISE		ICP/AES
	C1	C2	C3	C3
C WyNa 01	3.0	4.9	4.6	4.0
C WyNa 02	5.5	8.6	7.8	5.5
C WyNa 03	6.5	-	7.6	3.8
C WyCa 04	1.7	1.7	1.8	6.7
C WyCa 05	4.1	3.4	4.2	7.8
C WyCa 06	8.8	7.3	6.1	7.0

6.4 Discussion and conclusions

We found that the Gaines-Thomas selectivity coefficient K_{GT} for calcium-sodium exchange in Wyoming montmorillonite under confined conditions is very similar to what has been found in batch experiments, /e.g, Bradbury and Baeyens 2003/ report K_{GT} = 2.6 M for Wy-Na and /Missana and García-Gutiérrez 2007/ find an average value of 4.5 M in homoionic Na-FEBEX bentonite. In addition we have found that K_{GT} can be estimated by solving the Poisson-Boltzmann equation /Jönsson and Wennerström 1980/ for two parallel charged surfaces in equilibrium with an external NaCl/$CaCl_2$ mixed solution. Integration of the ion concentration profiles obtained from the PB equation gives the occupancy of Na^+ and Ca^{2+} in the clay. This information together with the composition of the external electrolyte is all that enters the calculation of K_{GT}. In principle one should go beyond the PB equation when there are divalent ions present /Guldbrand et al. 1984, Kjellander et al. 1988/ because correlation among the ions establishes an attractive potential that greatly influences swelling pressures. However, in these PB calculations we do not aim to compute thermodynamic quantities directly related to the free energy, e.g. the swelling pressures, but the total compositions of Na^+ and Ca^{2+}. Such an integrated quantity is less sensitive to the neglect of correlations so here PB is still a reasonable zeroth-order approximation.

In the calculations, we have assumed the area per negative surface charge to be 145 $Å^2$, which is close to the charge density in Wy-Na. For the dense systems (layer separations h = 6 and 10 Å) the populations of Ca and Na ions are evaluated over the whole interlayer, whereas for the dilute system (h =200 Å) the density profile (Figure 6-8) is integrated up to 6 Å from the surface, which roughly corresponds to two layers of water molecules. In all cases studied 75–90% of the charge is located within 6 Å. We have also confirmed that the surface potentials are essentially identical for interlayer separations of 200 and 1,000 Å so the values reported for 200 Å interlayer distance could be compared with batch experiments.

The findings from the calculations based on the PB equation are shown in Table 6-8. Particularly in the confined systems we find very little variation of K_{GT} with the composition of the external solution. For interlayer separation of 6 Å, K_{GT} = 8–8.1 M and for 10 Å the values are between 5.1 and 5.3 M. For the low density system h = 200 (or 1,000) Å we find a larger spread in the values. The upper limit varies between 4.3 and 4.7 M and the lower limit between 3.2 and 4 M. Note that these are not comparable to limits or error bars in an experiment. In the calculation the two limits originate from two different approaches of performing the numerical integration, which, for reasons specific to the particular PB computer code used, is less accurate at large h. Thus one needs to be cautious when interpreting the variation in K_{GT} with the ionic composition of the external solution for the dilute system (h = 200 Å). The theoretical prediction that K_{GT} increases with decreasing interlayer distance can be explained in terms of electrostatics and the fact that the Boltzmann distribution favours divalent ions over monovalent. When the distance between the two charged surfaces decreases, the magnitude of the electrostatic potential, $\Phi(x)$ increases, i.e. Φ becomes more negative, at all positions x in the interlayer. Since the population of ions in the interlayer is related to the external concentration, c_0 through the Boltzmann factor $c(x) = c_0 \exp(-ze\Phi(x) / k_BT$ where ze is the charge of the ion /Evans and Wennerström 1999/, one sees that divalent counterions are more favoured than monovalent counterions when the potential becomes more negative, and as a result K_{GT} increases. The calculations presented here show that the K_{GT} varies from 3–4 M in the dispersed system up to about 8 M for compacted clay, i.e. a factor of two. Such difference in K_{GT} between the dispersed and compacted clay is essentially insignificant for the sodium-calcium equilibrium between the clay and an external solution at low ionic strength. It follows from Equation 6-1 that the fraction of calcium in the clay is proportional to K_{GT} and more importantly, inversely proportional to the square of the sodium concentration in the external solution. Therefore, calcium will be preferential over sodium in the clay when the external solution has low total concentrations. Our measured selectivity coefficients for compacted montmorillonite show possibly the expected trend of being higher compared to those measured in batch. This means that the compacted clay is at least as preferential for divalent ions as the dispersed clay. In view of the discussion above, the value K_{GT} = 4.5 M used in the mapping of the sol formation zone (Chapter 7) is justified both from our and others' measurements as well as from fundamental theoretical considerations. Furthermore, these calculations demonstrate that selectivity coefficients for Ca-Na exchange can be determined from electrostatics alone without invoking special sorption mechanisms or surface complexation.

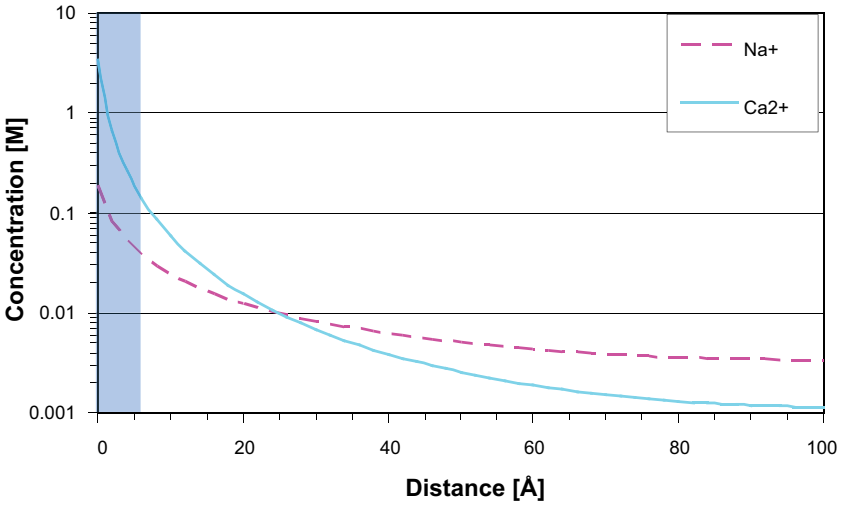

Figure 6-8. *Ion profiles outside a montmorillonite surface located at 0. The concentrations in the external solution are 1 mM NaCl and 0.1 mM $CaCl_2$. More than 80% of the charge is located within the blue-shaded region 0–6 Å away from the surface.*

Table 6-8. Selectivity coefficient (Gaines-Thomas convention) calculated using the Poisson-Boltzmann equation for different layer separations and compositions of the external solute.

Debye length [Å]	$C(Na^+)$ [mM]	$C(Ca^{2+})$ [mM]	K_{GT} h = 6 Å	K_{GT} [M] h = 10 Å	K_{GT} [M] h = 200 Å
5.2	200	50	8.1	5.3	4.0–4.7
6.4	200	10	8.1	5.3	3.8–4.5
6.8	200	1	8.1	5.3	3.7–4.4
12.0	50	5	8.0	5.2	3.5–4.3
13.3	50	1	8.0	5.1	3.4–4.2
19.4	10	5	8.0	5.1	3.4–4.3
27.0	10	1	8.0	5.1	3.4–4.3
85.2	1	0.1	8.0	5.1	3.2–4.3

7 Sol formation of Na/Ca-montmorillonite with excess ions

7.1 Introduction and overview

The montmorillonite in naturally occurring bentonites always contains several types of counterions. Furthermore, the counterion population of the buffer will change during the KBS-3 repository lifetime due to ion exchange with the ground water of the host rock. For KBS-3 conditions, the dominating counterions are sodium and calcium, which in pure systems give very different montmorillonite properties with regard to colloid release, as was shown in Chapter 5. Hence, in order to assess under what conditions sol formation could occur in the buffer, it is of decisive importance to investigate the sol formation properties of a mixed Na/Ca-montmorillonite contacted with a Na/Ca-solution.

In the montmorillonite systems studied so far, the ion exchange process is suppressed, either because the systems have contained only one type of cation (Ca or Na) or because the external solutions have been ion free. In this more realistic case, however, the process of ion exchange will be completely central for an accurate description of sol formation.

This chapter focuses on presenting a framework for how to describe a general Ca/Na-montmorillonite system. Using information on the Ca/Na exchange process (Chapter 6) and on sol formation properties in pure systems (Chapter 5), calcium and sodium concentration limits are derived for possible sol formation in the mixed Ca/Na-system.

Further, the sol formation ability of Wyoming type montmorillonite in various $CaCl_2$/NaCl-solutions has been extensively studied and compared to the expected behaviour based on information on the pure systems discussed in Chapter 5. This comparison shows that the sol formation ability in a mixed Ca/Na-system with excess ions is much lower than what would be expected only from electrostatic screening by ions in the external solution. It is therefore concluded that the explicit presence of excess calcium ions, also in relatively small amounts, dramatically lowers the sol formation ability of a Ca/Na-system. It is also argued that this mechanism must be associated with the edge-to-face interactions of the separate montmorillonite layers.

Finally some erosion tests made with mixed Ca/Na-solutions on both pure montmorillonite and natural MX-80 bentonite are presented which to a large extent support the findings of suppressed sol formation ability with the presence of excess calcium ions. The results indicate that typical ion concentrations of glacial meltwaters (0.1–1 mM) could be enough to chemically prevent buffer erosion.

7.2 Ion exchange equilibrium

When montmorillonite is in contact with an external Ca/Na-solution, the process of ion exchange between the clay and the solution becomes central for describing the system.

The law of mass action for the Ca^{2+}/Na^{+} exchange reaction can be expressed in the Gaines-Thomas convention (see further Chapter 6)

$$\frac{X \cdot \left[Na^{+}\right]^2}{(1-X)^2 \left[Ca^{2+}\right]} = K_{GT} \qquad (7\text{-}1)$$

where K_{GT} is the selectivity constant and X is the equivalent charge fraction of Ca^{2+} in the clay.

Because the reaction requires two Na ions from the external solution to exchange one Ca ion in the clay, the process will favour the Ca population in the clay (X closer to 1) in external solutions with low concentrations, as illustrated in Figure 7-1. Furthermore, the selectivity coefficient, which reflects the intrinsic preference of the clay for one type ion over the other, favours Ca over Na with a value in the range 3–8 M (see further Chapter 6).

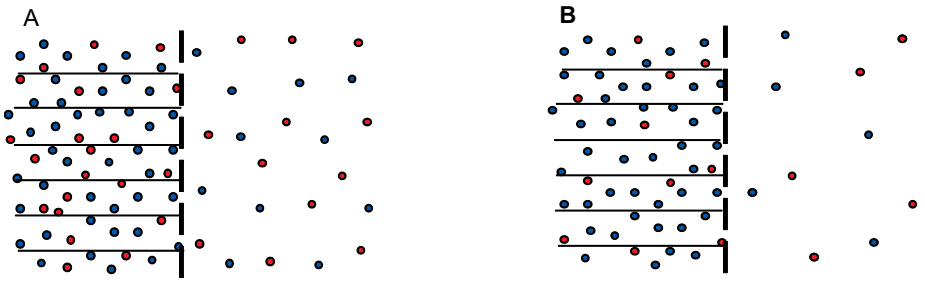

Figure 7-1. *Illustration of ion exchange equilibrium between montmorillonite (left compartment) an external solution (right compartment) in high (A) and low (B) total external concentration. Calcium ions are coloured blue and sodium ions red. At lower total external concentration (B), calcium population in the clay increases (and sodium population decreases) for the same concentration ratio.*

7.3 Possible sol formation zone

From the previous section it is clear that any specific Ca/Na-solution (specific values of $[Na^+]$ and $[Ca^{2+}]$) in equilibrium with montmorillonite results in a specific ion population in the clay (X) as given by Equation 7-1.

Two types of phase transitions have been observed in the montmorillonite systems studied so far (Chapter 5):

- A transition from a sol to a gel in pure Na-montmorillonite as the external Na concentration was increased. This transition is assumed to depend on the ionic strength of the external solution (due to screening of the electrostatic potential).
- A transition from a non-sol forming to a sol forming material in deionized water as the Na fraction increased in a mixed Ca/Na-montmorillonite.

When discussing the phase diagram in a general Ca/Na-system it is therefore convenient to make use of the variables X (clay ion population) and I (ionic strength). In the specific case of having mono-valent anions in the system (e.g. a $CaCl_2$/NaCl solution) the ionic strength is

$$I = [Na^+] + 3 \cdot [Ca^{2+}] \qquad (7\text{-}2)$$

Using the variables X and I, two functions can be defined:

- $X_{crit}(I)$ – critical Ca fraction needed for the material to be non-sol forming, at a given ionic strength.
- $I_{sol-gel}(X)$ – ionic strength at which the sol – gel transition occurs for a clay with a given Ca/Na population.

In the pure Na-systems investigated earlier, it was shown that $I_{sol-gel}(0)$ was strongly dependent on clay type. For Wyoming type montmorillonite, $I_{sol-gel}(0)$ = 25mM. Furthermore, the study of mixed clays in deionized water ($I = 0$) showed that $X_{crit}(0) \approx 0.9$ for any of the investigated types of clays.

To get an idea what ion concentrations sol formation might occur in a general Ca/Na system we will assume that the two above defined functions are constant and equal to the values found in the earlier studied special cases. Monte Carlo calculations of the primitive model confirm that $X_{crit}(0) \approx 0.9$, but also suggests that this function has a lower value at higher ionic strengths /Jönsson et al. 2009/. Thus, to approximate this function with its value at zero ionic strength is a conservative assumption. Also, to put $I_{sol-gel}(X)$ equal to its value in the pure Na-system ($X = 0$) could be considered conservative, since the ability to form a sol is definitely not expected to increase as the Ca-fraction of the clay increases (if anything, $I_{sol-gel}(X)$ is expected to decrease with increasing X).

Figure 7-2 shows lines of constant I and X in a $[Ca^{2+}]$-$[Na^+]$-diagram assuming a single mono-valent anion (Eq. 7-2). Note that the y- and x-axes in the $[Ca^{2+}]$-$[Na^+]$-diagram obviously corresponds to the curves for a pure Na-system ($X = 0$) and a pure Ca-system ($X = 1$), respectively.

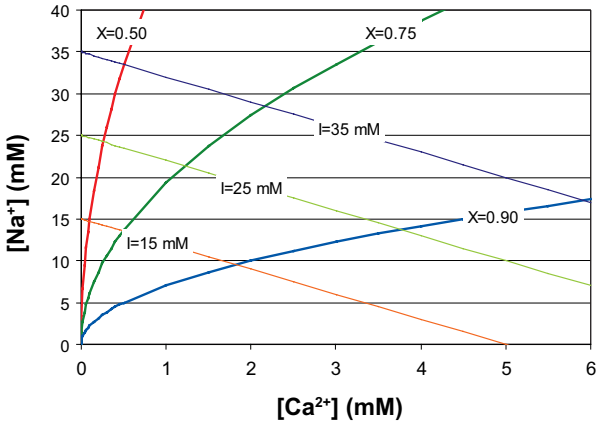

Figure 7-2. *Lines of constant ion population and lines of constant ionic strength in montmorillonite contacted with an external Ca/Na-solution with monovalent anions. The selectivity coefficient equals 4.5 M in the calculations.*

With the above assumptions, and specifying to Wyoming type montmorillonite, a zone of possible sol formation in the $[Ca^{2+}]$-$[Na^{+}]$-diagram is limited from above by the line

$$I_{sol-gel}(X) = 25 \text{ mM} \tag{7-3}$$

Wyoming type montmorillonite in equilibrium with Ca- and Na-concentrations above this line is expected to form a gel in accordance with the observations of a pure NaCl-system. The possible sol formation zone (SFZ) is also limited from below by the line

$$X_{crit}(I) \approx 0.9 \tag{7-4}$$

since systems in equilibrium below this line are expected to be non-sol forming. The possible SFZ for Wyoming type montmorillonite and a mono-valent anion (e.g. Cl^{-}) is pictured in Figure 7-3.

The beak-shaped sol formation zone reveals several interesting features of a $CaCl_2$/NaCl-montmorillonite system. Firstly, we see that only 3-4 mM of $CaCl_2$ (for the case of Wyoming type montmorillonite) will give a system which in equilibrium does not form a sol regardless of the magnitude of the ionic strength – the system is "to the right" of the SFZ. Note that the ionic strength of 4 mM $CaCl_2$ is 12 mM which is substantially lower than 25 mM, the limit for gel formation in a pure sodium state of a Wyoming type montmorillonite.

Secondly, we see that a sol could start to form by *increasing* the ionic strength of the system. If, for example, the system is in equilibrium with a pure $CaCl_2$-solution of 2 mM, the counterion population obviously is $X = 1.0$ and no sol is formed ($X > X_{crit}$). By adding NaCl to the system, it moves towards the SFZ from below (since the clay becomes more and more populated by sodium ions) and at a NaCl-concentration of approximately 10 mM a sol is expected to form ($X < X_{crit}$, $I < I_{gel\text{-}sol}(X)$). With a continued increase of the NaCl-concentration (and thus an increase of the ionic strength), the sol formation is expected to cease and a gel state to appear at a NaCl-concentration of approximately 19 mM.

Thirdly, by experimentally mapping out the SFZ, much information can be gained about the $CaCl_2$/NaCl-montmorillonite system. For instance, the red line in Figure 7-3 (I =25 mM) is an upper limit for the SFZ while the shape of the actually observed zone would answer the question at what ionic strength gel formation occurs for a clay of a given counterion population, i.e. give the function $I_{sol-gel}(X)$ (or show whether X is an appropriate variable to use for describing the behaviour of the system). Furthermore, fitting the lower limit (black line) to experimental data would be a means to better quantify the critical Ca – population where sol formation does not occur (i.e. give the function $X_{crit}(I)$). The shape of the SFZ is a sensitive function of this value, as is indicated by the curves in Figure 7-2. Also the selectivity coefficient for the Ca/Na exchange reaction could in principle be quantified by comparison with the experimentally obtained SFZ. However, the shape of the SFZ is not as sensitive to the value of K_{GT} as it is to X_{crit}.

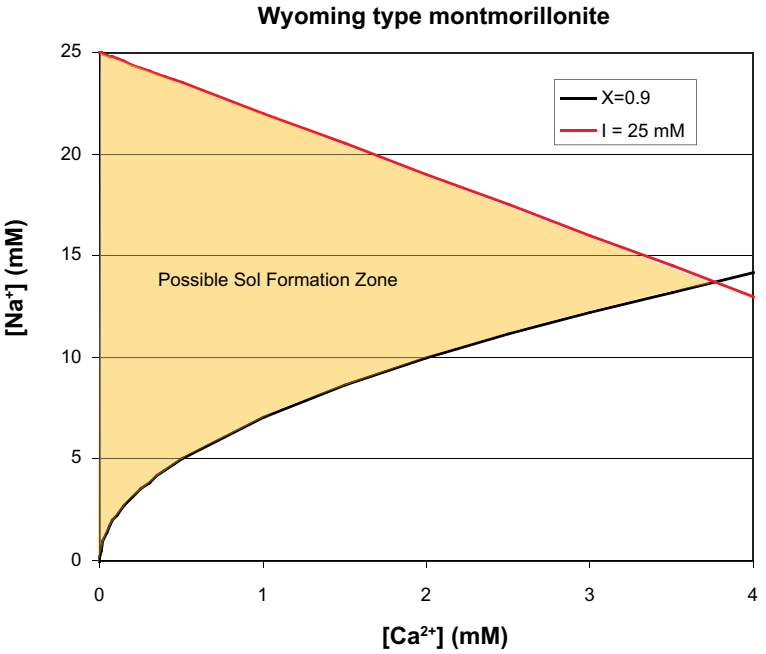

Figure 7-3. *Limitations of a possible sol formation zone for Wyoming type montmorillonite in equilibrium with an external Ca/Na-solution and mono-valent anions (e.g. Cl^-).*

In Figure 7-4 is seen the corresponding SFZ for Kutch type montmorillonite based on the same values of the constants as before (X_{crit} = 0.9, K_{GT} = 4.5 M) and the fact that gel formation in the pure Na-state of this clay occurs already at an ionic strength of 5 mM (i.e. $I_{sol-gel}(X)$ = 5 mM). It is seen that the SFZ in this case is dramatically diminished in comparison to Wyoming type montmorillonite, which is a direct consequence of the much lower concentration at which the gel-sol transition occurs for this clay under pure NaCl-conditions.

Looking at Figure 7-3 and Figure 7-4 it is seen that a definition of a critical coagulation concentration (CCC), a limiting concentration where gel formation occurs, can only be made unambiguously in the case of a pure Na-system (or a pure Ca-system where it is *zero*). A pure Na-system corresponds to the points on the y-axis in the $[Ca^{2+}]$-$[Na^+]$-diagram and the CCC in this case corresponds to the concentration where the red line intercepts this axis, i.e. it is the critical NaCl-concentration inferred from experiments in the first place.

For a montmorillonite system with a counterion population of both Ca and Na, the above discussion and figures show that defining a CCC becomes cumbersome since not only does e.g. the critical Na-concentration depend on the present Ca-concentration, there is also both an upper and a lower limit for each value of $[Ca^{2+}]$. In other words, instead of a single parameter (CCC) the whole SFZ must be specified in order to quantify the sol formation ability of a Ca/Na-system.

7.3.1 Practical concerns

The above section discussed the Ca/Na-montmorillonite system from an equilibrium point of view. This section presents practical formulas for describing equilibrium concentrations in specific experimental situations with e.g. a specified solid-to-water ratio. The variables describing the system are illustrated in Figure 7-5.

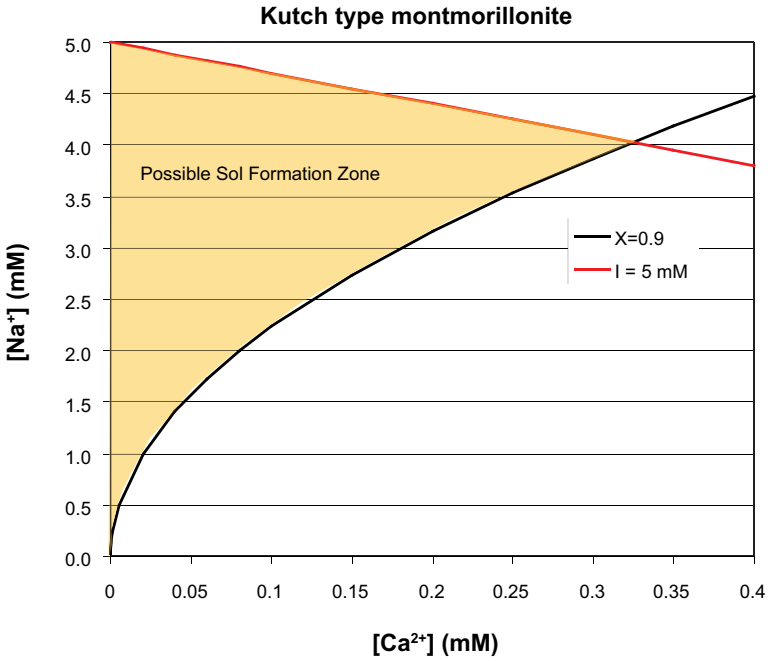

Figure 7-4. *Limitations of a possible sol formation zone for Kutch type montmorillonite in equilibrium with an external Ca/Na-solution and mono-valent anions (e.g. Cl^-).*

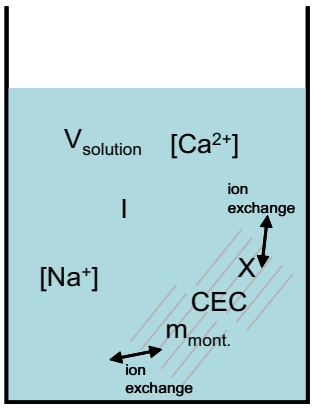

Figure 7-5. *Variables describing the system in a typical experimental situation. Montmorillonite of mass m_{mont} and cation exchange capacity CEC is immersed in a solution of volume $V_{solution}$. The ion content of the clay is described by the equivalent charge fraction of calcium, X and the ion content in the solution by calcium and sodium concentrations. Ionic strength is denoted I.*

7.3.1.1 Fixed amount of ions

In these types of experiments montmorillonite with an initial ion population (X_0) is immersed in a Ca/Na solution with initial concentrations $[Ca2^+]_0$ and $[Na^+]_0$. Usually the initial solution is not in equilibrium with the initial ion population of the clay and ions are redistributed between clay and solution until ion exchange equilibrium is achieved (Equation 7-1). The relation between initial and equilibrium concentrations is

$$\begin{aligned}\left[Ca^{2+}\right] &= \left[Ca^{2+}\right]_0 + (X_0 - X)\frac{u}{2} \\ \left[Na^{+}\right] &= \left[Na^{+}\right]_0 + (X - X_0)\cdot u\end{aligned} \tag{7-5}$$

where

$$u \equiv \frac{m_{clay}\cdot CEC}{V}\ . \tag{7-6}$$

Combining Equations 7-5 and 7-1 gives

$$K_{GT} = \frac{X\cdot\left(\left[Na^{+}\right]_0 + (X - X_0)\cdot u\right)^2}{(1-X)^2\cdot\left(\left[Ca^{2+}\right]_0 + (X_0 - X)\frac{u}{2}\right)}, \tag{7-7}$$

a third order algebraic equation in X, which easily can be solved in the general case (at least numerically).

The mathematical complexity is less for the problem of calculating the required initial concentrations, given the equilibrium concentrations and initial clay ion population. Solving Eq. 7-1 for X gives

$$X = 1 + \frac{R - \sqrt{R\cdot(4+R)}}{2} \tag{7-8}$$

where

$$R \equiv \frac{\left[Na^{+}\right]^2}{K_{GT}\cdot\left[Ca^{2+}\right]}$$

Combining Equations 7-5 and 7-8 gives

$$\begin{aligned}\left[Ca^{2+}\right]_0 &= \left[Ca^{2+}\right] + \left(1 + \frac{R - \sqrt{R\cdot(4+R)}}{2} - X_0\right)\frac{u}{2} \\ \left[Na^{+}\right]_0 &= \left[Na^{+}\right] - \left(1 + \frac{R - \sqrt{R\cdot(4+R)}}{2} - X_0\right)\cdot u\end{aligned} \tag{7-9}$$

7.3.1.2 Ion concentrations set by mineral equilibrium

Another experimentally interesting situation is when pure Na-montmorillonite ($X_0 = 0$) is put in a solution where the Ca-concentration is kept constant by equilibrium with a mineral rather than having a fixed amount of Ca-ions in the system (as presented in Chapter 2). The equilibrium condition (Eq. 7-1) then simplifies to

$$K_{GT} = \frac{X^3\cdot u^2}{(1-X)^2\cdot\left[Ca^{2+}\right]} \tag{7-10}$$

Note that sol formation in this case is not a question of calcium concentration alone, but must be related to a solid-to-water ratio. With $X_{crit} = 0.9$ and an assumed calcium concentration of $[Ca^{2+}] \approx 0.5$ mM (e.g. set by calcite at a partial CO_2-pressure of $10^{-3.5}$ bar) we get

$$u_{crit} = \sqrt{\frac{(1-X)^2 \cdot K_{GT} \cdot \left[Ca^{2+}\right]}{X^3}} = \sqrt{0.0137 \cdot 4.5 \cdot 0.0005}\ \mathrm{M} = 0.0056\ \ \mathrm{M}$$

which corresponds to a critical solid-to-water ratio of

$$\left(\frac{m_{clay}}{V}\right)_{crit} = \frac{u_{crit}}{CEC} = \frac{0.0056\,\mathrm{M}}{0.00085\,\mathrm{mol/g}} = 6.5\,\mathrm{g/l}$$

In Figure 7-6, the swelling of initially pure Na-montmorillonite of Milos type in a pure Ca-solution set by calcite is shown for two values of the solid-to-water ratio, above and below the critical value. When the solution volume is large, swelling is seen to have ceased and the clay is in a gel state. This example shows that when evaluating this type of sol formation ability, it is important to consider the solid-to-water ratio, i.e. what solid-to-water ratios are considered (too) small. The effect of an explicit dependence on the solid-to-water ratio does not show up in the previously treated experimental situation with a fixed amount of ions in the system. Instead the solid-to-water ratio governs the size of the difference between initial and equilibrium concentrations in the external solution. The observed sol formation ability should of course be related to the values at equilibrium in that case.

An additional interesting conclusion is that the subtle effects of the solid-to-water ratio is never at play if the calcium concentration instead is set by gypsum (see Chapter 2) since the solubility of this mineral puts the system in a state far away from the SFZ ($[Ca^{2+}] \approx 15.6$ mM).

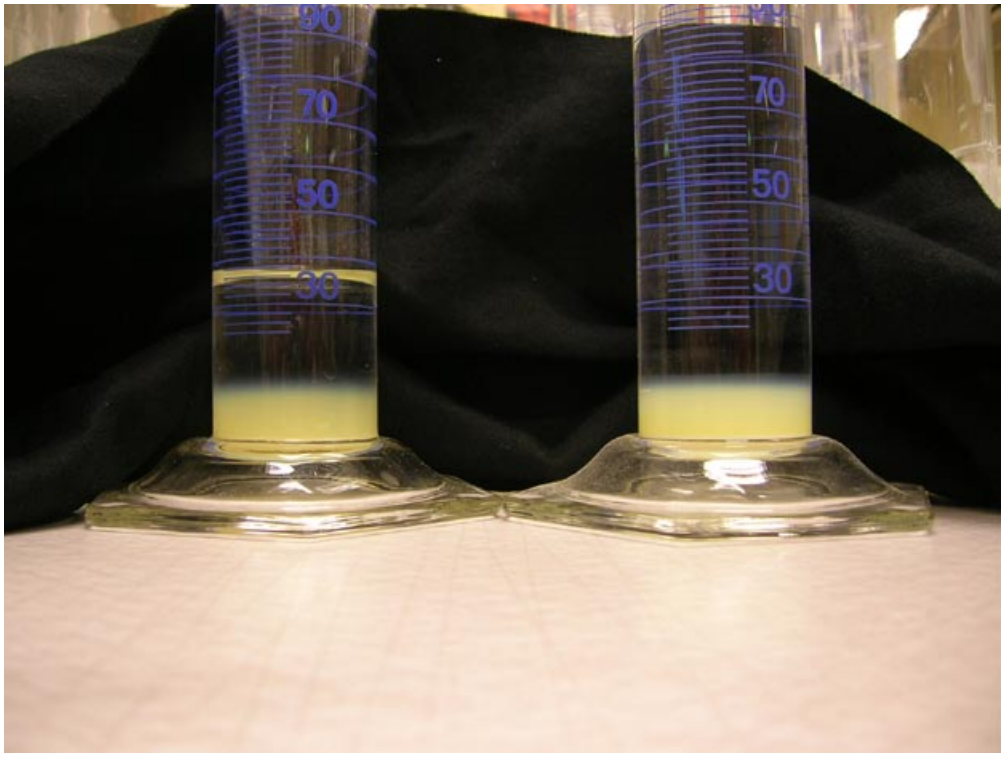

Figure 7-6. *Free swelling of initially pure Na-montmorillonte of Milos type in two different volumes of calcite saturated water. In the test tube to the right the volume is large enough for the exchange equilibrium to put the clay in a state where Ca dominates its behaviour (the solid to water ratio is below the critical 6.5 g/l) and swelling has ceased (the clay/water interface is sharp).*

7.4 Measured sol formation zone of Wyoming type montmorillonite in $CaCl_2$/NaCl-solution

A large series of sedimentation and swelling tests have been performed on Wyoming type montmorillonite in solutions of different $CaCl_2$- and NaCl- concentrations in order to study the sol formation ability and to compare the behaviour with the theoretical predictions from previous sections.

7.4.1 Sedimentation tests

7.4.1.1 Method

These tests were basically identical to the ones discussed in Section 5.3.2.1.

Small glass vials were filled with 20 mg of clay, appropriate amounts of 10 mM $CaCl_2$- and 50 mM NaCl-solutions, and deionized water (in that order) in order to achieve the clay/solution systems to study. The total amount of solution was 10 ml giving a mean solid-to-water ratio of 2 g/l. The vial was closed with a lid and shaken. The system was then allowed to equilibrate overnight.

After equilibration, the vial was properly shaken (either manually or by use of an ultra sonic bath) and turbidity at different times was measured at a point approximately 12–13 mm from the bottom using a turbidimeter TN-100 from Eutech instruments. For details regarding turbidity measurements, see Section 5.2. During the period of sampling of the sedimentation process, which could extend to several weeks or months, the vial was kept undisturbed for obvious reasons. An example of a sedimentation curve, i.e. turbidity as a function of time, is shown in Figure 7-7.

In addition to turbidity as a function of time, also a qualitative description of the system evolution was noted, e.g. if original (dry) clay grains persisted in the solution (see Figure 7-18), if and when a gel phase was visible, and the extension (volume) of this gel phase (see e.g. Figure 7-16).

A rather large number of test series have been performed in order to cover the interesting part in the [Ca]-[Na]-diagram. In these test series, one of the cation concentrations (either the initial or the equilibrium concentration) has been kept constant while the other has been varied.

In most of the performed sedimentation tests, pure Ca-montmorillonite was used (i.e. $X_0 = 1$ in Equations 7-7 and 7-9). Hence, as the Na/Ca exchange process takes the system to equilibrium there will be an increase of Ca-concentration and a decrease of the Na-concentration in the solution as compared to the initial values.

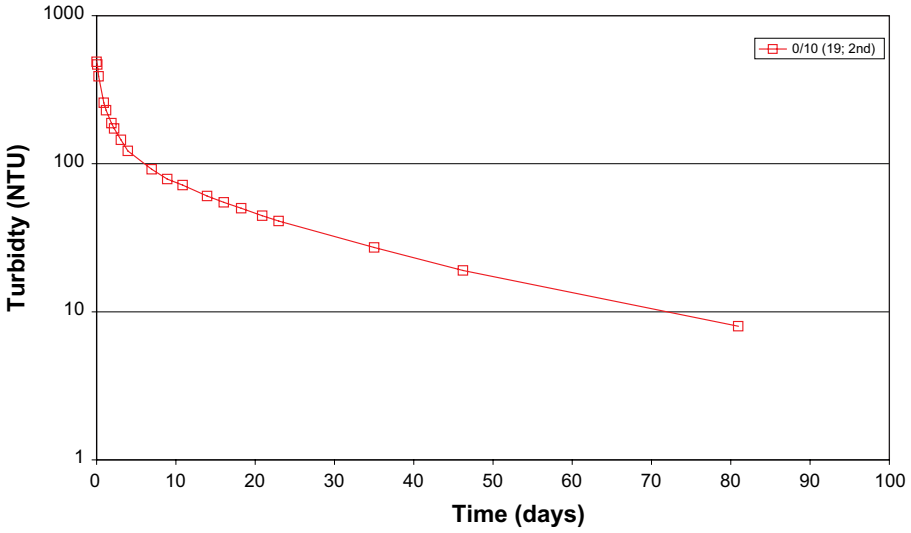

Figure 7-7. *An example of a sedimentation curve, i.e. turbidity as a function of time. This particular case corresponds to an initially pure Ca-montmorillonite, equilibrated with an initially pure NaCl-solution of 10 mM.*

Specifying Equation 7-7 to the specific case of pure Ca-montmorillonite put in a $CaCl_2$/NaCl-solution gives

$$u\cdot\left(\frac{K_{GT}}{2}+u\right)X^3-\left(K_{GT}\cdot\left[Ca^{2+}\right]_0+\frac{3K_{GT}}{2}-2u\cdot\left[Na^{+}\right]_0+2u^2\right)X^2$$
$$+\left(2K_{GT}\cdot\left[Ca^{2+}\right]_0+\frac{3K_{GT}\cdot u}{2}+\left(\left[Na^{+}\right]_0-u\right)^2\right)X-\left(K_{GT}\cdot\left[Ca^{2+}\right]_0+\frac{K_{GT}\cdot u}{2}\right)=0 \quad (7\text{-}11)$$

After solving this equation for X for specific values of the initial concentrations, the equilibrium concentrations can be calculated using Equation 7-5.

Some of the tests were instead performed with initially pure Na-montmorillonite. In this case the Na-concentration increases and the Ca-concentration decreases in the solution due to the ion exchange process. Equation 7-7 now reads

$$u\cdot\left(\frac{K_{GT}}{2}+u\right)X^3-\left(K_{GT}\cdot\left[Ca^{2+}\right]_0+K_{GT}\cdot u-2u\cdot\left[Na^{+}\right]_0\right)X^2$$
$$+\left(2K_{GT}\cdot\left[Ca^{2+}\right]_0+\frac{K_{GT}\cdot u}{2}+\left[Na^{+}\right]_0^2\right)X-K_{GT}\cdot\left[Ca^{2+}\right]_0=0 \quad (7\text{-}12)$$

In the test series where constant equilibrium concentrations were aimed for, the initial concentrations to use are given by Equation 7-9. In the following the values CEC=0.87 mol/kg and K_{GT} = 4.5 M have been used.

7.4.1.2 Results

The consistency of the method was tested by preparing identical samples and comparing their sedimentation curves. Such a comparison is shown in Figure 7-8 for the case of an initially pure Ca-montmorillonite in an initially pure 10 mM NaCl-solution (See Table 7-2 for details). Three different samples were compared in which also the equilibration time was varied. As can be seen from Figure 7-8 the system will be affected if the equilibration time is chosen too short: The first sedimentation curve of sample 32 was recorded without any time for equilibration, for sample 31 the equilibration time was 3 hours and for sample 19, equilibration was allowed overnight. It is seen that sample 32 in this case, and also sample 31 to a smaller extent, sediments faster than sample 19. The explanation is that without a proper equilibration time, larger grains of original Ca-montmorillonite still persist in the solution and fall to the bottom more quickly.

However, Figure 7-8 also shows that if the sedimentation process is repeated all three samples reproduce the same curve very precisely: The second time sample 19 was sedimented, it behaved exactly as the first time, showing that overnight equilibration is sufficiently long. The second time sample 32 was sedimented it very precisely reproduced the curves of sample 19, showing also that the sample preparation can be made consistent, i.e. the concentration variability for different samples prepared to give identical concentrations can be neglected.

Table 7-1 summarizes the performed test series. Below follows comments on each individual series.

7.4.1.2.1 Test series Ca-I-1 ($[CaCl_2]_0$ = 0 mM, $[NaCl]_0$ = 2.5–25 mM)

The performed tests of series Ca-I-1 are summarized in Table 7-2 and corresponding sedimentation curves are shown in Figure 7-9. The nomenclature used in the diagrams for most of the sedimentation curves is "$[Ca^{2+}]_0/[Na^{+}]_0$ (sample ID; order)" where the concentration unit is mM. For example "1/25 (9; 2nd)" means $[Ca^{2+}]_0$ =1 mM, $[Na^{+}]_0$ = 25 mM, sample ID is 9 and that the curve corresponds to the second time the systems is being sedimented.

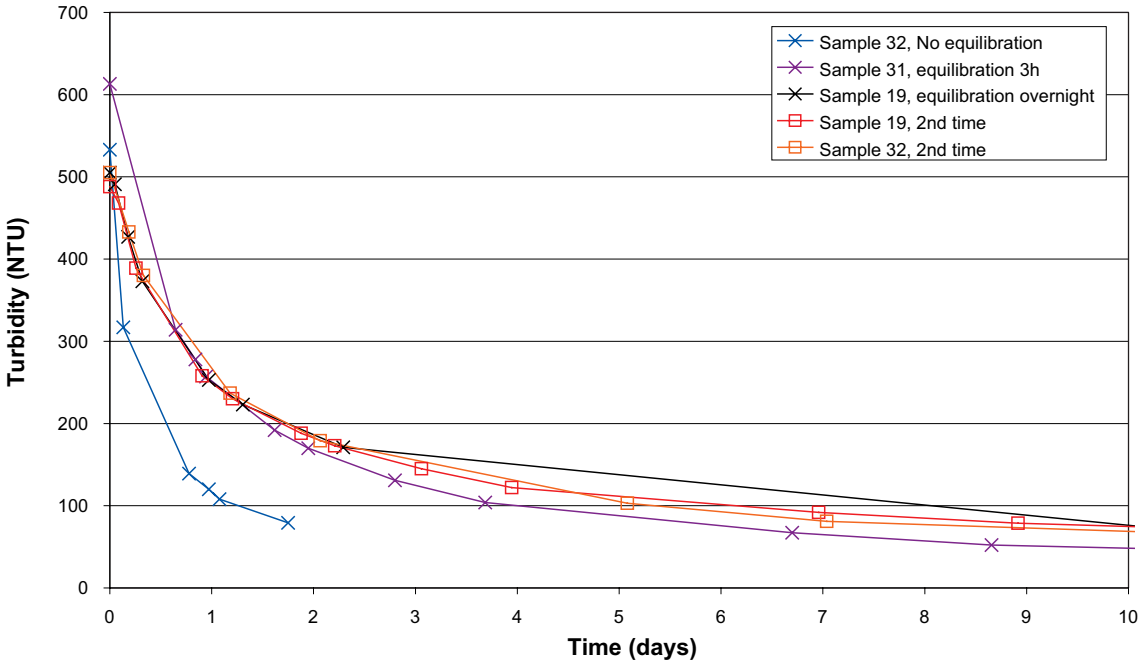

Figure 7-8. *Sedimentation curves of different samples prepared to give identical concentrations. This particular case corresponds to an initially pure Ca-montmorillonite, equilibrated with an initially pure NaCl-solution of 10 mM.*

Table 7-1. Performed sedimentation experiments.

Test Series	Initial clay (X_0)	$CaCl_2$	NaCl	No. of samples
Ca-I-1	pure Ca-montmorillonite (1)	0.0 mM (initially)	2.5–25 mM (initially)	8
Ca-I-2	pure Ca-montmorillonite (1)	0.25 mM (initially)	2.5–20 mM (initially)	10
Ca-I-3	pure Ca-montmorillonite (1)	0.5 mM (initially)	2.5–20 mM (initially)	6
Ca-I-4	pure Ca-montmorillonite (1)	1.0 mM (initially)	0–25 mM (initially)	9
Ca-I-5	pure Ca-montmorillonite (1)	3.0 mM (initially)	0–30 mM (initially)	10
Ca-E-1	Pure Ca-montmorillonite (1)	0.4 mM (in equilibrium)	2–14 mM (in equilibrium)	7
Ca-E-2	Pure Ca-montmorillonite (1)	0.3 mM (in equilibrium)	2–14 mM (in equilibrium)	2
Na-E-1	Pure Na-montmorillonite (0)	0.1 mM (in equilibrium)	5–22 mM (in equilibrium)	4
Na-E-2	Pure Na-montmorillonite (0)	0.2 mM (in equilibrium)	5–15 mM (in equilibrium)	3
Na-I-1	Pure Na-montmorillonite (0)	0.75–1.5 mM (initially)	0.0 mM (initially)	5

Table 7-2. Performed sedimentation experiments of test series Ca-I-1.

ID	$[CaCl_2]_0$ nominal (mM)	$[NaCl]_0$ nominal (mM)	V_{Ca} (ml)	V_{Na+Ca} (ml)	V_{tot} (ml)	$[CaCl_2]_0$ (mM)	$[NaCl]_0$ (mM)	$[CaCl_2]$ calc. (mM)	[NaCl] calc. (mM)	I calc. (mM)	X calc. (-)
28	0.00	2.50	0.00	0.49	9.99	**0.00**	**2.47**	0.09	2.29	2.57	0.89
23	0.00	5.00	0.00	0.99	9.99	**0.00**	**4.98**	0.15	4.69	5.14	0.83
19	0.00	10.00	0.00	1.99	9.98	**0.00**	**9.96**	0.22	9.51	10.17	0.74
31	0.00	10.00	0.00	1.99	10.01	**0.00**	**9.95**	0.22	9.50	10.16	0.74
32	0.00	10.00	0.00	1.98	9.98	**0.00**	**9.93**	0.22	9.48	10.14	0.74
20	0.00	15.00	0.00	2.99	9.99	**0.00**	**14.97**	0.29	14.40	15.27	0.67
21	0.00	20.00	0.00	3.98	9.99	**0.00**	**19.94**	0.34	19.27	20.29	0.61
22	0.00	25.00	0.00	4.99	10.00	**0.00**	**24.95**	0.38	24.19	25.33	0.56

The tables show sample ID, nominal values of initial concentrations of $CaCl_2$ and NaCl, the actual volumes of the different solutions added (V_{Ca} denotes the volume of 10 mM $CaCl_2$ solution added, V_{Ca+Na} denotes the combined volume of the $CaCl_2$ solution and 50 mM NaCl solution and V_{tot} denotes total volume of added $CaCl_2$ solution, NaCl solution and deionized water), the actual initial concentrations (in bold), calculated equilibrium concentrations (using Equations 7-5 and 7-11), calculated ionic strength (Equation 7-2) and calculated equivalent charge fraction of calcium in the clay (Equation 7-11).

It is seen (Figure 7-9) that the sedimentation behaviour as a function of initial NaCl concentration is rather complex. For systems with higher ionic strength (>10 mM NaCl initially; samples 20, 21 and 22) a gel was formed, which contracted under the influence of gravity leaving a clear liquid phase in the top of the vial. The sedimentation curves for the gels show a quick drop at the time when the top surface of the gel passes the point at which the turbidity is measured, clearly illustrated by sample 20 at around day 20 in Figure 7-9.

For the samples with lower ionic strength (2.5 and 5.0 mM NaCl initially; samples 28 and 23) no gel phase was observed, neither were any original grains from the Ca-montmorillonite, indicating that the calcium population of the clay is lower than the critical value of 0.9. These systems showed a rather slow sedimentation behaviour – it took 80 days or longer to reach a turbidity value below 10 NTU. However, the time scale is still considerably smaller than the corresponding time scale for pure NaCl-systems (see Figure 5-13).

From only investigation of Figure 7-9 it may seem that sample 19 was not showing gel behaviour. However, a thin gel was observed also in this sample as shown by Figure 7-10, which shows some of the systems after long sedimentation time (> 100 days). It is clearly seen that the final volumes of the gels (which are stable in the gravity field) increases with increasing ionic strength, consistent with the observations of gels in pure Na-systems (see Section 5.3.2.1).

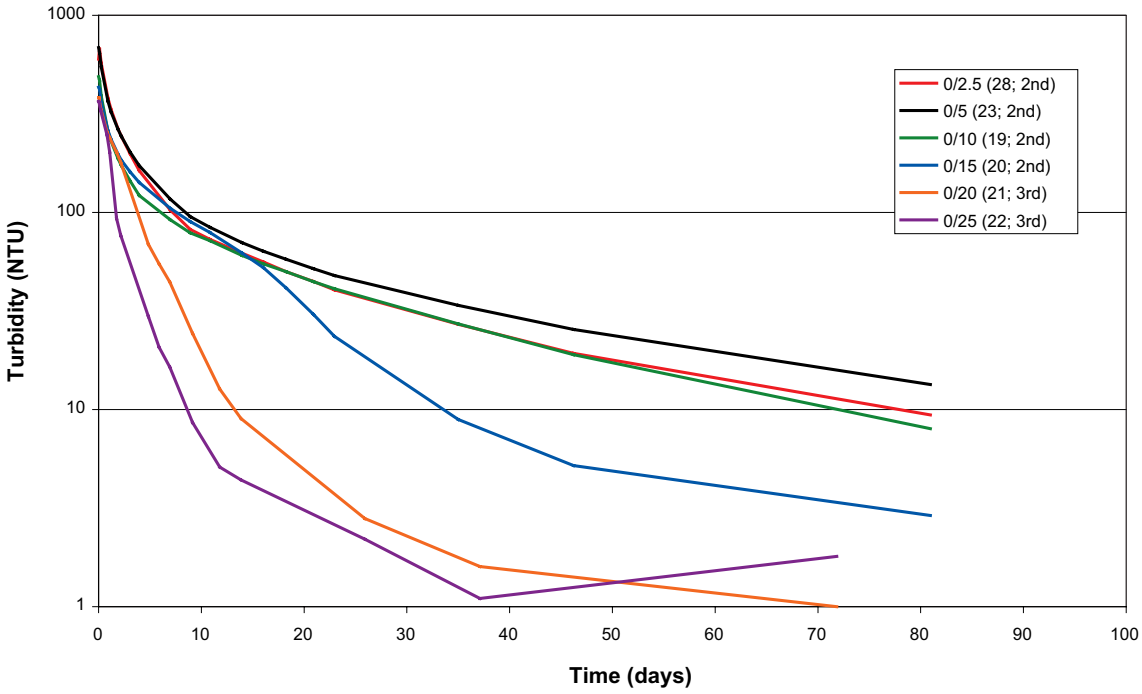

Figure 7-9. *Sedimentation curves for an initially pure Ca-montmorillonite in solutions with initially pure NaCl in the range 2.5–25 mM.*

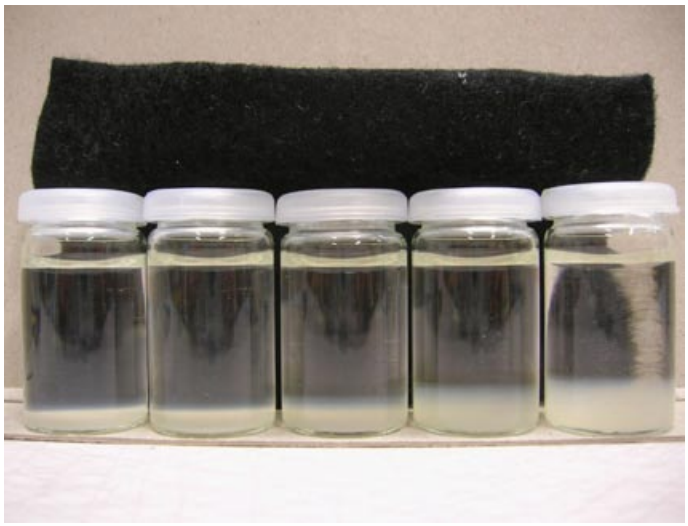

Figure 7-10. *Systems after long time of sedimentation (> 100 days). From left to right: 2.5, 5, 10, 15, and 20 mM NaCl in the initial solution (samples 28, 23, 19 ,20 and 21). Initially, no $CaCl_2$ in solution. Note how the gel phase volume in the three rightmost vials increases with ionic strength. The two leftmost vials show no gel phase.*

7.4.1.2.2 Test series Ca-I-2 ($[CaCl_2]_0$ = 0.25 mM, $[NaCl]_0$ = 2.5–20 mM)

The performed tests of series Ca-I-2 are summarized in Table 7-3 and corresponding sedimentation curves are shown in Figure 7-11. An explanation of the notations in tables and diagrams are given in the section describing test series Ca-I-1.

As for the case of no $CaCl_2$ in the initial solution (test series Ca-I-1), the sedimentation behaviour as a function of NaCl concentration is complex also for this series. A gel phase whose volume increases with NaCl content is observed in several of the samples (Figure 7-12). According to the shape of the sedimentation curves (discussed in the previous section) gels start to form in the range 5–7.5 mM NaCl.

In the sample with the lowest NaCl concentration (2.5 mM NaCl initially; sample 33) original Ca-montmorillonite grains are visible, indicating that the calcium population of the clay is higher than the critical value. This is also confirmed when comparing sedimentation curves (Figure 7-11); initially, sample 33 falls off faster than sample 24 (5 mM NaCl initially) although its ionic strength is lower.

It is also worth noticing that in both of these samples in which no gel was formed (samples 24 and 33), the sedimentation rate was much faster than in the systems which did not form a gel in test series Ca-I-1, which had less calcium in the system (see previous section). The slowest system for the Ca-I-2 case needed approximately 40 days to reach a turbidity value of 10 NTU which is less than half the time as compared to the longest time in series Ca-I-1.

7.4.1.2.3 Test series Ca-I-3 ($[CaCl_2]_0$ = 0.5 mM, $[NaCl]_0$ = 2.5–20 mM)

The performed tests of series Ca-I-3 are summarized in Table 7-4 and corresponding sedimentation curves are shown in Figure 7-13. An explanation of the notations in tables and diagrams are given in the section describing test series Ca-I-1.

Sedimentation curves are shown in Figure 7-13. In these systems the sedimentation behaviour is significantly faster in comparison to systems with 0 or 0.25 mM $CaCl_2$ initially (series Ca-I-1 and Ca-I-2) – the slowest system (sample 35) only needed approximately 15 days to reach a turbidity value below 10 NTU. Note, however, that the sedimentation speed decreases when increasing the initial NaCl concentration from 2.5 to 5.0 mM.

In the two samples with lowest NaCl concentration (sample 29 and 35) original grains of Ca-montmorillonite persisted. In all other samples, gel phases where the gel volume increased with NaCl-concentration were observed.

Table 7-3. Performed sedimentation experiments of series I-2 with initially pure Ca-montmorillonite and specified initial NaCl- and CaCl-concentrations.

ID	$[CaCl_2]_0$ nominal (mM)	$[NaCl]_0$ nominal (mM)	V_{Ca} (ml)	V_{Na+Ca} (ml)	V_{tot} (ml)	$[CaCl_2]_0$ (mM)	$[NaCl]_0$ (mM)	$[CaCl_2]$ calc. (mM)	[NaCl] calc. (mM)	I calc. (mM)	X calc (-)
33	0.25	2.50	0.25	0.75	9.99	**0.25**	**2.48**	0.30	2.37	3.27	0.94
43	0.25	2.50	0.26	0.76	10.07	**0.26**	**2.45**	0.31	2.35	3.28	0.94
24	0.25	5.00	0.26	1.27	10.00	**0.26**	**5.03**	0.36	4.83	5.91	0.89
44	0.25	5.00	0.25	1.24	9.99	**0.25**	**4.96**	0.35	4.76	5.81	0.89
45	0.25	7.50	0.25	1.75	9.99	**0.25**	**7.49**	0.39	7.21	8.38	0.84
25	0.25	10.00	0.26	2.25	9.99	**0.26**	**9.94**	0.43	9.60	10.89	0.80
46	0.25	10.00	0.26	2.27	10.01	**0.26**	**10.04**	0.43	9.70	10.99	0.80
47	0.25	12.50	0.25	2.76	10.00	**0.25**	**12.55**	0.45	12.14	13.49	0.77
26	0.25	15.00	0.24	3.24	10.02	**0.24**	**14.96**	0.47	14.49	15.90	0.73
34	0.25	20.00	0.25	4.25	10.00	**0.25**	**20.02**	0.53	19.45	21.04	0.67

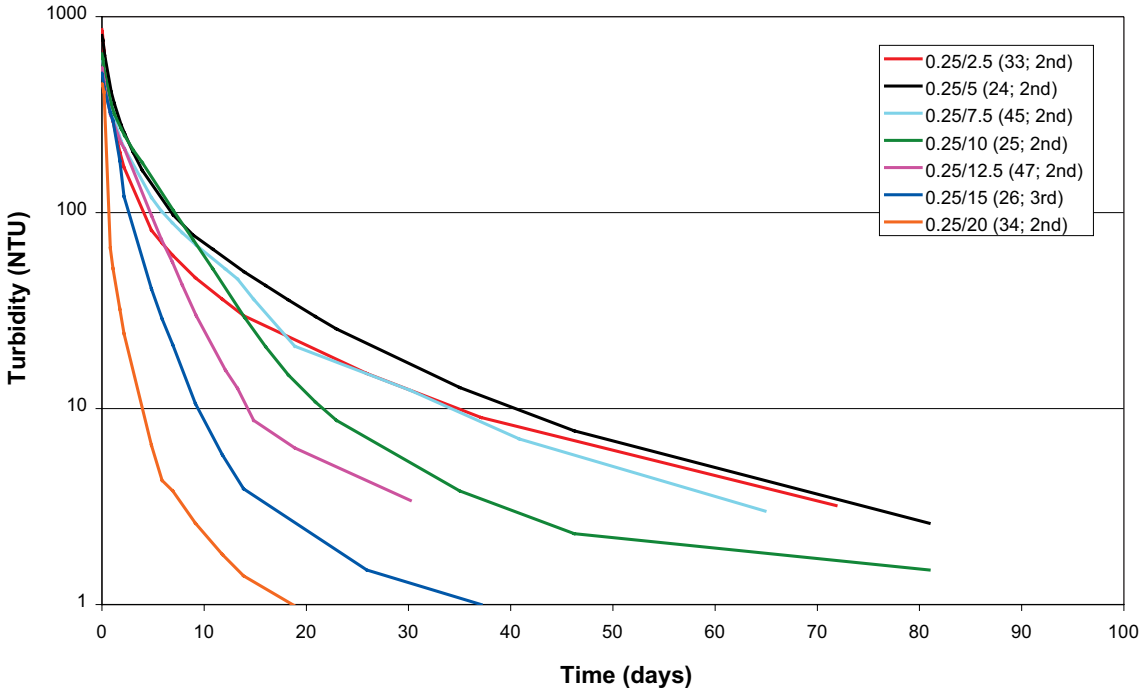

Figure 7-11. *Sedimentation curves for an initially pure Ca-montmorillonite in solutions with initially 0.25 mM $CaCl_2$ and 2.5–20 mM NaCl.*

Figure 7-12. *Systems after long time of sedimentation (> 100 days). From left to right: 2.5, 5, 7.5, 10 and 12.5 mM NaCl in the initial solution (Samples 33, 24, 45, 25 and 47). Initially 0.25 mM $CaCl_2$.*

Table 7-4. Performed sedimentation experiments with initially pure Ca-montmorillonite and with specified initial NaCl- and CaCl-concentrations.

ID	$[CaCl_2]_0$ nominal (mM)	$[NaCl]_0$ nominal (mM)	V_{Ca} (ml)	V_{Na+Ca} (ml)	V_{tot} (ml)	$[CaCl_2]_0$ (mM)	$[NaCl]_0$ (mM)	$[CaCl_2]$ calc. (mM)	[NaCl] calc. (mM)	I calc. (mM)	X calc (-)
29	0.50	2.50	0.48	0.99	10.00	**0.48**	**2.54**	0.52	2.45	4.01	0.95
35	0.50	5.00	0.51	1.50	10.00	**0.51**	**4.98**	0.59	4.82	6.59	0.91
60	0.50	7.50	0.50	2.01	10.01	**0.50**	**7.51**	0.61	7.29	9.12	0.87
36	0.50	10.00	0.50	2.50	10.00	**0.50**	**10.02**	0.64	9.73	11.65	0.83
37	0.50	15.00	0.51	3.53	10.00	**0.51**	**15.08**	0.71	14.68	16.81	0.77
30	0.50	20.00	0.50	4.50	10.01	**0.50**	**19.97**	0.75	19.48	21.73	0.72

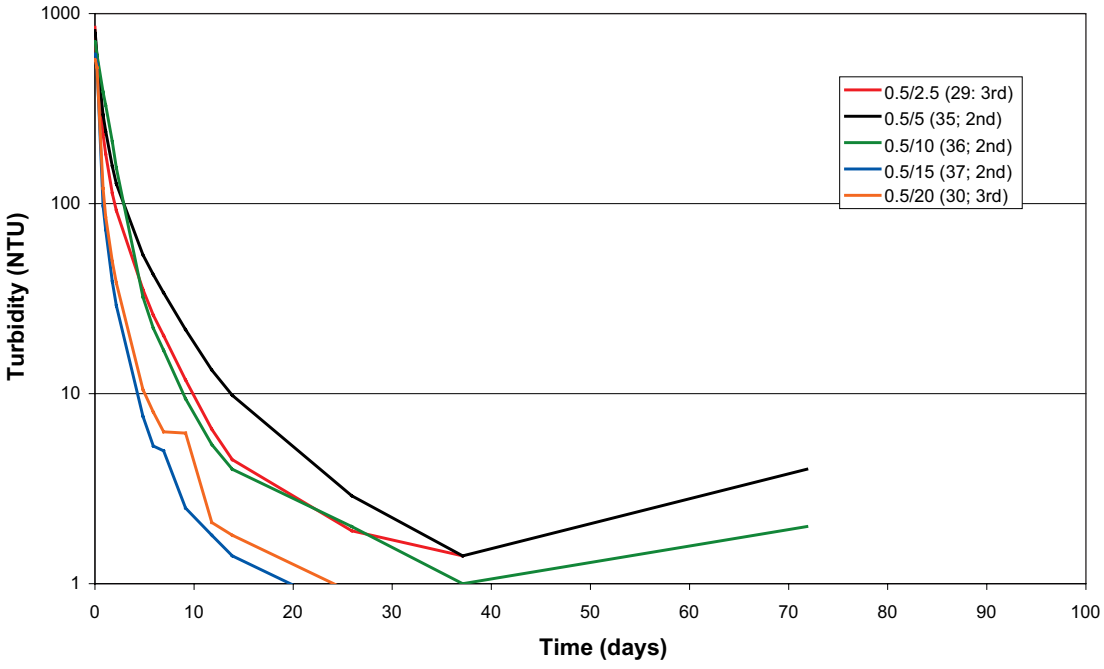

Figure 7-13. *Sedimentation curves for an initially pure Ca-montmorillonite in solutions with initially 0.5 mM $CaCl_2$ and 2.5–20 mM NaCl.*

Figure 7-14. *From left to right: 2.5, 5, 10, and 15 mM NaCl in the initial solution (Samples 29, 35, 36 and 37). Initially 0.5 mM $CaCl_2$.*

7.4.1.2.4 Test series Ca-I-4 ($[CaCl_2]_0$ = 1 mM, $[NaCl]_0$ = 0–25 mM)

The performed tests of series Ca-I-4 are summarized in Table 7-5 and corresponding sedimentation curves are shown in Figure 7-15. An explanation of the notations in tables and diagrams are given in the section describing test series Ca-I-1.

All systems sedimented very fast, and rather similar, as compared with the previous series, as can be seen in Figure 7-15.

For samples with low or no initial NaCl concentration in the solution, original montmorillonite grains could be observed. At higher NaCl concentrations, the sediment resembles a gel phase whose volume increases with the NaCl content. In Figure 7-16, the resulting sedimented phases are pictured for samples 1, and 5 to 9. Note how the height of the sedimented gel phase grows with increasing NaCl-content.

Table 7-5. Performed sedimentation experiments with initially pure Ca-montmorillonite and with specified initial NaCl- and CaCl-concentrations.

ID	$[CaCl_2]_0$ nominal (mM)	$[NaCl]_0$ nominal (mM)	V_{Ca} (ml)	V_{Na+Ca} (ml)	V_{tot} (ml)	$[CaCl_2]_0$ (mM)	$[NaCl]_0$ (mM)	$[CaCl_2]$ calc. (mM)	[NaCl] calc. (mM)	I calc. (mM)	X calc (-)
1	1.00	0.00	1.00	1.00	9.99	**1.00**	**0.00**	1.00	0.00	3.00	1.00
2	1.00	2.50	1.00	1.52	9.99	**1.00**	**2.59**	1.03	2.53	5.62	0.96
3	1.00	5.00	1.00	2.01	10.12	**0.99**	**4.97**	1.06	4.85	8.03	0.93
4	1.00	7.50	1.00	2.53	10.00	**1.00**	**7.65**	1.09	7.47	10.74	0.90
5	1.00	10.00	1.00	3.00	9.99	**1.00**	**10.02**	1.11	9.80	13.13	0.87
6	1.00	15.00	1.00	3.98	10.01	**1.00**	**14.91**	1.16	14.59	18.07	0.82
7	1.00	20.00	1.00	5.00	10.00	**1.00**	**19.98**	1.20	19.58	23.18	0.77
8	1.00	22.50	1.00	5.62	10.00	**1.00**	**23.10**	1.23	22.65	26.34	0.74
9	1.00	25.00	1.00	5.99	9.99	**1.00**	**24.95**	1.24	24.46	28.18	0.72

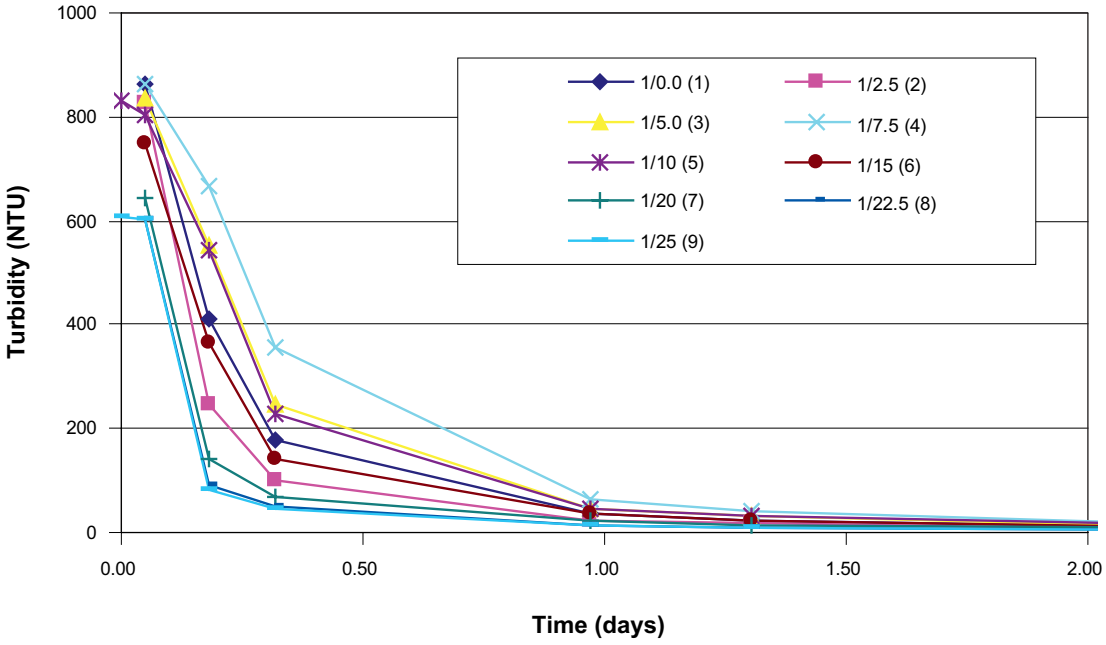

Figure 7-15. *Sedimentation curves (here given on a linear scale) for an initially pure Ca-montmorillonite in solutions with initially 1 mM $CaCl_2$ and 0–25 mM NaCl.*

Figure 7-16. *From left to right: 0, 10, 15, 20, 22.5 and 25 mM NaCl in the initial solution (Samples 1, 5,6,7,8 and 9). Initially 1.0 mM $CaCl_2$.*

7.4.1.2.5 Test series Ca-I-5 ($[CaCl_2]_0$ = 3 mM, $[NaCl]_0$ = 0–30 mM)

The performed tests of series Ca-I-5 are summarized in Table 7-6 and corresponding sedimentation curves are shown in Figure 7-17. An explanation of the notations in tables and diagrams are given in the section describing test series Ca-I-1.

As can be seen in the figure all systems sedimented very fast, even faster than the corresponding systems with initial solution containing 1 mM $CaCl_2$ (series Ca-I-4).

Original montmorillonite grains could be observed in some of the vials (Figure 7-18).

7.4.1.2.6 Test series Ca-E-1 ($[CaCl_2] = 0.4$ mM, [NaCl] = 2–14)

Instead of looking at the sedimentation behaviour as a function of *initial* concentrations of the solution, the following series of samples were aimed at having a constant *equilibrium* concentration of $CaCl_2$. In contrast to using initial concentration to specify the system, the initial concentrations now must be calculated using Equations 7-11 and 7-9. This means that there is an uncertainty in the exact value of the equilibrium concentrations, which depends on the accuracy of the selectivity coefficient.

In this manner, a series of samples, Ca-E-1, was produced aimed at having a fixed $CaCl_2$ concentration of 0.4 mM and different NaCl concentrations in equilibrium. The performed tests of series Ca-E-1 are summarized in Table 7-7 and corresponding sedimentation curves are shown in Figure 7-19. An explanation of the notations in tables and diagrams are given in the section describing test series Ca-I-1.

Table 7-6. Performed sedimentation experiments with initally pure Ca-montmorillonite and with specified initial NaCl- and CaCl-concentrations.

ID	$[CaCl_2]_0$ nominal (mM)	$[NaCl]_0$ nominal (mM)	V_{Ca} (ml)	V_{Na+Ca} (ml)	V_{tot} (ml)	$[CaCl_2]_0$ (mM)	$[NaCl]_0$ (mM)	$[CaCl_2]$ calc. (mM)	[NaCl] calc. (mM)	I calc. (mM)	X calc (-)
10	3.00	0.00	3.00	3.00	9.99	**3.00**	**0.00**	3.00	0.00	9.00	1.00
11	3.00	5.00	3.00	4.00	9.99	**3.00**	**4.99**	3.04	4.92	14.04	0.96
12	3.00	7.50	3.00	4.50	10.12	**2.97**	**7.42**	3.02	7.31	16.37	0.94
13	3.00	10.00	3.00	5.01	10.00	**3.00**	**10.03**	3.07	9.89	19.10	0.92
14	3.00	12.50	3.00	5.50	9.99	**3.00**	**12.50**	3.09	12.33	21.60	0.90
15	3.00	15.00	3.00	6.00	10.01	**3.00**	**14.97**	3.10	14.77	24.07	0.88
16	3.00	17.50	3.00	6.49	10.00	**3.00**	**17.45**	3.12	17.22	26.58	0.86
17	3.00	20.00	3.00	6.99	10.00	**3.00**	**19.96**	3.13	19.69	29.08	0.85
18	3.00	22.50	3.00	7.45	9.99	**3.00**	**22.28**	3.15	21.99	31.44	0.83
27	3.00	30.00	2.99	9.01	9.99	**2.99**	**30.12**	3.18	29.74	39.28	0.78

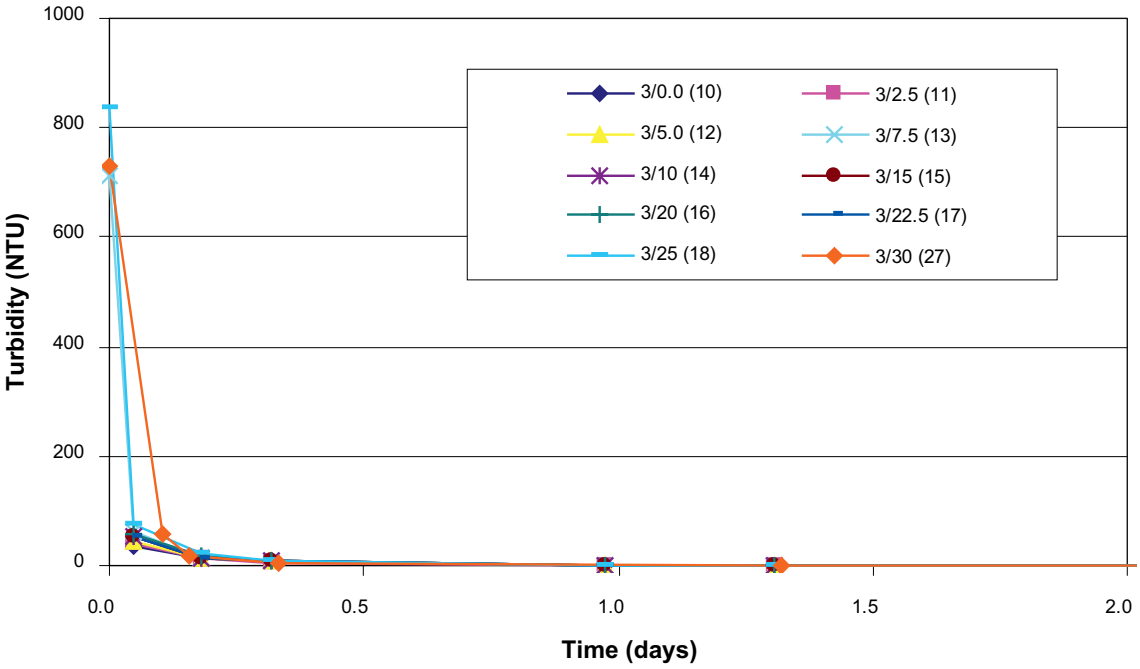

Figure 7-17. *Sedimentation curves (here given on a linear scale) for an initially pure Ca-montmorillonite in solutions with initially 3 mM $CaCl_2$ and 0–25 mM NaCl.*

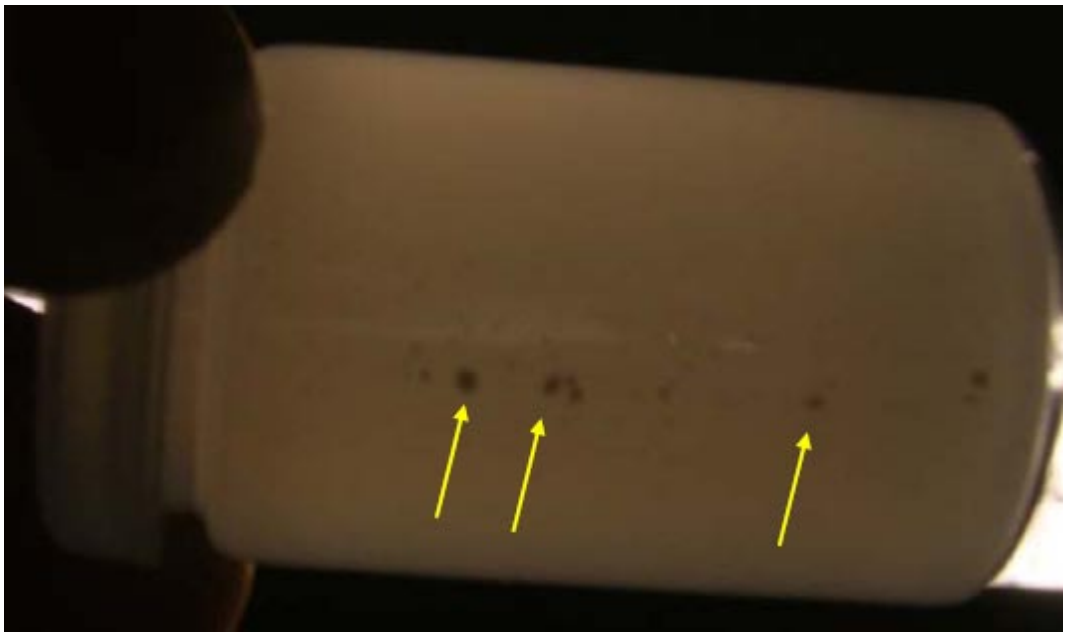

Figure 7-18. Initial grains persist in Ca-dominated systems. The picture shows sample 10 (pure Ca-montmorillonite in 3 mM $CaCl_2$).

Table 7-7. Performed sedimentation tests of series Ca-E-1.

ID	$[CaCl_2]_0$ nominal (mM)	$[NaCl]_0$ nominal (mM)	V_{Ca} (ml)	V_{Na+Ca} (ml)	V_{tot} (ml)	$[CaCl_2]_0$ (mM)	$[NaCl]_0$ (mM)	$[CaCl_2]$ calc. (mM)	[NaCl] calc. (mM)	I calc. (mM)	X calc (-)
49	0.36	2.10	0.37	0.81	10.00	**0.37**	**2.19**	0.41	2.11	3.34	0.95
50	0.32	4.20	0.33	1.26	10.00	**0.33**	**4.64**	0.42	4.47	5.73	0.90
51	0.29	6.25	0.30	1.54	10.00	**0.30**	**6.21**	0.41	5.99	7.22	0.87
52	0.25	8.30	0.24	1.91	10.00	**0.24**	**8.34**	0.39	8.04	9.21	0.83
53	0.22	10.40	0.23	2.30	10.00	**0.23**	**10.37**	0.41	10.01	11.24	0.79
54	0.19	12.45	0.19	2.67	10.03	**0.19**	**12.38**	0.40	11.96	13.16	0.76
55	0.16	14.50	0.16	3.05	10.00	**0.16**	**14.45**	0.40	13.97	15.17	0.72

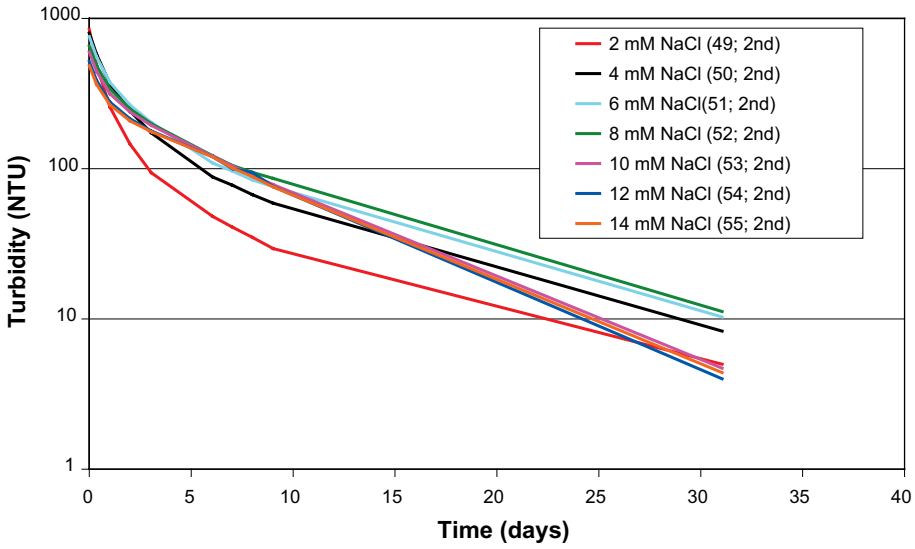

Figure 7-19. Sedimentation curves for an initially pure Ca-montmorillonite in solutions aimed at having a constant equilibrium $CaCl_2$ concentration of 0.4 mM and variable equilibrium NaCl concentrations.

There are several interesting features in Figure 7-19. It is seen that the fastest sedimenting system is that with the lowest ionic strength; with increasing NaCl concentration from 2 to 8 mM, the system sediments increasingly slowly. At around 10 mM of NaCl, the shape of the sedimentation curve indicates that a gel state has been formed.

By observation (Figure 7-20) it is seen that a gel phase appears already for 8 mM. The volume of the gel phase increases also in this series with the amount of NaCl.

7.4.1.2.7 Test series Ca-E-2 ($[CaCl_2]$ = 0.3 mM, [NaCl] = 5–10 mM)

The performed tests of series Ca-E-2 are summarized in Table 7-8. An explanation of the notations in the table is given in the section describing test series Ca-I-1.

None of the samples showed persisting original grains of montmorillonite. Sample 71 formed a gel.

7.4.1.2.8 Test series Na-E-1 ($[CaCl_2]$ = 0.1 mM, varied equilibrium [NaCl] = 1.6–22 mM)

With pure Ca-montmorillonite as starting material it is not possible to reach regions close to the y-axis in the $[Ca^{2+}]$-$[Na^{+}]$-diagram. To explore these regions some test series were performed with initially pure Na-montmorillonite. Below follows a summary of these series.

The performed tests of series Na-E-1 are summarized in Table 7-9 and corresponding sedimentation curves are shown in Figure 7-21. An explanation of the notations in tables and diagrams are given in the section describing test series Ca-I-1.

Figure 7-20. *Samples with 0.4 mM $CaCl_2$ in equilibrium solution. From left to right: 2, 4, 6, 8, and 10 mM NaCl in the equilibrium solution (samples 49, 50, 51, 52, and 53).*

Table 7-8. Performed sedimentation tests of series Ca-E-2.

ID	$[CaCl_2]_0$ nominal (mM)	$[NaCl]_0$ nominal (mM)	V_{Ca} (ml)	V_{Na+Ca} (ml)	V_{tot} (ml)	$[CaCl_2]_0$ (mM)	$[NaCl]_0$ (mM)	$[CaCl_2]$ calc. (mM)	[NaCl] calc. (mM)	I calc. (mM)	X calc (-)
70	0.19	5.22	0.18	1.23	9.99	**0.18**	**5.22**	0.29	5.00	5.87	0.87
71	0.09	10.41	0.09	2.17	9.99	**0.09**	**10.38**	0.30	9.97	10.87	0.76

Table 7-9. Performed sedimentation tests of series Na-E-1.

ID	$[CaCl_2]_0$ nominal (mM)	$[NaCl]_0$ nominal (mM)	V_{Ca} (ml)	V_{Na+Ca} (ml)	V_{tot} (ml)	$[CaCl_2]_0$ (mM)	$[NaCl]_0$ (mM)	$[CaCl_2]$ calc. (mM)	[NaCl] calc. (mM)	I calc. (mM)	X calc (-)
73	0.89	0.42	0.91	0.91	9.99	**0.91**	**0.00**	0.10	1.61	1.92	0.93
74	0.81	0.48	0.85	1.15	10.00	**0.85**	**1.48**	0.10	2.99	3.28	0.87
63	0.79	3.62	0.80	1.54	10.01	**0.80**	**3.69**	0.11	5.07	5.40	0.80
59	0.65	8.91	0.68	2.46	9.99	**0.68**	**8.91**	0.12	10.04	10.40	0.65
61	0.48	17.24	0.48	3.92	10.00	**0.48**	**17.23**	0.10	17.99	18.29	0.44
62	0.42	21.36	0.42	4.68	10.01	**0.42**	**21.29**	0.10	21.93	22.23	0.39

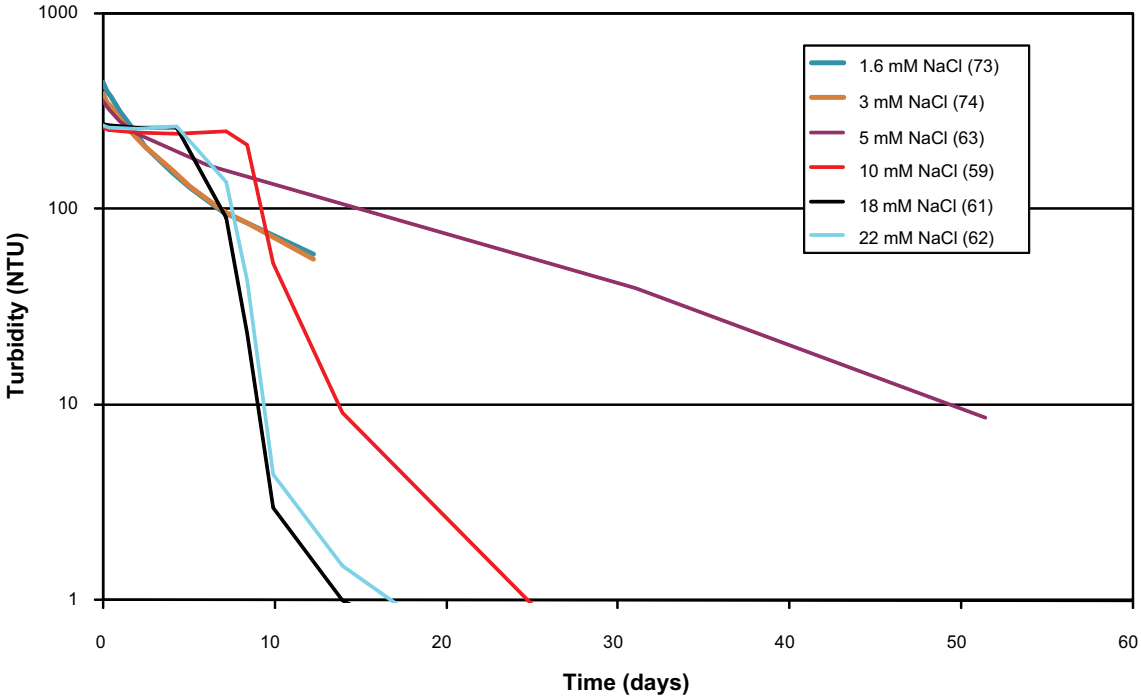

Figure 7-21. *Sedimentation curves of initially pure Na-montmorillonite aimed to have an equilibrium $CaCl_2$ concentration of 0.1 mM and variable equilibrium NaCl concentrations.*

All of these samples show gel behaviour but the three samples with lowest amount of NaCl (samples 63, 73, and 74 with equilibrium concentration 5 mM, 1.6 mM and 3 mM respectively) sediment completely differently as compared to the three samples with high NaCl concentration (samples 59, 61, and 62, with equilibrium concentrations 10 mM, 18 mM, and 22 mM respectively).

The gel states can be seen in Figure 7-22. Note that the volumes of these gel states are independent of the ionic strength of the system.

7.4.1.2.9 Test series Na-E-2 ($[CaCl_2]$ = 0.2 mM, varied equilibrium [NaCl] = 5–15 mM)

The performed tests of series Na-E-1 are summarized in Table 7-10. An explanation of the notations in the table is given in the section describing test series Ca-I-1.

All samples formed a gel, looking very similar to the samples in Figure 7-22.

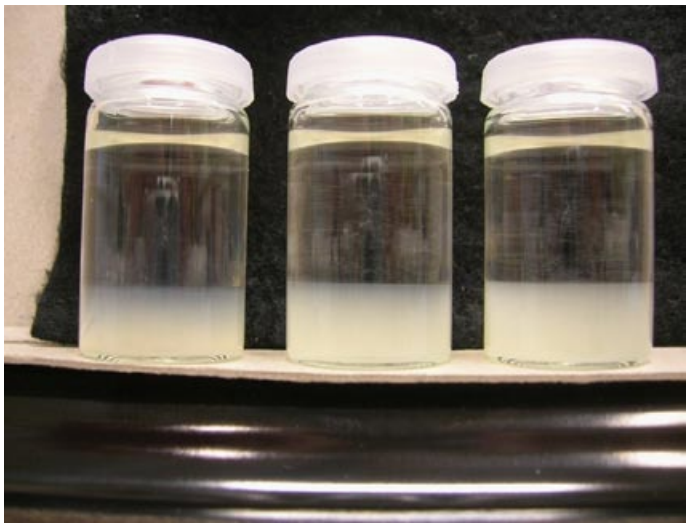

Figure 7-22. *Samples with 0.1 mM $CaCl_2$ in equilibrium solution obtained from initially pure Na-montmorillonite. From left to right: 5, 10, and 18 mM NaCl in the equilibrium solution (Samples 63, 59 and 61).*

Table 7-10. Performed sedimentation tests of series Na-E-2.

ID	$[CaCl_2]_0$ nominal	$[NaCl]_0$ nominal	V_{Ca}	V_{Na+Ca}	V_{tot}	$[CaCl_2]_0$	$[NaCl]_0$	$[CaCl_2]$ calc.	[NaCl] calc.	I calc.	X calc
	(mM)	(mM)	(ml)	(ml)	(ml)	**(mM)**	**(mM)**	(mM)	(mM)	(mM)	(-)
67	0.94	3.53	0.93	1.63	10.00	**0.93**	**3.50**	0.19	4.97	5.54	0.85
68	0.82	8.75	0.82	2.58	10.00	**0.82**	**8.77**	0.20	10.02	10.62	0.72
69	0.73	13.94	0.73	3.52	10.27	**0.71**	**13.59**	0.18	14.64	15.18	0.60

7.4.1.2.10 Test series Na-I-1 ($[CaCl_2]_0$ = 0.75–1.5 mM, $[NaCl]_0$ = 0.0 mM)

The systems ended up in gel phases in all except for one sample, in which the initial $CaCl_2$ concentration was 0.75 mM (sample 41). Sedimentation curves for this system and the system with initial $CaCl_2$ concentration 1.0 mM (sample 40) are shown in Figure 7-23. Note that in sample 41 there is not enough Ca in the system for a complete conversion of the clay to Ca-state (*u/2* = 0.87 mM). Sample 41 is the only system tested with initial pure Na-montmorillonite in which a gel was not observed.

The gel states are pictured in Figure 7-24. Also for these conditions, the gel volumes are not correlated with the ionic strength of the system. Note that for the two samples with highest initial $CaCl_2$-concentration, 1.25 and 1.5 mM respectively (samples 39 and 42), the gel has a rough surface, indicating a tensile strength. This is in contrast to the gel phase of sample 40 and also the gel states observed in the previously described test series (see Figure 7-22.).

Table 7-11. Performed sedimentation tests of series Na-I-1.

ID	$[CaCl_2]_0$ nominal (mM)	$[NaCl]_0$ nominal (mM)	V_{Ca} (ml)	V_{Na+Ca} (ml)	V_{tot} (ml)	$[CaCl_2]_0$ (mM)	$[NaCl]_0$ (mM)	$[CaCl_2]$ calc. (mM)	[NaCl] calc. (mM)	I calc. (mM)	X calc (-)
41	0.75	0.00	0.75	0.75	9.99	**0.75**	**0.00**	0.02	1.47	1.53	0.84
40	1.00	0.00	0.98	0.98	10.00	**0.98**	**0.00**	0.16	1.64	2.12	0.94
39	1.25	0.00	1.25	1.25	10.00	**1.24**	**0.00**	0.40	1.67	2.87	0.96
38	1.50	0.00	1.51	1.51	10.01	**1.51**	**0.00**	0.67	1.69	3.70	0.97
42	1.50	0.00	1.50	1.50	10.00	**1.50**	**0.00**	0.66	1.69	3.67	0.97

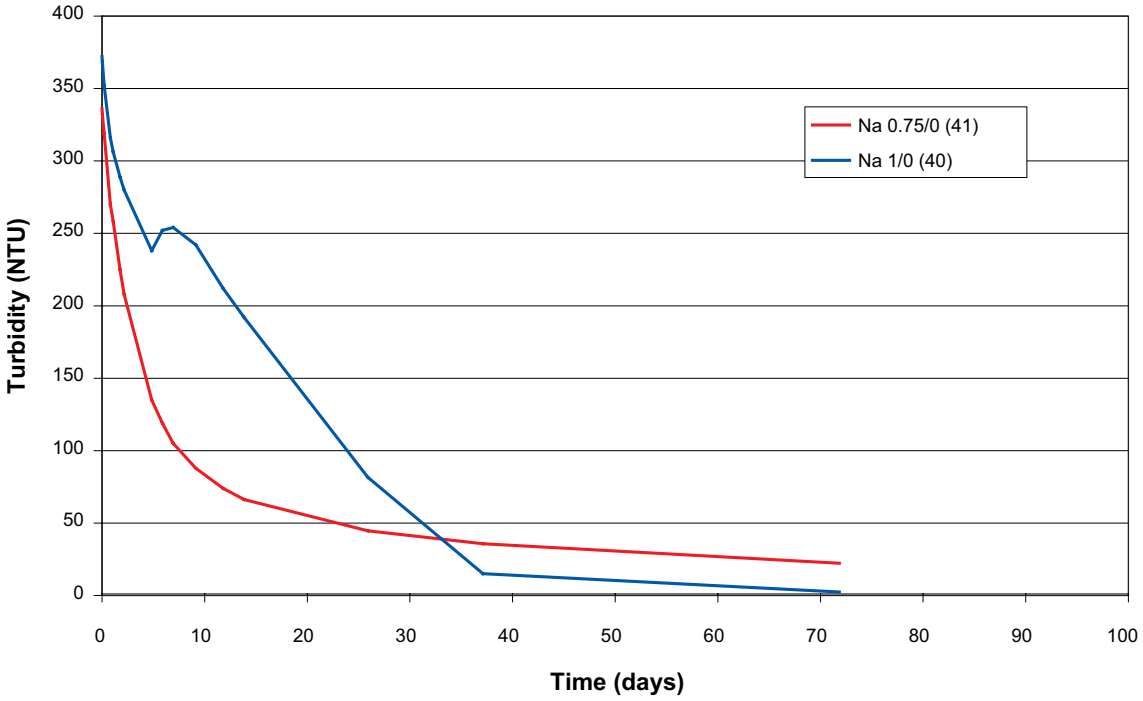

Figure 7-23. *Sedimentation curves of initially pure Na-montmorillonite in solutions with initial NaCl concentration 0.0 mM and initial $CaCl_2$ concentrations of 0.75 mM and 1.0 mM respectively.*

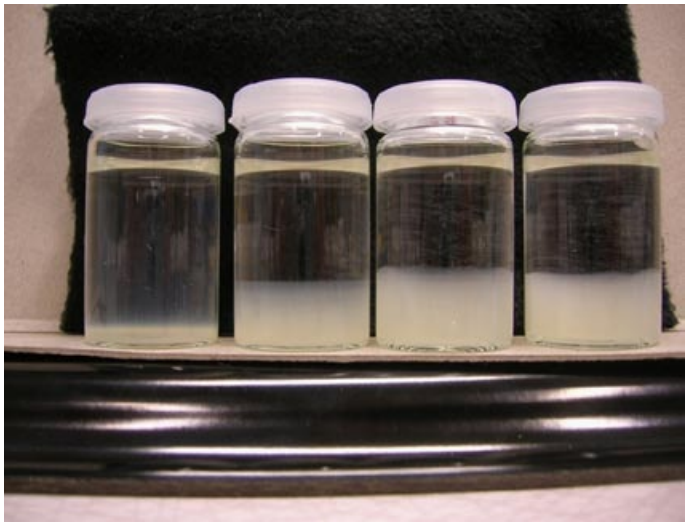

Figure 7-24. *From left to right: 0.75, 1.0, 1.25 and 1.5 mM $CaCl_2$ in the initial solution (samples 41, 40, 3,9 and 42). Intially 0.0 mM NaCl.*

7.4.2 Swelling tests

The sedimentation tests were complemented with series of swelling tests in specified solutions of NaCl/$CaCl_2$. These were performed in both the same type of vials as was used for the sedimentation tests but also in larger test tubes. All tests were performed with initially pure Na-montmorillonite as it has a much larger capacity to swell during the transient phase where the process of reaching ion exchange equilibrium is ongoing, i.e. if no sol formation is observed in these tests for specific $CaCl_2$- and NaCl-concentrations, it can be concluded that the system at equilibrium is non sol-forming.

7.4.2.1 Results

7.4.2.1.1 Swelling in small vials (10 ml)

These tests were basically identical to the swelling tests described in Section 5.3.2. 20 mg of montmorillonite of Wyoming type was dried in at the bottom of the same type of test vials as used in the sedimentation experiments after which appropriate amounts of 50 mM NaCl-solution, 10 mM $CaCl_2$-solution and deionized water were added in order to obtain the desired conditions. After addition of solution the vial was left undisturbed apart from occasional measurements of turbidity profiles, i.e. turbidity as a function of vial height, using a rebuilt turbidimeter (see Section 5.3.2.3 for details). The performed tests are listed in Table 7-12.

One test (sample 72) was performed in deionized water in order to compare with swelling in the other systems. The concentrations of test samples 64, 65 and 66 were chosen to be identical with samples 63, 59 and 62 of the sedimentation test series Na-E-1. In this way a direct comparison between sedimentation and swelling could be made.

The turbidity profiles of samples 64 and 72 for three different times are presented in Figure 7-25, where it is seen that the swelling is limited and no sol is formed in sample 64. The swelling was also limited in the other tests made and by visual observation it was confirmed that none of these systems (except sample 72, of course) showed any sol formation.

7.4.2.1.2 Swelling in measure cylinders (250 ml)

500 mg of Wy-Na montmorillonite was placed at the bottom of 250 ml measure cylinders after which appropriate $CaCl_2$/NaCl-solutions were added in order to obtain the desired conditions. After addition of solution the vessel was left undisturbed, i.e. turbidity was not measured, only visual observations were made.

Four systems were prepared, designed to have a NaCl-concentration of 5 mM and $CaCl_2$-concentrations of 0 mM, 0.01 mM, 0.05 mM and 0.1 mM in equilibrium. The resulting fully swollen systems after 74 days are pictured in Figure 7-26, where it is seen that sol formation only occurs in the pure NaCl-system and the system with equilibrium concentration of $CaCl_2$ of 0.01 mM. It can further be noted that the texture of the surfaces are very different in the two tests showing sol formation (smooth horizontal surfaces) and the two more Ca-rich samples (rough “lunar landscape”). The latter systems resemble the structure seen in pure NaCl-systems at much larger ionic strengths (compare with Figure 5-17).

The measure cylinders were later tilted horizontally and observed. The pure NaCl system was dispersing whereas the two systems containing the larger calcium amounts remained unaffected. A small fraction of clay at the top of the system with Ca^{2+} concentration of 0.01 mM dispersed. However the bulk of the material stayed unchanged at the bottom and appeared similar to the system in Figure 7-28, thus demonstrating a certain strength of the remaining presumably attractive gel.

Table 7-12. Performed swelling tests of initially pure Na-montmorillonite in 10 ml vials.

ID	$[CaCl_2]_0$ nominal (mM)	$[NaCl]_0$ nominal (mM)	V_{Ca} (ml)	V_{Na+Ca} (ml)	V_{tot} (ml)	$[CaCl_2]_0$ (mM)	$[NaCl]_0$ (mM)	$[CaCl_2]$ calc. (mM)	[NaCl] calc. (mM)	I calc. (mM)	X calc (-)
48	1.50	0.00	1.50	1.50	10.00	**1.50**	**0.00**	0.66	1.69	3.67	0.97
64	0.79	3.62	0.80	1.54	10.01	**0.80**	**3.69**	0.11	5.07	5.40	0.80
65	0.65	8.91	0.80	2.46	9.99	**0.80**	**8.27**	0.12	10.04	10.40	0.65
66	0.42	21.36	0.80	4.68	10.01	**0.80**	**19.40**	0.10	21.93	22.23	0.39
72	0.0	0.0	0.0	0.0	10.00	**0.0**	**0.0**	0.0	0.0	0.0	0.0

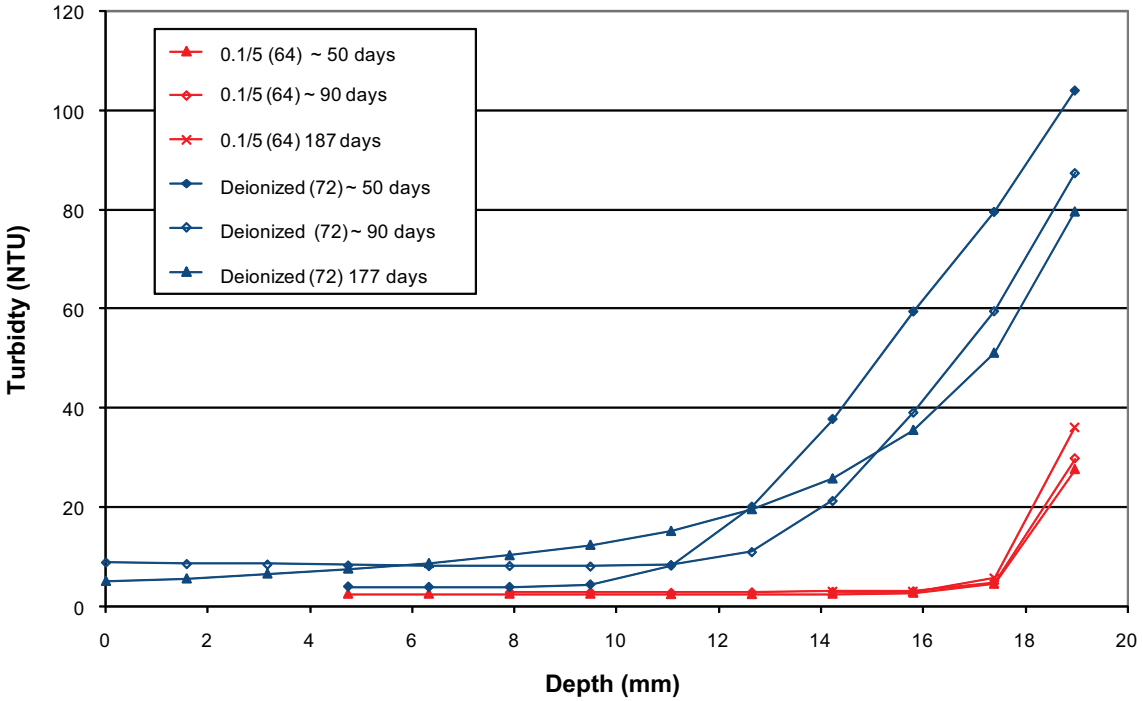

Figure 7-25. *Turbidity profiles of sample 64 (0.1 mM $CaCl_2$ and 5 mM NaCl in equilibrium) at different times. The system is compared to swelling of Na-montmorillonite in deionized water (sample 72).*

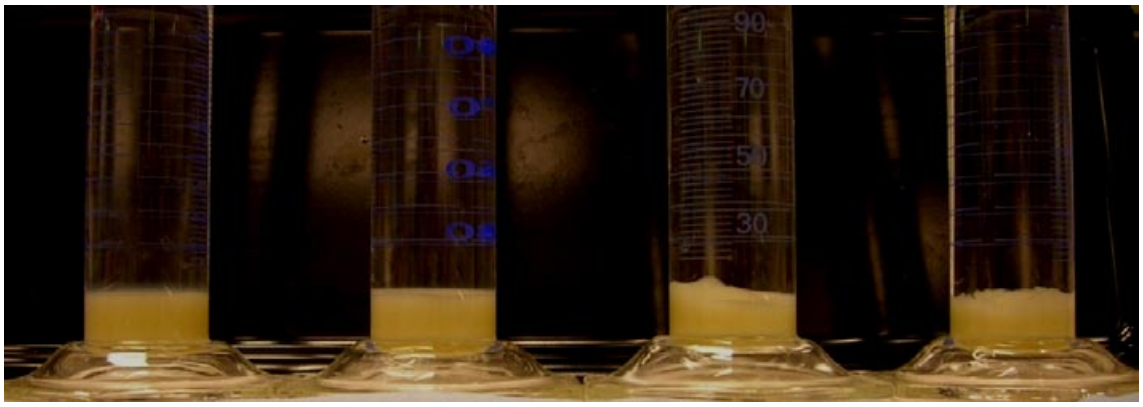

Figure 7-26. *Swelling of initially pure Na-montmorillonite in different Na/Ca-solutions. The systems are designed to have an equilibrium NaCl concentration of 5.0 mM and increasing $CaCl_2$ concentration of (left to right) 0.0 mM, 0.01 mM, 0.05 mM and 0.1 mM. The corresponding X-values are 0, 0.48, 0.72 and 0.79 respectively.*

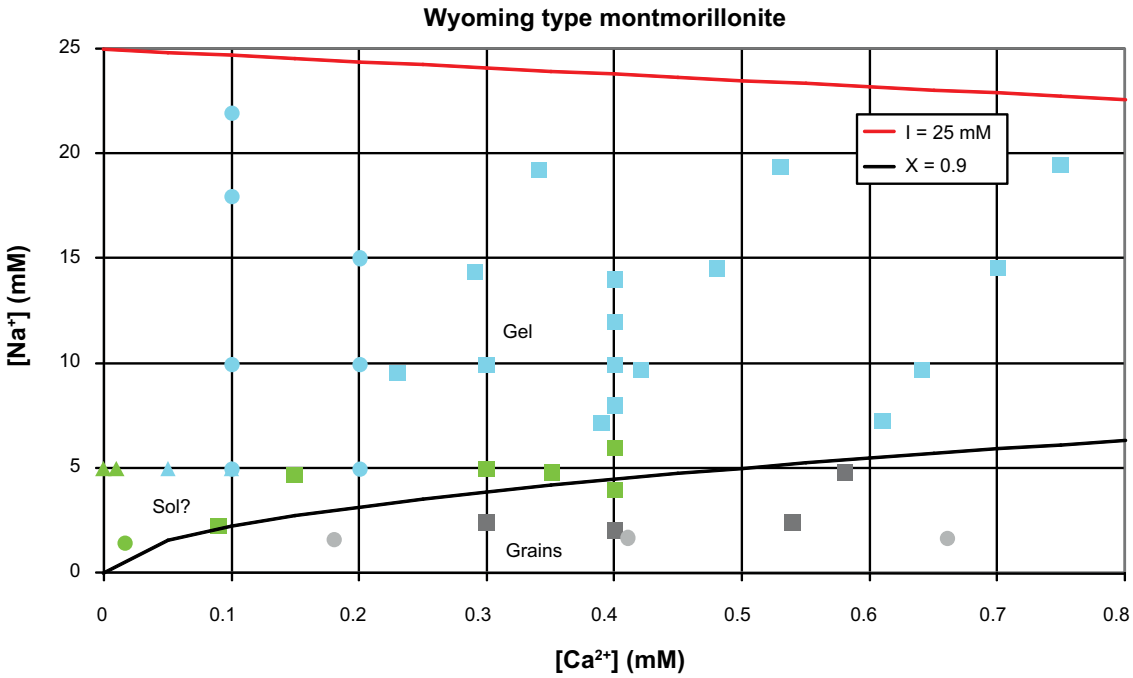

Figure 7-27. *Phases of the measured systems in comparison with the "theoretical" SFZ for Wyoming type montmorillonite. The red line indicates constant ionic strength of 25 mM and the black curve the points where the Ca-population in the clay is 90% according to the exchange reaction. The other symbols are explained in the text.*

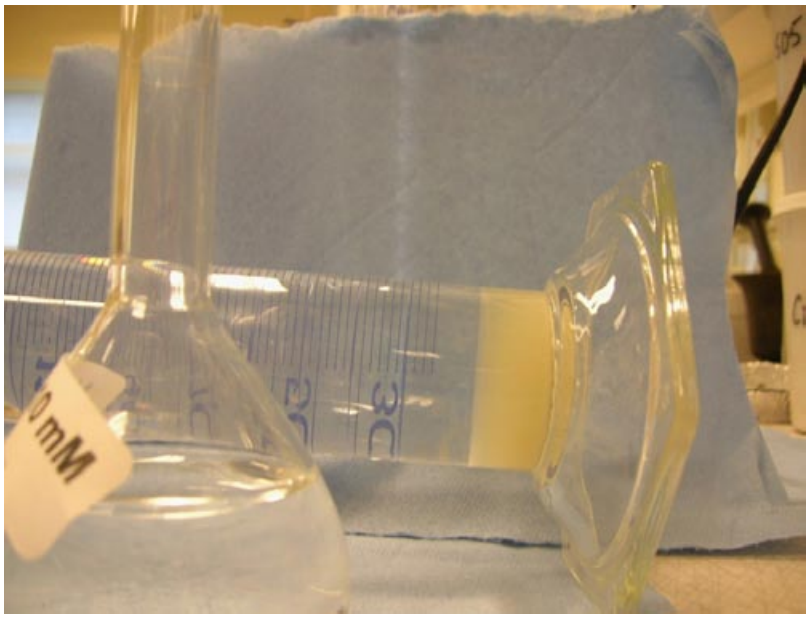

Figure 7-28. *Demonstration of the strength of a formed gel phase. The system contains initially pure Wyoming type Na-montmorillonite, equilibrated in calcite saturated solution. The water to solid mass ratio is >100 and the ionic strenght is only a few mM.*

7.4.3 Summary: Sol formation zone of Wyoming type montmorillonite

The majority of the sedimentation and swelling tests performed are summarized in the $[Ca^{2+}]$-$[Na^{+}]$-diagram in Figure 7-27. Sedimentation tests with Ca-montmorillonite initially are labelled with a square symbol, sedimentation tests with Na-montmorillonite initially are labelled with a disc symbol and the swelling tests (which all had Na-montmorillonite initially) are labelled with a triangle. The different final states have also been categorized into three different groups:

- Systems which ended up in a gel state (see e.g. Figure 7-10 and Figure 7-22). These are coloured turquoise in Figure 7-27.
- Systems which show signs of structural heterogeneity. In this group is included systems of initially pure Ca-montmorillonite in which original grains persists (see Figure 7-18) as well as systems of initially pure Na-montmorillonite which ended up in gel phases with a "rough" structure (see Figure 7-24). This group is interpreted to be dominated by calcium, i.e. $X > X_{crit}$, and the corresponding systems are coloured gray in Figure 7-27.
- Systems in which none of the above appears to happen (see e.g. Figure 7-10 and Figure 7-24). These states are coloured green in Figure 7-27.

The following points can be made:

- Sedimentation of initially pure Ca-montmorillonite
  - At low ionic strengths, where the calcium population of the clay is very large, grains of the initial Ca-montmorillonite are observed to persist. Further, no significant percolation gel is observed in these systems. These states are interpreted as being above the critical calcium population and thus being non sol forming. Looking at Figure 7-27, it is seen that the notion that $X_{crit} \approx 0.9$, which was shown to hold for systems in ion free water (see Section 5.3.1) is confirmed also for systems with excess ions at these ionic strengths.
  - At higher ionic strengths, set by larger concentrations of NaCl, the sediments form attractive gels whose strength increases with increasing NaCl concentration (or ionic strength). These gels are interpreted as percolation gels as they are formed at high solid-to-water mass ratios, similarly as the gels seen in sedimentation experiments for pure Na-systems. The ionic strength at which these gels start to form is significantly smaller than was expected from the simple theoretical discussion of Section 7.3.
  - When increasing the Na concentration at a constant Ca concentration, the sedimentation speed decreases for systems which do not form percolation gels (see e.g. Figure 7-19).
  - The sedimentation speed is dramatically increased when the Ca-concentration is increased (compare e.g. Figure 7-9 and Figure 7-13).
  - The systems which neither show original grains, nor any significant gel phase are located in a narrow region around the $X = X_{crit}$ line. From the sedimentation experiments alone it cannot be concluded if a separate sol phase exists in this region or if this is only the behaviour of sedimenting initial Ca-montmorillonite in the limit between the grain phase and the gel phase.
- Sedimentation of initially pure Na-montmorillonite
  - All but one of the tests formed gels. The system in which a gel was not formed (sample 41; see Figure 7-23, Figure 7-24 and Table 7-11) had a very low calcium concentration in solution (the calcium population in the clay is rather large, due to the low ionic strength, but the total amount of calcium in the system is not enough to reach the critical $X = 0.9$).
  - The gel volumes do not show a dependence on ionic strength, in contrast to the gels formed when sedimenting initial Ca-montmorillonite or when sedimenting Na-montmorillonite in a pure NaCl-system. The gel volume is generally larger than that seen in the sedimentation tests with initial Ca-montmorillonite.
  - The gels show two types of appearances. In systems with calcium population above the critical value, the gel surface is rough, while in gels in higher NaCl concentration the surface is smooth. The smooth one may be a percolation gel similar to the ones described for pure Wy-Na above the CCC, whereas in the rough type it is conceivable that the attractions are caused by correlation, but the system is locked in a non-equilibrium configuration preventing the emergence of a more compact face-to-face configuration, where correlation attraction is maximized.

  - Comparing with sedimentation tests with initial Ca-montmorillonite, it can be concluded that the sedimentation process and final states are hugely dependent on the initial state of the clay (Ca- or Na-montmorillonite). This is illustrated by comparing e.g. sample 63 (Table 7-9, Figure 7-21, and Figure 7-22) with sample 23 (Table 7-2, Figure 7-9, and Figure 7-10) which have very similar equilibrium concentrations and ion populations. Comparison of sample 39 (Table 7-11 and Figure 7-24) and sample 49 (Table 7-7, Figure 7-19 and Figure 7-20) is another example.

- Swelling (of initially pure Na-montmorillonite)
  - Swelling was shown to be limited in all tested systems, except for the ones containing no or only very small amounts of calcium in the equilibrium solution. This shows that the sol formation zone is limited to a region very close to the [Na^+]-axis (diagram). Also, this result indicates that several of the systems which could not be categorized as grain or percolation gel states in the sedimentation tests of initially pure Ca-montmorillonite are not sol states.

The main conclusion from the sol formation tests is that the sol formation zone is limited to a very narrow region close to the [Na^+]-axis. Systems containing such small calcium concentration as 0.1 mM have been shown to be non sol-forming at rather low ionic strengths.

Thus, the initial notion that ionic strength is the controlling parameter for gel formation in a Ca/Na-montmorillonite system does not hold. Instead a large effect of introducing only small (external) concentrations of calcium is identified, giving very limited ability for the montmorillonite to form a sol state.

Note that this calcium effect is different from the well documented correlation effect in lamellar swelling, which causes the swelling of Ca-montmorillonite to be limited to the nm-scale. The latter effect needs a very large fraction of calcium in the clay to be manifested ($X > X_{crit}$) while the observed effect in this study seems to function also with relatively small amounts of calcium.

Since it has been shown that attractive gel formation, and thereby also sol formation is a mechanism governed by interactions different from the conventional “face-to-face” interaction (DLVO, etc.) – most probably associated with edge sites of the individual montmorillonite layers – the newly observed effect of calcium must also be associated with these sites and their interactions.

However, even if ionic strength alone is not controlling the system, the lines of constant ionic strength equal to the CCC in a pure Na-system as a limit for sol formation, e.g. Equation 7-3 have been demonstrated to be very conservative, as is clearly illustrated in Figure 7-27.

An important question to answer is whether the attractive gel states formed in a mixed Ca/Na-system are stable enough not to be transported away with flowing ground water in a fracture under real repository conditions. Note that the gel states reported in this chapter are in most cases not the same types of gels on which rheological characterization was performed in Chapter 3. In Chapter 3 the studied gels were either repulsive gels or in the case where one from our knowledge of the sol-formation zone would expect attractive gels the method of preparation (Section 3.4.4) disrupts the network of attractive bonds that is not reformed during the shearing experiments. For example, the solid to water mass ratio of the gels pictured in e.g. Figure 7-22 and Figure 7-24 is approximately 150–200, a region where the systems in Chapter 3 are modelled as Newtonian fluids (region C2 in Table 3-6). Nevertheless, all gels achieved in the tests in this chapter do show quite high stability. This is demonstrated in Figure 7-28, which shows an initially pure Na-montmorillonite which has equilibrated in a calcite saturated solution. The clay is dominated by calcium (due to the large solid-to-volume ratio) and the system is located below the SFZ in the [Ca^{2+}]-[Na^+]-diagram. The gel has been tilted to a vertical configuration and stayed stable for several months.

Although most of the rheological tests in Chapter 3 were done on repulsive gels or systems where the attractive bonds were disrupted there are a few vane tests in Section 3.6.4 on MX-80 where at least one of the systems is actually an attractive gel. These tests are performed on MX-80 in initially distilled water at different solid to water mass ratios between 15 and 40. In these systems the ionic strength is basically given by dissolution of gypsum and therefore varies with the water to solid mass ratio, i.e. the lower the water to solid mass ratio the higher ionic strength. In Figure 3-37 the clay/electrolyte blends have had 21 days of resting time which is more than sufficient for re-establishing eventual attractive bonds. For the gel with water to solid mass ratio 30 a yield stress above 9 Pa is

found. A water to solid mass ratio of 30 corresponds to 33.3 g MX-80 per litre and with a content of 0.7% gypsum (see further Section 7.5.2) the concentration of gypsum (molar weight 172 g/mol) can be estimated to 33.3×0.007/172=1.36 mM. At such low ionic strength and low water to solid mass ratio essentially all calcium remains in the clay and the external electrolyte consists basically of Na_2SO_4, thus the concentration of Na^+ is around 2.7 mM. It has also been verified separately that MX-80 at an *average* water to solid mass ratio of 30 does not swell to fill the total volume and that the clay shows no sign of flow when the beaker is left tilted (after more than three weeks the clay surface is still parallel to the bottom of the beaker). These observations strongly suggest that this system is an attractive gel.

7.5 Erosion tests

7.5.1 Erosion tests of initially pure Na-montmorillonite

The influence of mixed Ca/Na-solutions on the erosion rate of a (initially) pure Na-montmorillonite has been tested in a small set of tests similar to the ones presented in Chapter 4 and Section 5.5. In four experimental set-ups identical to that pictured in Figure 4-1, different electrolyte solutions were circulated over 10 µm filters and swelling pressure exerted by the clay as well as turbidity in the external circulating solution were measured. In the case where a specific solution did not stop erosion, it was replaced with a solution of the same kind but with a higher concentration. The different electrolyte solutions were

- $CaCl_2$
- A 50/50 mixture of $CaCl_2$ of a specific concentration and NaCl of twice as high concentration, corresponding to equal charge equivalent fractions of calcium and sodium
- Gypsum ($CaSO_4$) saturated solution.
- Calcite ($CaCO_3$) saturated hydrochloric acid solution of increasing concentration.

For comparison, an additional erosion test with deionized water as circulating solution was run in parallel.

The swelling pressure response as a function of time for the five tests is shown in Figure 7-29. The test consisted of shorter periods of solution circulation and longer periods of stopped circulation in order to recover a stable swelling pressure for the systems which showed erosion. If a specific system did not show erosion (i.e. pressure drop), the solution was circulated continuously. After stopping circulation, in a system showing erosion, the circulating solution was replaced with one of higher concentration.

Looking at the pressure response for the system consisting of only deionized water in Figure 7-29 (denoted H_2O) it can be seen when circulation was going on (steep pressure drop) and when it was switched off (levelling out to a plateau).

Below follows a short discussion on each specific test

7.5.1.1 Gypsum saturated solution

The gypsum saturated solution stopped erosion immediately. The initial pressure drop seen in Figure 7-29 is due to an initial circulation of deionized water in order to check that the set-up was functioning.

The prevention of erosion by a gypsum saturated solution was expected because of the rather high ionic strength and relatively large calcium concentration (15.6 mM).

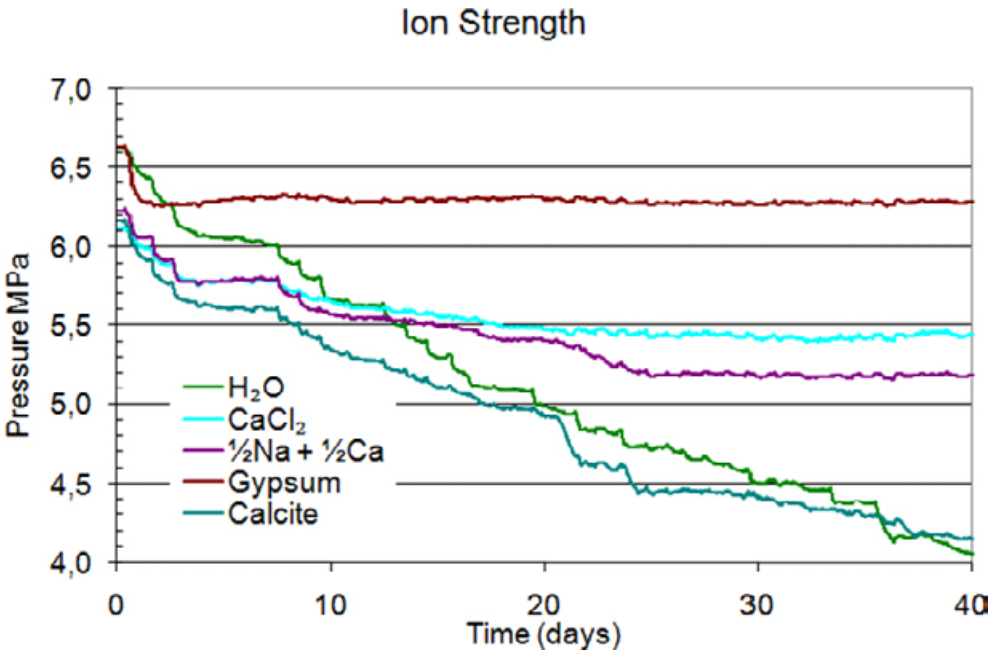

Figure 7-29. *Swelling pressure response for the four tested systems with different circulation Ca or Ca/Na solutions over an initially pure sample of Na-montmorillonite. Also shown is a sample with deionized water for comparison (labelled H_2O).*

7.5.1.2 $CaCl_2$ solution

Solution concentration was increased in the sequence 0.0 mM, 0.05 mM, 0.1 mM, 0.5 mM, 1 mM, 1.5 mM and 2.5 mM. Initially erosion is clearly recorded but between the change from 1.5 mM to 2.5 mM, erosion ceased.

Since the initial sample is a pure Na-montmorillonite, there is an ion exchange process present. The maximum amount of calcium which could have been exchanged is 0.1L·(0.05 + 0.1 + 0.5 + 1.0 + 1.5 + 2.5)mM = 0.565 mmol, while the amount of Na^+ in the clay is estimated by CEC·m_s·1 mol/eq = 0.87 meq/g·7 g·1 mol/eq = 6.1 mM (a typical sample in these tests weighs approximately 7 g). Hence, at most, the clay has converted to a calcium population of $X_{max} = 0.565 \cdot 2/6.1 \approx 0.18$.

The final solution, 2.5 mM $CaCl_2$, was circulated for several weeks. Since the sample still is very dominated by Na, the ion exchange process will basically put only sodium in the outer solution, i.e. it will be close to a pure 5 mM NaCl solution. The situation when erosion has stopped is obviously very interesting, where a hugely Na-dominated montmorillonite is prevented from eroding by an approximately 5 mM NaCl solution with small amounts of $CaCl_2$.

7.5.1.3 $CaCl_2$ + NaCl solution

Solution concentration was increased in the sequence presented in Table 7-13. Just as in the test with pure $CaCl_2$ solution, ion exchange is expected which will put Ca in the clay and Na in the external solution. The maximum amount of Ca which could have been exchanged in this test is 0.1 L·(0.025 + 0.05 + 0.125 + 0.25 + 0.5 + 0.75 + 1.25 + 2.5) = 0.545 mmol, which corresponds to $X_{max} \approx 0.18$, which is the same population as was estimated for the pure $CaCl_2$ case. In this case, however, the final solution contains approximately 10 mM NaCl since the final solution contributes with 5 mM in itself. Still, this test seems to end up in a rather similar situation as the previously treated, with a hugely Na-dominated montmorillonite being prevented from eroding by a solution consisting of mostly NaCl and minor concentrations of $CaCl_2$.

Table 7-13. Sequence of solution concentration for the erosion test with a circulation $CaCl_2$ + NaCl solution.

Sol no.	[NaCl] (mM)	[$CaCl_2$] (mM)
1	0.0	0.0
2	0.05	0.025
3	0.1	0.05
4	0.25	0.125
5	0.5	0.25
6	1.0	0.5
7	1.5	0.75
8	2.5	1.25
9 (final)	5.0	2.5

7.5.4.4 Calcite + HCl

Test solutions consisted of specified HCl solutions which were saturated with calcite. The composition of the tests solutions after circulation as measured with ion selective electrodes are presented in Table 7-14.

In this case, erosion was not stopped as shown in Figure 7-29. However, Table 7-14 also show that the system is very far from equilibrium in every measurement. As calcite sets a constant calcium concentration, the experimental conditions are those discussed in Section 7.3.1.2. Using Equation 7-10 with $u \approx 0.06$ M and $K_{GT} = 4.5$ M gives equilibrium values of X ranging between 0.57 and 0.70 depending on the measured calcium concentrations (0.7–3.0 mM). This, in turn, corresponds to Na-concentrations in equilibrium between 34 and 42 mM. The measured Na-concentrations (Table 7-14), on the other hand, are several orders of magnitudes lower than this indicating that almost no ion exchange has occurred in the tests. The accumulated amount of exchanged Na corresponds to 0.1 L·1.3 mM·1 eq/mol = 0.13 meq which gives $X_{final} = 0.13/6.1 \approx 0.02$. The ion population of the clay is then extremely dominated by sodium for any of the circulating solutions. The observed erosion should then be associated with properties of (in principle) pure Na-montmorillonite, which also in equilibrium has been shown to be much more dispersive than mixed Ca/Na-systems.

Table 7-14. Measurements of calcite saturated HCl solutions after clay exposure.

	Measured with ion selective electrode after circulation		
Initial Solution	[Ca^{2}+] mM	[Na+] mM	pH
0	0.7	0.002	8.57
0.2 mM HCl	0.8	0.04	8.74
0.4 mM HCl	3.3	0.02	8.67
0.6 mM HCl	3.6	0.03	8.5
0.8 mM HCl	1.4	0.03	8.43
1.0 mM HCl	1.5	0.02	8.3
1.2 mM HCl	1.3	0.02	8.05
1.4 mM HCl	2.3	0. 02	8.18
1.6 mM HCl	2.0	0. 02	8.13
1.8 mM HCl	2.0	0.03	8.04
2.0 mM HCl	2.0	0.13	8.2
2.2 mM HCl	2.2	0.04	8.06
2.4 mM HCl	2.5	0.22	8.07
2.6 mM HCl	2.3	0.13	7.92
2.8 mM HCl	2.8	0.17	8.04
3.0 mM HCl	2.8	0.23	8.14
3.2 mM HCl	2.1	0.17	7.95

7.5.2 Erosion test of MX-80 bentonite

The influence of a mixed Ca/Na-solution on the erosion rate of a sample of MX-80 bentonite has been examined in a test similar to the ones presented in Chapter 4, Section 5.5 and Section 7.5.1.

7.5.2.1 Preparation phase

MX-80 bentonite of approximate dry weight 7.6 g was prepared in a set-up identical to the one showed in Figure 4-1. The MX-80 material is produced from mixing naturally occurring soils and contains relatively small variable amounts of readily soluble minerals, predominantly gypsum. In the first phase of the test, the sample was drained of these excess ions by flushing the system with an initially deionized solution. In order to avoid erosion at this stage the flushing was done intermittently. Due to the prescribed boundary conditions the flux out of the sample is expected to be Na_2SO_4 which is further discussed and investigated in Chapter 8. The electrical conductivity in the external solution was recorded and correlated to a Na_2SO_4 concentration. After a few days, when the external concentration had increased to 1.3 mM, the circulation of the external solution was done continuously without any erosion occurring. This is yet another example of what was observed in some of the experiments performed on pure montmorillonite where a sodium dominated clay ($X_{Ca} < 0.3$ in the MX-80 montmorillonite) is prevented from eroding by a rather weak sodium solution (and small amounts of calcium).

The flushing was continued until no further rise of concentration of the external solution was recorded. The final concentration was 3.0 mM, which corresponds to an original gypsum ($CaSO_4 \cdot 2H_2O$, molar weight 172 g/mol) amount of 0.1 L·3 mM·0.172 g/mmol = 0.0516 g. This, in turn, corresponds to approximately 0.7% of the weight of the dry mass of the sample, in good agreement with other content specifications of MX-80 /Karnland et al. 2006/. The pressure response of the sample was recorded during the entire test and is presented for the described preparation phase in Figure 7-30. The initial pressure increase during flushing is a simple consequence of lowering the salt concentration in the solution in the filters by dilution. This, in turn, increases the water activity outside the clay, and is directly reflected in an increased swelling pressure.

7.5.2.2 Erosion phase

After the preparation phase the circulating solution was replaced by a new amount (0.1 L) of deionzied water. In this solution electrical conductivity, turbidity and pH were measured. The measured turbidity values were converted to accumulated mass of eroded montmorillonite using the approximate relation 100 NTU = 1 g/L (see Section 5.2).

After several days of continuous circulation and occasional replacement with fresh deionzied water, the solution was replaced once again, this time with a weak NaCl/$CaCl_2$-solution with initial concentrations [NaCl] = 0.7 mM and [CaCl] = 0.2 mM. This solution was allowed to circulate for 4 days, with occasional replacements to keep a fairly constant boundary condition, before a change to deionzed water was once again conducted. This switching between deionzed water and NaCl/$CaCl_2$-solution was repeated and the corresponding mass loss response during the first part of the erosion phase is shown in Figure 7-31. It is evident that erosion occurred when deionzied water was circulated (simultaneous pressure drop and mass loss) while erosion stoped when the prescribed NaCl/$CaCl_2$-solution was circulated.

The solution was not replaced in the second period of using the NaCl/$CaCl_2$-solution (day 35 to 42). This means that the ion exchange process between the clay and the solution could reach equilibrium, which was confirmed by measuring very a low calcium concentration (0.01 mM or less) with ion selective electrode at day 42. Thus, at this point the outer solution can be concluded to contain basically pure 1.1 mM NaCl solution. It should be noted that 0.1 L of 0.2 mM $CaCl_2$ contains 0.04 meq exchangeable charge, which is less than one percent of the exchange capacity of the sample (7.6 g·0.75 meq/g = 5.7 meq). Hence, the ion population of the sample has not changed significantly during the test.

After day 42, the circulating solution was again switched to deionized water and mass loss was once again detected by turbidty measurements, but this time no pressure loss was observed. At day 46, a new amount of the previously used NaCl/$CaCl_2$-solution was contacted to the sample. This solution was circulated for a period of approximately 63 days (day 46–109) without any pressure drop. Also the turbidity measurements indicated almost no erosion during this time period. The small recorded increase in eroded mass is expected to come from material already present in the tubes at this stage.

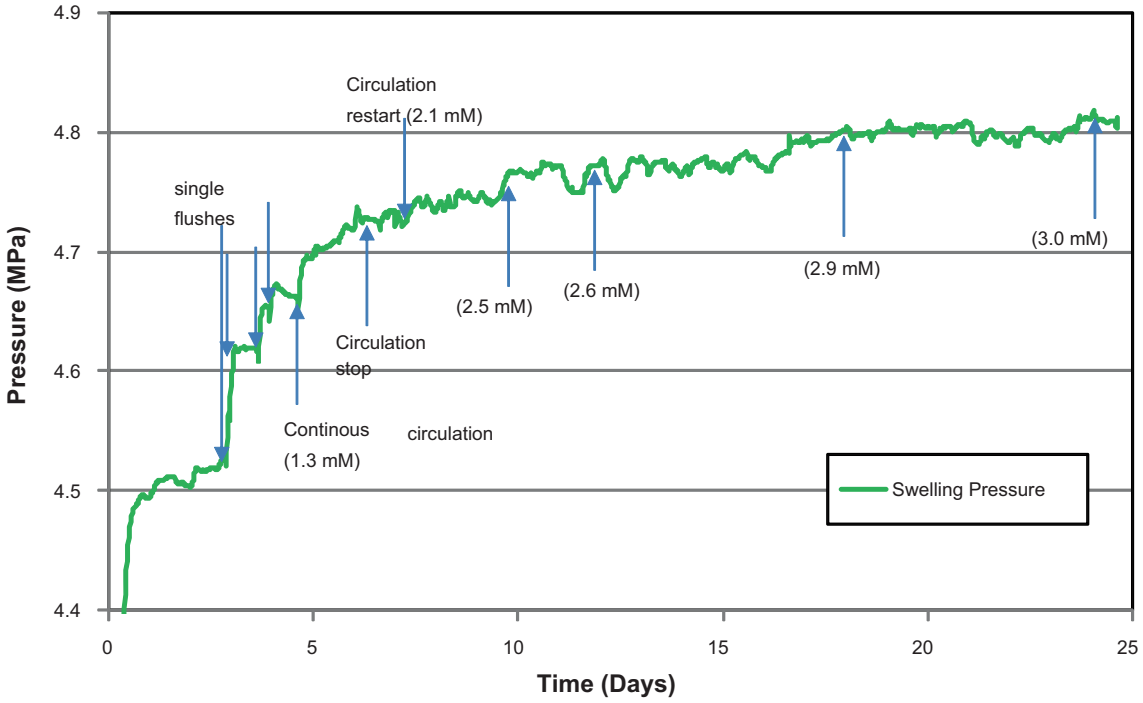

Figure 7-30. *Pressure response of the MX-80 sample during preparation phase. The measured Na_2SO_4-concentration in the outer circulating solution is also indicated.*

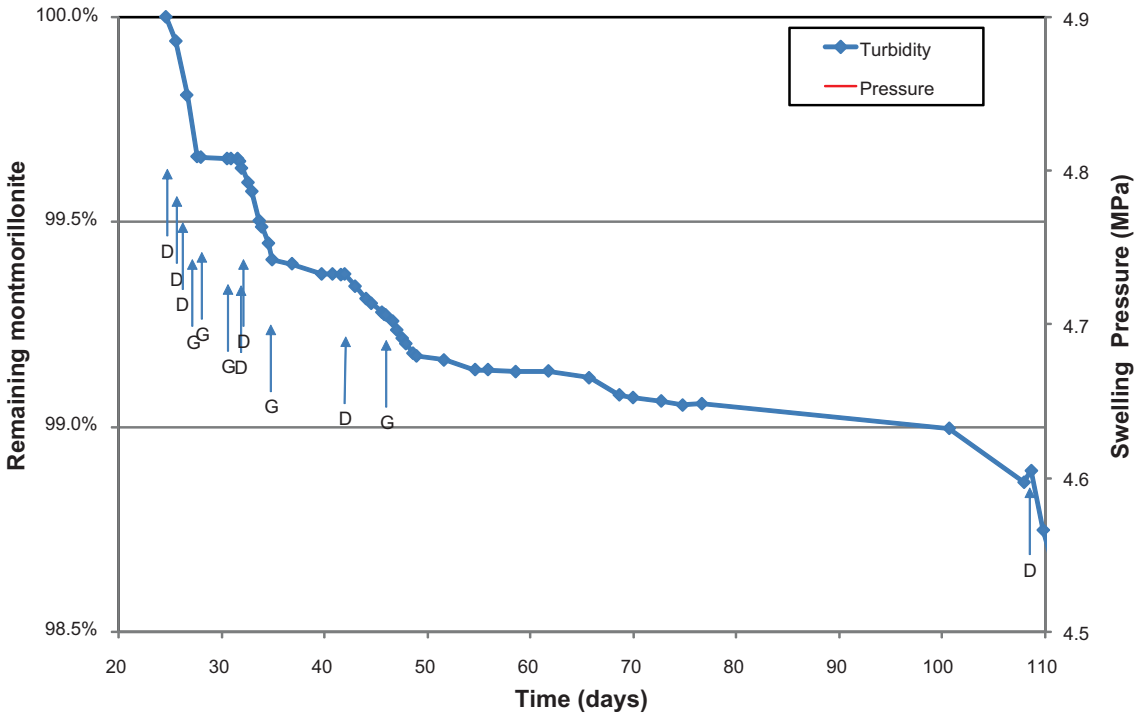

Figure 7-31. *Remaining amount of montmorillonite as deduced from turbidity measurements, and recorded swelling pressure of the MX-80 sample during days 20–110 in the MX-80 erosion experiment. D denotes events when the circulating solution was replaced by deionized water. G denotes events when the ciruclating solution was replaced by a $NaCl/CaCl_2$ with initial concentrations [NaCl] = 0.7 mM, $[CaCl_2]$ = 0.2 mM.*

At day 109, the circulating solution was replaced with deionzied water and erosion was immediately detected, with simultaneous pressure drop and recorded mass loss (Figure 7-32). This erosion process was observed to accelerate, and at day 112 the sample was contacted with a NaCl/$CaCl_2$-solution of half the concentration compared to the one used before (i.e. [$CaCl_2$] = 0.1 mM and [NaCl] = 0.35 mM, initially). Although an initial slowdown of the erosion process was observed, this solution did not stop the erosion. Also at these conditions the erosion process accelerated. At day 119, the pumping rate was lowered by a factor of 7 and a new amount of the weaker NaCl/$CaCl_2$-solution was contacted to the sample. The erosion was initially slowed down but then once again accelerated erosion took place.

At day 129, the solution was replaced by deionzed water and the pumping rate was put back to normal. Here very strong erosion occurred with a mass loss of over 1% during just a few hours. The sample was then contacted with a new NaCl/$CaCl_2$-solution of the original type ([NaCl] = 0.7 mM and [$CaCl_2$] = 0.2 mM) which was not replaced for a period of ca 63 days. Initially, the erosion was slowed down, but again an acceleration of the mass loss and pressure drop was observed. At day 136, the pumping rate was lowered by a factor of 7 and erosion stopped. Except for a mass loss event occurring between day 140 and 143, no further erosion occurred until the circulating solution was switched back to deionized water at day 192 (the small recorded mass loss during days 143–192, which is not correlated with a corresponding pressure drop, is most certainly coming from material lying in the tubes and not from the pressurized sample). At day 188 the pumping rate was put back to normal without any erosion occurring.

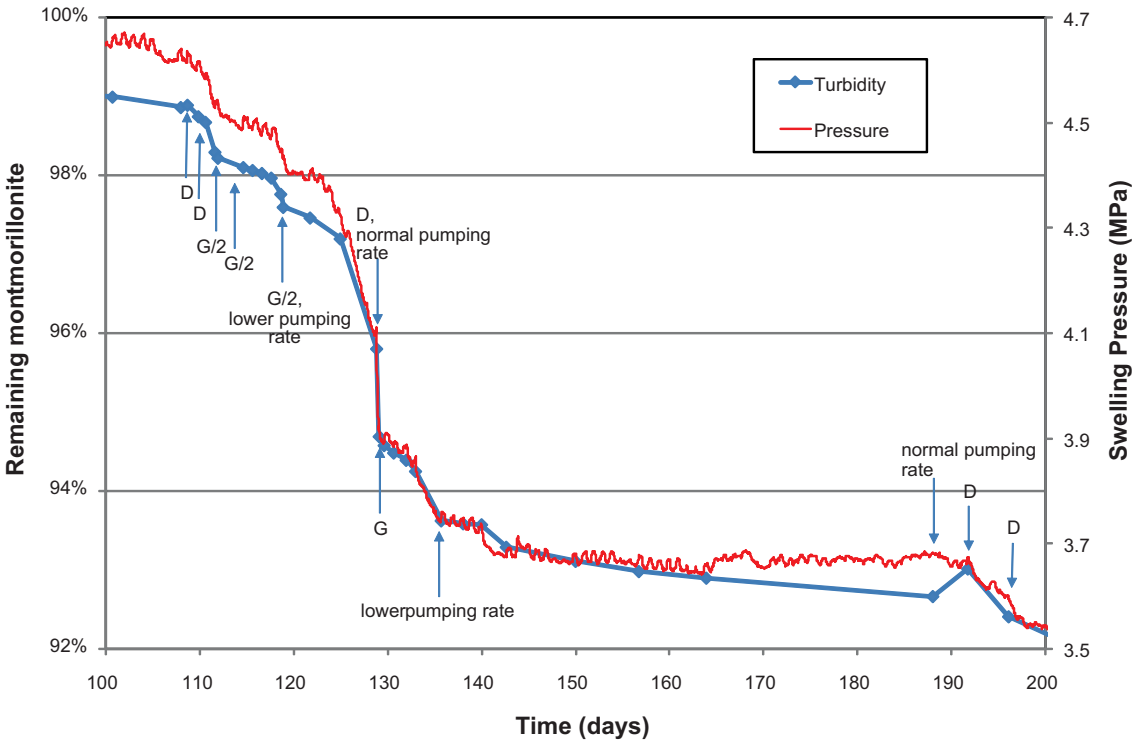

Figure 7-32. *Remaining amount of montmorillonite as deduced from turbidity measurements and recorded swelling pressure of the MX-80 sample during days 100–200 in the MX-80 erosion test. D denotes events when the circulating solution was replaced by deionized water. G denotes events when the ciruclating solution was replaced by a NaCl/$CaCl_2$ with initial concentrations [NaCl] = 0.7 mM, [$CaCl_2$] = 0.2 mM. G/2 denotes event when the circulating solution was replaced by a NaCl/$NaCl_2$ with initial concentrations [NaCl] = 0.35 mM, [$CaCl_2$] = 0.1 mM. Occations when the pumping rate of the circulating solution was changed are also denoted.*

Deionized water was circulated over the sample between day 192 and 213. Erosion was clearly recorded (Figure 7-33), but with a much lower rate as compared to the erosion events observed around day 129 (where the same type of solution was circulated at the same pumping rate); here approximately a mass loss of 1% was recorded during a time period of 6 days. At day 209, the pumping rate was increased by a factor of 7 which initially increased the erosion rate significantly. The erosion was however later slowed down, as seen in Figure 7-33.

At day 213, the circulating water was replaced by a weak NaOH solution of initial pH 10.7. This solution was circulated for about 14 days and pH was occasionally measured. The pH declined with time in the solution and seemed to level out at a value around 8.1. Although pH was larger than 10 for at least 4 days when circulating the NaOH solution, erosion was slowed down and eventually stopped.

At day 227, deionized water was circulated over the sample and an erosion rate of 1% the mass in only about 1.5 days was observed.

7.5.2.3 Summary: erosion test of MX-80 bentonite

The performed erosion test of MX-80 bentonite do show erosion when deionzed water is circulated although the erosion rate can vary widely for identical external conditions (i.e. identical pumping rates of the circulating water). Furthermore, by increasing the pumping rate, the erosion rate has increased (see day 209, Figure 7-33). These observations suggest that the observed erosion process not only involves the out-transport of a formed sol phase, but also have a contribution from mechanical erosion where flowing water tears off clay from the gel phase. The mechanical part depends on how the clay is swelling into the confining filters and how the circulating water is flowing over and in the filters. The influence of this mechanical component is difficult to quantify with the current setup.

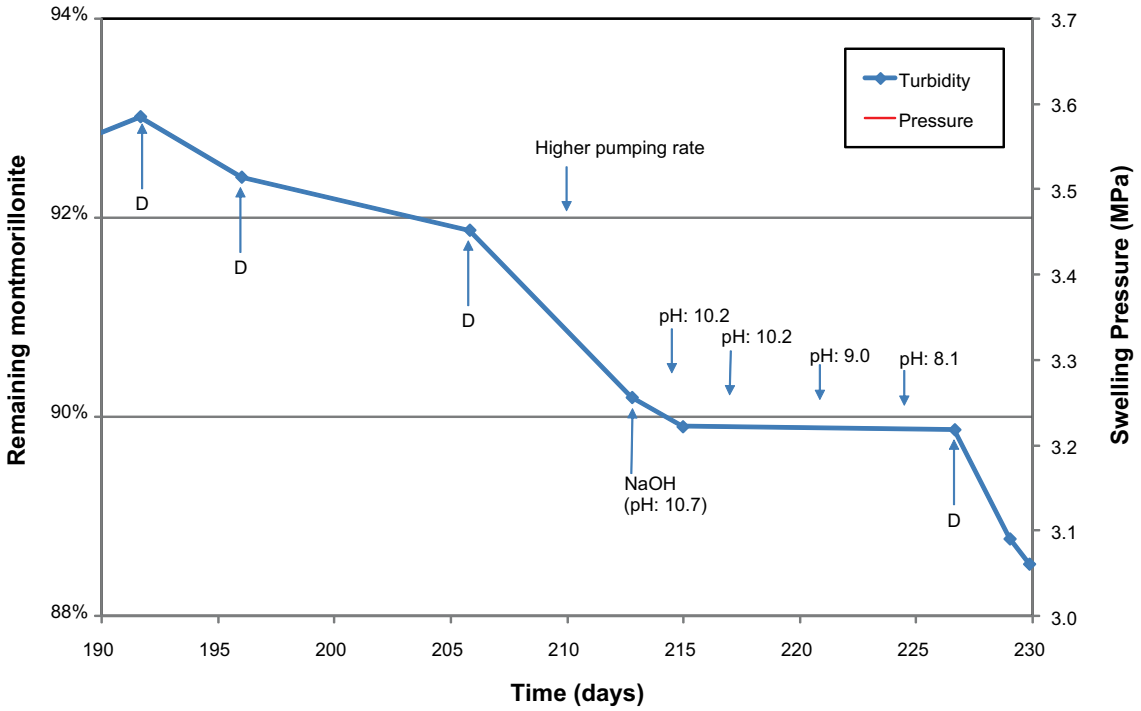

Figure 7-33. *Remaining amount of montmorillonite as deduced from turbidity measurements and recorded swelling pressure of the MX-80 sample during days 190–230 in the MX-80 erosion test. D denotes events when the circulating solution was replaced by deionized water. Indicated are also occations when the pumping rate of the circulating solution was changed and when the cirulating solution was replaced by a NaOH solution of approximate pH 10.7 Values of measured pH is indcated.*

The test has also demonstrated that the erosion can be turned off by circulating the prescribed NaCl/$CaCl_2$-solution (or rather a 1.1 mM NaCl solution, which is the state at equilibrium). Note that both of the suggested erosion mechanisms are turned off under these chemcial conditions. This means that the clay is not only non-sol forming but is strong enough to withstand mechanical erosion due to local flow in or near the filters. Furthermore, since the erosion process can be turned on again by switching to deionized conditions, the effect is clearly "chemcial", i.e. the cessation of erosion is not an effect of a permanent erosion hindrance such as an accumulation of particles of accessory minerals.

The test actually indicates that no filter cake is built-up by the accessory minerals. If this would be the case, the erosion rate under deionized contions would decline during the course of the experiment. No such systematic trend is observed (compare day 24 with day 129, or day 210 with day 230).

It should also be noted that the erosion process is insensitive to pH in the investigated range. The initial pH of the deionzied water and the prescribed NaCl/$CaCl_2$-solution is approximately 5.7 but increases in proportion to exposure time as a consequence of H^+ ion exchange (and possibly other mechanisms such as calcite dissolution or surface complexation reactions). Figure 7-34 shows eroded material mass and pH of the test solutions at replacement of the solutions (except for the pH-values measured between days 213 and 227 ,where the solution was not replaced, see Figure 7-33). From this figure and the known initial pH it is seen that erosion during deionized conditions have occurred in this test for pH ranging between 5.7–7.3, while the erosion have been stopped due to increased salt concentration (the NaOH or NaCl/$CaCl_2$ solutions) at pH-values up to 10.2.

7.5.3 Erosion tests of pure Ca/Na-montmorillonite

The erosion behaviour of mixed Ca/Na-clay at low ionic strength was further investigated by tests on pure montmorillonites with specified Ca/Na population. Different types of montmorillonite, both with respect to ion population and origin, of dry weights in the range 2.6–2.9 g were prepared in set-ups similar to the one showed in Figure 4-1. The only difference with the set-up shown in Figure 4-1 was that in these tests metal cells (steel or titanium) of diameter 20 mm were used.

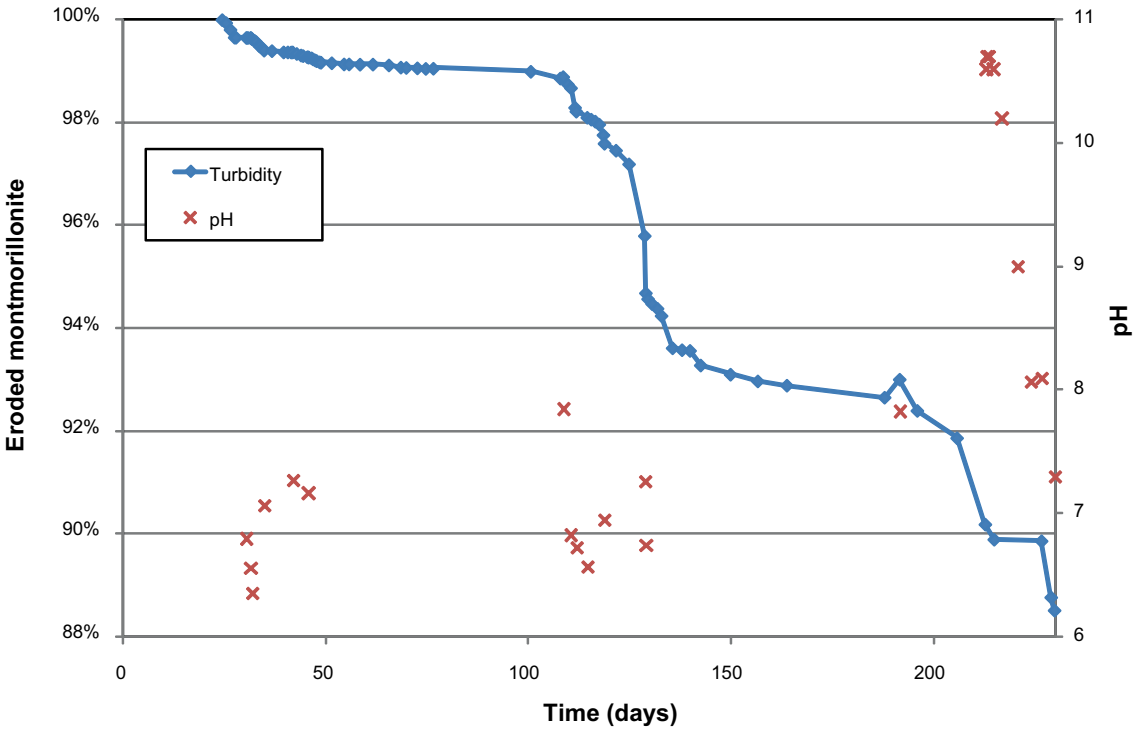

Figure 7-34. Accumulated eroded mass montmorillonite of the MX-80 sample and recorded pH of the circulating solutions during the entire MX-80 erosion test.

By circulating initially pure NaCl solutions, the amount of ion exchange required to reach equilibrium was very small due to the low ionic strength (nearly all calcium in the system sticks to the clay, see Section 7.2). Solution concentration and pumping rate was varied and pressure evolution and turbidity in the circulating solution were measured.

The results were similar to the results of the test with MX-80 bentonite (Section 7.5.2). In particular, also the results from these tests suggest an additional form of erosion due to mechanical shering of the clay gel. This is illustrated in Figure 7-35 where an erosion process occurring at a circulating solution of 2 mM spontaneously ceases.

Table 7-15 presents the lowest concentration of the circulating solution for which stable (i.e. non-decreasing) swelling pressures could be achieved for each of the tested samples. These values, which are in the range 0.5–4 mM, should not be considered as characterizing each separate clay since they most certainly are affected by uncontrolled factors in the experimental set-up (local flow, filters etc.). However, the obtained concentration range covers the corresponding limiting concentration of the erosion test of MX-80 bentonite (1.1 mM, Section 7.5.2). This indicates that the presence of accessory minerals do not significantly influence the erosion mechanisms. Furthermore, comparison of the four tests made on montmorillonite of Milos type (CaNaErosion01, 02, 03 and 04) shows that there is no significant influence on the erosion mechanism by varying the calcium content of the clay between 25 and 75 percent. This is yet a strong indication that the underlying mechanism which governs the present type of erosion in mixed Ca/Na-systems is different from the face-to-face correlation effect which appear at high calcium content (see Section 5.4.3).

Finally, from the results of Table 7-15 it can be concluded that the erosion process shows no significant dependency on the investigated clay types (Milos, Kutch or Wyoming).

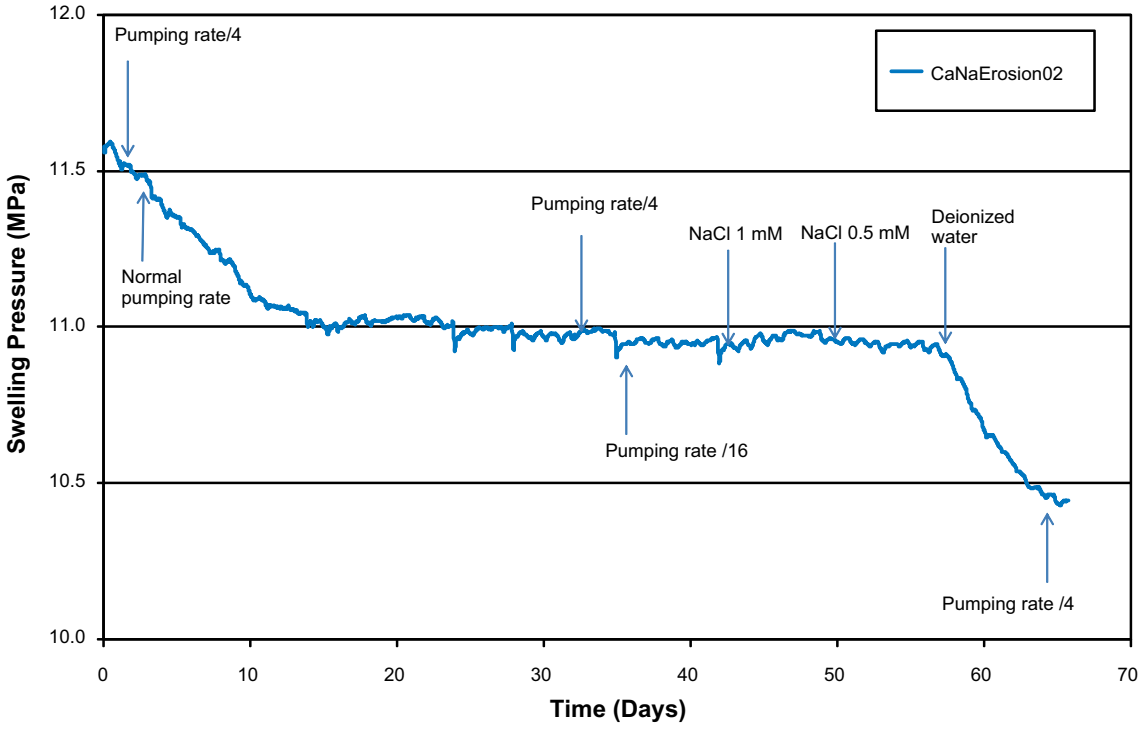

Figure 7-35. *Swelling pressure evolution of eroding test CaNaErosion02. The clay is of Milos type and the ion population is 50/50 Ca/Na. The circulating solution is 2 mM NaCl at the beginning of the displayed time period. The pumping rate have been lowered by a factor of 4 or 16 compared to original rate throughout the test period. The events of changing pumping rate is indicated in the diagram. Indicated is also when the circulating solution has been replaced with a solution of lower concentration. Note that the erosion stop at around day 15 is occuring spontaneosly, without changing pumping rate or circulating solution.*

Table 7-15. Summary of the conducted erosion experiments with Ca/Na-montmorillonite. X denontes the charge fraction of calcium in the clay. The column "Observed stability" lists the lowest NaCl concentration for which no (or undetectable) erosion occurred (As examplified in Figure 7-35).

Sample	Clay Type	X	Observed stability
CaNaErosion01	Milos	0.5	2 mM
CaNaErosion02	Milos	0.5	0.5 mM
CaNaErosion03	Milos	0.25	1 mM
CaNaErosion04	Milos	0.75	3 mM
CaNaErosion05	Wyoming	0.5	4 mM
CaNaErosion06	Kutch	0.5	1 mM

7.6 Conclusions

The present work has derived theoretical limits for a sol formation zone in the $[Ca^{2+}]$-$[Na^{+}]$-diagram for montmorillonite limited at low ionic strength by a curve representing the Na/Ca-exchange reaction at a Ca population in the clay of approximately 90% (charge wise). At high ionic strengths the theory puts an upper limit by the line of constant ionic strength equal to the concentration at which the pure Na-system forms a gel.

From supporting sedimentation measurements for the case of Wyoming type montmorillonite, a comparison between measurements and theory has been made. The measurements show that the zone of sol formation, is localized very close to the $[Na^{+}]$-axis in the $[Ca^{2+}]$-$[Na^{+}]$-diagram. This observation suggests that the ability to form a sol is not just a matter of ionic strength but also explicitly depend on the calcium content of the system: relatively small amounts of calcium reduce the ability to form a sol significantly. This effect of calcium is additional to the well-documented correlation effects on lamellar swelling and must be associated with interactions involving the edges of separate montmorillonite layers.

Further comparison between measurements of the sol formation zone and the theoretical considerations shows that the lower limit (exchange reaction) of the sol formation zone is marked, i.e. there is a transition from non-swelling behaviour of Ca-montmorillonite to something which disperses much more easily at around 90% of Ca population even in Ca/Na systems containing excess ions.

A quite different behaviour was observed for the systems prepared from initially pure Na-montmorillonite and initially pure Ca-montmorillonite, and it remains to determine if this is an effect of the initial state or not. Systems with initially pure Na-montmorillonite seem to form different gels above and below the sol formation zone. It is of interest to investigate if these gels are constructed differently on a microscopic scale. Visual observations, however, suggests that both gel types have a rather high strength.

The additional stabilizing effect of calcium has also been confirmed in erosion tests where highly Na-dominated clays (both pure montmorillonite and MX-80 bentonite) have been shown to be prevented from eroding by solutions containing only small concentrations of calcium and NaCl concentrations far below the corresponding CCC in a pure Na-system. The effect has been shown to be insensitive to the precise value of the calcium charge fraction of the clay in the range of 20 to 75 percent. Thus, as long as the calcium content of the clay stays above 20 percent, it is not important if the system is in exchange equilibrium or not. This observation, in turn, suggests that a pragmatical critical concentration for erosion to occur in mixed Ca/Na-clays could be defined based on charge concentration rather than specific ion concentrations, since charge is conserved in the ion exchange process. The performed experiments show that an upper limit for this type of critical concentration in mixed Ca/Na-clay is 4 mM charge equivalents.

8 Diffusion of Ca^{2+}, Na^{+} and SO_4^{2-} in compacted montmorillonite

8.1 Introduction

As has been shown in the previous chapters, the ion population (X) of the clay is one of the key variables which determine the sol formation ability in a Ca/Na-system. It follows that it is of great importance to be able to predict the evolution of the counterion population of the bentonite buffer in the KBS-3 repository in order to quantify possible mass loss due to colloidal release. Ions redistribute in the buffer mainly for two reasons; either by interaction with the groundwater or due to dissolution (or precipitation) of accessory minerals initially present in the bentonite. Since gypsum is the most soluble mineral present in many bentonites (e.g. MX-80) and also a source for calcium it is of specific interest to investigate the fate of this phase in the KBS-3 buffer.

Therefore, and also to gain understanding of the dissolution process of accessory minerals in water saturated bentonite, ion diffusion tests were performed in pure montmorillonite systems contacted either with crystalline gypsum in a controlled geometry or with a gypsum saturated solution.

8.2 Experimental

The experimental setup is schematically pictured in Figure 8-1. Thin pieces of precipitated gypsum were placed between two 2.5 mm discs of pre-saturated pure montmorillonite of either Na- or Ca-type. The gypsum/montmorillonite sample was mounted between two steel filters in a test cell and deionized water was circulated on the opposite side in two separate circuits (top and bottom).

A through-diffusion test was also performed. In this case the sample consisted only of pure Ca-montmorillonite, the bottom reservoir source contained gypsum saturated solution and the top solution deionized water.

8.2.1 Materials

Montmorillonite was obtained from purification of Wyoming type bentonite (MX-80) and ion exchanged to pure Na-form by repeated washing in 1 M NaCl-solution and subsequent dialysis. The amount of dry material was chosen to achieve a dry density of approximately 1.5–1.6 g/cm^3.

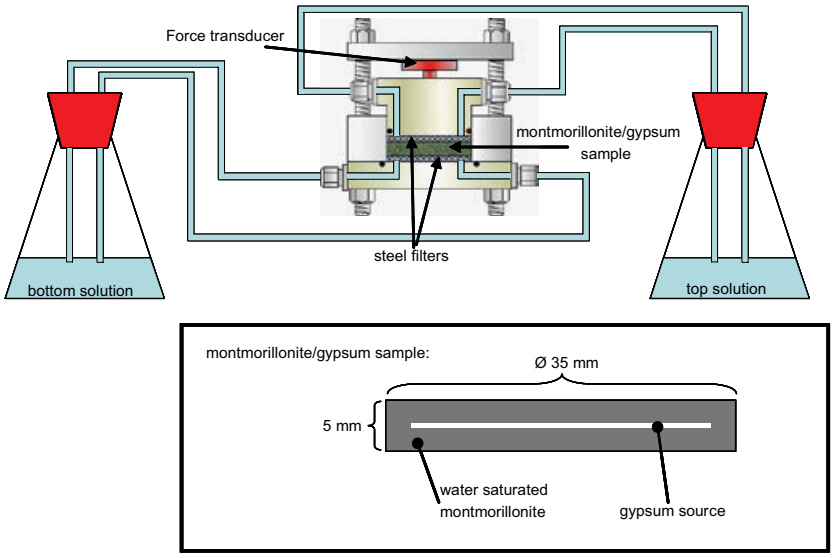

Figure 8-1. *Schematic view of experimental set-up.*

8.2.2 Test cells

The test cells consist of PEEK and are held together with steel bolts. The inner diameter is 35 mm and the height was adjusted to 5 mm. When Ca-montmorillonite was used, the pore size of the filters used was 10 µm, and 0.2 µm-filters were used for the case of Na-montmorillonite due to the great ability for this material to form colloids which escapes the cell ("infinite" swelling) when contacted with solutions with low enough ionic strength. A transducer continuously sampled the force, and thereby the pressure, exerted by the swelling clay. The pressure measurements are a good indicator of achieved density, since swelling pressure has large density dependence (see e.g. Karnland et al. 2006). At a dry density of 1.5–1.6 g/cm^3, the swelling pressure for Wy-Ca and Wy-Na montmorillonite contacted with deionized water is 5–15 MPa (/Karnland et al. 2006/). Furthermore, monitoring the pressure is a convenient method to guarantee that the sample is not modified during measurement, e.g. due to mass loss.

8.2.3 Sample preparation

The montmorillonite/gypsum samples were prepared by first water saturating two Na- and two Ca-montmorillonite samples of height 2.5 mm. Water saturation was achieved by circulating deionized water over both top and bottom filters of the test cell until the swelling pressure was stable over a long time (several days or even weeks). After saturation all test cells were opened. A thin layer of crystalline gypsum was placed on top of one of the Na-montmorillonite samples, while the other Na-sample was removed from its test cell and placed on top of the gypsum. The cell containing Na-montmorillonite – Gypsum – Na-montmorillonite was reassembled and its confining pressure adjusted to 5–10 MPa. Exactly the same procedure was performed to prepare the Ca-montmorillonite/gypsum sample.

The pure Ca-montmorillonite sample of height 5 mm used in the through-diffusion test was also water saturated by circulating deionized water over both filters. Swelling pressure evolutions of all three samples during the test phase are plotted in Figure 8-2.

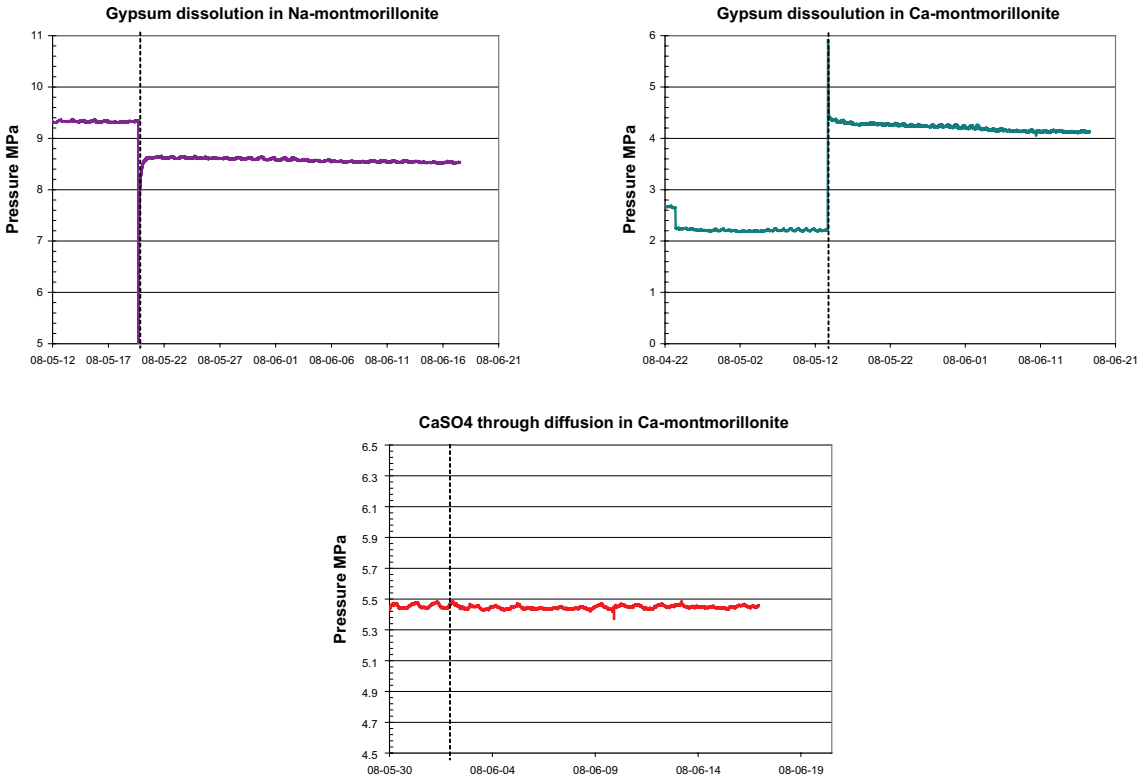

Figure 8-2. *Pressure evolution in the three tests. The dashed vertical lines indicate start of the diffusion tests.*

8.2.4 Diffusion tests

The diffusion tests were performed by contacting the water saturated montmorillonite/gypsum samples by 100 grams of deionized water on each side. The target solutions were circulated in separate circuits. By this design, each sample actually constituted two identical diffusion tests. Comparison of the diffusive flux into each target reservoir gave a good indication whether the intended geometry was achieved and that no preferential paths was formed in the cells during preparation where mobility would be increased.

The through-diffusion test was performed by replacing the deionized bottom solution (from water saturation phase) with gypsum saturated solution. The top circuit (target) was contacted with 100 grams of deionized water.

The accumulation of ions in the target reservoirs as a function of time was determined both by activity measurements using Na^+- and Ca^{2+}- selective electrodes and with electrical conductivity measurements in the case of Ca-montmorillonite. Electrical conductivity measurements are not applicable when the system contains both Na^+ and Ca^{2+} ions as no one-to-one relation can be established between Na/Ca-concentrations and electrical conductivity.

The measured activities and conductivities were correlated to Na_2SO_4 and $CaSO_4$ concentrations by careful calibration to reference solutions.

When needed, the target solutions were replaced in order to maintain the correct boundary conditions (i.e. to keep the target reservoirs virtually ion free).

8.3 Theory

Let n_{acc} (t) denote the accumulated diffused amount of a specific ion at time t (as moles per second) in a diffusion experiment. Typically (if boundary concentrations are constant) this function becomes a linear function of t for large times and can be fitted to

$$n_{\text{acc}}(t) = \mathrm{k}_0 + \mathrm{k}_1 \cdot t \qquad \text{large } t \tag{8-1}$$

where k_0 and k_1 are fitting parameters. The steady state flux is then given by

$$j_{\text{s.s.}} = \frac{1}{A}\frac{dn_{acc}(t)}{dt} = \frac{\mathrm{k}_1}{A} \quad \text{large } t \tag{8-2}$$

where A is the cross sectional area of the sample. From this quantity the effective diffusion coefficient can be determined

$$D_{\text{e}} = -\frac{j_{\text{s.s.}}}{\nabla c} = \frac{l \cdot \mathrm{k}_1}{A \cdot \left(c_{\text{source}} - c_{\text{target}}\right)} \tag{8-3}$$

where c_{source} is the concentration at the source, c_{target} the target concentration (equal to zero in all cases treated here) and l is the length between target and source. Note that the effective diffusion coefficient here is defined for external concentrations, i.e. exterior to the clay. The actual clay concentrations are modified by ion equilibrium effects /Birgersson and Karnland 2009/.

Usually the n_{acc} (t) curve shows a breakthrough behaviour. The breakthrough time, t_{BT}, defined as the time where the large-t linear fit intercept the time axis

$$0 = \mathrm{k}_0 + \mathrm{k}_1 \cdot t_{\text{BT}} \Leftrightarrow t_{\text{BT}} = -\frac{\mathrm{k}_0}{\mathrm{k}_1} \tag{8-4}$$

is related to the actual diffusion coefficient in the clay by /Crank 1975/

$$D_c = \frac{l^2}{6 \cdot t_{\text{BT}}} = -\frac{l^2 \cdot \mathrm{k}_1}{6 \cdot \mathrm{k}_0}\,. \tag{8-5}$$

8.4 Results

8.4.1 Gypsum dissolution in Ca-montmorillonite

In the case of gypsum dissolution in Ca-montmorillonite, the system only contains one type of cation and one type of anion. Due to charge neutrality, the flux detected in the target solutions must be a $CaSO_4$-flux. In Figure 8-3 the accumulated $CaSO_4$ with time is plotted as measured both with electrical conductivity measurements and with the Ca^{2+}-selective electrode. A trend is seen that the conductivity measurements give higher values and also a somewhat higher flux (slope of the curve). This could be due to some systematic error in the calibration, but probably reflects the fact that the montmorillonite phase itself is slowly dissolving in contact with deionized water, thereby producing additional ions which contributes to the electrical conductivity to a much higher degree than to the activity of Ca^{2+}. In the following we will use the data achieved from ion specific electrodes for evaluating transport parameters, still the electrical conductivity measurements are a good way to control the consistency of the activity measurements.

Another good check whether we are actually observing ion diffusion through montmorillonite is to compare the ion accumulation in the two separate circuits over the test cell. This comparison is made in Figure 8-4. The good agreement between the two curves is a very strong indication that there were no preferential paths, through which ions diffuse more easily, introduced during the preparation of the montmorillonite/gypsum sample.

The small deviation of flux on the two target sides seen in Figure 8-4, is probably an indication of a small off-centre displacement of the gypsum source in the montmorillonite.

The behaviour of the accumulation curve (Figure 8-4) shows a steady-state behaviour after only a few days (the curve is linear). The corresponding average steady state flux is $j_{s.s.} = 1.0 \cdot 10^{-8}$ mol/s/m^2 if the full cross sectional area of the test cell is used in Equation 8-2. Since the gypsum source did not cover the entire cross section, this evaluated flux is most probably a slight underestimation of the actual flux. Assuming the $CaSO_4$-concentration at the source to equal the solubility of gypsum in bulk water, $c_{sat.gypsum}$, an effective diffusion coefficient can be determined using Equation 8-3.

$$D_e^{Ca^{2+}/Ca} = D_e^{SO_4^{2-}/Ca} = -\frac{j_{s.s.} \cdot L/2}{c_{sat.gypsum}} = -\frac{1.0 \cdot 10^{-8}\,\text{mol/s/m}^2 \cdot 0.0025\,\text{m}}{15.6\,\text{mol/m}^3} = 1.6 \cdot 10^{-12}\ \text{m}^2/\text{s}$$

The notation $D_e^{M/N}$ refers to diffusion of ion M in N-montmorillonite and L denotes the length of the montmorillonite/gypsum sample (= 0.005 m).

It is also interesting to note that the ions appear to move quickly enough through the thin sample that any break-through behaviour in the accumulation curve is hard to resolve. Hence, no sulphate diffusion coefficient in the clay could be estimated (Equation 8-5).

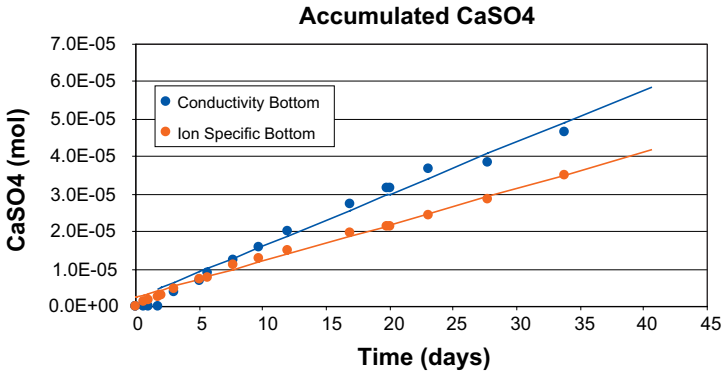

Figure 8-3. *Amount of $CaSO_4$ in the bottom target solution as a function of time as measured with Ca^{2+} specific electrode and electrical conductivity for the case of gypsum dissolution in Ca-montmorillonite. $P_s \approx 4$ MPa.*

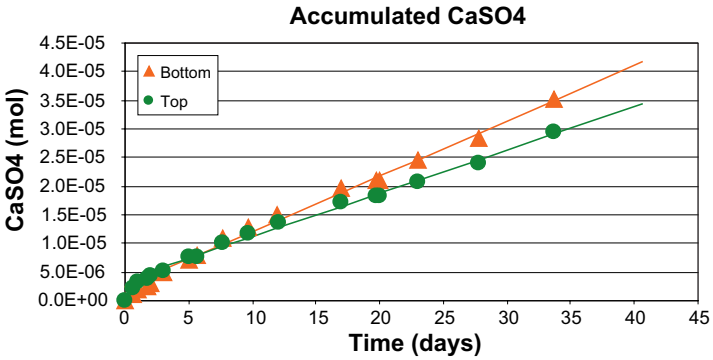

Figure 8-4. *Comparison of top and bottom target solutions as a function of time. The reproducibility is good. $P_s \approx 4$ MPa.*

8.4.2 Gypsum dissolution in Na-montmorillonite

Looking at gypsum dissolution in Na-montmorillonite, the accumulated amounts of cations in the bottom target is pictured in Figure 8-5. Note that even though gypsum is a source of calcium ions, the flux consists entirely of sodium ions. Obviously, this Na-flux must be accompanied by a SO_4^{2-}-flux of half the magnitude in order to maintain charge neutrality.

It is also seen in Figure 8-5 that a steady state like behaviour is rather quickly established for the Na-flux. After approximately 20 days this flux is suddenly changed to a new steady state-like flux. This behaviour is interpreted as a partial depletion of the gypsum source. A strong indication that this interpretation is correct is given by comparing at the accumulated Na^+ in both target reservoirs, as seen in Figure 8-6. The behaviour is very similar in both targets, and preferential paths can be excluded as an explanation for the abrupt behaviour.

Looking at the first steady-state phase, the average Na-flux equals $j_{s.s.}^{Na^+} = 8.9 \cdot 10^{-8}\,\mathrm{mol/s/m^2}$ (again with a slight overestimation of cross sectional area) and the associated SO_4^{2-} flux is then $j_{s.s.}^{SO_4^{2-}} = 1/2 \cdot j_{s.s.}^{Na^+} = 4.5 \cdot 10^{-8}\,\mathrm{mol/s/m^2}$. Assuming once again saturated gypsum concentration at the source, the effective diffusion coefficient for SO_4^{2-} can be estimated

$$D_e^{SO_4^{2-}/Na} = \frac{j_{s.s.}^{SO_4^{2-}} \cdot L/2}{c_{sat.\,gypsum}} = \frac{4.5 \cdot 10^{-8}\,\mathrm{mol/s/m^2} \cdot 0.0025\,\mathrm{m}}{15.6\,\mathrm{mol/m^3}} = 7.2 \cdot 10^{-12}\ \mathrm{m^2/s}$$

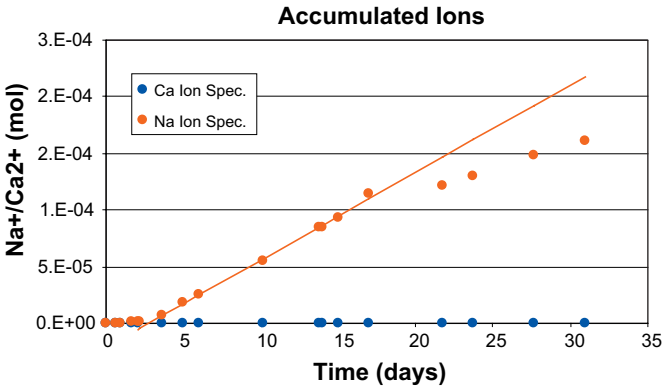

Figure 8-5. *Amount of Ca^{2+} and Na^+ in the bottom target solution as a function of time measured with ion specific electrodes for the case of gypsum dissolution in Na-montmorillonite. $P_s \approx 8.5$ MPa.*

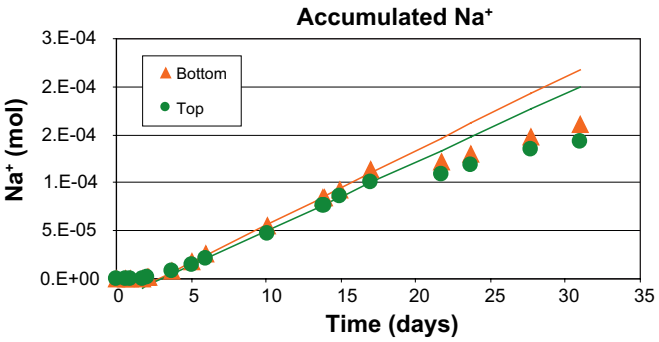

Figure 8-6. *Comparison accumulated Na^+ ions in top and bottom target solutions as a function of time for the case of gypsum dissolution in Na-montmorillonite. $P_s \approx 8.5$ MPa.*

Note that this value is approximately four times larger than the corresponding value for SO_4^{2-} in Ca-montmorillonite. The Na-montmorillonite sample has a higher swelling pressure, and hence a slightly higher density, as compared to the Ca-montmorillonite sample. From a density consideration alone one would therefore expect the diffusion coefficient to be smaller in the Na-montmorillonite since diffusivity is a density dependent quantity.

As can be seen in Figure 8-6, a breakthrough behaviour can be resolved in the accumulation curve in contrast to the case with gypsum in Ca-montmorillonite. This indicates that SO_4^{2-} has a lower mobility in Na-montmorillonite as compared to Ca-montmorillonite.

From the linear fit a sulphate diffusion coefficient in the clay can be quantified (Equation 8-5) $D_c^{SO_4^{2-}/\mathrm{Na}} = 4.2 \cdot 10^{-12}$ m^2/s $t_{BT} \approx 66$ hours in this case). This value could be compared to the corresponding value in bulk water of $D_{bulk\ water}^{SO_4^{2-}} = 1.1 \cdot 10^{-9}$ m^2/s /Lasaga 1998/.

The measured SO_4^{2-} fluxes are compared in Figure 8-7 for all targets and samples.

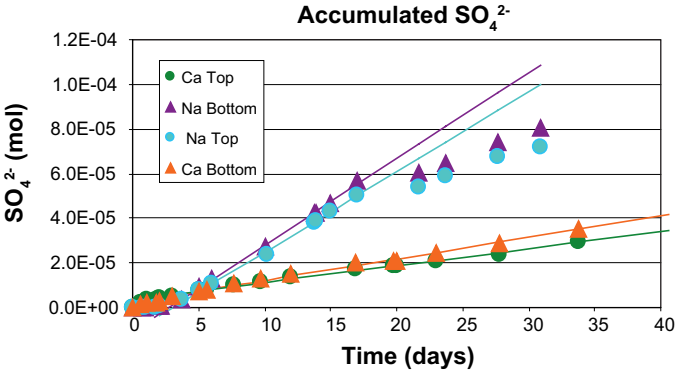

Figure 8-7. *Comparison of accumulated SO_4^{2-} in top and bottom target solutions as a function of time for gypsum dissolution in both Na- and Ca-montmorillonite. $P_s \approx 4$ MPa for the Ca-montmorillonite and $P_s \approx 8.5$ MPa for the Na-montmorillonite.*

8.4.3 Through-diffusion of $CaSO_4$ in Ca-montmorillonite

Through-diffusion of $CaSO_4$ in Ca-montmorillonite was performed in order to compare to the results of gypsum in Ca-montmorillonite. The accumulation curve is shown in Figure 8-8. The steady state flux is $j_{s.s.} = 8.9 \cdot 10–9$ mol/s/m^2, giving

$$D_e^{Ca^{2+}/Ca} = D_e^{SO_4^{2-}/Ca} = -\frac{j_{s.s.}}{c_{sat.\,gypsum}/L} = -\frac{8.9 \cdot 10^{-9}\,\text{mol/s/m}^2}{15.6\,\text{mol/m}^3/0.005\,\text{m}} = 2.9 \cdot 10^{-12}\ \text{m}^2/\text{s}$$

since diffusion occurs across the entire sample length in this case. In this case no underestimation is done when using the entire cross sectional area since the solution is penetrating everywhere. This effective diffusion coefficient is approximately 1.5 times larger than what was evaluated for the case of gypsum dissolution in Ca-montmorillonite. It should be kept in mind, however, that in the latter case the actual cross sectional area of the gypsum mineral was smaller (and not totally controlled) than the total cross sectional area of the test cell. The evaluated through diffusion coefficient above is then rather an upper limit to what would be expected in the gypsum dissolution experiment. In this perspective the closeness of these two values indicates that it is actually the solubility of gypsum in bulk water (modified by ion equilibrium effects) which sets the concentration gradient in the case of dissolving gypsum as well.

A break-through behaviour is clearly seen in Figure 8-8 and the diffusion coefficient in the clay is estimated to $D_c^{SO_4^{2-}/Ca} = 1.9 \cdot 10^{-11}$ m^2/s (break-through time is approximately 60 hours). Note that this value is around four times larger than the corresponding value evaluated in Na-montmorillonite.

This relatively large value also explains why no break-trough was resolved in the case of gypsum in Ca-montmorillonite. In that test the diffusion length was only half of the length in the through-diffusion test. Since break-through time is proportional to the square of the diffusion length (Equation 8-5), the break-through occurred only after a few hours.

All measured and estimated parameters in the three performed diffusion tests are summarized in Table 8-1.

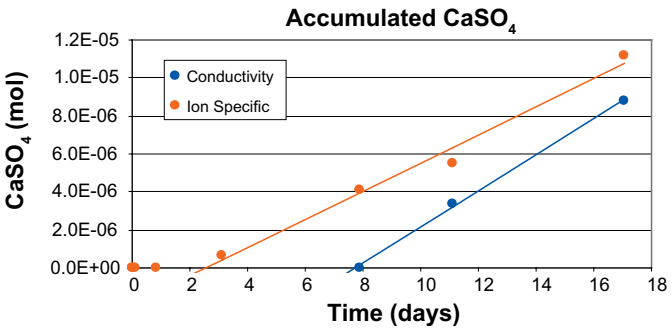

Figure 8-8. *Through diffusion of CaSO4 in Ca-montmorillonite. The mismatch between conductivity and activity measurements are due to the fact that concentrations are so low in the target reservoir that the calibration for the conductivity measurements are not valid. $P_s \approx 5.4$ MPa.*

Table 8-1. Summary of performed diffusion experiments. The dry density was evaluated from water to solid mass ratios measured after termination of the tests. The fluxes refers to steady state values (in the case of Na-flux in the test with gypsum in Na-montmorillonite, it refers to the first period of "quasi" steady state, see e.g. Figure 8-5). The corresponding values for bulk water are taken from /Lasaga 1998/.

Test	P (MPa)	ρ_d (g/cm³)	$j_{SO_4^{2-}}$ (mol/s/m²)	$j_{Ca^{2+}}$ (mol/s/m²)	j_{Na^+} (mol/s/m²)	$D_e^{SO_4^{2-}}$ (m²/s)	$D_e^{Ca^{2+}}$ (m²/s)	$D_e^{Na^+}$ (m²/s)	$D_c^{SO_4^{2-}}$ (m²/s)
Gypsum diss. in Ca-mont	4.0	1.34	$1.0\cdot10^{-8}$	$1.0\cdot10^{-8}$	-	$1.7\cdot10^{-12}$	$1.7\cdot10^{-12}$	-	-
Gypsum diss. in Na-mont.	8.5	1.46	$4.5\cdot10^{-8}$	0.0	$8.9\cdot10^{-8}$	$7.2\cdot10^{-12}$	0.0	∞	$4.2\cdot10^{-12}$
Through-diff. in Ca-mont	5.4	n.d.	$8.9\cdot10^{-9}$	$8.9\cdot10^{-9}$	-	$2.9\cdot10^{-12}$	$2.9\cdot10^{-12}$	-	$1.9\cdot10^{-11}$
					Values in bulk water:	$1.1\cdot10^{-9}$	$7.9\cdot10^{-10}$	$1.3\cdot10^{-9}$	$1.1\cdot10^{-9}$

8.5 Discussion

Two processes are of importance for describing ion diffusion in montmorillonite /Birgersson and Karnland 2009/.

- Donnan equilibrium

This type of equilibrium between ions in an external solution and ions in the clay applies to both cations and anions and leads to a lowering of the concentration of externally introduced ions in the clay as compared to the concentration in the outer solution /Birgersson and Karnland 2009/.

- Cation exchange equilibrium

This process applies only to cations. Exchange processes will only contribute to the diffusive mass transfer if more than one type of cation is present in the system.

8.5.1 $CaSO_4$ diffusion in Ca-montmorillonite

For the case of gypsum dissolution in Ca-montmorillonite, the system contains only one type of cation and exchange reactions are of no concern. Hence only Donnan equilibrium is at play. The similar diffusive behaviour of $CaSO_4$ observed in the through-diffusion test and the mineral dissolution test performed in Ca-montmorillonite explicitly demonstrates that the same type of (Donnan) equilibrium prevail in both situations. This behaviour is expected from a thermodynamic point of view as the chemical potential of $CaSO_4$ is the same in the mineral and in the saturated solution. The observation that Donnan equilibrium controls the diffusion behaviour of $CaSO_4$ has rather large implications.

For instance, the dissolution of minerals in a water saturated bentonite can be (rather dramatically) delayed as compared to what is predicted by traditional reactive transport calculations, due to the fact that Donnan equilibrium always sets a lower concentration gradient than what is given by bulk solubility.

8.5.2 $CaSO_4$ diffusion in Na-montmorillonite

How the ion concentration gradients are controlled in the gypsum-in-Na-montmorillonite test is more difficult to identify. However, from the design of the test it can be directly stated that no exchange processes can occur over the clay/filter interface since the target solutions are kept at low (zero) concentration.

It can then directly be stated that each pair of sodium ions ending up in the target solutions must be accompanied by one SO_4^{2-} ion. Furthermore, due to the imposed boundary conditions, it can also be stated that no strict steady state situation can occur until the entire (initial) Na-clay has been converted to a pure Ca-clay or until the gypsum source is depleted. This is due to the fact that in the limit of low concentration (which is the boundary condition on the filter sides) Ca^{2+} will be basically infinitely more preferred than Na^+ in the clay. Thus, it is actually not surprising that Na^+ is diffusing out of the system.

If complete Ca-conversion should occur, we would get back the same steady state that has been studied in the other gypsum dissolution test where the clay is of Ca-form to begin with. If instead the gypsum source became depleted, any ion flow would soon cease, and the clay would be left in a state where the counterions are of both Ca- and Na-type.

Still, a "quasi" steady-state is rather quickly established for the $Na_2SO_4^{2-}$ flux. Because of the time independence of the flux it can be concluded that the SO_4^{2-} concentration in the clay must resemble a straight line. How the Na and Ca are distributed in the clay in this "quasi" steady state can on the other hand not be inferred from the information given by the experiment.

But comparing the effective diffusion coefficient for SO_4^{2-} in this state to the coefficient obtained in the case of gypsum in pure Ca-montmorillonite, it is seen that it is significantly larger. This would suggest that either the mobility of SO_4^{2-} is larger in Na dominated montmorillonite as compared to pure Ca-montmorillonite, or that the solubility of SO_4^{2-} is influenced by the type of counterions in the clay. The significant (approximately a factor of 4) difference of SO_4^{2-} diffusivity in Ca- and Na- montmorillonite, on the other hand shows that the SO_4^{2-} mobility is *lower* in Na dominated montmorillonite. This observation leads to the conclusion that it is actually the solubility of gypsum that is influenced by the type of counterions present in the clay.

A speculation is that it is the solubility of Na_2SO_4 which sets the boundary condition in the case of gypsum dissolution in Na-montmorillonite (modified by Donnan equilibrium, of course). A through-diffusion test of saturated Na_2SO_4 solution in Na-montmorillonite would shed some light on this matter.

8.6 Conclusions

By comparing the diffusion behaviour of Ca^{2+}- Na^+- and SO_4^{2-}-ions in montmorillonite either by gypsum dissolution surrounded by water saturated clay or by through diffusion, we have shown that the mass transport cannot be described by single diffusion coefficients. Instead the ion equilibrium across any interface with the clay (mineral phase or external solution) must be considered.

We have demonstrated that gypsum dissolving in Na-montmorillonite, contacted to deionized water will result in a Na_2SO_4 flux over the clay/external solution interface. Such behaviour is qualitatively easily explained by considering the basically infinite preference for Ca^{2+}- ions in clay for these types of boundary conditions.

Furthermore, it has been demonstrated that the (initial) SO_4^{2-} flux is approximately 4 times larger in the sample where gypsum is dissolving in Na-montmorillonite as compared to the sample where gypsum is dissolving in Ca-montmorillonite, despite the fact that the mobility of SO_4^{2-} ions in the Na-montmorillonite sample is considerably lower. This implies a higher solubility of gypsum in Na-montmorillonite as compared to Ca-montmorillonite, an effect which can be explained by the lower Ca^{2+}-activity in the former system.

9 Conclusions

The primary aim with this report has been to give a description of the basic principles for possible montmorillonite particle release from a bentonite buffer material and to investigate the occurrence of colloid release at various clay densities and chemical environments.

9.1 Detailed conclusions

Below follows a list of comments and main conclusions from each chapter of the report

- "Swelling ability of bentonite"
  - The swelling process takes place on a short time scale.
  - There is "unlimited" swelling for montmorillonite with monovalent counterions (Na^+) at *low* ionic strength, resulting in sol formation.
  - There is limited swelling for montmorillonite with only divalent counterions (Ca^{2+}) at *any* ionic strength.
  - There is a definite transition from limited to "unlimited" swelling in deionized water for Na/Ca-montmorillonite systems at a calcium population of less than about 90% (charge wise).
  - Sol formation does not occur in montmorillonite with more than 90% of calcium as counterions.
- "Rheology"
  - Measured rheological properties of bentonite and Na-montmorillonite are hugely dependent on sample preparation and sample history. Several preparation methods were investigated and the most conservative was chosen, where initial thixotropic effects were reduced by stirring.
  - The rheological properties of bentonite and pure Na-montmorillonite depend strongly on water content and four rheological domains have been identified and quantified at low ionic strength.
    - Na-montmorillonite with a water to solid mass ratio below 35 is a repulsive gel with non-zero shear strength.
    - Between 35 and 100 in water to solid mass ratio, Na-montmorillonite is a non-Newtonian fluid.
    - Between 100 and 1,000 in water to solid mass ratio, Na-montmorillonite is a Newtonian fluid with a viscosity larger than that for water.
    - Above 1,000 in water to solid mass ratio, the influence of montmorillonite is lost.
  - MX-80 bentonite behaves essentially as Na-montmorillonite, but the water to solid mass ratio limits for the different rheological regions are generally lower.
  - A modelling of bentonite swelling into fractures was performed. In the model the penetration is in space driven by the repulsive forces causing swelling pressure and limited by friction against the fracture surfaces and in time limited by the water flow into the swelling bentonite. The model is based on empirical relations for swelling pressures and hydraulic conductivities. These empirical relations are determined in the region where the clay is a repulsive gel and therefore only swelling but not attractive gel formation was taken into account in the modelling. In the model, clay that reach a certain low swelling pressure (1 or 10 Pa) in the fracture is assumed to be immediately lost. The calculations show that when only repulsive forces are accounted for, the swelling rate is so high that the loss of bentonite in the time scale 100,000 years is unacceptable. The immediate loss of bentonite at the tip of the gel needs to be replaced by a transport model of the bentonite sol. This conclusion is independent of whether an empirical relation or the Poisson-Boltzmann equation is used.
- "Filtering"
  - Na-montmorillonite readily penetrates filters of pore sizes 10 and 2 μm, while pore sizes of 0.5 and 0.2 μm stop erosion within the actual detection limit. These results correlate well with evaluated lateral dimension of a typical single montmorillonite layer.
  - Ca-montmorillonite does not actively penetrate filters of pore size up to 100 μm. This observation agrees well with the observed limited swelling of this material.

- Highly compacted filter cakes of kaolinite and diatomite have been demonstrated to prevent penetration of Na-montmorillonite, while a highly compacted filter cake of MX-80 accessory minerals strongly retarded the penetration of Na-montmorillonite. However, ionic strength effects stemming from mineral dissolution is clearly noticed in the performed tests. Thus, the tests so far performed do not exclusively show that there is a mechanical filter effect of these materials.

- "Sol formation without influence of ion exchange"
  - In deionized water, correlation effects prevents sol formation of a mixed Ca/Na-montmorillonite when the Ca content is 90% or larger.
  - Na-montmorillonite in pure NaCl solution show sol behaviour below a certain critical coagulation concentration which is different for the different montmorillonite studied. For Wyoming type the CCC is 25 mM, for Milos type it is 10 mM and for Kutch type it is 5 mM.
  - It was demonstrated that the sol formation ability is related to interactions of the edge sites on individual montmorillonite layers. Consequently, this type of coagulation cannot be described by conventional "face-to-face" interaction (DLVO theory).
  - It was also demonstrated that the erosion of pure Na-montmorillonite could be stopped by increasing the NaCl concentration of a circulating solution to the CCC.
  - Gels could be formed even at pH above 9. In the pH range 7–9 there are no significant variations in CCC.

- "Ca/Na ion exchange equilibrium"
  - The selectivity coefficient for the Ca/Na exchange reaction in montmorillonite was found to be in the range 4–8 M (Gaines-Thomas convention), in good agreement with earlier studies.
  - No significant dependence of the selectivity coefficient on density was found.
  - The measured selectivity coefficient also compares well with what is calculated using the Poisson-Boltzmann equation.

- "Sol formation of Na/Ca-montmorillonite with excess ions"
  - The transition from a non-sol forming to a sol forming material occurs at an equivalent charge fraction of calcium of approximately 90% (as was the case in deionized water) in the case of external solutions containing excess calcium and sodium ions (at rather low concentrations).
  - The ability of a mixed Ca/Na-montmorillonite to form a sol in the solution with which it is in equilibrium is dramatically lowered as compared to a pure Na-system.
  - The two calcium effects described in the previous points are different phenomena. The first is associated with face-to-face interactions, while the second seems to be associated with the interactions of the edge sites of separate montmorillonite layers.
  - The gels formed in the performed sedimentation and swelling tests showed a rather high strength.
  - Several of the erosion tests have shown that NaCl-solutions of concentrations in the range 1–4 mM are able to stop erosion of clay whose ion population is dominated by sodium by as much as 80%.
  - The erosion tests have also shown the ability of mixed Ca/Na-clays to erode is insensitive to calcium population in the range 20–75%. The expected population in natural systems lie in this range.

- "Diffusion of Ca^{2+}, Na^{+} and SO_4^{2-} in compacted montmorillonite"
  - The mass transport of ions in montmorillonite cannot be described by single diffusion coefficients. Instead the ion equilibrium across any interface with the clay, e.g. a mineral phase or an external solution, must be considered.
  - Gypsum dissolving in Na dominated montmorillonite, contacted to deionized water will result in a Na_2SO_4 flux over the clay/external solution interface.
  - Gypsum solubility appears to increase substantially depending on the state of the montmorillonite (Na- or Ca-type).

9.2 Implications for the KBS-3 saftey assessment

In this report the modelling of bentonite swelling into fractures, based on empirical relations for swelling pressures, hydraulic conductivities and friction against the fracture surfaces, has been performed. The results show that the swelling rate is so high that the loss of bentonite in the time scale 100,000 years is unacceptable if immediate loss of bentonite at the tip of the gel takes place. A realistic transport modelling of the bentonite sol is needed.

However the experimental work reported here shows that there are additional attractive forces in montmorillonite associated to edge-face interactions that governs the formation of attractive gels already at low ionic strengths, 1–4 mM charge equivalents for mixed Ca/Na-montmorillonite containing 20–75% calcium, or 5–25 mM NaCl for Na-montmorillonite depending on the source of the montmorillonite. For homoionic Na-montmorillonite one may use the term critical coagulation concentration (CCC) for the concentration where attractive gels are formed. For mixed mono and divalent systems the concept of a CCC is not practical and may even be misleading. One cannot, as is sometimes seen done in the literature, speak of a CCC of Ca^{2+} for a Na-montmorillonite because as we have shown here there is always ion exchange involved. The external concentrations of Na^{+} and Ca^{2+} at equilibrium determine the ratio of Na^{+} and Ca^{2+} in charge compensation position in the clay. Some of these combinations lead to a sol (this defines the sol formation zone), and others give attractive gels, either such that are held together by correlation forces where Ca^{2+} population in the interlayer is larger than 90% or gels that are formed through edge-face interactions. For Na-montmorillonite the edge-face interaction is demonstrated in several experiments by the use of NaOH that weakens the gel or by adding tetrasodium pyrophosphate that screen the positive edge charges so effectively that the CCC increases by an order of magnitude. For the mixed Ca/Na systems we have not as explicitly demonstrated the edge-face interaction (e.g. calcium pyrophosphate would precipitate), but this is inferred from the emergence of percolation gels at high water to solid mass ratio, where face-to-face van der Waals interactions as well as correlation effects are negligible.

The homoionic montmorillonites of either sodium or calcium types are two extremes that are not realistic in a repository for spent nuclear fuel, especially not at the onset of the contact with glacial meltwater. The likely scenario is that the content of divalent ions in the interlayer will be in the range of 20–80% of CEC and in the mapping of the sol formation zone we have found that under such conditions sols are only formed when the external solution contains less than 2–4 mM charge equivalents.

The performed erosion experiments using swelling pressure test cells and circulating saline solutions have shown that erosion does not occur when the solution contains above 4 mM charge equivalents. This is also in agreement with the sol formation zone. Some of the experiments actually indicate that erosion stops at even lower concentrations (1.1 mM) that are comparable with glacial meltwaters.

The experiments thus show that erosion is stopped at and above 4 mM charge equivalent, which means that the buffer will be stable during non-glacial conditions. The experimental results cannot, due to, e.g. experimental uncertainties rule out erosion due to sol formation during glacial conditions.

References

Abend S, Lagaly G, 2000. Sol-gel transition in sodium montmorillonite dispersions. Applied Clay Science 16, 201-227.

Avena M J, Mariscal M M, De Pauli C P, 2003. Proton binding at clay surfaces in water. Applied Clay Science 24, 3-9.

ben-Avraham D, 1993. Diffusion-limited three-body reactions in one dimension, Physical Review Letters **71**, 3733-3735.

Birgersson M, Karnland O, 2009. Ion equilibrium between montmorillonite interlayer space and an external solution – Consequences for diffusional transport. Geochimica et Cosmochimica Acta **73**, 1908-1923.

Bradbury M H, Baeyens B 2003. Porewater chemistry in compacted re-saturatedMX-80 bentonite. Journal of Contaminant Hydrology **61**, 329–338.

Brindley G W, Brown G (eds), 1980. Crystal Structures of Clay Minerals and Their X-Ray Identification, Mineralogical Society Monograph No.5

Brookfield Engineering Labs Inc. More solutions to sticky problems – a guide to getting more from your Brookfield viscometer.

Börgesson L, Pusch R, Fredriksson A, Hökmark H, Karnland O, Sandén T, 1991. Final Report of the Rock Sealing Project – Sealing of the Near Field Rock Around Deposition Holes by Use of Bentonite Grouts. SKB, TR 91-34, Svensk Kärnbränslehantering AB.

Börgesson L, Johannesson L-E, Sandén T, Hernelind J, 1995. Modelling of the physical behaviour of water saturated clay barriers. Laboratory tests, material models and finite element application. SKB TR-95-20, Svensk Kärnbränslehantering AB.

Börgesson L, Hernelind H, 2006. Consequences of loss or missing bentonite in a deposition hole – A theoretical study. SKB TR-06-13, Svensk Kärnbränslehantering AB.

Cadene A, Durand-Vidal S, Turq P, Brendle J, 2005. Study of individual Na-montmorillonite particles size, morphology, and apparent charge. Journal of Colloid and Interface Science **285**, 719–730.

Connaughton C, Rajesh R, Zaboronski O, 2008. Constant flux relation for diffusion-limited cluster-cluster aggregation. Physical Review E **78**, 041403, 1–9.

Crank J, 1975. The Mathematics of Diffusion, 2nd ed.; Oxford University. Press, Oxford.

Duc M, Gaboriaud F, Thomas F, 2005. Sensitivity of the acid-base properties of clays to the methods of preparation and measurements 1. Literature review. Journal of Colloid Interface Science **289**, 139–147.

Evans D F, Wennerström H, 1999. The Colloidal Domain, 2nd ed. Wiley-WCH, New York.

Gaines G L, Thomas H C, 1953. Adsorption studies on clay minerals. II. A formulation of the thermodynamics of exchange adsorption. Journal of Chemical Physics **21**, 714–718.

Guldbrand L, Jönsson B, Wennerström H, Linse P, 1984. Electrical doube-layer forces. A Monte Carlo study. Journal of Chemical Physics **80**, 2221–2228.

Hansbo S, 1975. Jordmateriallära. Almqvist och Wiksell förlag AB, Stockholm 1975.

Hetzel F, Doner H E, 1993. Some colloidal properties of beidellite: comparison with low and high charge montmorillonite. Clays and Clay Minerals **41**, 453–460.

Iwasaki T, Watanabe T, 1988. Distribution of Ca and Na ions in dioctahedral smectites and interstratified dioctahedral mica/smectites. Clays and Clay Minerals **36**, 73–82.

Jiang Y, Gang H, BenKun M, 1990. Critical property and universality in the generalized Smoluchovski coagulation equation, Physical Review B **41**, 9424–9429.

Jönsson B, Wennerström H, 1980. Ion condensation in lamellar liquid crystals, Chemica Scripta **15**, 40–44.

Jönsson B, Labbez C, Cabane B, 2008. Interaction of nanometric clay platelets. Langmuir **24**, 11406–11413.

Jönsson B, Åkesson T, Jönsson B, Segad Meehdi M, Janiak J, Wallenberg R, 2009. Structure and forces in Bentonite MX-80**.** SKB TR-09-06, Svensk Kärnbränslehantering AB.

Karnland O, Muurinen A, Karlsson F, 1995. Bentonite swelling pressure in NaCL solutions –Experimentally determined data and model calculations. In: Alonso E.E. Ledesma A. (Eds) Advances in understanding engineered clay barriers. A.A. Balkema Publishers, Leiden.

Karnland O, Olsson S, Nilsson U, 2006. Mineralogy and sealing properties of various bentonites and smectite-rich clay material. SKB TR-06-30, Svensk Kärnbränslehantering AB.

Kjellander R, Marcelja S, Quirk J P, 1988. Attractive double-layer Interactions between calcium clay particles. Journal of Colloid and Interface Science 126, 194–211.

Kraepiel A M L, Keller K, Morel F M M, 1998. On the acid-base chemistry of permanently charged minerals. Environmental Science and Technology **32**, 2829–2838.

Lagaly G, Ziesmer S, 2003. Colloid chemistry of clay minerals: the coagulation of montmorillonite dispersions. Advances in Colloid and Interface Science **100–102**, 105–128.

Laird D A, 2006. Influence of layer charge on swelling of smectites**.** Applied Clay Science **34**, 74–87.

Lasaga A C, 1998. Kinetic theory in the earth sciences, Princeton University Press.

Liu J, Neretnieks I, 2006. Physical and chemical stability of the bentonite buffer. SKB R-06-103, Svensk Kärnbränslehantering AB.

Martin C, Pignon F, Piau J-M, Magnin A, Lindner P, Cabane B, 2002. Dissociation of thixotropic clay gels. Physical Review E **66**, 021401, 1–11.

Mason M, Weaver W, 1924. The settling of small particles in a fluid. Physical Review 23: 412–426.

Meier L P, Kahr G, 1999. Determination of the cation exchange capacity (CEC) of clay minerals using the complexes of copper(II) ion with triethylenetetraamine and tetraethylenepentamine. Clays and Clay Minerals **47**, 386–388.

Michot L, Bihannic I, Porsch K, Maddi S, Baravian C, Mougel J, Levitz P, 2004. Phase diagrams of Wyoming Na-montmorillonite clay. Influence of particle anisotropy. Langmuir, **20**, 10829–10837.

Missana T, García-Gutiérrez M, 2007. Adsorption of bivalent ions (Ca(II), Sr(II) and Co(II) onto FEBEX bentonite. Physics and Chemistry of the Earth **32**, 559–567.

Mongondry P, Nicolai T, Tassin J-F, 2004. Influence of phosphate or polyethylene oxide on the aggregation and gelation of aqueous laponite dispersions, Journal of Colloid and Interface Science **275**, 191–196.

Newman A C D, Brown G, 1987. The Chemical Constitution of Clays*,* In Chemistry of Clays and Clay Minerals – Mineralogical Society Monograph No.6, (ed A C D Newman), Longman Scientific and Technical, Essex, U.K.

Norrish K. 1954. The swelling of montmorillonite Discussions Faraday Soc. **18**, 120–134.

Secor R B, Radke C J, 1985. Spillover of the diffuse double layer on montmorillonite particles. Journal of Colloid Interface Science **154**, 236–243.

Shainberg I, Otoh H, 1968. Size and shape of montmorillonite particles saturated with Na/Ca ions (inferred from viscosity and optical measurements). Israel Journal of Chemistry **6**, 251–259.

Stauffer D, Aharony A, 1994. Introduction to Percolation Theory, 2nd ed Taylor and Francis, London.

Tanaka H, Meunier J, Bonn D, 2004. Nonergodic states of charged colloidal suspensions: Repulsive and attractive glasses and gels. Physical Review E **69**, 031404, 1–6.

Tertre E, Caset S, Berger G, Loubet M, Giffaut E, 2006. Surface chemistry of kaolinite and Na-montmorillonite in aqueous electrolyte solutions as 25 and 60°C: Experimental and modeling study. Geochimica et Cosmochimica Acta **70**, 4579–4599.

Tombácz E, Szekeres M, 2004. Colloidal behaviour of aqueous montmorillonite suspensions: the specific role of pH in the presence of indifferent electrolytes. Applied Clay Science **27**, 75–94.

Verburg K, Baveye P, 1994. Hysteresis in the binary exchange of cations on 2:1 clay minerals: A critical review. Clays and Clay Minerals **42**, 207–220.

Wanner H, Albinsson Y, Karnland O, Wieland E, Wersin P, Charlet L, 1994. The acid/base chemistry of montmorillonite. Radiochima Acta **66/67**, 157–162.

Equilibrium after swelling into the slot without considering in-plane stresses

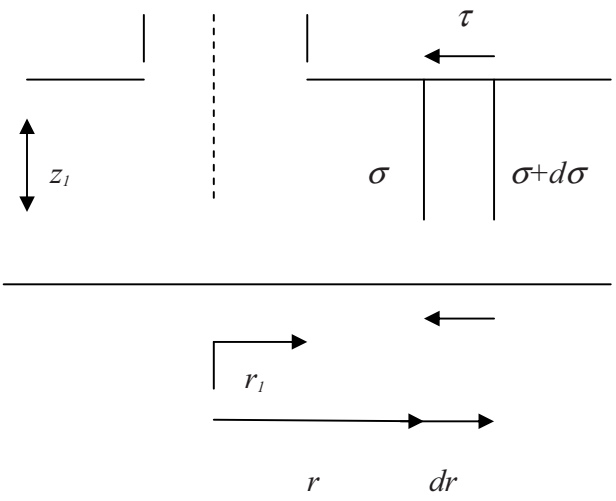

Force equilibrium in radial direction:

$$\sigma \cdot 2\pi r z_1 - (\sigma + d\sigma)2\pi(r + dr)z_1 = \left[\pi(r + dr)^2 - \pi r^2\right] \left(\sigma + \frac{d\sigma}{2}\right) \cdot \tan\phi \cdot 2$$

$$-\sigma dr - r d\sigma = \sigma r dr \cdot \frac{2\tan\phi}{z_1}$$

$$-\frac{dr}{r} - \frac{d\sigma}{\sigma} = dr\frac{2\tan\phi}{z_1}$$

Integrating from r_1 to a specified distance r_2:

$$-\int_{\sigma_1}^{\sigma_2}\frac{d\sigma}{\sigma} = \int_{r_1}^{r_2}\frac{dr}{r} + \frac{2\tan\phi}{z_1}\int_{r_1}^{r_2} dr$$

$$\ln\sigma_1 - \ln\sigma_2 = \ln\frac{r_2}{r_1} + (r_2 - r_1)\frac{2\tan\phi}{z_1}$$

$$\ln\sigma_2 = \ln\sigma_1 - \ln\frac{r_2}{r_1} - \frac{r_2 - r_1}{z_1} \cdot 2\tan\phi \qquad (1)$$

Equilibrium after swelling into the slot (general case):

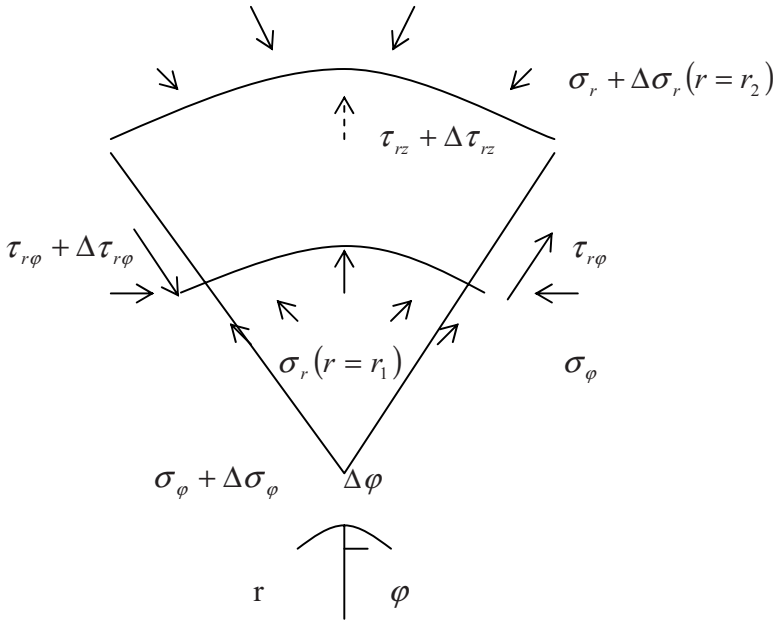

$$-(\sigma_r + \Delta\sigma_r)(r + \Delta r)\Delta\varphi \cdot \Delta z + \sigma_r \cdot r\Delta\varphi\Delta z + \tau_{r\varphi} \cdot \Delta r \cdot \Delta z - (\tau_{r\varphi} + \Delta\tau_{r\varphi}) \cdot \Delta r\Delta z + \cdot$$

$$(\sigma_\varphi + \sigma_\varphi + \Delta\sigma_\varphi) \cdot \Delta r \cdot \Delta z + \frac{\Delta\varphi}{2} + [(\tau_{rz} + \Delta\tau_{rz}) - \tau_{rz}] \cdot \Delta\varphi \cdot \left[\frac{(r+\Delta r)^2}{2} - \frac{r^2}{2}\right] = 0$$

$$-\sigma_r r\Delta\varphi\Delta z - \sigma_r \Delta r\Delta\varphi\Delta z - \Delta\sigma_r r\Delta\varphi\Delta z - \Delta\sigma_r \Delta r\Delta\varphi\Delta z + \sigma_r r\Delta\varphi\Delta z - \Delta\tau_{r\varphi}\Delta r\Delta z + \sigma_\varphi \Delta r\Delta z\Delta\varphi +$$
$$\Delta\sigma_\varphi \Delta r \frac{\Delta\varphi}{2} \cdot \Delta z + \Delta\tau_{rz} \cdot \Delta\varphi\left(r \cdot \Delta r + \frac{\Delta r^2}{2}\right) = 0$$

$$(\sigma_\varphi - \sigma_r) - \Delta\sigma_r\left(\frac{r}{\Delta r} + 1\right) + \Delta\sigma_\varphi / 2 - \frac{\Delta\tau_{r\varphi}}{\Delta\varphi} + \frac{\Delta\tau_{rZ}}{\Delta z} \quad r + \frac{\Delta r}{2} \quad = 0$$

$$\Delta\sigma_\varphi = 0$$

$$\frac{\Delta\tau_{r\varphi}}{\Delta\varphi} = 0$$

$$\Delta\tau_{rZ} = -2\sigma_r \cdot \tan\phi$$

$$\Rightarrow$$

$$(\sigma_\varphi - \sigma_r) - \Delta\sigma_r \frac{r}{\Delta r} - \frac{2\sigma_r \tan\phi}{\Delta z} \cdot r = 0 \qquad (2)$$

Assuming isotropic swelling pressure:

$$\sigma_r = \sigma_\varphi$$

$$\Rightarrow$$

$$-\Delta\sigma_r \frac{r}{\Delta r} - \frac{2\sigma_r \tan\phi}{\Delta z} \cdot r = 0$$

$$-\frac{d\sigma_r}{\sigma_r}\Delta z = 2\tan\phi \cdot \Delta r$$

$$-\ \ln\frac{\sigma_2}{\sigma_1}\ \cdot h = 2\tan\phi(r_2 - r_1)$$

$$\sigma_2 = \sigma_1 \cdot e^{-\frac{2\tan\phi(r_2 - r_1)}{h}} \qquad (3)$$

Assuming anisotropic swelling pressure:

$$\sigma_\varphi / \sigma_r = \nu/(1-\nu) \Rightarrow$$

$$\sigma_\varphi - \sigma_r = \sigma_r\left(\tfrac{\upsilon}{1-\upsilon} - 1\right)$$

$$K = \ \frac{\nu}{1-\nu} - 1 \ \Rightarrow$$

$$\sigma_\varphi - \sigma_r = \sigma_r \cdot K$$

Insert into Eqn 2 yields

$$-\Delta\sigma_r \frac{r}{\Delta r} + \sigma_r \ + K - \frac{2\tan\phi}{\Delta z} \cdot r \ = 0$$

$$\frac{d\sigma_r}{\sigma_r}\Delta z = \ K\frac{dr}{r}\Delta z - 2\tan\phi dr$$

$$\ln\frac{\sigma_2}{\sigma_1}\ h = K \cdot h \cdot \ln\frac{r_2}{r_1} - 2\tan\phi(r_2 - r_1)$$

$$\frac{\sigma_2}{\sigma_1} = \cdot e^{K\ln(\frac{r_2}{r_1}) - 2\tan\phi(\frac{r_2 - r_1}{h})}$$

$$\ln\sigma_2 = \ln\sigma_1 + K\ln\frac{r_2}{r_1} - \frac{r_2 - r_1}{z_1} \cdot 2\tan\phi \qquad (4)$$

ν	K
0	-1
0.3	-0.57
0.5	0

Thus ν=0 in Eqn 4 yields Eqn 1 and ν=0.5 yields Eqn 3

ISSN 1404-0344
CM Gruppen AB, Bromma, 2010